Universite du Quebec
Institut National de la Recherche Scientifique
Centre Energie, Materiaux et Telecommunications

Ion-Driven Hydrogel-Based Portable Electric-Generators and Self-Powered Pressure Sensors

Par

Xiaofeng Pan

These presentee pour l'obtention du grade
de Philosophiae Doctor (Ph.D.)
en sciences de l'énergie et des matériaux

Jury d'évaluation

Président du jury et examinateur interne	Prof. François Vidal INRS-EMT
Examinateur externe	Prof. Yixiang Wang McGill university
Examinateur externe	Prof. Fabio Cicoira Polytechnique Montreal
Directeur de recherche	Prof. Fiorenzo Vetrone INRS-EMT
Codirecteurs internes	Prof. Federico Rosei INRS-EMT

ACKNOWLEDGEMENTS

Upon the completion of the thesis, I would like to express my sincere gratitude to all those who have supported and encouraged me over the past four years.

First and foremost, I am deeply thankful to my supervisors, Professor Federico Rosei, Professor Fiorenzo Vetrone, and Professor Yonghao Ni, for their unwavering support, guidance, and encouragement throughout my doctoral journey. Their profound knowledge, insightful advice, and the open, collaborative research environment they fostered have been essential to my academic and personal growth. It has been a true privilege to study under their supervision.

I would also like to express my heartfelt gratitude to my parents, Ms. Guizhen Liu and Mr. Jinsong Pan, and to my girlfriend, Ms. Qinhua Wang, for their unconditional love, unwavering support, and deep understanding across time zones and distance. Their quiet strength has been a steady source of motivation, helping me persevere through challenges and self-doubt. I could not have come this far without them. Their constant encouragement has been a source of strength throughout this journey.

I am especially grateful to Dr. Daniele Benetti and Dr. Lei Jin, who have been both exceptional mentors and supportive friends. Their guidance in my research and manuscript writing has been invaluable, and their encouragement has made a lasting impact.

My thanks also go to the NanoFemtoLab members—Dr. Xin Liu, Dr. Li Shi, Dr. Yuting Lei, Dr. Jiabin Liu, Dr. Faying Li, Mingzhu Wang and Dr. Tingzhou Yang—for their technical assistance and constructive discussions. I also feel fortunate to have met so many wonderful friends during my time here, especially Yang Liu, Fang Dong, Hao Yu, Wenqiang Xiang, and Miao Liu, whose companionship made this journey more meaningful.

I would like to acknowledge the administrative and technical staff at INRS-EMT for their professionalism and continuous support, as well as the China Scholarship Council (CSC) for providing financial support during my studies.

Finally, I sincerely thank Professor Shuhui Sun, Professor François Vidal, Professor Yixiang Wang, Professor Fabio Cicoira, and Professor Andreas Ruediger for serving on my thesis committee and for their valuable feedback and time.

To all who have supported me along the way—thank you.

ABSTRACT

To support efficient human–machine interaction, wearable pressure sensors have gained significant attention for their outstanding performance. Thanks to their softness, biocompatibility, and tunable properties, hydrogels are well-suited for such applications. Traditional sensors rely on external power, while self-powered designs based on triboelectric nanogenerators (TENGs) or piezoelectric nanogenerators (PENGs) produce alternating current (AC) that requires rectification, adding complexity to the system. Therefore, developing hydrogel-based direct current (DC) generators and self-powered pressure sensors is of great importance.

In the first project, a polyelectrolyte generator was developed using poly (acrylic acid) (PAA) hydrogel. As a typical polyelectrolyte, PAA contains fixed negative groups ($–COO^-$) backbone and mobile protons (H^+). Under compression, a difference in local ion concentration drives directional proton migration, producing a measurable DC signal in the external circuit. At around 50% compressive strain, the device generated an output of ~6 mV. It remained stable under prolonged loading (over 1000 seconds), showing excellent resilience and reliability. Demonstrations showed its potential for self-powered position and sound sensing. This mechanism can also be extended to other polyelectrolyte hydrogel systems.

The second project aimed to boost voltage output by building an internal ion gradient. The bilayer hydrogel generator consists of two functional hydrogel layers: one is a polyvinyl alcohol (PVA) hydrogel incorporating either an anionic polyelectrolyte (lignosulfonate sodium, LS) or a cationic polyelectrolyte (quaternary chitosan, QC), and the other is a pure PVA hydrogel layer. This gradient-driven structure enabled a single device to reach a maximum output of ~130 mV. When ten units were connected in series, the total output rose to ~1.3 V, enough to power small commercial electronics like calculators. The device also functioned as a self-powered pressure sensor, responding to external pressure without the need for an external power source.

The third project introduced a paper–hydrogel hybrid generator. It combined a silver-coated filter paper as the bottom electrode with a layer of polyacrylamide (PAM) hydrogel. The porous paper facilitated ion generation and transport, while the silver coating reacted with moisture to enhance the output. This setup produced voltages up

to 0.6 V and showed excellent long-term performance. With added glycerol to retain moisture, the device operated stably for over 1000 hours. Its modular design allowed easy scaling—ten units in series delivered up to 6 V—making it suitable for powering larger devices or charging energy storage units. Besides power generation, the device also served as a flexible and reliable pressure sensor.

In summary, the strategies proposed and the ion-driven hydrogel devices developed in this work exhibit significant improvements in DC output and demonstrate potential for powering small electronics and enabling self-powered sensing. This work may offer a promising foundation for advancing efficient, sustainable, and potentially commercializable hydrogel-based DC generators and sensors.

Keywords: Wearable pressure sensor, self-powered pressure sensing, electric generator, hydrogels, polyelectrolyte-gradient, ion-gradient, filter paper, lignosulfonate sodium (LS), quaternary chitosan (QC)

RÉSUMÉ

Pour favoriser une interaction homme–machine efficace, les capteurs de pression portables suscitent un vif intérêt en raison de leurs performances remarquables. Grâce à leur souplesse, leur biocompatibilité et leurs propriétés modulables, les hydrogels sont particulièrement adaptés à ces applications. Les capteurs traditionnels dépendent d'une source d'alimentation externe, tandis que les dispositifs auto-alimentés basés sur des nanogénérateurs triboélectriques (TENGs) ou piézoélectriques (PENGs) produisent un courant alternatif (AC), qui nécessite un redressement, ce qui complique le système. Ainsi, le développement de générateurs à courant continu (DC) à base d'hydrogel et de capteurs de pression auto-alimentés revêt une grande importance.

Dans le premier projet, un générateur à polyelectrolyte a été conçu en utilisant un hydrogel de poly (acide acrylique) (PAA). Le PAA, en tant que polyelectrolyte typique, contient des groupes négatifs fixes ($–COO^–$) et des protons mobiles (H^+). Lors d'une compression, une différence locale de concentration ionique induit une migration directionnelle des protons, générant un signal DC mesurable dans le circuit externe. Sous environ 50 % de déformation, l'appareil a produit une tension d'environ 6 mV. Il a montré une grande stabilité sous contrainte prolongée (plus de 1000 secondes), avec une bonne résilience. Ce dispositif a démontré son potentiel pour détecter des positions ou des sons sans alimentation externe. Ce principe peut également être appliqué à d'autres hydrogels polyelectrolytes.

Le deuxième projet visait à augmenter la tension de sortie en créant un gradient ionique interne. Le générateur à hydrogel en double couche est composé de deux couches fonctionnelles : l'une est un hydrogel de polyalcool vinylique (PVA) contenant un polyelectrolyte anionique (lignosulfonate de sodium, LS) ou cationique (chitosane quaternisé, QC), l'autre est un hydrogel de PVA pur. Cette structure à gradient a permis à un seul dispositif d'atteindre une tension maximale d'environ 130 mV. En connectant dix unités en série, la sortie totale est montée à environ 1,3 V, suffisante pour alimenter de petits appareils électroniques comme une calculatrice. L'appareil peut aussi servir de capteur de pression auto-alimenté, sensible aux forces externes sans besoin d'une source d'énergie.

Le troisième projet a introduit un générateur hybride papier–hydrogel. Il associe un

papier filtre recouvert d'argent comme électrode inférieure et une couche d'hydrogel de polyacrylamide (PAM). Le papier poreux facilite la génération et le transport des ions, tandis que la couche d'argent réagit à l'humidité pour renforcer la production d'électricité. Ce système a généré jusqu'à 0,6 V et a démontré une excellente stabilité à long terme. Avec l'ajout de glycérine pour conserver l'humidité, l'appareil a fonctionné de manière stable pendant plus de 1000 heures. Son design modulaire permet une mise à l'échelle facile : dix unités en série peuvent atteindre jusqu'à 6 V, ce qui le rend adapté à l'alimentation d'appareils plus puissants ou au stockage d'énergie. En plus de la production électrique, il fonctionne aussi comme un capteur de pression souple et fiable.

En résumé, les stratégies proposées et les dispositifs à hydrogel ioniques développés dans ce travail ont montré une nette amélioration de la sortie en courant continu, et offrent un réel potentiel pour l'alimentation de petits appareils électroniques ainsi que pour la détection auto-alimentée. Ces travaux ouvrent la voie à des générateurs et capteurs à hydrogel plus efficaces, durables et potentiellement commercialisables.

Mots-clés : Capteur de pression portatif et souple, détection de pression auto-alimentée, générateur électrique, hydrogels, gradient de polyelectrolyte, gradient ionique, papier filtre, lignosulfonate de sodium (LS), chitosane quaternaire (QC)

TABLE OF CONTENTS

LIST OF FIGURES

LIST OF TABLES

LIST OF SYMBOLS

AA	Acrylic Acid
AC	Alternating Current
AI	Artificial Intelligence
AM	Acrylamide
APS	Ammonium Persulfate
AgNPs	Silver Nanoparticles
AuNWs	Gold Nanowires
$BaTiO_3$	Barium Titanate
CA	Contact Angle
CB	Carbon Black
CMC	Carboxymethyl Cellulose
CNN	Convolutional Neural Network
CNTs	Carbon Nanotubes
CS	Compressive Stress
$CaCl_2$	Calcium Chloride
DC	Direct Current
DES	Deep Eutectic Solvents
DMSO	Dimethyl Sulfoxide
DSC	Differential Scanning Calorimetry
EDAX	Energy-Dispersive X-ray Analysis
FTIR	Fourier Transform Infrared Spectroscopy
GSM	Gram per square meter
HC	High Concentration

HEG	Hydorgel Electric Generator
ILs	Ionic Liquids
KPFM	Kelvin Probe Force Microscope
LC	Low Concentration
LCR	Inductance (L), Capacitance (C), and Resistance (R) meter
LS	Lignosulfonate sodium
LiCl	Lithium Chloride
Li_2SO_4	Lithium Sulfate
MBA	N,N'-Methylenebisacrylamide
MEGs	Moisture-Electric Generators
MWCNTs	Multi-Walled Carbon Nanotubes
MXene	2D Transition Metal Carbides/Nitrides
NTf_2^-	Bis(trifluoromethylsulfonyl)imide
NaCl	Sodium Chloride
OFET	Organic Field-Effect Transistor
PAA	Polyacrylic Acid
PAM	Polyacrylamide
PANI	Polyaniline
PDMS	Polydimethylsiloxane
PEDOT	Poly(3,4-ethylenedioxythiophene)
PENGs	Piezoelectric Nanogenerators
PEG	Paper Electric Generator
PET	Polyethylene Terephthalate

PGHEG	polyelectrolyte-gradient hydrogel electricity generator
PHEG	paper-hydrogel electricity generator
PI	Polyimide
PNIPAM	Poly(N-isopropylacrylamide)
PPy	Polypyrrole
PU	Polyurethane
PVA	Polyvinyl Alcohol
PVA–LS	Polyvinyl Alcohol–Lignosulfonate sodium
PVA–QC	Polyvinyl Alcohol–Quaternary Chitosan
PVDF	Poly(vinylidene fluoride)
QC	Quaternary Chitosan
R	Electrical Resistance
RH	Relative Humidity
RT	Room Temperature
SEM	Scanning Electron Microscope
TA	Tannic Acid
TEGs	Thermoelectric Generators
TENGs	Triboelectric Nanogenerators
TMEDA	Tetramethylethylenediamine
VHB	Very High Bond
XPS	X-ray Photoelectron Spectroscopy
$ZnCl_2$	Zinc Chloride
ZnO	Zinc Oxide

1. INTRODUCTION

1.1 Wearable electronics

Wearable electronics refer to flexible devices that can be directly worn on the human body. [1, 2] They are lightweight, capable of real-time sensing and interactive control, and are widely used in areas such as health monitoring (Figure 1.1), intelligent control, and human–machine interaction.[3] Compared to conventional rigid devices, wearable electronics offer better softness and conformity, allowing them to attach closely to the skin while maintaining comfort and portability.

These devices can continuously collect a range of physiological signals, including electrophysiological activity, blood glucose, blood pressure, and mechanical strain, providing reliable data for health assessment and rehabilitation.[4, 5] In addition, the sensed information can be converted into control signals for operating external systems and enabling interactive functions. With the integration of data processing and pattern recognition techniques, the responsiveness and adaptability of such systems continue to improve, laying the groundwork for more flexible and efficient human–machine collaboration.[6-8]

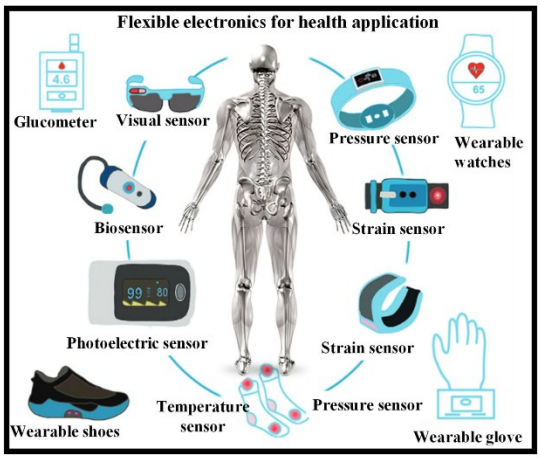

Figure 1.1 Wearable electronics for human health applications. [9]

1.1.1 Wearable pressure sensors

Pressure sensors are essential components in wearable devices, capable of converting subtle mechanical stimuli from the body or external sources into detectable electrical signals.[10] With ongoing research, the development of flexible, lightweight, and skin-conformal sensors has advanced steadily. These devices exhibit excellent compliance,

allowing them to closely adhere to skin and maintain stable performance under various movement conditions, while ensuring comfort during extended wear. [11] They can be integrated into clothing or directly attached to skin, and are widely used in applications such as real-time monitoring of physiological signals like pulse and respiration, gait analysis, and rehabilitation support.[12] As shown in Figure 1.2, the wearable pressure sensor collects subtle pulse signals from the human body and transmits them in real-time via Bluetooth.

Figure 1.2 Real-time acquisition and wireless transmission of subtle pulse signals by a wearable pressure sensor. [13]

Looking ahead, continued innovation in flexible electronics is poised to push the boundaries of what wearable pressure sensors can achieve—particularly in terms of sensitivity, power efficiency, and adaptability. Such advancements will not only improve the precision of physiological data acquisition but also enable more responsive and personalized healthcare solutions. In parallel, the integration of these systems into robotics and interactive technologies will deepen the synergy between humans and machines.[14] Over time, a wearable pressure sensor is expected to become a core component of next-generation bio-integrated systems, blending seamlessly into everyday applications and redefining how we interact with our environments (Figure 1.3).

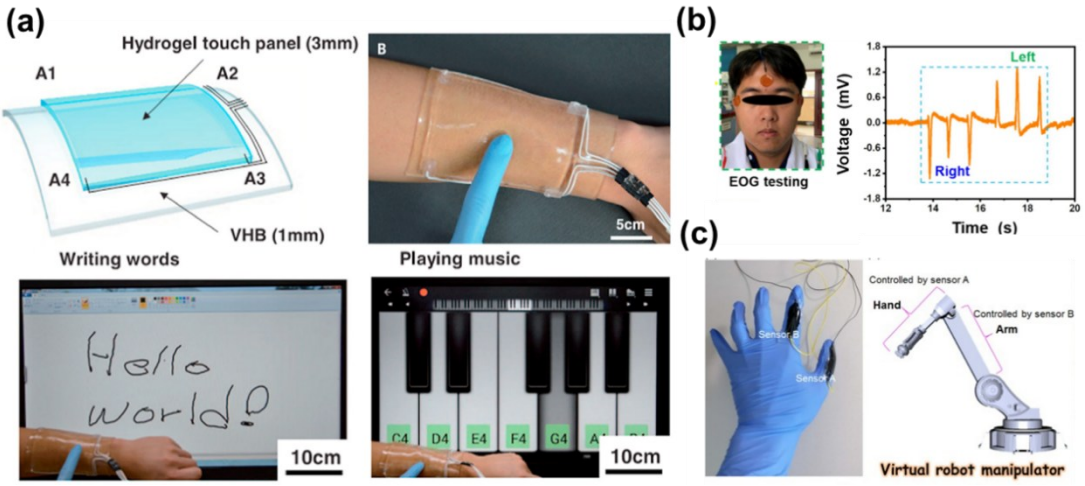

Figure 1.3 Wearable electronics utilizing force sensing for a) text input and remote piano operation, [15] b) human EOG signal collection, [16] and c) robotic arm control.[17]

1.1.2 Substrates for wearable pressure sensors

Achieving accurate force sensing in wearable pressure sensors requires substrate materials that not only perform well but also feel natural on the body. Ideally, the substrate should mimic the mechanical properties of human skin—flexible, stretchable, durable, and biocompatible—to ensure both functionality and comfort.

Common materials like polyurethane (PU), polydimethylsiloxane (PDMS), polyimide (PI), and polyethylene terephthalate (PET) are widely used due to their strength and ease of processing.[18, 19] However, they struggle to match the skin's dynamic movements. For instance, while PDMS and PU offer some stretchability, they remain stiffer than real skin, which can lead to discomfort and poor mechanical conformity (Figure 1.4). Their limited biocompatibility also raises concerns for long-term wear, potentially causing irritation or immune responses. PI and PET, though mechanically stable, are too rigid for applications requiring flexibility.[20]

In contrast, hydrogels have emerged as promising alternatives. Their high-water content, softness, and tissue-like properties offer better adaptability to skin movements and improved long-term comfort. These features make hydrogels strong candidates for next-generation wearable electronics.[21]

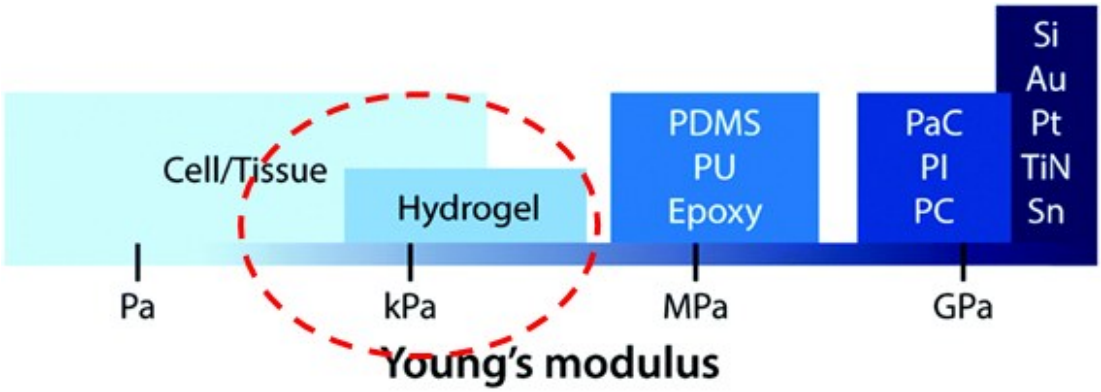

Figure 1.4 Young's modulus of cells, tissues, and commonly used materials.[22]

1.2 Hydrogels and their functional design for wearable electronic

Hydrogels are semi-solid materials with a three-dimensional network of hydrophilic polymers that can retain large amounts of water without dissolving (Figure 1.5).[23] Their strong hydration ability comes from functional groups like hydroxyl, amine, and carboxyl, while crosslinked structures—formed via covalent bonds or physical interactions such as hydrogen bonding or electrostatic forces—ensure mechanical stability.[24, 25]

Figure 1.5 Schematic diagram of a soft hydrogel
(produced from http://www.jat.net.cn/pageslevel2/type_1_16.html).

In wearable electronics, especially skin-contact applications, hydrogels offer clear advantages.[26] Their high water content gives them a soft, skin-like feel, improving comfort and reducing irritation.[22] This not only enhances user experience but also helps improve signal quality. Moreover, their structure can be precisely engineered to adjust properties like biocompatibility, toughness, conductivity, anti-freezing, anti-drying, adhesion, self-healing, and pressure sensitivity. [27] These tunable features make hydrogels highly promising for next-generation flexible electronics.

1.2.1 Classification of hydrogels

The classification of hydrogels is primarily based on the type of polymer used, which can be broadly categorized into natural hydrogels, synthetic hydrogels, and hybrid hydrogels (Figure 1.6).

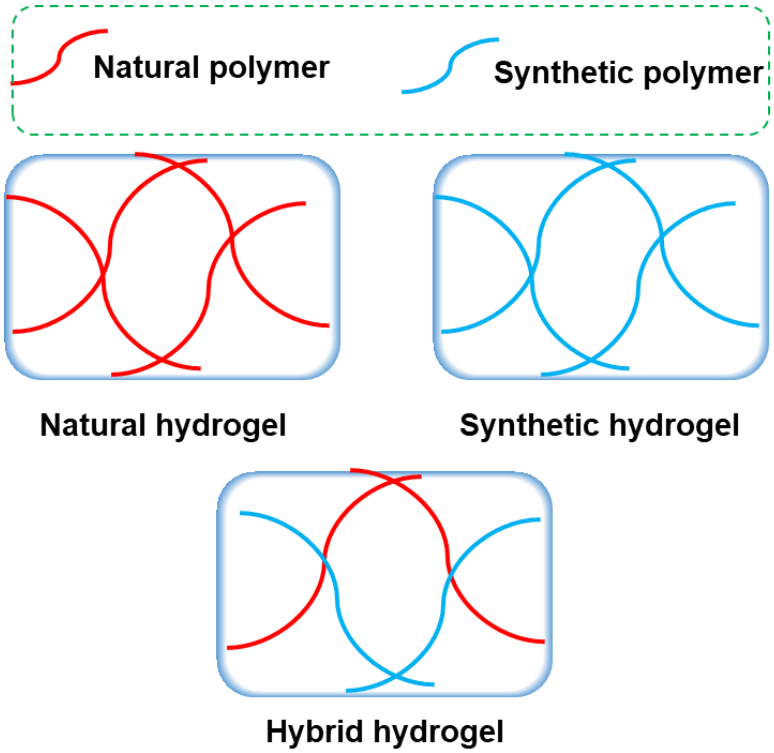

Figure 1.6 Schematic diagram of hydrogels composed of natural, synthetic, and hybrid polymers (by Xiaofeng Pan).

Natural hydrogels

Natural polymer hydrogels, mainly derived from polysaccharides, lignin, and proteins, offer a wide spectrum of functional properties.[28] Polysaccharide-based hydrogels—such as agar, alginate, hyaluronic acid, chitosan, and cellulose derivatives—are widely used due to their excellent hydrophilicity and biocompatibility.[29, 30] Protein-based hydrogels like collagen, gelatin, and fibrin add structural and functional diversity. Materials such as gelatin and agarose are valued for their thermos-reversible gel-sol behavior, making them indispensable in fields like food processing.[31] Sodium alginate, capable of ion-induced crosslinking (*e.g.*, with Ca^{2+}), is a staple in bioprinting.[32] Cellulose-based hydrogels can be produced through methods such as

dissolution–regeneration, chemical crosslinking, or functionalization, supporting applications from pollutant adsorption to flexible electronics.[33, 34] However, natural hydrogels often suffer from low mechanical strength and fast degradation, limiting their long-term use (Figure 1.7a). [28]

Synthetic hydrogels

Unlike natural hydrogels, synthetic hydrogels are made from man-made polymers such as polyacrylic acid (PAA), polyacrylamide (PAM), polyvinyl alcohol (PVA), and poly(N-isopropylacrylamide) (PNIPAM).[35] They are typically crosslinked—either chemically or physically—into stable three-dimensional networks. PAM and PAA are commonly prepared through monomer polymerization followed by chemical crosslinking, offering good mechanical robustness.[36] PVA-based hydrogels, formed via freeze–thaw cycles or crosslinking agents, also exhibit high mechanical strength. Compared to their natural counterparts, synthetic hydrogels generally demonstrate superior mechanical durability and environmental stability (Figure 1.7b). However, concerns over the toxicity of certain monomers and crosslinkers can limit their use in applications requiring high biocompatibility, such as wearable electronics or biomedical devices.[37]

Hybrid hydrogels

To bridge the gap between strength and biocompatibility, hybrid hydrogels—combining natural and synthetic polymers—have gained growing attention.[38] By integrating the favorable properties of both components, these materials can overcome the weaknesses of each. For example, Gu *et al*. developed a lignin–PVA hybrid hydrogel with enhanced mechanical properties and improved biocompatibility (Figure 1.7c).[39]

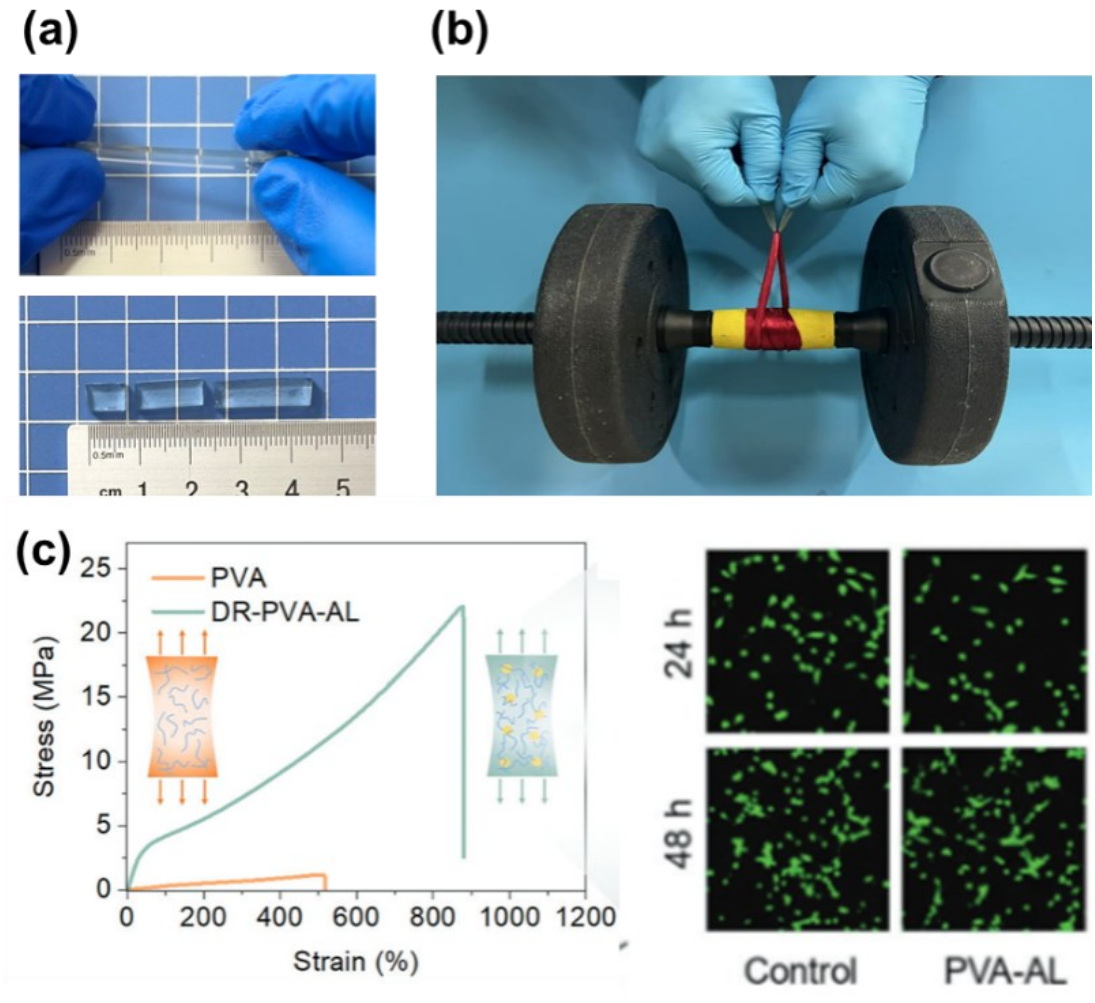

Figure 1.7 Schematic illustration of the mechanical strength of a) gelatin (by Xiaofeng Pan) and b) PVA hydrogels [40], along with c) the mechanical strength and cytotoxicity of PVA-Lignin hybrid hydrogel. [39]

1.2.2 Tunable design of hydrogel mechanical properties

In wearable electronics, the mechanical behavior of hydrogels is key to both comfort and performance. As shown in Figure 1.8, soft hydrogels can closely conform to the skin and irregular surfaces thanks to their flexibility, improving wearer comfort and sensing accuracy.[41] Tough hydrogels, on the other hand, resist stretching, bending, and friction, making them suitable for applications that demand long-term mechanical stability under repeated stress. [42] For optimal function, hydrogel properties should be tailored to meet the specific mechanical requirements of different use scenarios.

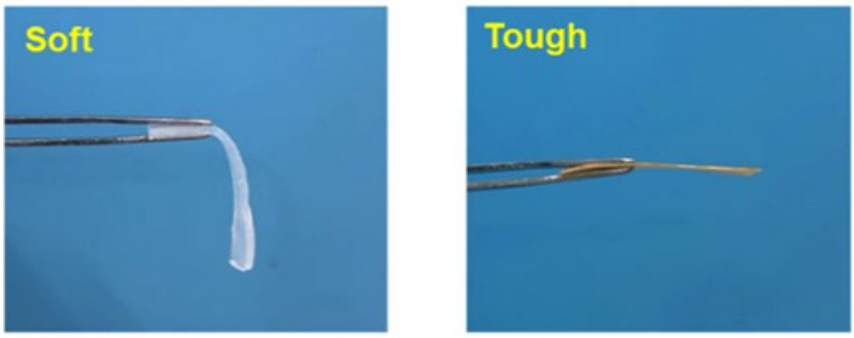

Figure 1.8 Schematic illustration of soft and tough hydrogels (by Xiaofeng Pan).

To improve the mechanical strength of hydrogels, several effective strategies have been developed.[43] A common approach is the dual-network design, which combines a rigid network with a flexible one to achieve both strength and toughness.[44] Nanofiller reinforcement—using materials like cellulose nanofibers or graphene—can further enhance mechanical properties.[45] Dynamic and reversible crosslinking, based on hydrogen bonding or metal coordination, also contributes to toughness by improving energy dissipation and structural resilience.[46]

On the other hand, reducing hydrogel strength is sometimes desirable, especially in applications requiring high flexibility. This can be achieved by lowering the crosslinking density to soften the network, or by increasing water content to reduce modulus through controlled swelling.[47] Copolymerization with components such as lignin or tannic acid (TA) can also adjust chain rigidity, making the hydrogel more stretchable and adaptable.[48]

1.2.3 Tunable design of hydrogel conductive properties

Conductivity plays a crucial role in hydrogel-based pressure sensors, enabling effective signal collection, transmission, and processing.[49] While hydrogels are highly flexible and biocompatible, they are inherently non-conductive.[50] To overcome this, conductive materials or networks are often introduced, allowing hydrogels to function as soft, stretchable conductors without sacrificing their mechanical compliance (Figure 1.9). [51]

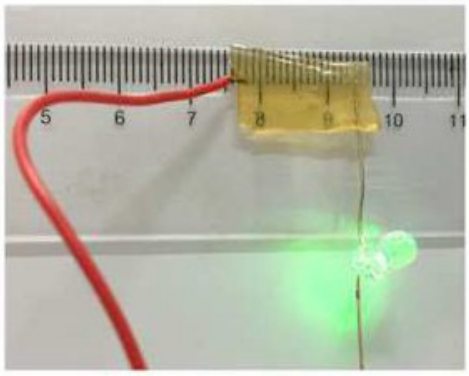

Figure 1.9 Schematic illustration of conductive hydrogel acting as a conductor in a circuit, enabling a battery to power a small LED bulb.[52]

This electrical functionality is key to converting mechanical stimuli into measurable signals, supporting real-time sensing and feedback. [53] Typically, hydrogel conductivity is enhanced through three main approaches: electronic conduction, ionic conduction, and polyelectrolyte-based systems (Table 1.1). [54]

Table 1.1 Approaches for enhancing the conductivity of hydrogels

Strategy	Conductive mechanism	Conductive materials
Electronically conductive	Electron transport through conductive fillers	Carbon-based materials, conductive polymers, metal nanomaterials
Ionically conductive	Ion migration	Metal salts, ionic liquids (ILs), and deep eutectic solvents (DES)
Polyelectrolyte-based conductive	Ion migration	Polyelectrolytes

Electronically conductive hydrogel

Electronic conductive materials used in hydrogels mainly include carbon-based materials, conductive polymers, and metal nanomaterials, each offering distinct advantages for flexible electronics.[55] Carbon-based fillers like carbon black (CB), multi-walled carbon nanotubes (MWCNTs), and MXene provide efficient electron transport through their highly conductive nanostructures.[56] Conductive polymers—such as polyaniline (PANI), polypyrrole (PPy), and poly(3,4-ethylenedioxythiophene) (PEDOT)—offer tunable conductivity via molecular design and doping, while maintaining good flexibility and processability.[57] Metal nanomaterials, including

silver nanoparticles (AgNPs), gold nanowires (AuNWs), and copper nanosheets, leverage their high surface area and nanoscale geometry to enhance charge transport and conductivity.[58]

To incorporate these materials into hydrogels, hydrophilic modification is often necessary to ensure uniform dispersion in water. Once dispersed, they can form continuous conductive networks within the hydrogel matrix, greatly improving electrical performance. For instance, Han *et al*. (Figure 1.10a) modified CNTs with polydopamine to enhance water dispersibility, achieving a conductivity of 8 S/m after embedding them into a polymer hydrogel. Wang *et al*. (Figure 1.10b) synthesized a water-soluble conductive filler via in-situ polymerization of EDOT on lignosulfonate sodium (LS), yielding a hydrogel with a conductivity of 0.065 S/cm. In another example, Zhu *et al*. (Figure 1.10c) introduced hydroxyl groups to silver nanowires using bis(2-hydroxyethyl) disulfide, facilitating their incorporation into a PVA–borax system and resulting in a hydrogel with 3.59 S/m conductivity.

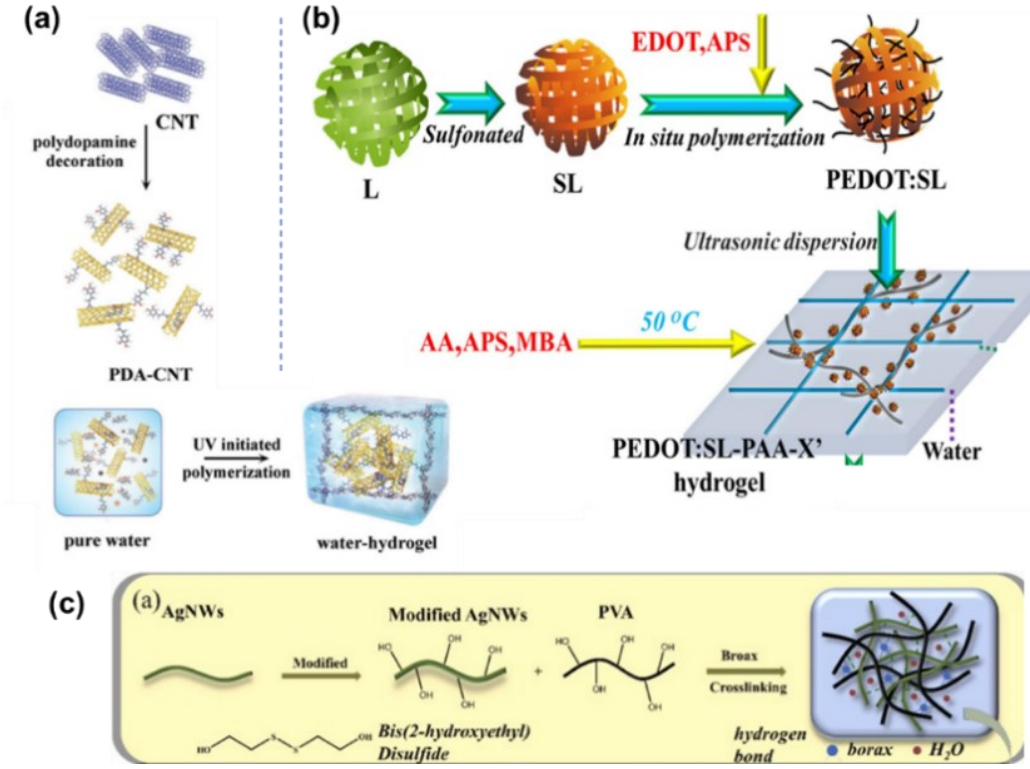

Figure 1.10 Hydrophilized electronic conductive fillers are uniformly dispersed and embedded into the hydrogel network to form a stable hydrophilic conductive structure. [59-61]

Ionically conductive hydrogel

The Suo team first proposed the concept of ionic conductive hydrogels, where charge transport relies on mobile ions rather than electrons.[62, 63] Their conductivity arises from the high water content and the presence of ionizable additives such as metal salts (e.g., NaCl, LiCl), ILs, and DES. [64, 65] These additives dissociate in water to release cations and anions, enabling ion-based conduction within the hydrogel network.

Metal salts like NaCl dissolve readily, producing free Na^+ and Cl^- ions that migrate under an electric field, forming the basis for salt-based conductive hydrogels. ILs and DES offer alternative ion sources. ILs typically consist of bulky organic cations (*e.g.*, imidazolium, pyridinium) and small anions (*e.g.*, $CF_3SO_3^-$, NTf_2^-), providing high ionic strength, low volatility, and wide electrochemical stability.[66] However, their high viscosity, synthesis cost, and potential toxicity remain concerns. In contrast, DES—formed from hydrogen bond donors (*e.g.*, amino acids, lactic acid) and acceptors (e.g., acetylcholine, $ZnCl_2$)—are more environmentally friendly and biocompatible, though they generally exhibit lower conductivity and thermal stability. [67] Both ILs and DES are highly hydrophilic and can be mixed with water in any ratio.

To introduce these conductive species into hydrogels, two main strategies are used. One method adds the conductive additive directly during gel preparation to ensure uniform dispersion. For example, Bai *et al*. prepared a PAM/Carboxymethyl cellulose (CMC) hydrogel incorporating $CaCl_2$, achieving an ionic conductivity of 3.37 S/m (Figure 1.11a). The other method involves soaking a pre-formed hydrogel in a conductive solution, allowing ions to diffuse into the network. Zhang *et al*., for instance, replaced water with DES in a PVA system to produce a uniformly conductive hydrogel (Figure 1.11b).

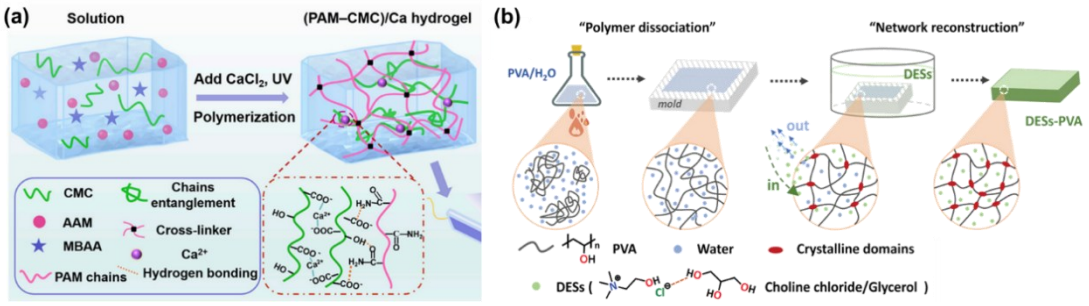

Figure 1.11 Two approaches for preparing ionic hydrogels include: a) incorporating ionic components before gel formation; [68] b) allowing ionic components to diffuse into the gel through solution replacement after gelation. [69]

Polyelectrolyte-based conductive hydrogel

Polyelectrolyte-based hydrogels conduct electricity through dissociable ionic groups along the polymer backbone.[70] Typical examples include carboxyl groups in PAA and sulfonic acid groups in LS, which release mobile ions upon hydration. [48] These ions migrate under an electric field, enabling ionic—rather than electronic—conduction. Depending on their charge type, polyelectrolytes can be classified as cationic, anionic, or zwitterionic, with the latter capable of releasing both cations and anions. This built-in ionic functionality allows polyelectrolyte hydrogels to achieve conductivity without the need for additional conductive fillers. Their conductivity depends on several factors, including ion dissociation degree, ion mobility, solvation, solvent content, and polymer architecture.[71] By carefully selecting and designing the polymer structure, conductive hydrogels can be prepared cost-effectively and straightforwardly.

1.2.4 Tunable design of anti-freezing and anti-dryness properties in hydrogels

Similar to human skin, hydrogels are highly responsive to environmental changes. However, conventional hydrogels tend to freeze at low temperatures and lose water at high temperatures, leading to brittleness and loss of function.[61] By optimizing molecular composition and network structure, their resistance to freezing and dehydration can be significantly improved.[72] As a result, hydrogels can maintain flexibility, mechanical integrity, and conductivity under extreme conditions, making them more reliable for wearable electronic applications.[73]

Anti-freezing hydrogel

In everyday life, salt is often spread on icy roads to lower the freezing point of water and reduce ice formation. Antifreeze fluids in vehicles, typically containing ethylene glycol, prevent ice crystal growth and protect engines in cold weather. In nature, polar fish produce antifreeze proteins that inhibit intracellular ice, a strategy also applied in frozen food preservation to reduce cell damage. Inspired by these examples, researchers have developed several approaches to enhance the antifreeze performance of hydrogels. Four main strategies are commonly used in their design (Figure 1.12).[74]

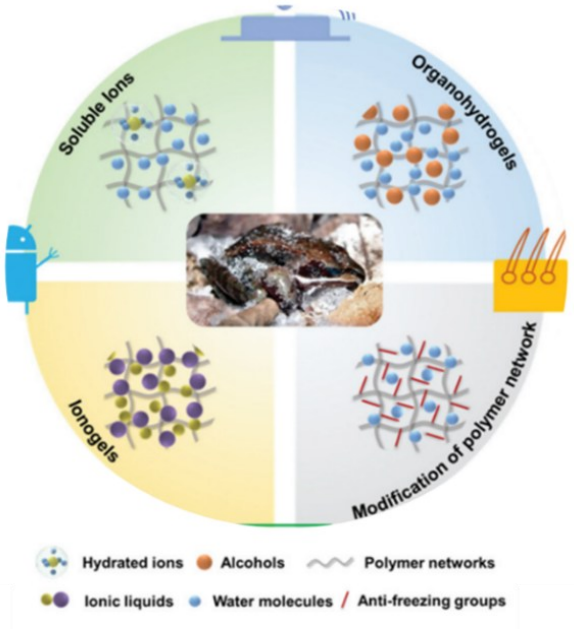

Figure 1.12 Schematic illustration of four strategies for enhancing the anti-freezing performance of hydrogels.[74]

Adding salts to hydrogels is an effective way to suppress ice crystal formation by lowering the freezing point. The presence of dissolved ions increases the osmotic pressure, limits the mobility of water molecules, and disrupts the hydrogen bonding network, thereby reducing the amount of freezable water. [75] This collectively leads to a depression in freezing temperature, allowing the hydrogel to remain soft and flexible at low temperatures, and avoiding shrinkage or brittleness. Inspired by this, Vlassak *et al*. incorporated $CaCl_2$ into polymer hydrogels, enabling the composite hydrogel to remain stretchable even at -57°C.[76]

Some organic solvents, such as glycerol, ethylene glycol, and DMSO, function as antifreeze agents by lowering the freezing point of water, and inhibiting ice crystal formation. Through hydrogen bonding with water molecules, they reduce the free water content and help maintain water fluidity at low temperatures, effectively preventing freezing-related issues. For instance, Zhou's team gradually replaced water in polymer hydrogels with glycerol, glycol, and sorbitol, successfully developing an organic hydrogel that remains unfrozen even at –80°C.[75] However, unlike salt-based antifreeze agents, organic solvents may compromise the hydrogel's conductivity.

In addition, ILs exhibit low melting points, minimal volatility, and excellent ionic conductivity, enabling them to stay liquid even at extreme temperatures like -50°C.[77]

This makes them highly effective antifreeze agents. By disrupting the hydrogen bond network and promoting water molecule hydration, ILs help hydrogels remain flexible in cold environments while preserving conductivity.

Certain biomolecules, such as antifreeze proteins, fish collagen, trehalose, and glucose, enhance the freeze resistance of hydrogels by stabilizing water molecules and inhibiting ice crystal growth through hydrogen bonding. [74, 78] For example, Jiang's group incorporated glucose into a PAM hydrogel, progressively lowering its freezing point.[79] In addition, introducing hydrophilic groups (*e.g.*, carboxyl, hydroxyl, and sulfonic groups) into the polymer network strengthens water interactions, increasing the fraction of unfrozen water and further enhancing antifreeze performance.[80]

Anti-dryness hydrogel

To improve the water retention and anti-drying performance of hydrogels, two main strategies are typically employed. The first enhances water–hydrogel interactions by introducing hydrophilic groups, incorporating superabsorbent polymers, or adding water-stabilizing agents such as ILs, DES, and sugars. [81] These modifications reduce water evaporation and are often associated with improved antifreeze properties, as freeze resistance and water retention tend to reinforce each other.

The second strategy aims to physically limit moisture loss by introducing external barriers, such as water-repellent coatings or dense protective layers. In some cases, both approaches are combined for greater effectiveness. As shown in Figure 1.13, a PVA hydrogel was modified with a glycerol–salt mixture and covered with a compact polymer film.[82] This combination significantly reduced water loss, highlighting the benefit of integrating chemical and physical water-retention mechanisms.

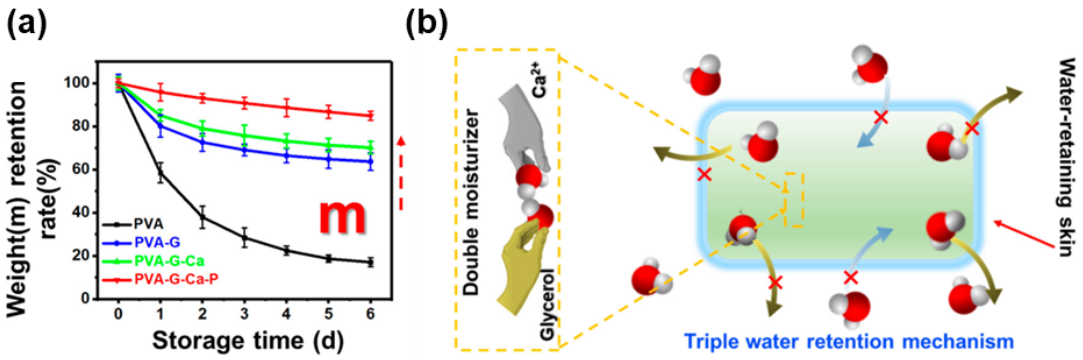

Figure 1.13 a) Weight variation of different PVA composite hydrogels during storage, including

the original hydrogel, hydrogel with glycerol, hydrogel with glycerol and $CaCl_2$, and hydrogel with glycerol, $CaCl_2$, and a dense protective coating. b) Schematic representation of the water retention mechanism in hydrogels.[82]

1.2.5 Tunable design of self-healing properties in hydrogels

The self-healing ability of human skin is driven by a coordinated network of biological processes. Inspired by this, researchers have developed hydrogel-based wearable electronics capable of autonomously restoring their structure, mechanical strength, and conductivity after damage.

This functionality is typically achieved through reversible crosslinking mechanisms—such as dynamic covalent bonds, hydrogen bonding, and ionic interactions—that allow the material to reconfigure and recover mechanical integrity.[83] As illustrated in Figure 1.14a, PVA–borax hydrogels self-heal via reversible bonds between borate ions and hydroxyl groups on the polymer chains, enabling mechanical recovery. Conductivity can also be restored through interfacial reconnection or molecular diffusion. For example, a DES-based hydrogel incorporating MXene and P(AA–co–AM) regains conductivity immediately after being rejoined (Figure 1.14b).

Such self-healing behavior helps hydrogels maintain flexibility and function under prolonged use or mechanical stress. This not only enhances device durability in harsh environments but also reduces the need for frequent replacement, making them more practical for flexible electronic applications.[84]

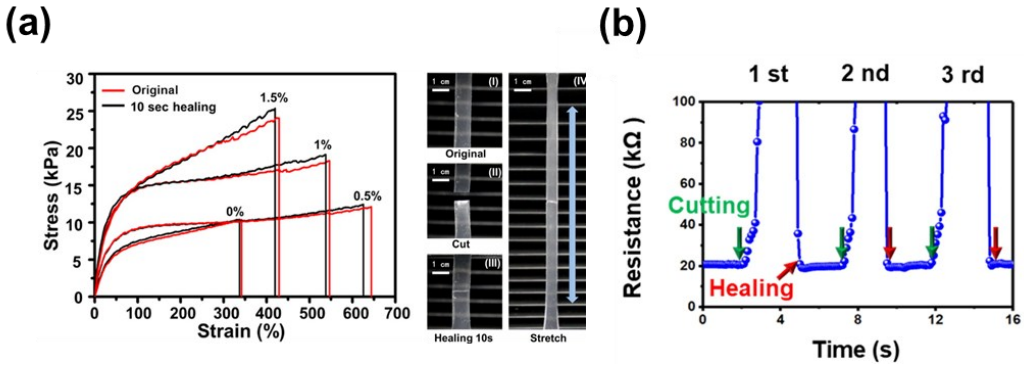

Figure 1.14 a) Schematic representation of mechanical strength recovery in hydrogels; [85] b) Schematic depiction of the self-healing of hydrogel conductivity. [86]

1.2.6 Tunable design of self-adhesive properties in hydrogels

The self-adhesive property of wearable electronics is critical for stable operation in

applications such as physiological monitoring, soft robotics, and medical devices. Strong adhesion ensures reliable contact with skin or tissue during motion, bending, or sweating, minimizing signal loss and improving data accuracy.[87] It also allows the device to follow skin deformation, which is especially important in high-strain areas like joints. Enhancing the adhesive performance of hydrogel-based electronics improves their durability, signal consistency, and adaptability under demanding conditions.[88]

One effective strategy to improve hydrogel adhesion is incorporating substances rich in functional groups—such as TA, dopamine, lignin, amino acids, soy protein, or gelatin—into the polymer network. [89, 90] These components enhance interfacial bonding through hydrogen bonds, electrostatic forces, covalent interactions, and hydrophobic effects. As shown in Figure 1.15a, TA is first coated onto the substrate and then embedded into the hydrogel, forming a stable adhesive interface (Figure 1.15b). The deliberate molecular design of such components not only strengthens adhesion but also improves environmental tolerance and overall wearability, making hydrogels more suitable for flexible electronics and related applications (Figure 1.15c). [91]

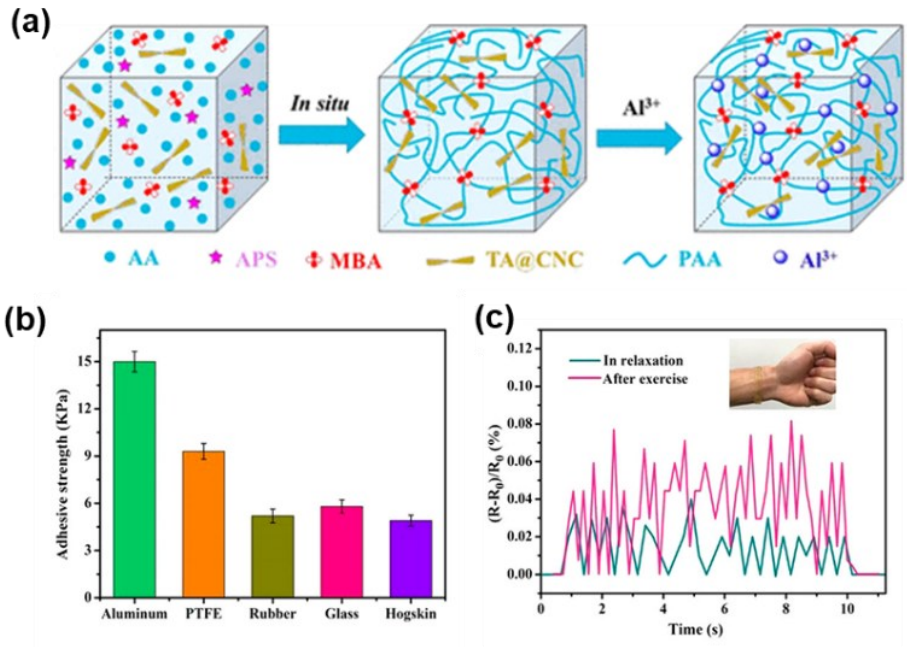

Figure 1.15 a) Schematic illustration of the preparation process of adhesive hydrogels; b) Adhesion strength on different substrates; c) Application as a self-adhesive wearable sensor for monitoring human pulse signals. [91]

1.3 Hydrogel-based wearable pressure sensors (external power supply)

This section focuses on hydrogel design strategies for externally powered pressure sensors. These devices primarily operate through piezoresistive or capacitive mechanisms, converting applied pressure into electrical signals. Hydrogels contribute to sensing performance through their viscoelasticity, conductivity, and deformation sensitivity, enabling accurate detection of pressure variations.[26] However, their function typically depends on a stable external power supply.

1.3.1 Hydrogel-based capacitive piezoresistive sensor

The viscoelastic and conductive properties of hydrogels form the basis for their use in pressure sensing within flexible electronics. As illustrated in Figure 1.16, hydrogel-based piezoresistive sensors typically consist of a conductive hydrogel layer placed between two metal electrodes. When external pressure is applied, the hydrogel deforms elastically, leading to a change in its geometry. This deformation alters the electrical resistance (R) according to the basic principles of conductivity, allowing the applied pressure to be quantitatively detected.

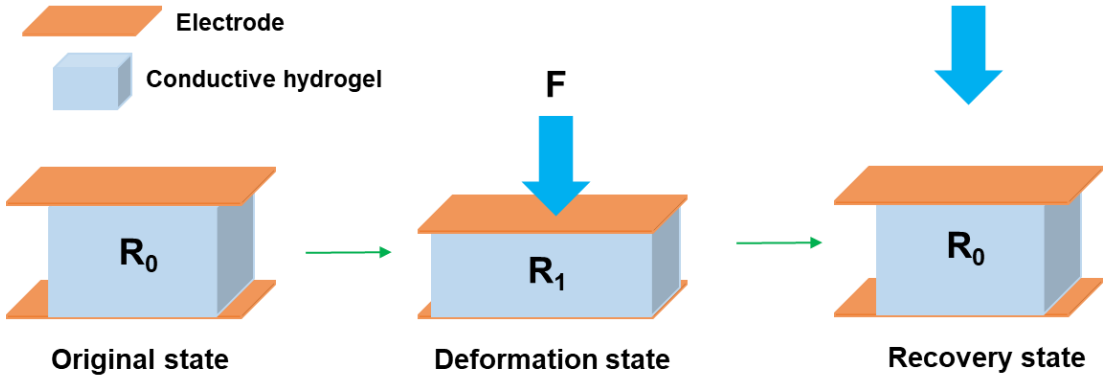

Figure 1.16 Working principle of a conductive hydrogel-based piezoresistive sensor (by Xiaofeng Pan).

The conductivity (σ) of hydrogels is measured using the following formula:

$$\sigma = \frac{L}{RA} \qquad \textbf{Equation 1.1}$$

where σ (S/m) represents conductivity, L (m) is the sample length, R (Ω) is the measured resistance, and A (m^2) is the cross-sectional area.

If the hydrogel is considered a uniform conductor with consistent conductivity, applied pressure causes deformation, altering the length and cross-sectional area of the conductive pathway and, consequently, its resistance.[92] This deformation effectively

translates pressure into a resistance change. Once the force is removed, the hydrogel elastically returns to its original shape, restoring the resistance to its initial value and completing the pressure-sensing process. For example, Zhang incorporated MXene into PVA hydrogel to create a conductive hydrogel, which was then used to construct a piezoresistive sensor for handwriting recognition and sound detection. These sensors detect changes in R signals caused by hydrogel deformation, enabling the recognition of handwriting and letters.[93]

Piezoresistive sensors offer high sensitivity, fast response, and ease of fabrication, but their performance is susceptible to environmental influences. For instance, temperature fluctuations can alter the resistance of hydrogels, leading to baseline drift.[94] Humidity variations can also affect resistance. [95] Although applying a protective film or coating with silicone oil can help minimize moisture interference, temperature changes are constant, making it challenging to fully eliminate their impact on the device.

1.3.2 Hydrogel-based capacitive pressure sensor

The core structure of a hydrogel-based capacitive pressure sensor typically consists of two conductive hydrogel electrodes and a dielectric layer in between, forming a parallel plate capacitor. The capacitance of a parallel plate capacitor is given by the following equation:

$$C = \frac{\varepsilon_r \varepsilon_0 A}{d} \qquad \textbf{Equation 1.2}$$

where C is the capacitance, A is the effective electrode area, ε_r is the dielectric constant of the dielectric material, ε_0 is the permittivity of vacuum, and d is the distance between the electrodes. According to this equation, the capacitance depends on the dielectric constant of dielectric material (ε_r), electrode area (A), and electrode spacing (d).

As shown in Figure 1.17a, when an external force is applied, the conductive hydrogel electrode deforms, changing the effective electrode area and altering the capacitance. Once the force is removed, the hydrogel returns to its original shape, restoring the capacitance and completing a pressure-sensing cycle. This deformation-driven capacitance variation enables the conversion of external force into electrical signals for precise pressure or touch detection.[63] For instance, Lei *et al*. developed an ionically conductive hydrogel and integrated it into a capacitive pressure sensor. The sensor detects pressure changes by utilizing the deformation of the hydrogel electrode caused

by falling water droplets, which leads to capacitance variation (Figure 1.17b).[96]

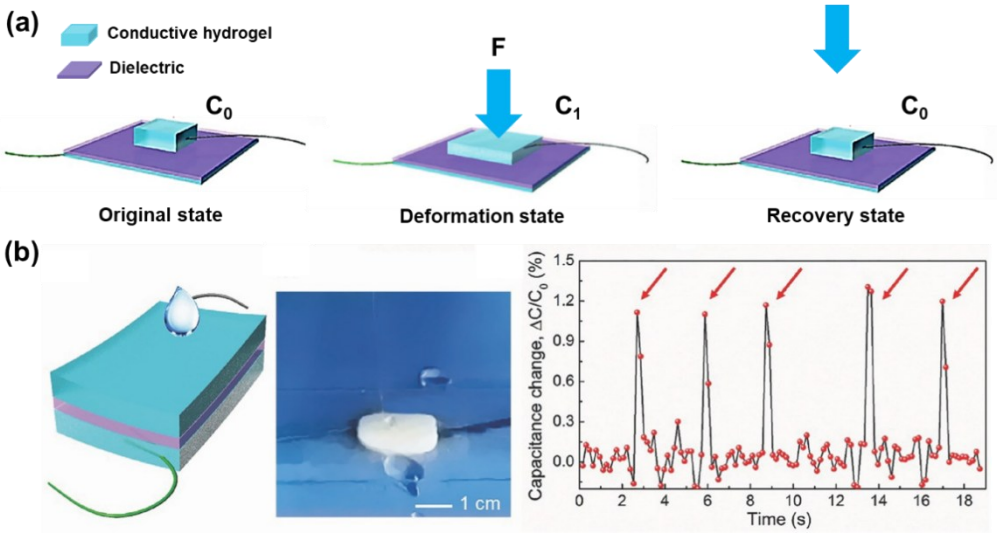

Figure 1.17 a) Working principle of a conductive hydrogel-based capacitive pressure sensor. b) Schematic illustration of a conductive hydrogel-based capacitive pressure sensor detecting falling water droplets. [96]

Compared to piezoresistive sensors, capacitive pressure sensors are structurally more complex and costlier. However, they are less sensitive to temperature and environmental factors, such as humidity, making them better suited for certain applications.

1.4 Hydrogel-based electric generators and self-powered pressure sensors

Flexible pressure sensors, remain in the early stages of development and face several challenges before large-scale adoption. Among them, energy supply is one of the most critical, as it directly affects device stability and usability. Unlike human skin, flexible electronics cannot generate power autonomously and typically rely on external energy sources. Although batteries are the most common solution, their need for frequent charging or replacement limits real-time performance. In addition, their rigid structure is incompatible with the stretchable nature of wearable systems. Ideally, these devices should operate continuously without regular charging—an objective that remains difficult to achieve.

To address this issue, self-powered sensing has become an important research focus. As shown in Figure 1.18, interest in self-powered hydrogel-based tactile sensors has grown steadily in recent years. The core concept is to harvest energy from the environment or human activity and convert it into electricity to support sensor function. Mechanisms

such as triboelectricity, piezoelectricity, thermoelectricity, and moisture-driven energy harvesting enable these devices to operate without traditional batteries.[97] Since the energy is derived from ambient sources, it is also cleaner compared to conventional battery systems, which often rely on fossil fuels. In addition to powering the sensor itself, the harvested energy can potentially supply other low-power components. This approach reduces dependence on external power sources and improves the flexibility and longevity of wearable electronics, offering promising prospects for wearable electronics.[98]

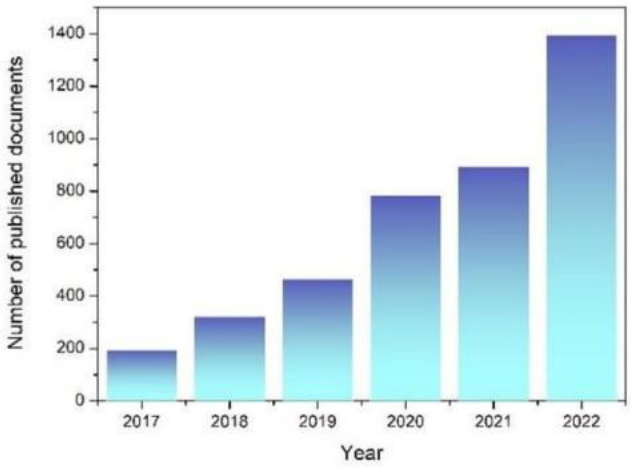

Figure 1.18 Number of research papers found using the keyword "hydrogel for self-powered tactile sensor" in the database (accessed on February 1, 2023).[99]

1.4.1 Hydrogel-based alternating current (AC) electric generators and self-powered pressure sensors

This section highlights the dual functionality of hydrogel-based flexible electronics, which can generate AC signals while simultaneously sensing external forces through voltage or current changes. Currently, most hydrogel-based AC generators and self-powered sensors fall into two main categories: triboelectric and piezoelectric. Both types can detect mechanical stimuli—such as pressure, deformation, or vibration—without relying on external power sources, by converting mechanical energy into electrical signals. This integration of sensing and energy harvesting enables continuous operation and supports the development of self-sustaining systems. Such technologies offer several advantages, including sustainable energy output and compatibility with compact, wearable, or implantable devices. In addition, hydrogel-based sensors can operate autonomously and supply power to other low-energy components, expanding

their potential for practical applications in healthcare, robotics, and portable electronics.

Triboelectric nanogenerators (TENGs)

TENGs, first reported by Wang's group in 2012, operate based on the principles of contact electrification and electrostatic induction.[100] When two materials with differing electron affinities come into contact and then separate, a potential difference arises due to surface charge transfer, generating current through an external circuit. Repeating this cycle produces AC, making TENGs a promising strategy for developing self-powered systems. Compared to conventional power sources, TENGs offer a lightweight, scalable, and environmentally friendly solution.[101]

Hydrogel-based TENGs typically operate in single-electrode mode, where the hydrogel is connected to an external circuit via a metal wire and encapsulated in an elastomer film. Based on their conduction mechanism, hydrogels are broadly categorized into ion-conductive and electron-conductive types, each with distinct energy harvesting behaviors. As illustrated in Figure 1.19a, ion-conductive hydrogels generate electricity through ion redistribution within the gel upon mechanical deformation. When contact is made between the dielectric and elastomer layers, surface charges are generated. Upon separation, a potential imbalance drives ion migration within the hydrogel, which subsequently induces electron flow in the external circuit. This mechanism enables AC generation without relying on traditional electron flow within the gel itself. In contrast, electron-conductive hydrogel-based TENGs follow a similar structural design but rely on electron mobility through the hydrogel (Figure 1.19b). The electrical output arises directly from charge transfer induced by electrostatic interactions between materials under repeated contact-separation motions. [102]

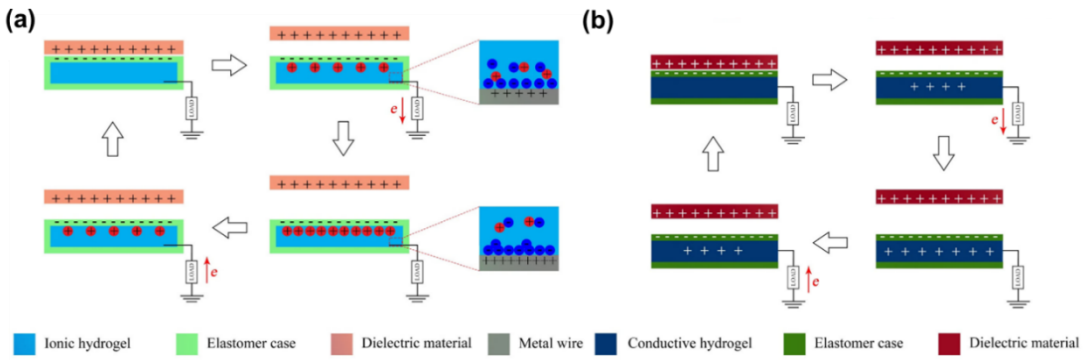

Figure 1.19 Schematic illustration of single-electrode TENGs utilizing a) ion-conductive

hydrogels and b) electron-conductive hydrogels. [102]

Hydrogel-based TENGs are gaining attention as a sustainable option for self-powered sensing. Beyond detecting pressure without external power, they can also provide usable energy for small electronic devices, and have shown durability under continuous use. That said, one key limitation is that TENGs generate AC, which must be rectified into direct current (DC) for most practical systems—a step that adds to circuit complexity and complicates device integration. For instance, Pu and co-workers designed a single-electrode TENGs by embedding an ion-conductive hydrogel in very high bond (VHB) tape (Figure 1.20a).[103] Their device not only converts pressure into consistent voltage signals, but after rectification, the output can also charge a capacitor or power a small electronic watch—demonstrating both sensing and energy supply capabilities in a single compact system (Figure 1.20b).

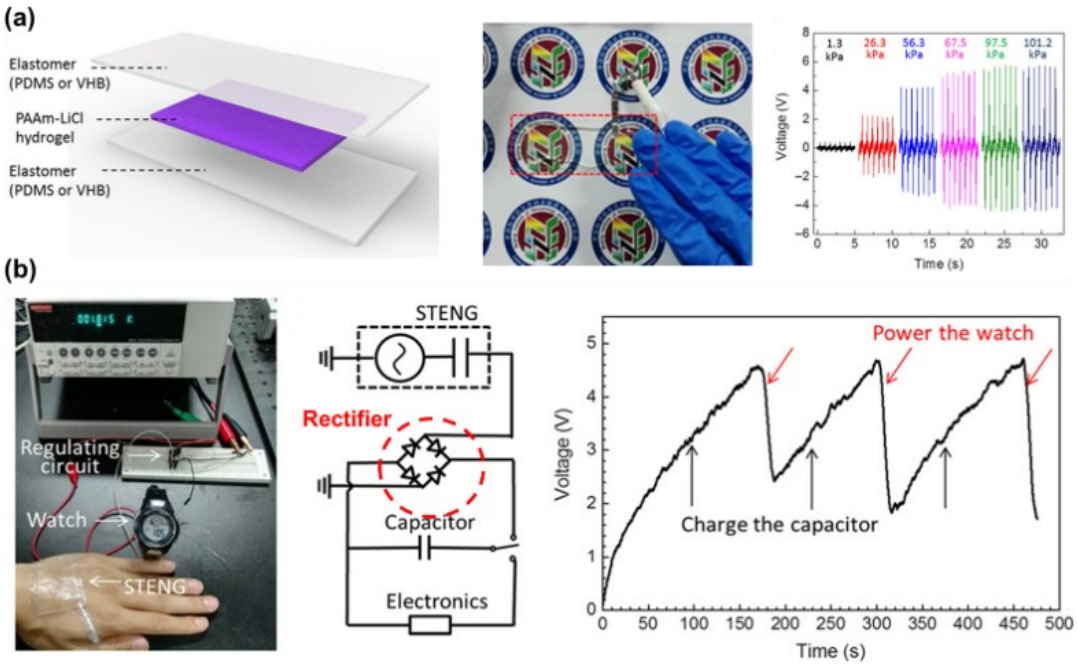

Figure 1.20 a) Schematic illustration of a single-electrode TENGs based on ionic conductive hydrogel and its self-powered pressure-sensing process. b) The AC output generated by the hydrogel TENGs can be rectified into DC to power small electronics.[103]

Piezoelectric nanogenerator (PENGs)

Hydrogel-based PENGs combine the mechanical flexibility of hydrogels with the energy conversion capabilities of piezoelectric materials, offering a promising platform for self-powered sensing and energy harvesting. By embedding piezoelectric elements

within a soft hydrogel matrix, mechanical deformation can be effectively translated into electrical signals via the piezoelectric effect (Figure 1.21).[104]

Depending on their composition and working mechanism, the piezoelectric materials used in PENGs are generally divided into two categories. Organic materials such as chitosan, silk fibroin, and poly (vinylidene fluoride) (PVDF) possess inherent dipole moments—arising from β-sheet structures or polar C–F bonds—that reorient under mechanical force to generate surface charge. In contrast, inorganic materials like ZnO, $PbTiO_3$, and $BaTiO_3$ respond to external stress through lattice deformation, shifting internal dipoles and producing piezoelectric polarization. [104] Integrating these materials into a hydrogel not only ensures mechanical compliance but also enables stable charge generation upon deformation, with external electrodes facilitating charge transfer. The working mechanism typically involves four steps: mechanical deformation, dipole realignment and charge separation, generation of electric potential and current flow, and finally, recovery to the original state inducing a reverse current. This cyclical process results in AC output. [105]

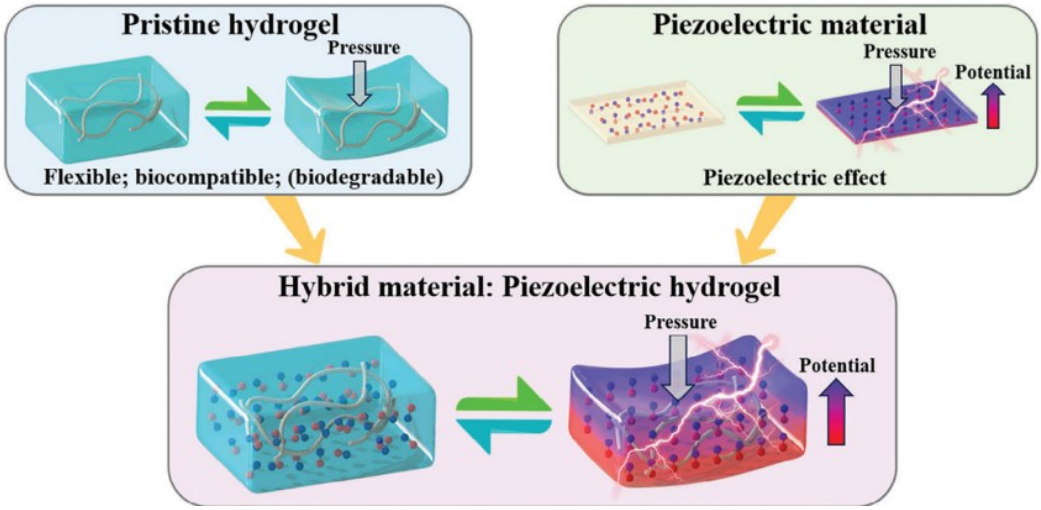

Figure 1.21 Schematic illustration of the assembly of a hydrogel-based PENGs.[104]

Similar to hydrogel-based TENGs, this device utilizes a green energy conversion mechanism for self-powered pressure sensing and power supply to other small electronics. However, like TENGs, it primarily generates AC, necessitating rectification to produce DC for practical use. This additional step increases circuit complexity and poses challenges for seamless system integration. To enhance the practicality of

hydrogel-based wearable electronics, developing generators and self-powered sensors capable of directly outputting DC remains a key research priority.

1.4.2 Hydrogel-based DC electric-generators and self-powered pressure sensors

This section focuses on hydrogel-based DC generators, particularly thermoelectric generators, which convert thermal energy into DC. In addition, when subjected to compression, conductive hydrogels deform, altering their internal resistance and influencing the electrical signal output. By tracking these signal variations, pressure sensing can be achieved.

Hydrogel-based thermoelectric generators (TEGs) and self-powered pressure sensors

Heat is an abundant and continuously dissipated energy form in the environment, much of which remains underutilized—particularly low-grade sources such as industrial waste heat and body heat. Thermoelectric technology presents a sustainable way to tap into this energy, converting it directly into DC electricity without moving parts or emissions.[106]

Among candidate materials, ionic hydrogels stand out due to their mechanical softness, high ionic conductivity, and adaptability, making them particularly well-suited for flexible, quasi-solid-state thermoelectric systems.[107] These materials are capable of harvesting ambient or body heat and converting it into usable electrical signals, providing a viable power source for wearables and low-power sensors. The thermoelectric response of hydrogels generally arises from two complementary mechanisms: the thermogalvanic and Soret effects. In thermogalvanic systems, redox reactions at electrodes held at different temperatures generate a voltage difference (Figure 1.22a). Ion pairs such as Fe^{3+}/Fe^{2+} and I^{-}/I_3^{-} are commonly used, producing thermopowers often exceeding 1mV/K.[108] In parallel, the Soret effect contributes by driving ions to diffuse from hot to cold regions, establishing concentration gradients and thereby inducing a voltage (Figure 1.22b). [109] While this mechanism does not involve redox chemistry and cannot maintain a continuous current on its own, it can reinforce the thermogalvanic output when the two effects are coupled—enhancing overall energy conversion efficiency.[110]

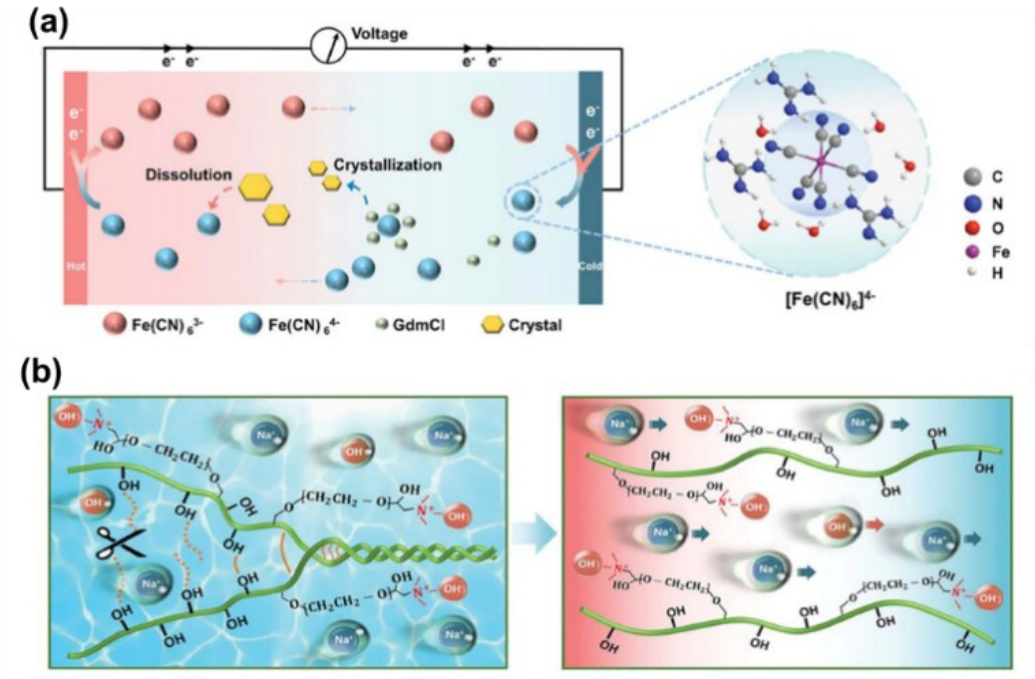

Figure 1.22 Two typical thermoelectric power generation modes based on ionic hydrogels: (a) thermogalvanic effect [108] and (b) Soret effect [109].

Hydrogel-based thermoelectric generators can also serve as self-powered pressure sensors. In a representative study (Figure 1.23a), Chen and colleagues developed a highly flexible hydrogel consisting of a PAM–calcium alginate dual network, with Li_2SO_4 introduced as the ionic conductor. The device harnesses the Soret effect to convert thermal gradients into electrical signals. Interestingly, when pressure is applied, the resulting deformation of hydrogel alters its internal resistance, leading to measurable voltage fluctuations (Figure 1.23b). This coupling between mechanical stress and electrical output allows the system to function as a self-powered pressure sensor.[111]

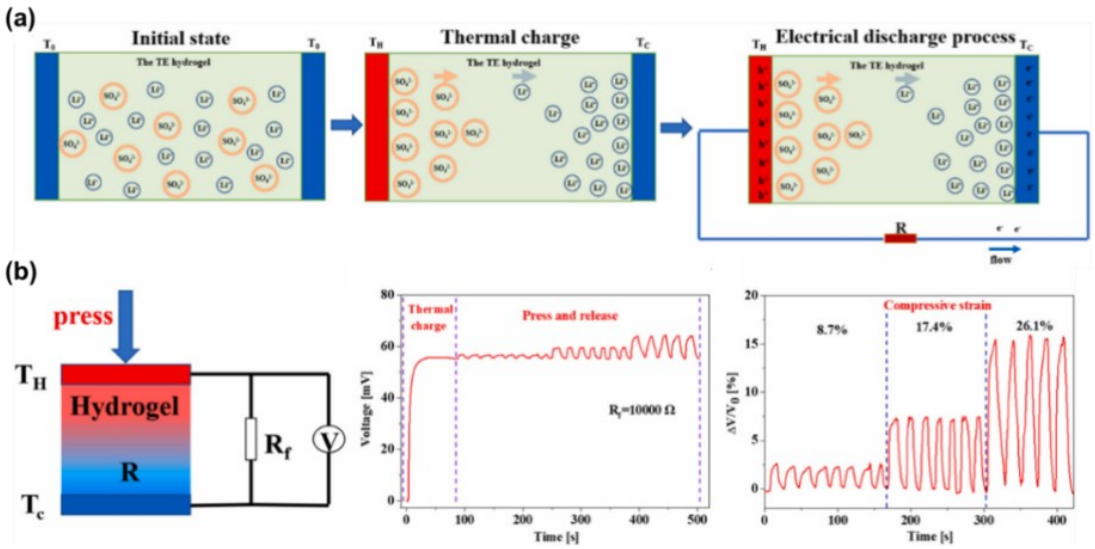

Figure 1.23 a) Schematic illustration of the DC power generation process of an ionically conductive hydrogel-based thermoelectric generator (Soret effect); b) Schematic illustration of the self-powered pressure sensing process. [111]

Experimental results have highlighted the promise of thermoelectric hydrogels as self-powered pressure sensors. However, several practical challenges must be addressed before they can be deployed reliably. One key issue is their sensitivity to ambient temperature fluctuations, which can interfere with signal accuracy. Furthermore, mechanical compression may bring the hydrogel into contact with unintended heat or cold sources, introducing additional variability and voltage drift. These factors compromise signal stability and limit the consistency of sensor performance in uncontrolled or dynamic environments.

1.4.3 Hydrogel-based moisture-enabled generators

Moisture-electric generators (MEGs) are micro-energy devices that convert ambient humidity into DC without external power input. Their ability to operate in diverse environments—including indoors, on cloudy days, or even on human skin—makes them well-suited for wearable electronics and low-power systems.[112]

For example, Yang *et al.* developed scalable MEGs based on ionic hydrogel, incorporating PVA, phytic acid, and a glycerol-water solvent to enhance moisture absorption and ion transport (Figure 1.24a). The device operates via humidity-driven ion migration. As moisture diffuses across a humidity gradient, ions move with it, forming a concentration imbalance. Since electrodes block ion flow, this gradient induces electron movement through the external circuit, generating DC output (Figure

1.24b).[113]

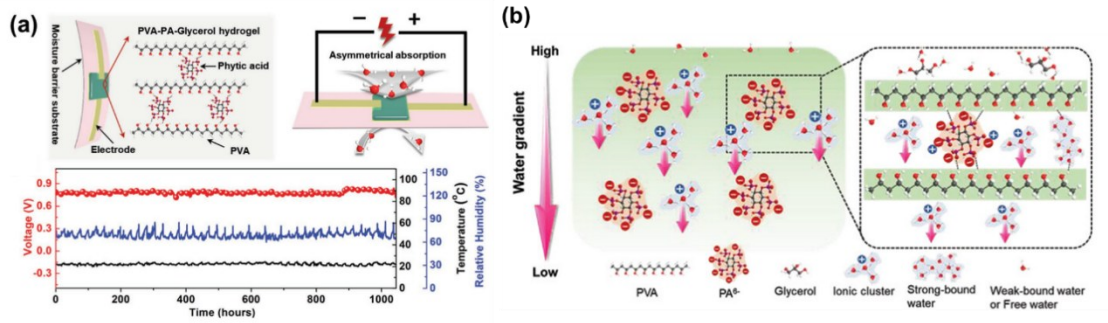

Figure 1.24 a) Schematic illustration of the structure and DC power generation of the hydrogel-based MEGs; b) Schematic diagram of the power generation mechanism of the hydrogel-based MEGs.[113]

Although this device can generate DC electricity, it is not well-suited for self-powered pressure sensing. Ambient humidity is often unstable and varies with location and time, making it difficult to ensure consistent signal output. Moreover, applying pressure can hinder moisture diffusion into the hydrogel, disrupting ion migration and leading to signal instability.

1.5 Motivation

To enable efficient human–machine interaction, wearable pressure sensors have attracted widespread attention and research due to their excellent functional properties. Hydrogels, with their softness, elasticity, and good compatibility with biological tissues, offer clear advantages for these applications. In recent years, efforts have focused on enhancing their mechanical and functional properties—such as improving their viscoelasticity, conductivity, stability under extreme temperatures, self-healing behavior, and adhesion—so they can perform reliably under repeated use and in complex environments.

Initial hydrogel-based sensors, including piezoresistive and capacitive types, could detect mechanical deformation but relied on external power, limiting integration and portability. To address this, self-powered designs using TENGs and PENGs mechanisms were introduced, allowing AC generation and pressure sensing under mechanical input. However, AC output requires rectification, increasing circuit complexity. As a result, interest has shifted toward TEGs hydrogel sensors, which generate DC by ion movement under temperature gradients and can respond to pressure through voltage changes. Still, their performance is vulnerable to environmental

interference.

Today, hydrogel-based pressure sensors are evolving toward DC, self-powered systems. Researchers are exploring two main approaches: one in which pressure directly induces DC generation, and another where a continuous DC signal is modulated by applied pressure. During our preliminary investigation, we found that the directional migration of ions in hydrogels can generate a DC in an external circuit. However, if both positive and negative ions move simultaneously, their charges may cancel out, preventing electron flow and thus failing to produce a current in an external circuit (Figure 1.25a). To achieve a DC output, selectively driving either positive or negative ions while keeping the oppositely charged ions fixed is essential (Figure 1.25b). This principle is similar to that observed in moisture-electric generation. By carefully designing the hydrogel composition and device structure, ion migration can be precisely controlled to generate DC, enabling self-powered pressure sensing.

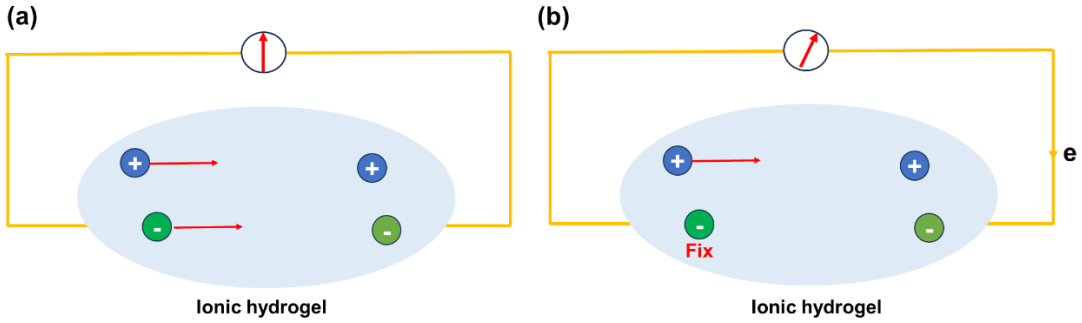

Figure 1.25 Schematic illustration of electron movement in the external circuit of an ionic hydrogel: a) simultaneous migration of positive and negative ions, and b) selective migration of a single ion species.

1.6 Thesis objectives and organization

Objectives: This work focuses on designing and building flexible hydrogel-based devices that can generate DC and act as self-powered pressure sensors. The main focus is to improve the DC output by controlling the directional movement of ions inside the hydrogel. To achieve this, the study explores the chemical composition of the hydrogel, optimizes the device structure, and introduces multi-layer functional designs to enhance overall performance. The goal is to prove that these devices can function as self-powered pressure sensors. Based on this objective, the research is divided into three parts.

Part I: This chapter presents a self-powered hydrogel-based pressure sensor that can generate DC, based on the different migration behaviors of cations and anions in solution. The working principle is similar to salinity-gradient energy generation. Specifically, we synthesized a PAA hydrogel with good elasticity and conductivity. PAA is a typical polyelectrolyte, which, after gelation, contains mobile protons (H^+) and fixed negative charges on the polymer backbone ($–COO^–$). Under mechanical compression, the local ion concentration increases. While the fixed anions cannot move, the protons migrate in one direction, producing a DC output in the external circuit. We verified this mechanic-electric conversion mechanism through theoretical modeling and experiments. The device was systematically evaluated under different compression strains, applied pressures, and contact areas to test its signal responsiveness, stability, and reversibility. We also demonstrated its potential for use in position detection and sound sensing. Finally, we extended this mechanic-electric conversion mechanism to other polyelectrolyte hydrogel systems.

Part II: In the previous chapter, we showed that mechanical force can create an ion concentration difference inside a polyelectrolyte hydrogel, leading to the directional movement of a single type of ion and generating a small DC voltage. However, the output was low (less than 10 mV), which limits its real-world use. To improve this, we designed a new hydrogel with a built-in ion concentration gradient to raise the voltage above 100 mV. This was done by stacking two layers of hydrogel—one made from PVA mixed with polyelectrolytes, and the other made from pure neutral PVA. This structure creates a natural gradient that helps drive ion flow more effectively. We also studied how the type of polyelectrolyte, the amount added, and the way the layers are arranged affect the output. Finally, we tested the device's ability to work as both a small power source and a self-powered pressure sensor.

Part III: To further improve the output performance, this chapter introduces a paper (with a thin silver coating)–hydrogel structure. This design increases the DC voltage to over 500 mV. The paper helps release ions, and the silver layer reacts with the moisture from hydrogel to boost the voltage through a galvanic effect. This setup is simple, low-cost, and easy to scale up. We tested how different factors—such as paper type, crosslinker amount, hydrogel thickness, and glycerol content—affect the output and stability. We also measured the discharge current, power output, and charging behavior

of the device. Finally, we showed that the device can give variable DC signals when pressed, making it useful for pressure sensing.

These three chapters together show a full process—from understanding the working principle to improving the structure and building a strong and useful hydrogel-based generator and self-powered pressure sensor. This work provides a good base for developing new flexible electronic devices.

Organization

Chapter 1 Introduction: This chapter first introduces wearable electronics and wearable pressure sensing. It then reviews hydrogels and hydrogel-based flexible wearable pressure sensors, including their design, fabrication, and working principles in non-self-powered systems. Recent advances in self-powered hydrogel-based pressure sensors are also discussed, followed by the motivation and objectives of this thesis.

Chapter 2 Experimental: This chapter provides detailed information on the materials, synthesis methods, and characterization techniques used for preparing and evaluating various hydrogel systems and paper-based components. It also includes the testing procedures for electrical output performance and the self-powered sensing behavior of the devices.

Chapter 3-5 Results and discussions for three projects: These chapters present the results and discussions of three research projects. Each section focuses on the device structure, material composition, and working mechanisms. The influence of key factors on the electrical output and stability is systematically analyzed. The potential applications of these devices as miniature power sources and self-powered pressure sensors are also demonstrated.

X. Pan, Q. Wang, D. Benetti*, Y. Ni*, F. Rosei*, Polyelectrolyte hydrogel: A versatile platform for mechanical-electric conversion and self-powered sensing, Nano Energy 103 (2022) 107718.

X. Pan, Q. Wang, D. Benetti*, L. Jin, Y. Ni*, F. Rosei*, Biomimetic polyelectrolyte-gradient hydrogel electricity generator: a green and portable energy source, Journal of Materials Chemistry A 11 (2023) 19506-19513.

X. Pan, Q. Wang*, L. Jin*, Y. Ni, F. Rosei*, Integrated paper-hydrogel structure for spontaneous and ultra-durable eco-friendly electricity generation, Nano Energy 136 (2025) 110730.

Chapter 6 Conclusions and perspectives: This chapter gives a short summary of the main findings and discusses possible directions for future work.

In line with INRS guidelines, a French summary of this thesis is provided in the appendix.

2. EXPERIMENTAL

2.1 Chemicals and Materials

Acrylic acid (AA, Aladdin Industrial Corporation), sodium persulfate (APS, Aladdin Industrial Corporation), N,N'-methylenebisacrylamide (MBA, Aladdin Industrial Corporation), polyvinyl alcohol-1799 (PVA, Aladdin Industrial Corporation, Shanghai), sodium alginate (Aladdin Industrial Corporation, weight-average molecular weight :~325 kDa), calcium chloride ($CaCl_2$, Aladdin Industrial Corporation), guar gum (Chengdu Aike Reagent Co., Ltd, ~987 kDa), borax (Aladdin Industrial Corporation), lignosulfonate sodium (LS, Aladdin Industrial Corporation, ~132 kDa), quaternary chitosan (QC, Kuer Technology, Beijing, ~468 kDa), acrylamide (AM, Aladdin Industrial Corporation), tetramethyl ethylenediamine (TMEDA, Aladdin Industrial Corporation).

In addition, different papers, cation exchange membranes, glass, PET, silver paint, and graphite electrodes were purchased from commercial stores. The specific parameters of different types of paper are listed in Table 2.1, and the resistance values before and after applying the conductive coating are shown in Table 2.2.

Table 2.1 Parameters of different papers

Paper type	Gram per square meter (GSM) g/m^2	Thickness /μm
Corrugated paper	210	272
Filter paper	85	156
Tissue paper	34	72
Printed paper	70	86

Table 2.2 The surface resistance of papers before and after Ag coating

Paper type	Surface resistance	Surface resistance (after Ag coating)
Corrugated paper	$2.6*10^7$ Ω	2.8 Ω
Filter paper	$3.9*10^7$ Ω	1.49 Ω
Tissue paper	$1.9*10^7$Ω	5.98 Ω
Printed paper	$6.3*10^7$ Ω	9.14 Ω

2.2 Preparation of hydrogels

Preparation of PAA hydrogel: First, 2.5 mL of AA was added to 7.5 mL of water and stirred well. Next, 0.025 g of APS was added to the above solution. Then, 0.005 g of MBA was added. Finally, the mixed solution was heated in a 60 °C water bath until the PAA hydrogel was formed.

Preparation of PVA hydrogel: First, 1.5 g of PVA was completely dissolved in 8.5 g of water (90 ℃), and then poured into a mold. The mold was frozen at −24 °C overnight and thawed for 4 h to obtain the final PVA hydrogel.

Preparation of sodium alginate hydrogel: First, 0.2 g of sodium alginate was completely dissolved in 9.8 g of deionized water (high temperature). The solution was cast into a mold and immersed in a 5.0 wt.% $CaCl_2$ solution at room temperature for 12 h to obtain the sodium alginate hydrogel.

Preparation of guar gum hydrogel: Guar gum hydrogel was prepared by dissolving 0.15 g of *guar gum* in 10 mL of deionized water, followed by the addition of 4.0 wt.% borax until gelation was complete.

Preparation of PVA–LS hydrogel:1.5 g of PVA and an appropriate amount of LS were dissolved in 8.5 g of deionized water and heated. The solution was poured into a mold, frozen at −24 °C overnight, and thawed for 4 h to obtain the PVA-LS hydrogel. See Table 2.3.

Table 2.3 The compositions of PVA-LS hydrogels

	LS/PVA (wt.%)	PVA (g)	Deionized water (g)
PVA-LS hydrogel	1	1.5	8.5
	10	1.5	8.5
	20	1.5	8.5
	50	1.5	8.5
	100	1.5	8.5

Preparation of PVA–QC hydrogel:1.5 g of PVA and an appropriate amount of QC were added to 8.5 g of deionized water and heated to dissolve. The solution was poured into a mold, frozen at −24 °C overnight, and thawed for 4 h to obtain the PVA-QC hydrogel. See Table 2.4.

Table 2.4 The compositions of PVA-QC hydrogels

	QC/PVA (wt.%)	PVA (g)	Deionized water (g)
PVA-QC hydrogel	1	1.5	8.5
	10	1.5	8.5
	20	1.5	8.5
	50	1.5	8.5

Preparation of PAM hydrogel: Specifically, 25 g of AM, 0.05 g MBA, 200 μL TMEDA, and 0.5 g APS were added to 100 g of deionized water and stirred. The solution gelled at 4 °C to form a PAM hydrogel. In addition, various PAM hydrogels were prepared by adjusting the composition (Table 2.5).

Table 2.5 Composition of different PAM hydrogels

Gel type	AM/g	APS/g	TMEDA/μL	MBA/g	Water/g	Glycerol/g
PAM–0.02 wt.% MBA	25	0.5	200	0.02	100	0
PAM–0.05 wt.% MBA (regular PAM hydrogel)	25	0.5	200	0.05	100	0
PAM–0.25wt.% MBA	25	0.5	200	0.25	100	0
PAM–0.5 wt.% MBA	25	0.5	200	0.5	100	0
PAM–30 wt.% glycerol	25	0.5	200	0.05	70	30
PAM–50 wt.% glycerol	25	0.5	200	0.05	50	50
PAM–80 wt.% glycerol	25	0.5	200	0.05	20	80

2.3 Characterization

The zeta potentials of AA, LS, QC, PAA, PAM hydrogel, and various papers were measured using a Malvern Zeta Sizer Nano ZS90 (UK). Note, the hydrogels were ground into particles using a cell crusher and then redispersed and diluted in deionized water for testing. The ionic conductivity of the PAA hydrogel precursor, as well as LS and QC solutions, was tested using a pH meter (Thermo Fisher Scientific Co., Ltd.). The microscopic morphology of LS, QC, original PAA hydrogel, PAA hydrogel (compression strain: 50%), PAM hydrogel, and different papers were examined via scanning electron microscopy (SEM, Thermo Scientific Verios G4 UC), and elemental mapping was performed using energy-dispersive X-ray analysis (EDAX, AMETEK).

Note: the hydrogels need to be freeze-dried before testing. In addition, The PVA hydrogel is assembled with PVA–LS (10 wt.%) and PVA–QC (10 wt.%) hydrogels and connected to a commercial multimeter, respectively. Then the PVA hydrogel is freeze-

dried and subjected to elemental analysis. FTIR spectra of LS and QC were recorded with a Nicolet 380 FTIR spectrometer (Thermo Electron Instruments Co., Ltd., USA). The surface chemistry of the filter paper was analyzed by X-ray photoelectron spectroscopy (XPS, Thermo Scientific ESCALAB 250Xi). Surface potential measurements of the filter paper and that with attached PAM hydrogel were carried out using a Kelvin probe force microscope (KPFM, Asylum MFP-3D Infinity). The water contact angle (CA) of the papers was measured using a contact angle meter (HARKE-SPCA−1, Beijing) at room temperature.

2.4 Hydrogel tests

Differential Scanning Calorimetry (DSC): The freezing temperatures of the PAA hydrogel and PAA organohydrogel were measured using a DSC 214 (NETZSCH). The samples were cooled from 20 °C to −120 °C at a rate of 5 °C/min.

Compression Tests: Compression tests were performed on cylindrical hydrogel samples using a digital stretching machine (KJ−1065B, Kejian Instrument Co., Ltd., Dongguan, China). The compressive stress (CS) was calculated using the formula:

$$CS = \frac{F}{A} \qquad \textbf{Equation 2.1}$$

, where F is the compressive load and A is the original cross-sectional area of the sample.

Conductivity Measurements: The conductivity of hydrogels was measured using an Inductance (L), Capacitance (C), and Resistance (R) meter (LCR, TH 2832) with an applied voltage of 1 V and a measurement frequency of 1 kHz. Conductivity (σ) was calculated according to the Equation 1.1.

Adhesion Test: The adhesion strength of PAM hydrogel to filter paper was evaluated by a 180-degree peel test using the digital stretching machine. The hydrogel-paper assembly was affixed to a PET film to limit crack tip deformation. During testing, force and displacement were continuously recorded.

Anti-Drying Measurements: The anti-drying capability of the hydrogel or device was assessed by monitoring weight changes during storage at room temperature (25 °C, 55% RH).

2.5 Device Assembly

Assembly of Mechanical-electric conversion hydrogel device: The electrodes of

hydrogels are thin graphite paper. PAA cylindrical hydrogel with different diameters is sandwiched between two electrodes to assemble mechanical-electric conversation devices and self-powered sensors.

Assembly of polyelectrolyte-gradient hydrogel electricity generator (PGHEG) devices: For anionic LS, PVA−LS hydrogels with various LS content (S: 23.74 cm^2, H: 5 mm) were placed on top of pure PVA hydrogels (S: 23.74 cm^2, H: 5 mm). Then, the double-layer hydrogel was sandwiched between two graphite paper electrodes to assemble the PGHEG. For cationic QC, PVA−QC hydrogels with different QC content (S: 23.74 cm^2, H: 5 mm) were placed under pure PVA hydrogels (S: 23.74 cm^2, H: 5 mm). Then, the double-layer hydrogel was sandwiched between two graphite paper electrodes to assemble the PGHEG.

Assembly of paper-hydrogel electricity generator (PHEG) devices: Apply conductive spray evenly on the upper surface of the paper. Then, attach the lower surface of the paper to the PAM hydrogel, and place a layer of graphite paper underneath to complete the device assembly.

2.6 Mechanical-electric conversion test

The performance test is achieved by combining a digital stretching machine and an electrochemical workstation (CHI 630E, Shanghai). The temperature of the upper and lower electrodes should be kept at the same temperature throughout the compression process; that is, there is no temperature difference between the two electrodes (Figure 2.1). Reminder, the compression area of the machine needs to be much larger than the hydrogel. In addition, ensure that the upper and lower sides of the electrode cannot touch and connect during the compression process.

Figure 2.1 Real and thermographic images of the hydrogel's mechanics-electric conversion testing process.

It should be *noted* that the hydrogel distribution is not uniform, so the initial output

voltage may already exist (very small). Therefore, the hydrogel electronics must be short-circuited before the test to eliminate the original voltage and current as much as possible. Nevertheless, we only recorded the pulses (relative output voltage) that convert mechanical energy into electricity. The mechanical energy-electric conversion signals of other polyelectrolyte hydrogels also use the same test methods. The electrical signal of the resistive sensor assembled with PAA hydrogel and graphite paper electrode is collected using an LCR meter.

2.7 The electrical output of PGHEG

The open-circuit voltage of PGHEG is measured and collected using an electrochemical workstation and a commercial multimeter. The short-circuit current of PGHEG is measured and collected using a source meter (Keithley Instrument Inc.). Note: the voltage must be set to 0 before the test. The local ambient temperature is regulated by the refrigerator and oven.

2.8 The electrical output of PHEG

The output voltage and current of various devices were measured and collected using an electrometer or a commercial multimeter. The test of dependence of the voltage and current on the electrical resistance of the external circuit is tested by connecting a PHEG with a resistance box.

The power output of the device is calculated by the following equation:

$$P = UI \qquad \textbf{Equation 2.2}$$

Where the U is the voltage tested on the resistance box; I is the current in the circuit.

2.9 Self-powered sensing testing

Connect the PGHEG or PHEG in series to a load resistance, with a voltmeter attached across the load. By applying pressure either manually or using a mechanical linear motor (Linmot, HF01–37), the resulting voltage changes are recorded, enabling self-powered pressure sensing.

2.10 Thermodynamic analysis of mechanical-electrical conversion

In hydrogel systems with asymmetric ion distributions (such as Na^+ from LS or H^+ from PAA), ions migrate through two competing mechanisms:(i) Spontaneous diffusion from

the high-concentration (HC) side to the low-concentration (LC) side, and (ii) Drift from the LC side to the HC side driven by an internally generated electric field. The diffusion current density is expressed as: [114-116]

$$J_{dif} = qFD\frac{dc}{dx} \quad \textbf{Equation 2.3}$$

The drift current density is:

$$J_{dri} = -qFcv\frac{dU}{dx} \quad \textbf{Equation 2.4}$$

where the ion mobility v is defined as:

$$v = D\frac{qF}{RT} \quad \textbf{Equation 2.5}$$

Here, q is the ionic valence, F is the Faraday constant, D is the diffusion coefficient, R is the gas constant, T is temperature, c is ion concentration, and U is the induced potential.

When diffusion and drift reach dynamic equilibrium (J_{dif}=−J_{dri}), a stable output voltage ΔU is generated, as described by the Nernst equation:

$$\Delta U = \frac{RT}{qF}ln\frac{C(H)}{C(L)} \quad \textbf{Equation 2.6}$$

where C_{HC} and C_{LC} represent the ion concentrations at the high and low concentration sides, respectively. This output voltage is directly determined by the concentration gradient of mobile ions, which can be modulated by the degree of compression or by controlling the content of ionizable groups in the hydrogel.

2.11 Finite element analysis

PAA hydrogel material properties are defined as elastic constitutive and then processed by hypermesh and solved by Abaqus to obtain the displacement distribution of local hydrogel during compression. To be closer to the actual compression state of PAA gels, we have considered Poisson's ratio (0.45), friction force, and elastic modulus (20 kPa) of the gels. Additionally, we used a uniform mesh instead of polymer chains to help us analyze the polyelectrolyte or ionic concentration locally in the gel.[117, 118]

2.12 Cost accounting of PHEG

The PHEG device is a hydrogel (2×2 cm^2) sandwiched between graphite paper electrodes (2×2 cm^2) and paper (2×2 cm^2) with a silver coating. We estimated the material costs based on the purchase prices of the materials, converted using the international exchange rate on the day of calculation. This estimation excludes labor,

facility, and other operational costs, serving as a reference for material expenses only. The total material costs are calculated based on surface area (per square meter) and are as follows: filter paper – \$0.245/m², graphite paper – \$30.34/m², electrode coating – \$1.10/m², and hydrogel (5 mm thickness) – \$37.69/m². In total, the device cost is approximately \$69.375 /m², which is equivalent to \$0.0277 per PHEG unit (2×2 cm^2).

3 POLYELECTROLYTE HYDROGEL FOR MECHANICAL–ELECTRIC CONVERSION

3.1 Introduction

As introduced in Chapter I, polymer hydrogels have been extensively investigated for applications in portable pressure sensors and electronic skins.[14, 22, 62, 119] Due to their high water content and adjustable mechanical properties, polymer hydrogels can perfectly match the tissues of the skin to achieve both high biological and mechanical compatibility.[96, 120, 121] In addition, thanks to its structural versatility the hydrogel system can be pre-doped and adjusted with unique functions and macro/microstructural characteristics.[122-125]

Polymer hydrogels can combine the great elastic properties of polymers with the electric-signal transport channel of conductive media.[52, 126, 127] This type of hydrogel-based sensor can induce the redistribution of the conductive channel and the subsequent adjustment of electrical signals through compression and stretching of the internal polymer network, to respond to external mechanical stimuli.[61, 72] Commonly, conductive nano-metals, intrinsically conductive polymers, and carbon materials are used as conductive fillers.[60] However, conductive fillers present several issues, such as easy aggregation, high-cost, challenging synthesis, and opacity of the hydrogel that hinder their use in wearable electronics.[52, 128, 129] Moreover, ionic conductive hydrogels are prone to ion leakage, which could present health hazards for the human body.[63, 130] In contrast, low-cost polyelectrolyte (high molecular polymer) hydrogels are polymerized and assembled by ionizable monomers or natural polysaccharides in water, exhibit sufficient conductivity, and do not leak.[131]

In addition, most hydrogel sensors have to rely on an external rigid power source to operate, so portable hydrogel electronics require the realization of self-powered pressure sensing.[132-136] Generally, the assembly of hydrogels into TENG results in high self-powered performance, yet there are obstacles such as micro-structural preparation and high cost.[103, 137] In addition, TENG's contact separation detection method affects the universality of signal recognition.[138-140]

It is known that a salt concentration gradient-driven ion selective permeation membrane can trigger the directional transport of a single ion (cation or anion), which leads to the

generation of electrical power.[141-143] Polyelectrolyte hydrogels possess both ions and ion transport channels to replicate this kind of electricity generation behavior. When the polyelectrolyte is fixed (crosslinked) in the hydrogel, only the dissociated ions can move freely.[144-148] By controlling the directional movement of free ions, electrical power can be generated, which is the basis for the design and preparation of self-powered hydrogel sensors.[149]

In this chapter, as a proof of concept, the common anionic electrolyte PAA is used as a backbone to assemble a highly elastic PAA covalent hydrogel as a platform for mechanical-electrical conversion and sensing. Based on theoretical simulations and experimental results, we observe that the local ion concentrations inside the elastic polyelectrolyte hydrogel can vary due to the change of its internal structure by external mechanical force, thereby completing the conversion of mechanical energy into electricity and accompanying the mechanical signal recognition. The self-powered response capability of the sensor is proven to be adjustable, which is closely related to the strain and pressure. Manipulating the direction of free ion transport allows the sensor to easily recognize where the pressure is applied. Lastly, the self-powered hydrogel exhibits more accurate sound detection capabilities than traditional resistive sensors. Overall, this simple and low-cost flexible device based on polyelectrolyte hydrogel is promising for applications in self-powered sensing and energy harvesting.

3.2 Results and Discussions

3.2.1 Design principle of self-powered polyelectrolyte hydrogel

In a salt solution, both cations and anions move randomly. When electric power is applied, the ions will move directionally to realize the electric conduction of the circuit.[150] If the anions and cations in the solution spontaneously move in opposite directions, the movement of electrons occurs in the external circuit connecting the two different directions.[151, 152] In addition, due to the concentration gradient, ionizable salt in the high-concentration region will autonomously diffuse to the low-concentration region. When an ion-selective membrane is used between the two regions, the movement of one type of ion (cation or anion) can be restricted and the directional diffusion of the oppositely charged ion can be obtained (Figure 3.1a). This will also induce the movement of electrons when connected to an external circuit. The internal 3D hole of the hydrogel can be used as a channel for ion transmission to achieve a

similar power generation effect (Figure 3.1b).[145, 153]

It is known that polyelectrolytes can ionize movable ions when water is present, but since the polyelectrolyte chain acts as a hydrogel skeleton, it is restricted from free movement. We assume that the compression of the anion polyelectrolyte hydrogel will increase the local (TOP of hydrogel) polymer concentration, which will cause the directional diffusion of free ions (+) inside the hydrogel and consequently, the movement of electrons in the external circuit (the polyelectrolyte chains cannot move freely and thus cannot offset the net displacement of cation). This reveals that the polyelectrolyte hydrogel can convert mechanical energy to electricity (Figure 3.1c). When the elastic network of the hydrogel recovers, the generated dynamic electrical signals (output voltage or current) will gradually disappear (Figure 3.1d). This hypothesis also supports the idea that polyelectrolyte hydrogel can realize self-powered pressure/strain sensing while achieving mechanical energy-electricity conversion.[154] In this work, we follow the electric-generating model based on ion concentration gradient-induced ion-directed motion in hydrogels.[114, 115, 151, 152, 155, 156] However, while this work was under revision, a new interpretation has been proposed. The study indicates that during compression, ions are squeezed and migrate to the uncompressed region. However, due to the difference in migration rates between cations and anions, the net displacement of charges is nonzero, thereby generating a DC electricity.[149] Our results are compatible with both models. Currently, the mechanism is still under debate.

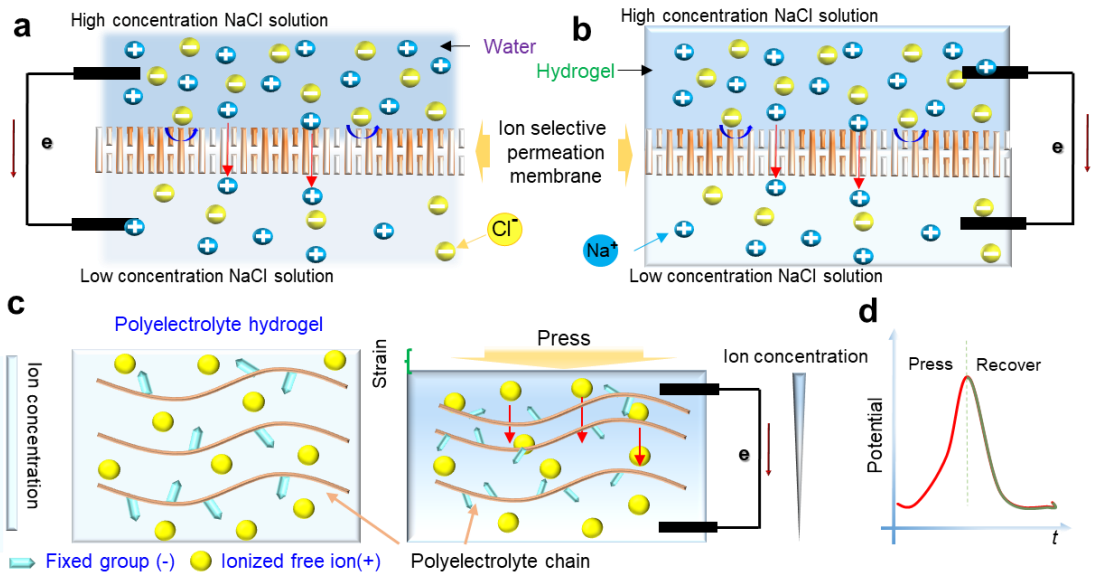

Figure 3.1 a) Schematic diagram of electric-generation caused by the diffusion of high-concentration salt (NaCl) solution to low-concentration salt solution through ion selective permeation membrane. b) Schematic diagram of electric-generation caused by the diffusion of hydrogel with high-concentration salt (NaCl) to hydrogel with low-concentration salt (NaCl) through ion selective permeation membrane. c) During the compression process, the anion polyelectrolyte hydrogel will have an uneven distribution of ion concentration and subsequent diffusion, resulting in the conversion of mechanical energy into electricity. d) After the elastic network of hydrogel is restored, the ion concentration will be restored uniformly, and the hydrogel completes self-powered strain sensing.

Herein, the typical anionic polyelectrolyte PAA hydrogel was prepared as a research model. This hydrogel is formed by covalently cross-linking PAA chains. PAA hydrogel is negatively charged (Figure 3.2a). Therefore, ionized PAA by deprotonation of the −COOH groups can provide the conductivity of the hydrogel (Figure 3.2b).

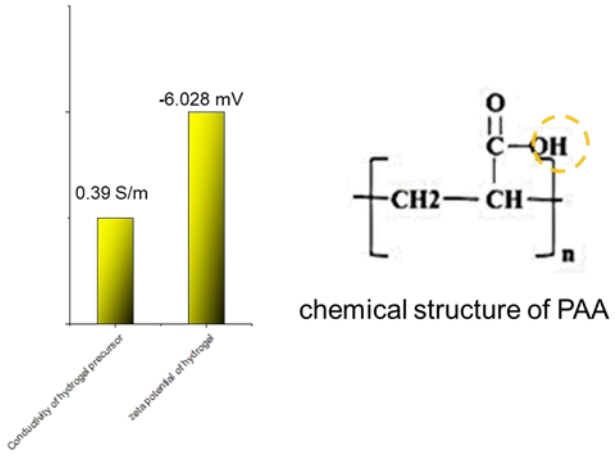

Figure 3.2 a) Zeta potentials of PAA hydrogel and conductivity of hydrogel precursor.

Figure 3.3a reveals a model diagram of a mechanical-electric converter assembled from a cylindrical PAA hydrogel (d=2.5 cm) combined with soft electrodes of graphite paper. According to Figure 3.3b, when the hydrogel is gradually compressed from the top with a press, its output voltage will increase rapidly.

These results demonstrate that the compression deformation of polyelectrolyte PAA hydrogel can be converted into electrical signals linearly. In particular, when the compression deformation of the hydrogel is maintained, the output signals are steady, which basically satisfies two of the three elements of strain/pressure sensing, that is, response and stability.[124, 157, 158]

The above results are consistent with our original hypothesis. The compression behavior of the PAA hydrogel may lead to a gradual decrease in the compression degree

(relative displacement) from the top to the bottom so that the H^+ concentration gradually decreases from the upper to bottom surfaces of the hydrogel (Figure 3.3b). Thanks to the H^+ concentration gradient, H^+ in the hydrogel will diffuse downward to generate an output voltage. The net charge displacement of H^+ and the PAA chains (-) caused by the compression process is zero, that is, the downward compression process does not generate electrical power. The power generation of the hydrogel stems entirely from the diffusion of H^+, which can also be proven by the result that the output voltage of hydrogel remains stable (not disappeared or significantly reduced) while maintaining compressive strain (50%).

The positive or negative movements of H^+ will increase or decrease the output voltage, which gradually decreases during reverse compression (Figure 3.3c), presenting strong evidence of the reverse movement of H^+ (Figure 3.2d). The two processes are almost symmetrical. Therefore, it can be concluded that the directed diffusion of H^+ underpins power generation. According to thermodynamic equilibrium, the output potential (ΔU) of PAA hydrogel can be described as

$$\Delta U = \frac{RT}{qF} ln \frac{C(H)}{C(L)} \qquad \textbf{Equation 3.1}$$

where R, T, q, and F are the gas constant, temperature, valence, and Faraday's constant respectively. In addition, $C(H)$ and $C(L)$ represent the H^+ concentration on the high-concentration side and the low-concentration side of the hydrogel surface, respectively. [114, 115, 155] This formula indicates that the intensity of the induced voltage (output voltage) is directly related to the concentration gradient of H^+, which in turn, is determined by the degree of compression (strain or force). Details of the formula are provided in **2.10**.

We further studied the local H^+ concentration of PAA hydrogel because of compression. As presented in Figure 3.3e, in reference to the original hydrogel, the compressed polymer network of PAA hydrogel (50% strain) will be denser. In addition, finite element method (FEM) simulation was used to analyze the local displacement and polymer mesh distribution of the columnar uniform hydrogel structure under various compressive strains (Figure 3.3f, see 2.11 for the detailed simulation process). The simulation results proved that compression of the hydrogel will cause the difference in displacement or deformation of the hydrogel from top to bottom. As the compressive

strain increases, the difference in compression of the polymer grids on the upper and lower surfaces of the gel gradually becomes larger. This also implies that the compression causes the H^+ concentration difference between the upper and lower surfaces of the gel to gradually increase.

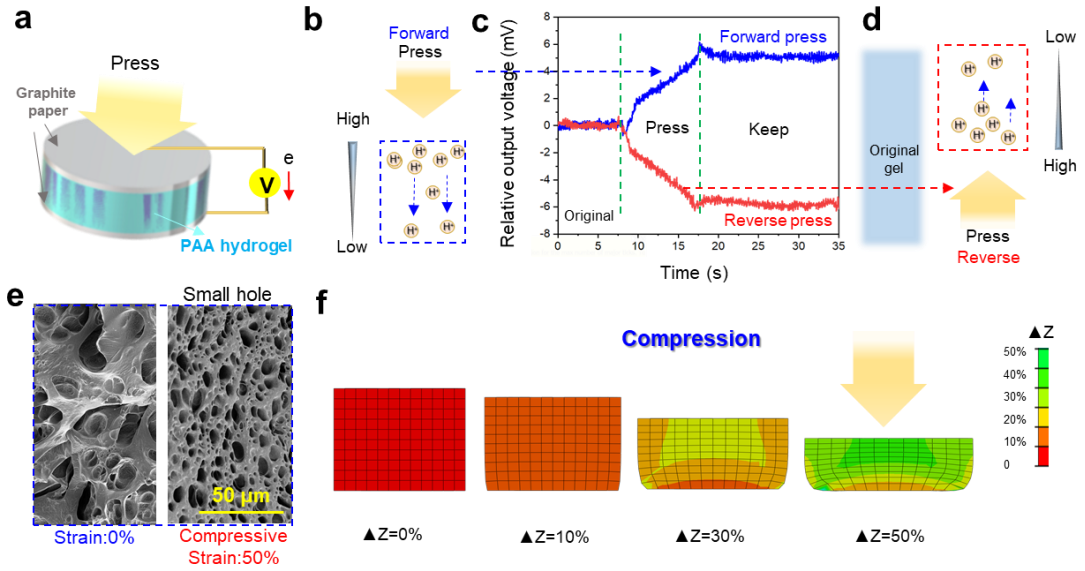

Figure 3.3 a) Schematic diagram of PAA hydrogel-based mechanical-electric conversion model. b) The working principle of PAA hydrogel converting mechanical energy into electrical energy during forward compression. c) The relative output voltage (pulse) of PAA hydrogel changes in response to external dynamic compression behavior. d) The working principle of PAA hydrogel converting mechanical energy into electricity during reverse compression. e) SEM images of the internal structure of PAA hydrogels under various compressive strains. f) Finite element simulation of local displacement distribution and PAA network state of hydrogels under different compressive strains (ΔZ represents displacement).

At a 50% compressive strain, the pressure and strain are held steady, and the relative output voltage and current of the hydrogel also remain stable (Figure 3.3c and 3.4). Therefore, the operating mechanism of PAA hydrogels that convert mechanical energy into electricity is attributed to the H^+ concentration difference of the hydrogel caused by external compression, which triggers the directional diffusion of H^+, ultimately generating electricity.

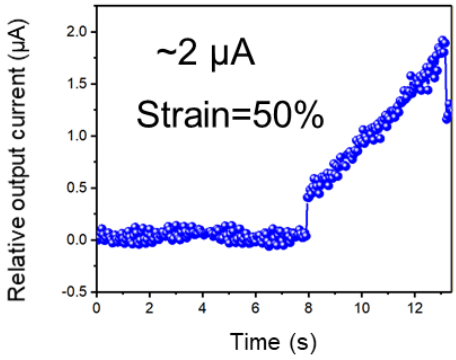

Figure 3.4 The relative current of PAA hydrogel changes in response to external compression behavior.

3.2.2 The self-powered sensing performance of polyelectrolyte hydrogels

As mentioned, the PAA hydrogel satisfies the two fundamental elements of strain/pressure sensors: response and stability. More importantly, high elasticity is essential for the proper operation of the hydrogel-based pressure/strain sensor, allowing full recovery of the initial shape and thus of the electronic signal.[159] In this work, we studied the signal recovery and stability of PAA hydrogel-based sensors. As shown in Figure 3.5a and b, the hydrogel exhibited almost identical response (~6 mV), drop curve, and programmed recognition time (~7 s) to four independent reciprocating mechanical compressions (strain: 50%). The stable compressive stress-strain curves confirm the elastic recovery and stability of the hydrogel, which is critical for a pressure/strain sensor (Figure 3.5c).

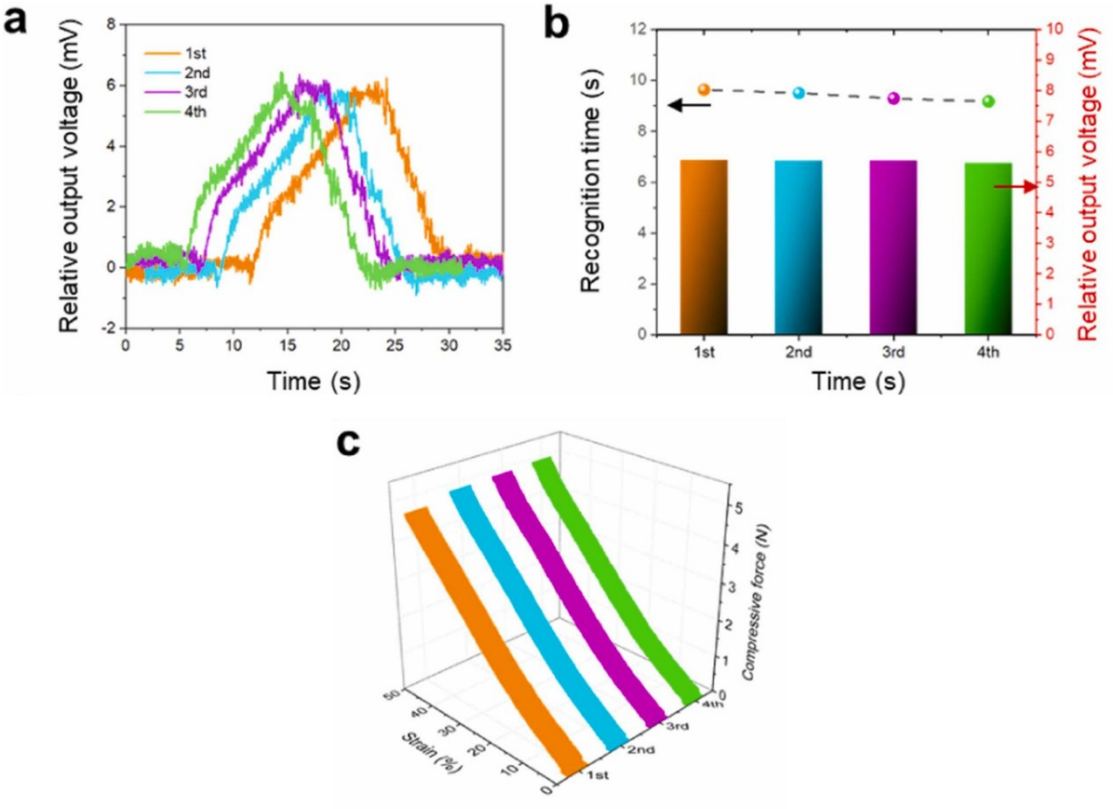

Figure 3.5 a) The relative output voltage changes in response to the four-independent compression (strain:50%)-recovery processes of the PAA hydrogel. b) The recognition time and response amplitude of hydrogel to compressive strain (50%). c) Four- independent compression force-strain curves of the hydrogel.

Moreover, compression speeds of 10, 50, 100 and 200 mm/min were applied to test the output voltage of the PAA hydrogel (strain: 50%). The results show that the output voltage is only related to the degree of compression (pressure or strain), but not directly related to the speed of compression (Figure 3.6a). The maximum detection limit of the PAA hydrogel device collected here is ~5N, while the minimum detection limit is ~0.05–0.1 N (Figure 3.6b).

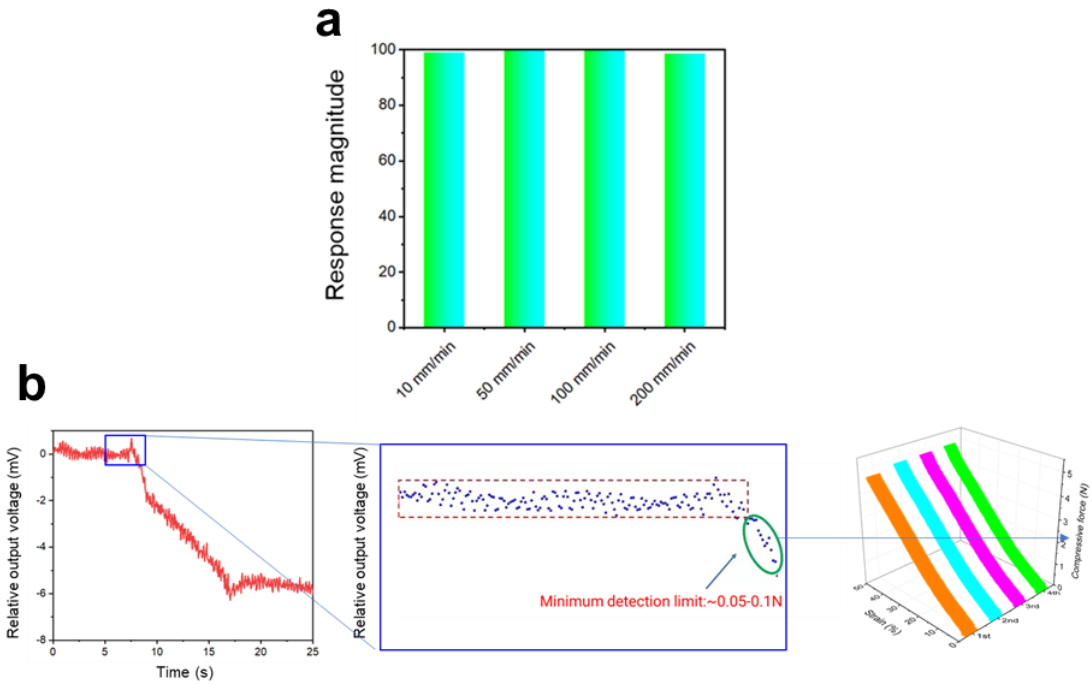

Figure 3.6 a) Response magnitude (voltage) of the gel at various compression speeds. b) Minimum detection limit for PAA hydrogel device.

When the hydrogel gradually recovers, the H^+ concentration difference at the corresponding position will decrease, causing the output voltage to drop until it reaches zero. These results indicate that polyelectrolyte PAA hydrogel has all the characteristics of self-powered pressure/strain sensing. The signal output of the hydrogel also has been proven to be adjustable. The output voltage/current can improve by increasing the strain/pressure amplitude (strain) (Figure 3.7a). Based on the adjustability of the output signals, the hydrogel can recognize and respond to various strains and pressures, thereby expanding its possible applications. To further confirm the stability of the external pressure sensing mechanism, the hydrogel was compressed applying strain for multiple cycles from 0% to 10%. We found that a stable response voltage pulse to the same strain (10%) within 1000 s can be maintained (Figure 3.7b).

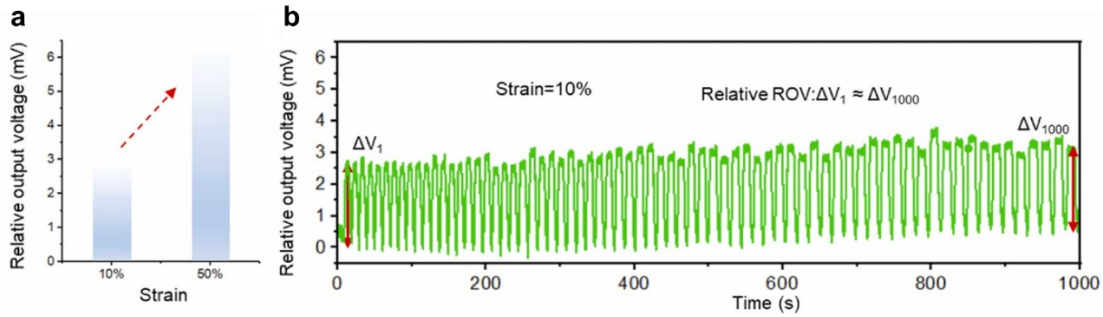

Figure 3.7 a) The relative output voltage changes (pulse) in response to the various compressive strains of the PAA hydrogel. b) The self-powered strain response stability of PAA hydrogel (strain:10%).

3.2.3 The self-powered sensing application of hydrogels

We have shown that polyelectrolyte hydrogels have direction-dependent self-powered sensing capabilities. Based on this feature, a self-powered orientation (position) recognition sensor was developed. As presented in Figure 3.8a, the sensor is composed of a PAA hydrogel and two graphite paper electrodes. It is possible to split this device into three regions from left to right, A, O and B (the left and right electrodes of the hydrogel recognizer need to be connected to the negative and positive electrodes of the test instrument respectively). When pressing different areas of the sensor, distinct output signals can be generated. As shown in Figure 3.8b, when part A is pressed, the output voltage increases rapidly. This is because the H^+ concentration in part A increases as a result of the compression, which subsequently causes H^+ to diffuse to the right side. On the other hand, when part B is compressed, the output voltage of the sensor decreases rapidly, which is caused by the H^+ of B part movement to the left side. Interestingly, when part O is pressed, no relative output voltage from the hydrogel sensor is generated. This is because, at part O (the center of the hydrogel detector) the net H^+ displacement is close to zero (the left and right diffusion is the same, with opposite directions).

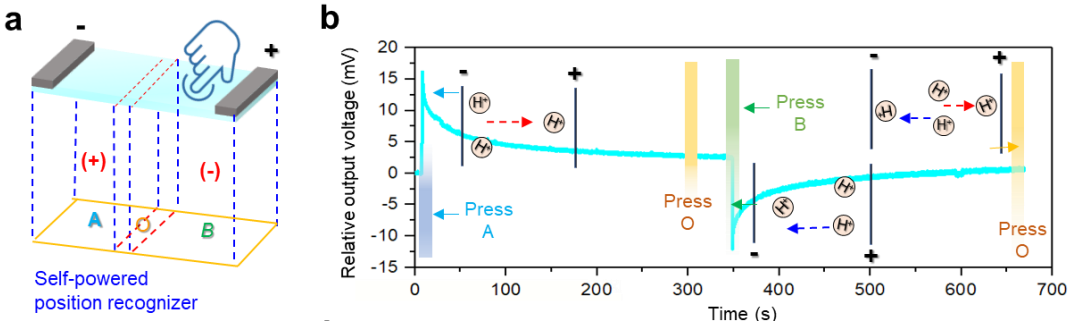

Figure 3.8 a) Application diagram of self-powered position recognizer. b) The relative output voltage changes of the detector in response to pressing of different positions of the recognizer.

In addition, we performed controlled experiments to consider the possible thermoelectric and triboelectric interferences caused by finger pressing on the gel. As shown in Figure 3.9, during the pressure test, the temperature of the two electrodes on the left and right sides is similar (~25 ℃). When a cold finger (~36.6 ℃) was maintained on part A of the gel (without pressing) for the whole test duration (Figure 3.9a and b), the output current did not show any response and change (Figure 3.9c). However, when the finger compresses part A, a positive current is rapidly generated and disappears after the compression is completed. A negative current appears when the finger is pressed on part B. To further show that the body heat did not affect the pressure sensing, a glass rod (~26°C) was used to apply pressure on the hydrogel; a similar response was obtained (Figure 3.9d).

The above results indicate that the electrical response of the gel comes from the compression process and is independent of the temperature difference (the instantaneous temperature difference hardly induces the gel to generate an output current). [160]At the same time, the gel was shown to identify the compression location, which was related to the compression-induced increase in ion concentration and the subsequent direction of ion diffusion.

Notably, a slow (~s level) and DC is generated during gel compression. In contrast, the output current from piezoelectric and triboelectric is rapid (~ms level) and AC.[161, 162]These results support that the mechanical-electric conversion effect of the gel does not originate from thermoelectric, piezoelectric, or triboelectric.[163-167]

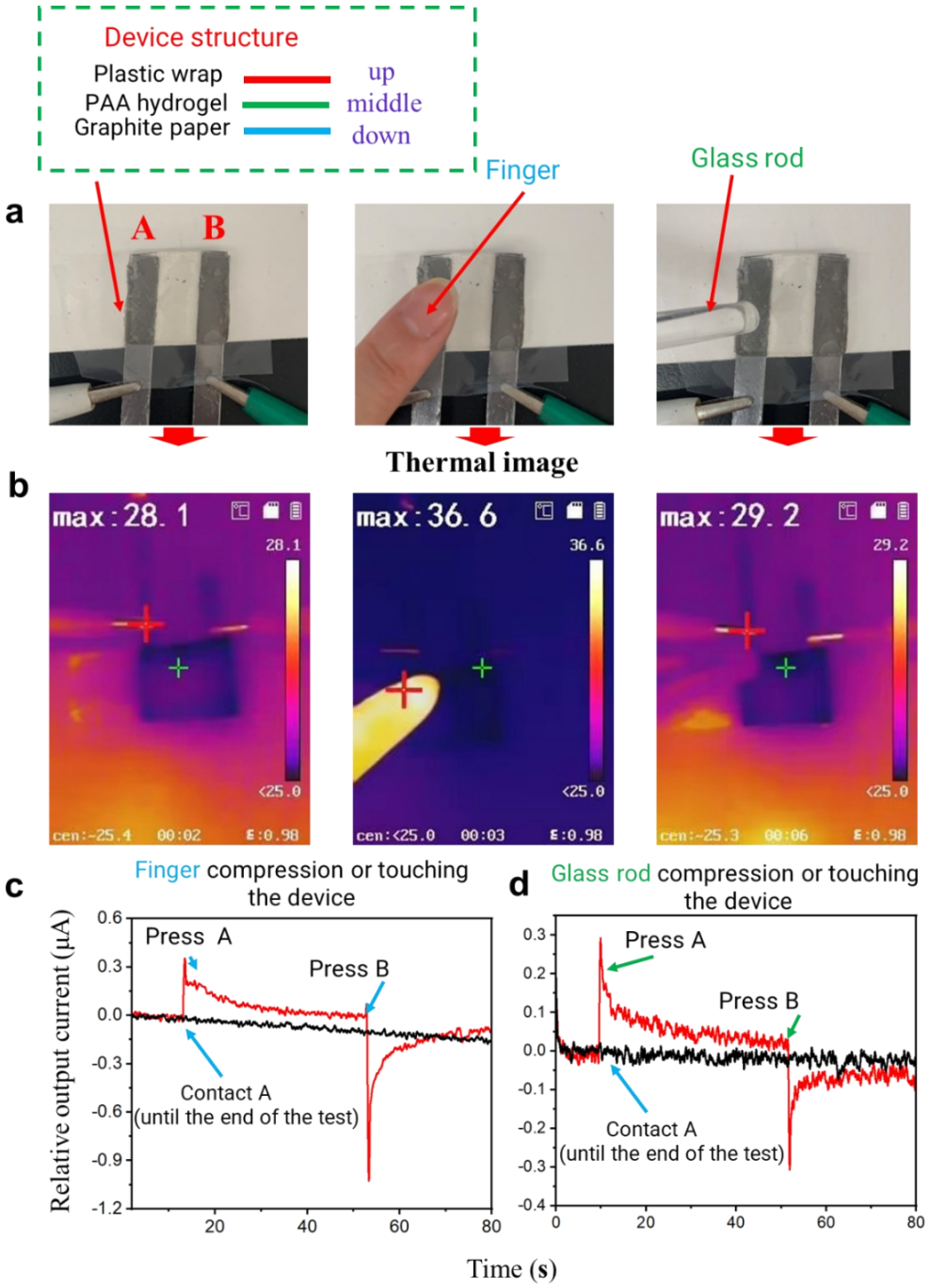

Figure 3.9 Influence of temperature on orientation recognition of PAA hydrogel. a) Photos and b) thermograms of the orientation sensor in different states, from left to right, are the original state, finger contact, and glass rod contact. c) The relative output current changes of the detector in response to finger pressing or touching of different positions. d)The relative output current changes of the detector in response to glass rod pressing or touching of different positions.

Importantly, traditional resistive sensors exhibit a non-directional response to pressing (Figure 3.10). [168] Pressing different regions (A, O, and B) of the resistive hydrogel sensor results in an increase in resistance in all cases, without any decrease observed. As a result, the sensor is unable to distinguish the specific location of the applied

pressure. This is due to the difference in the response mechanism from the direction-dependent self-powered sensing that is being developed in the present study. The external mechanical compression can change (increase or decrease) the resistivity, but in this type of device the pressing position cannot be easily detected.

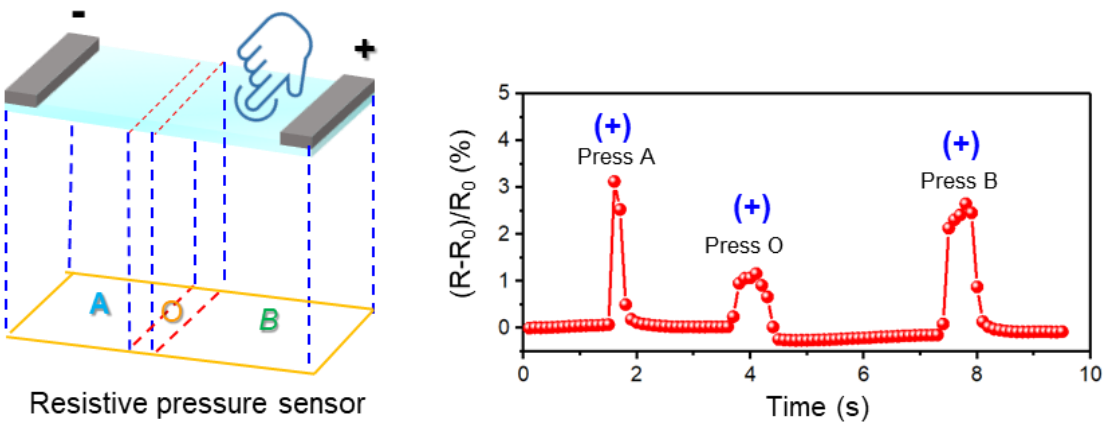

Figure 3.10 The relative resistance changes of the sensor in response to the different compressive positions of the resistive position device (the hydrogel substrate used for the test is PAA hydrogel).

The as-obtained direction-dependent self-powered PAA hydrogel sensor can not only complete the recognition of position and direction to operate like a switch, but also serve as a self-powered voice recognizers. Figure 3.11a presents a wearable and self-powered sound detector based on the PAA hydrogel. When a person wearing this detector pronounced particular words, such as “love” or “red flowers”, repeatable and distinguished curves of the electric signal were measured (Figure 3.11b). Compared to traditional resistive sensor-based sound monitors, the self-powered hydrogel exhibits multi-dimensional response characteristics that are very helpful for improving the accuracy of sound recognition (Figure 3.11c).

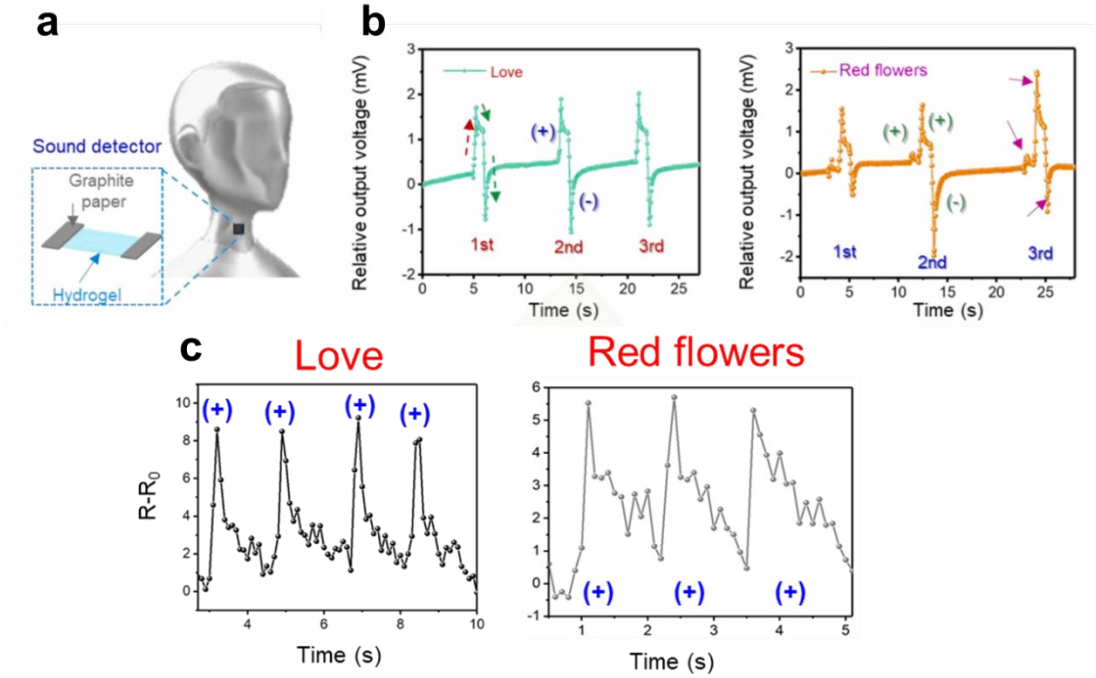

Figure 3.11 a) Schematic diagram of the PAA hydrogel-based sound detector. b) The relative output voltage changes of a detector in response to various sounding letters "love" and "red flowers". c)The relative resistance changes of the sensor in response to various sounding letters "love" and "red flowers" (the hydrogel substrate used for the test is PAA hydrogel).

Generally, hydrogel-based devices suffer from freezing at ultra-low temperatures (Figure 3.12a). However, PAA hydrogel can be readily imparted with antifreeze capability by simple solvent replacement, obtaining antifreeze PAA organo-hydrogel (Figure 3.12b). [76, 169] The latter can realize stable self-powered sensing also in sub-zero temperature environments (Figure 3.12c). The DSC curve shows that the regular PAA hydrogel gives a strong exothermic peak around –15 °C during cooling, indicating that it freezes at this temperature. In contrast, the PAA organohydrogel shows no exothermic peak throughout the cooling process, suggesting that it resists freezing and has good anti-freezing ability (Figure 3.12d).

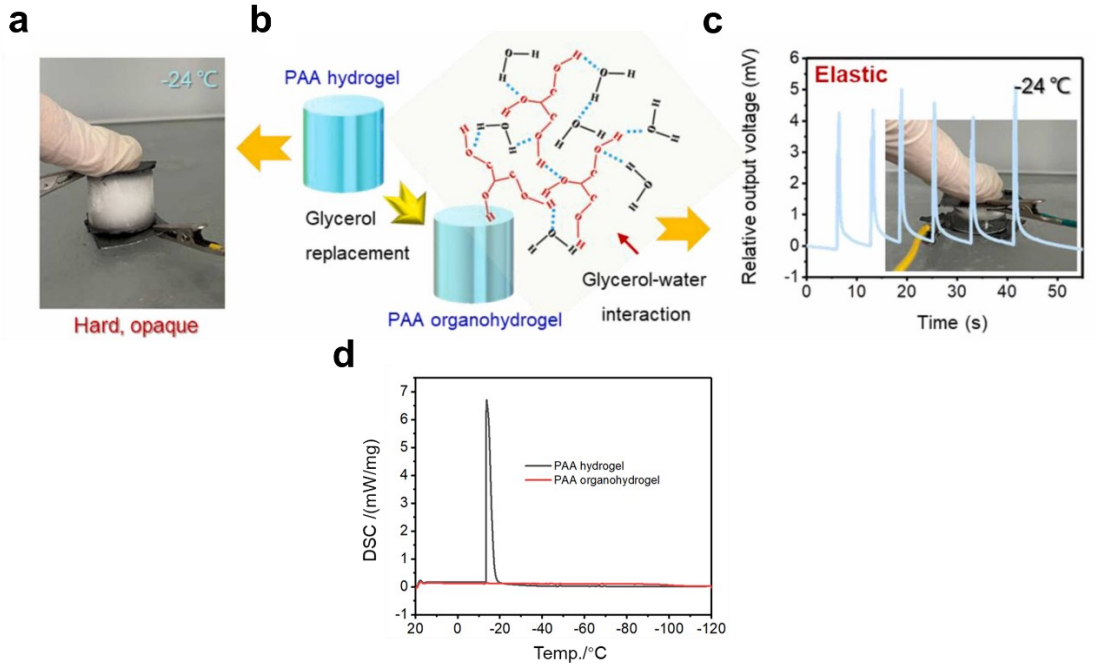

Figure 3.12 a) The original PAA hydrogel will freeze at -24 ℃ and lose its elasticity. b) PAA hydrogel undergoes glycerol solvent replacement to obtain PAA organohydrogel. c) PAA organohydrogel can realize self-powered sensing at low temperatures (–24℃). d)DSC thermograms of the PAA hydrogel and PAA organohydrogel from 20 ℃ to –120 ℃.

Moreover, the obtained PAA organo-hydrogel proved a long-lasting solvent retention that increases the service life (Figure 3.13). [170] Overall, PAA hydrogel possesses favorable characteristics for the design and application of a wide range of environmentally adaptable self-powered sensors.

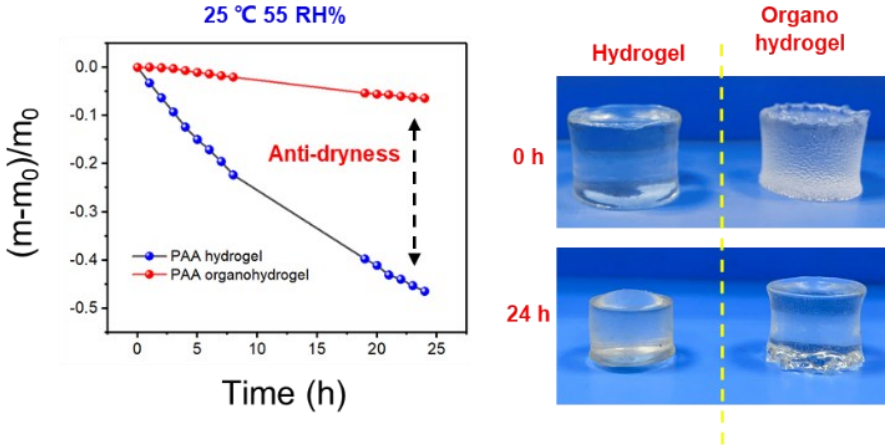

Figure 3.13 Anti-drying performance of PAA hydrogel and PAA organohydrogel at room temperature. m and m_0 represent the mass of the gel at a given time and its initial mass, respectively.

3.2.4 The mechanical energy collection of various polyelectrolyte hydrogels

Importantly, PAA hydrogel exhibits great processability and potential for large-scale production. For example, a large-size transparent PAA hydrogel (300 cm^2) can be prepared (Figure 3.14a). PAA hydrogels also have excellent customization capabilities: as demonstrated in Figure 3.14b, an insole incorporating a cropped PAA hydrogel-based device is fabricated. This insole can be placed in any pair of shoes to collect the mechanical energy generated by human motion. The new insole can effectively convert the mechanical energy associated with the leg's continuing movement to electricity (Figure 3.14c). Since the hydrogel is not completely uniform, and a small initial voltage output may already exist. Therefore, only the pulse (relative voltage output) that converts mechanical energy into electricity was recorded. Similarly, PAA organohydrogel, which has been replaced with glycerol, can also be used for mechanical energy collection at temperatures below zero (−24 °C, Figure 3.14d). Although the electrical output from the new insole may be small, this type of polyelectrolyte PAA hydrogel-based energy harvester is simple and low-cost. Thus, as a new type of mechanical energy collection device its potential in the continuous collection of daily walking energy can still be substantial. The concept discussed is also universally applicable to many hydrogels containing polyelectrolytes. In fact, like PAA hydrogels, other polyelectrolyte hydrogels, such as PVA, guar gum, and sodium alginate hydrogels, can convert mechanical energy into electricity (Figure 3.14e, f, and g).

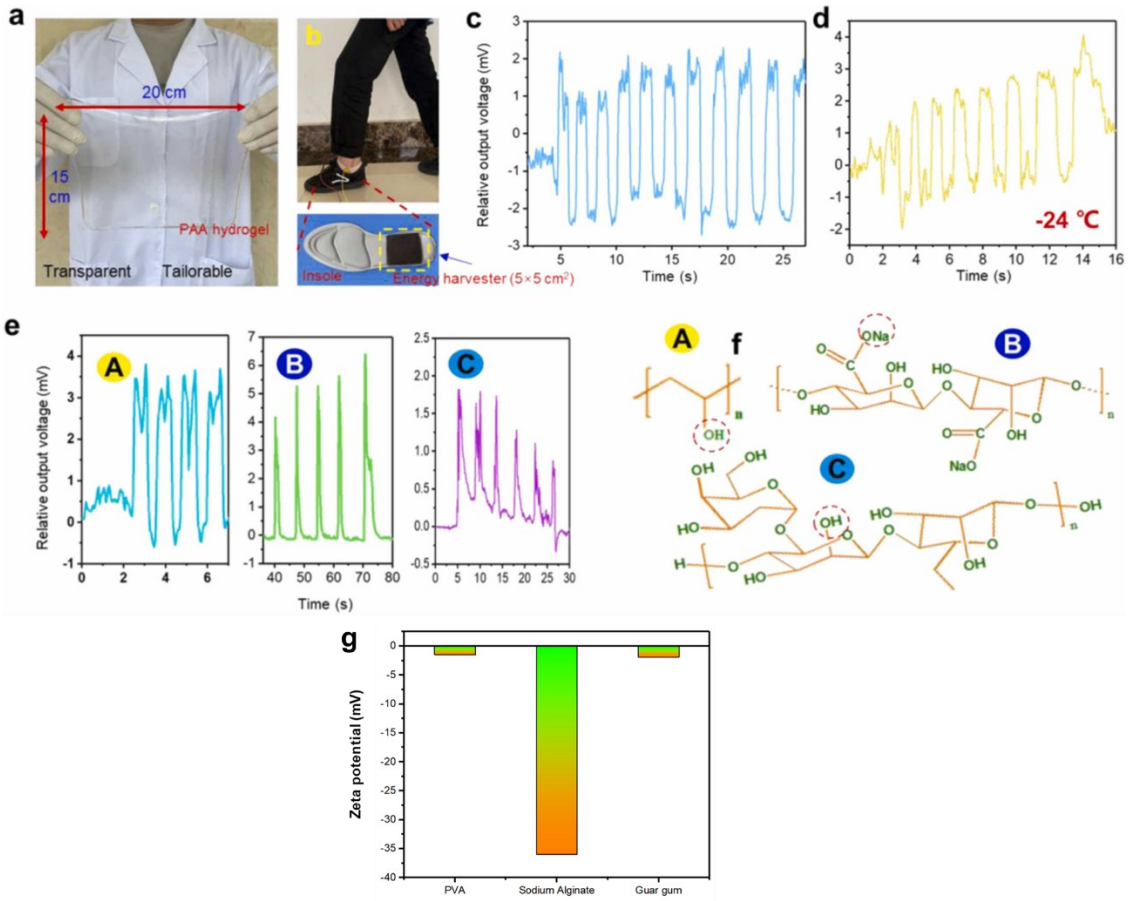

Figure 3.14 a) PAA hydrogels hold great transparency and are tailorable. b) The energy harvesting insole assembled by PAA hydrogel and graphite papers(electrode) can be applied for mechanical energy harvesting. c) The relative output voltage of the new insole containing PAA hydrogel changes in response to the dynamic walking behavior of humans. d) The relative output voltage of the new insole containing PAA organohydrogel changes in response to the dynamic walking behavior of humans. e) The mechanical energy harvesting result of various polyelectrolyte hydrogels. f) The chemical structure of different polyelectrolytes, A: polyvinyl alcohol; B: sodium alginate; C: guar gum. g) Zeta potentials of PVA (-), sodium alginate (-), and guar gum (-).

3.3 Conclusions

We designed and fabricated a polyelectrolyte PAA hydrogel inspired by salinity-gradient power generation, which can realize mechanical energy conversion and self-powered sensing. By combining simulations and experimental results we propose an interpretation of the mechanical energy-to-electricity conversion mechanism of PAA hydrogels, which is derived from the directional H^+ diffusion induced by compression deformation. Taking full advantage of the special self-powered sensing principle, we have developed both PAA hydrogel-based self-powered position recognizers and multi-dimensional sound detectors. Importantly, the mechanical-to-electric energy conversion concept is rather universal, and it is applicable to various polyelectrolyte

hydrogels. This mechanical-electric conversion device has large comprehensive advantages compared to common hydrogel-based piezoelectric and triboelectric electronics (Table 3.1).

Table 3.1 Comparison of this work with other hydrogel-based triboelectric[102, 161, 171-174] and piezoelectric[162, 175-177] devices

Sensing mechanisms		Detectable mechanical stimulus	Power source	Output voltage	Output current	Applicability	Current form	Responding speed	Orientation recognition	Ref.
Passive sensing mechanisms	Piezoelectric	Dynamic	Self-powered	Moderate	pA-μA	Negatively charged hydrogel	Alternating Current	High frequency (10^0-10^3Hz)	No	[2, 12-16]
	Triboelectric	Dynamic	Self-powered	Large	nA- μA	Piezoelectric material-doped hydrogels	Alternating Current	High frequency (10^0-10^3 Hz)	No	[3, 17-19]
	This work	Static and dynamic	Self-powered	Small	2 μA	All hydrogels containing polyelectrolytes	Direct current	Low frequency (0.05 Hz)	Yes	-

The novel mechanical-electric conversion technology discovered in this work applies to almost all polyelectrolyte-containing hydrogels without additional micro-nanostructure processing and precise chemical synthesis[178, 179]. Therefore, this technology has good universality and low-cost merits[180-182].

This simple and low-cost flexible device based on polyelectrolyte hydrogels is promising for several emerging technologies, including self-power sensing and energy harvesting.

4 POLYELECTROLYTE-GRADIENT HYDROGEL GENERATOR AND SELF-POWERED PRESSURE SENSOR

In the previous chapter, we showed that polyelectrolyte hydrogels can convert mechanical pressure into DC output for self-powered pressure sensing. This primarily arises from the diffusion of mobile ions during compression, while the oppositely charged polyelectrolyte chains are immobilized within the network, leading to an internal charge imbalance in the hydrogel and thereby driving electron flow in the external circuit. However, the output voltage was low (< 10 mV), limiting practical use. To improve output performance, this chapter introduces a bilayer hydrogel inspired by the asymmetric structure of red blood cells. By stacking a polyelectrolyte-rich layer with a near-neutral one, a strong ion concentration gradient forms, raising the initial DC voltage to over 100 mV. This enhanced functionality enables the device to serve both as a self-powered pressure sensor and a power source for small electronic devices.

4.1 Introduction

Water vapor-driven hydrogel-based green electric generators,[113, 114, 183-185] in particular water-driven polyelectrolyte hydrogels, can generate more than 100 mV output voltage under continuous moisture feeding.[94] This is due to the difference in ionizable ion concentration caused by moisture, which causes subsequent ion diffusion.[133, 186, 187] While the electricity generated is green, these devices rely heavily on the external moisture configuration. They can only operate in high moisture levels, which limits their practical applications.[153, 188, 189] A more effective solution can be obtained using an aqueous medium as a carrier for ion transport. In this case, ionic diffusion can generate electricity from a high-concentration salt-hydrogel through an ion-selective membrane to a low-concentration salt-hydrogel.[153, 190] However, the configuration and construction of three-layer substrates (membrane and hydrogels) are cumbersome; in particular, the preparation of ion-selective membranes that would match the hydrogel substrates is challenging.[191]

There are many asymmetric structures in nature, such as the lipid bi-layer structure in red blood cells.[192] Neutral lipids and anionic lipids are mainly located in the outer and inner leaflets.[193] The non-uniform distribution of charged polymers in the bi-layer structure leads to the generation of the transmembrane potential (Figure 4.1).[193-195]

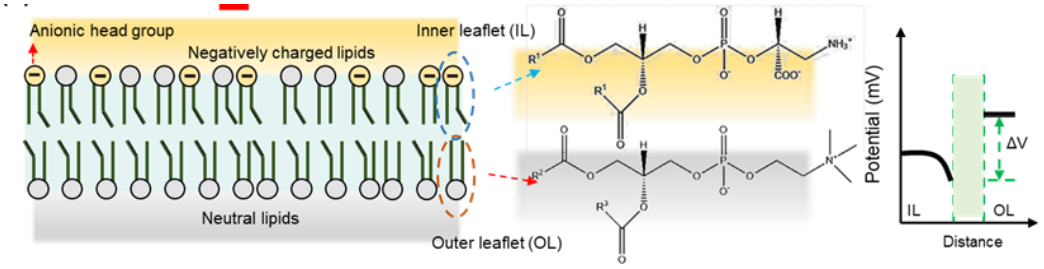

Figure 4.1 Schematic diagram of the asymmetrical lipid bilayer of red blood cells.

In this chapter, we applied a biomimetic approach, using the asymmetric charged structure of the red blood cell system as inspiration, and we proposed the concept of an asymmetric PGHEG. The directional migration of ions (Na^+ and Cl^-) driven by the difference in polyelectrolyte concentration also underpins the ability of PGHEG to generate direct electrical current power. As a proof of concept, biomass LS (anionic polyelectrolyte) or QC (cationic polyelectrolyte) doped PVA hydrogels (PVA–LS or PVA–QC hydrogel) and pristine PVA hydrogels (without polyelectrolyte doping), were fabricated and assembled into PGHEG. The generator's output voltage is directly related to the polyelectrolyte content in the gel. The LS-assembled PGHEG can generate a maximum output voltage of ~130 mV at room temperature. By assembling 10 PGHEG units in series, an output voltage as high as ~1.29 V can be obtained, which is sufficient to power a small electronic. Moreover, the device has been demonstrated to enable self-powered pressure sensing with a DC output.

4.2 Results and Discussions

4.2.1 Design principle

As PVA polymers have poor ionization characteristics,[195] we used PVA hydrogel as a neutral layer (PVA hydrogel contains no chemical crosslinkers or impurities). LS, a biomass-derived polyelectrolyte (Figure 4.2a), undergoes ionization in the presence of water, releasing Na^+ into the surrounding medium.[196, 197] At the same time, sulfonate groups ($–SO_3^-$) are fixed on the polymer chains.[132, 195] The LS we purchased has the same characteristic peaks as those in previous work (Figure 4.2b). And the spectrum of the LS displays the absorption peaks at 1033 cm^{-1} revealing the existence of $–SO_3^-$.[198]

QC, as a biomass-derived polycationic polymer, can release Cl^- upon ionization, while the quaternary ammonium groups ($–N^+$) remain fixed on the polymer backbone (Figure

4.2c).[199]The FTIR spectrum of QC showed the principal characteristic bands: the -OH stretching around 3430 cm^{-1}; The weak absorption bands at wavenumbers 2918 cm^{-1} and 2873 cm^{-1} corresponded to the C–H stretching of hydrocarbon in the chitosan backbone. The characteristic absorption band at wavenumbers 1374 cm^{-1} corresponded to the C–O stretching of the amide group. When chitosan was modified with quaternary ammonium salt, a new band at 1480 cm^{-1} corresponding to the methyl groups of ammoniums appeared (Figure 4.2d). [195, 200, 201] The zeta potentials of the two materials are shown in Figure 4.2e.

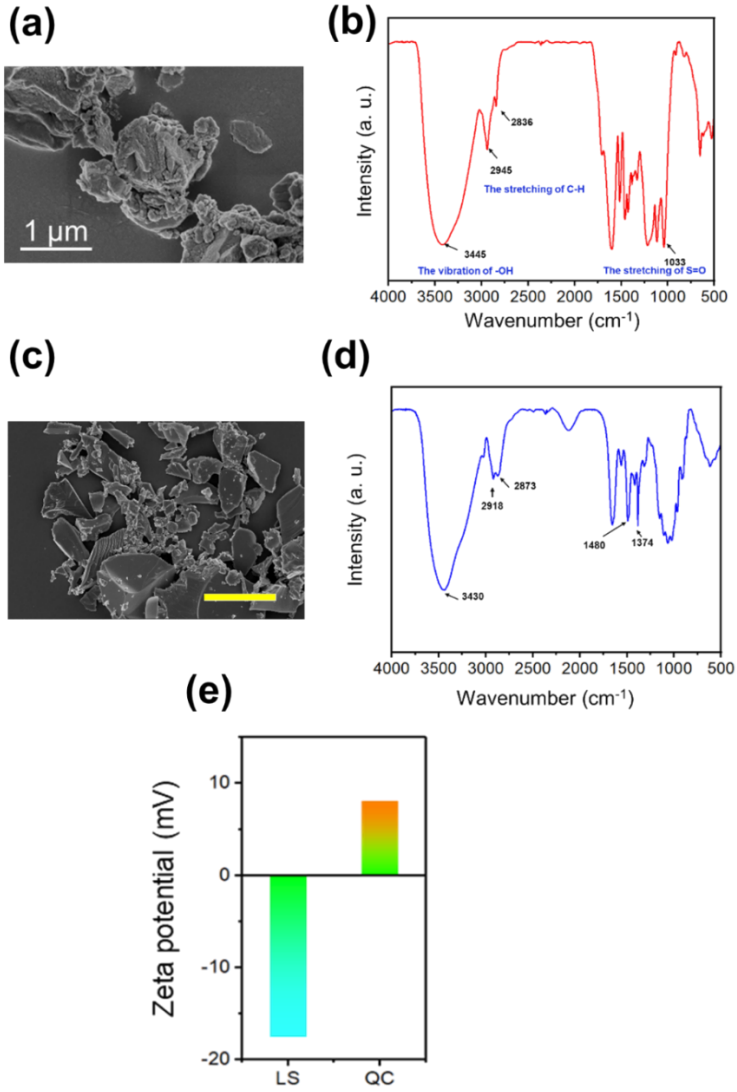

Figure 4.2 a) The microscopic morphology of LS. b) The FTIR spectra of LS. c)The microscopic morphology of QC. Scale bar: 10 μm. d)The FTIR spectra of QC. e) Zeta potentials of LS and QC.

For these reasons, LS was incorporated into the PVA hydrogel system to assemble the PVA–LS hydrogel as a negatively charged layer (Figure 4.3a). LS can ionize in the presence of water, yielding Na^+ that can move freely in the hydrogel (Figure 4.3b).

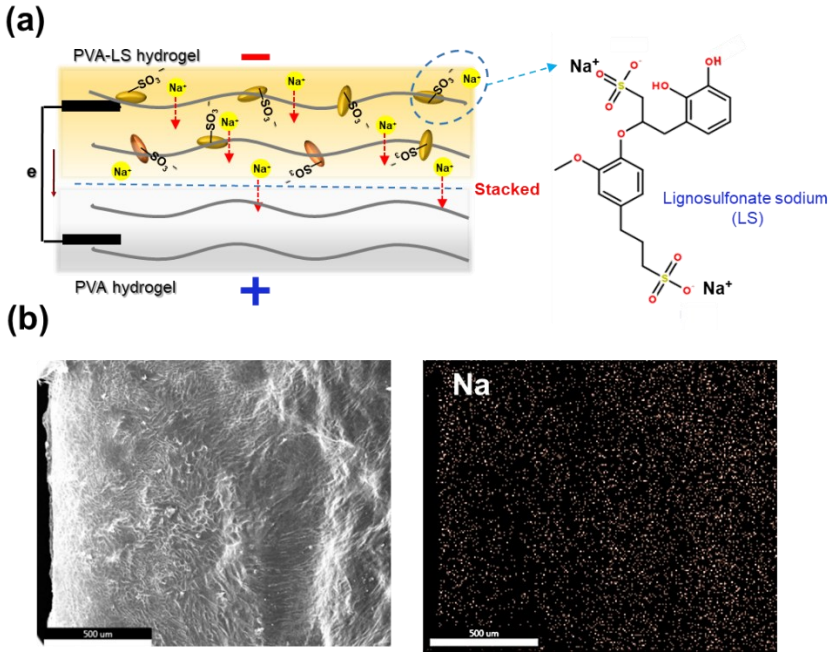

Figure 4.3 a) The operating principle of the electric generator of biomass LS (-) polyelectrolyte-gradient hydrogel. b) Microscopic morphology and Na distribution of PVA-LS hydrogel.

In this case, the PVA hydrogel doped with QC is applied as a positively charged layer (Figure 4.4a). QC can ionize in the presence of water, yielding Cl^- that can move freely in the hydrogel (Figure 4.4b).

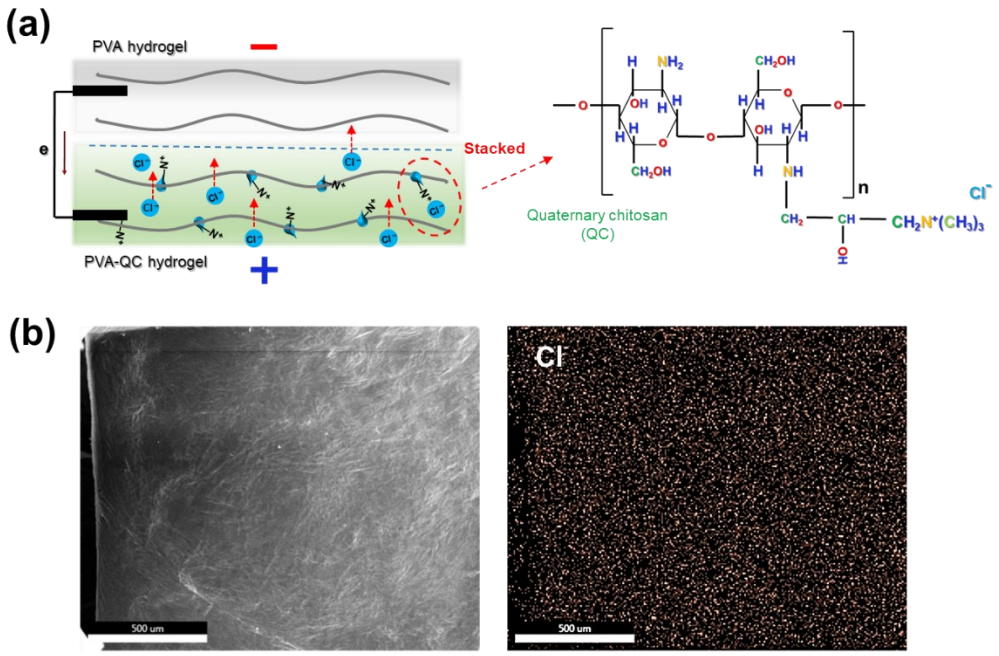

Figure 4.4 a) The operating principle of the electric generator of biomass QC (+) polyelectrolyte-gradient hydrogel. b) The microscopic morphology and Cl distribution of PVA-QC hydrogel.

The PVA–QC and PVA–LS hydrogels are then stacked on neutral PVA hydrogels to form the final devices. This structure mimics the blood cell structure to obtain directed ionic motion and generate electrical power. For instance, PVA hydrogels doped with LS can ionize more Na^+ than pure PVA hydrogels. When the two hydrogels bond together, Na^+ will move towards the low-concentration side (pure PVA hydrogel) in the water medium of the hydrogel. However, negatively charged groups on polymer chains typically lack mobility. So here, the ion concentration difference is the driving force for this device to generate electricity.

Generally, polyelectrolyte hydrogels/membranes can be used to prepare moisture generators.[94, 195, 202] These devices work only in the presence of moisture when there is no moisture difference between the upper and lower surfaces of polyelectrolyte membranes/hydrogels, they cannot generate electricity. [156] When one side is exposed to a high concentration of moisture and the other is sealed, the moisture will cause the polyelectrolyte chains to ionize, resulting in more ions. The difference in ion concentration induces the movement of ions in the direction of low concentration (sealed end). In this type of device, moisture molecules or water media act as transport media for ions.[203]

Therefore, the basic operating principle between the power generation mechanism of this device and that of the moisture generator is essentially the same, based on an ion gradient concentration. However, the moisture generator must rely on moisture to activate and function, while our device can directly generate electricity through a pre-set ion concentration difference, thus getting rid of the limitation of moisture. [204]

4.2.2 The performance of PGHEG constructed by anionic LS

To explore the influence of LS content on the electrical properties of composite hydrogels, PVA–LS hydrogels with various LS contents were prepared. As shown in Figure 4.5a, as the LS content increases, the appearance of the hydrogel changes from transparent to opaque black-brown.[131, 205] The increased LS content also improves the conductivity of the water medium and hydrogel due to the presence of more Na^+ ions in the system (Figures 4.5b and c). At the same time, the increased compressive strength of the hydrogel (Figure 4.5d) can also be attributed to the filling of LS in the hydrogel's pores.[52]

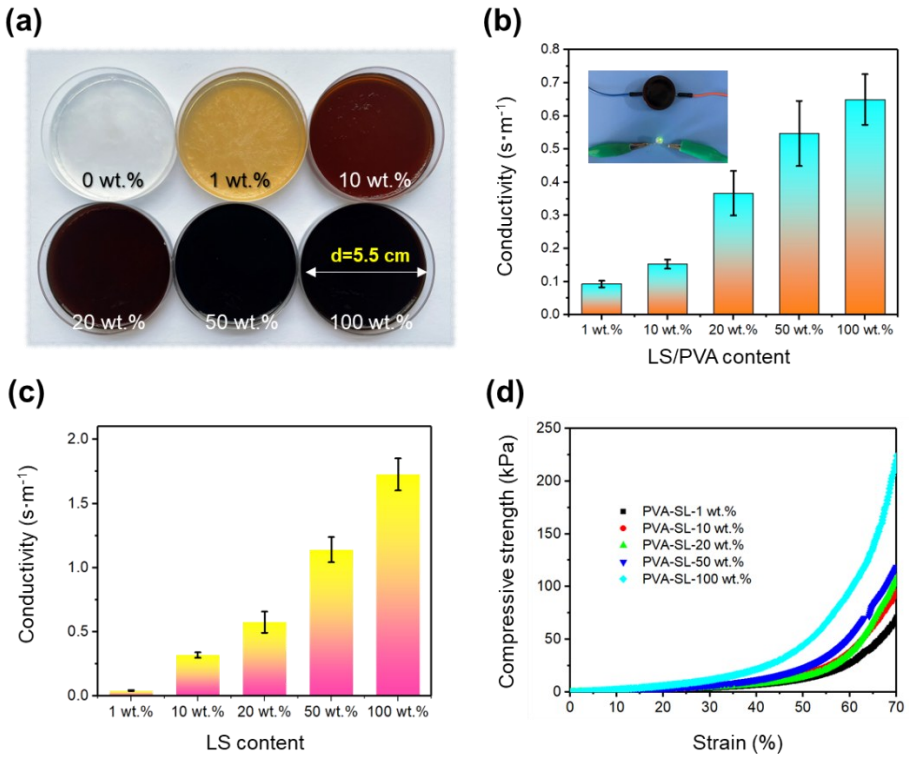

Figure 4.5 a) The actual appearance of PVA-LS hydrogel with various LS content (1 wt.% means the mass ratio of LS and PVA is 1%). b) The ionic conductivity of PVA-LS hydrogel with varying LS content. c) The ionic conductivity of the LS solution. d)The compressive stress-strain curve of the various PVA-LS hydrogels.

Different representative samples of disc-shaped PVA–LS hydrogels (diameter: 5.5 cm, thickness: 5 mm) with different %wt. of LS were prepared, and then positioned on the upper surface of pure PVA hydrogels of the same size. Next, the bilayer hydrogel is sandwiched between two graphite paper electrodes (thickness: 0.5 mm) to form a final PGHEG device. Figure 4.6 shows the effect of LS content on the device's output voltage. Increasing the LS content can increase the device's output voltage from ~20 to a max of ~125 mV at room temperature. A higher LS content leads to more Na^+, which creates a more significant concentration difference gradient (driving force) between the two layers of the hydrogel (the LS particles containing $–SO_3^-$ groups are fixed in the hydrogel network), thereby significantly increasing the output voltage. However, a further increase of LS showed only a limited output voltage increase. For this reason, as well as cost considerations, the 100 wt.% PVA–LS hydrogel was selected as a sample for the next phase of the study.

According to thermodynamic analysis, the output potential (ΔU) of the polyelectrolyte-gradient hydrogel device can be defined by:

$$\Delta U = \frac{RT}{qF} ln \frac{C(h)}{C(l)} \qquad \textbf{Equation 4.1}$$

where R, T, q, and F represent the gas constant, temperature, valence, and Faraday's constant, respectively. [115, 155, 206] Also, the Na^+ concentrations on the PVA-LS hydrogel and PVA hydrogel sides are expressed as C(h) and C(l), respectively. Details of the formula are provided in Chapter 2 (**2.10)**. It can be concluded that the output voltage is directly related to the concentration of mobile ions (Na^+). In this system, increasing the LS concentration results in a larger output voltage.

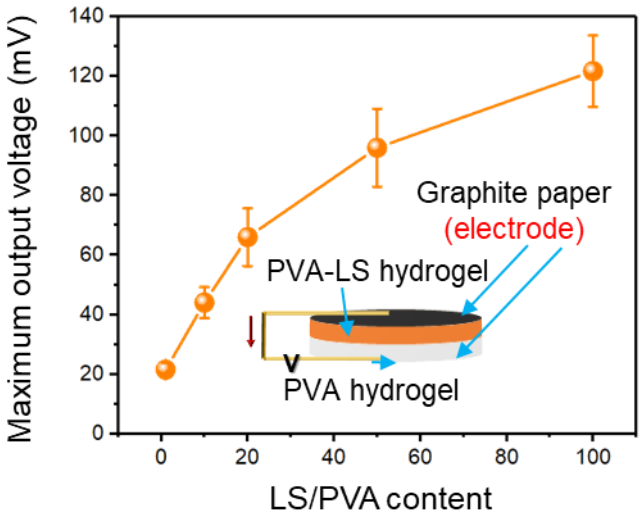

Figure 4.6 The output voltages of the PGHEG assembled by various PVA–LS hydrogels and pure PVA hydrogel.

The porous 3D structure of the PVA hydrogel provides a directional diffusional channel for Na^+, which is critical for electric power generation (Figure 4.7a). Figure 4.7b confirms that the neutral PVA hydrogel that has been in contact with PVA–LS hydrogel contains a significant amount of Na.

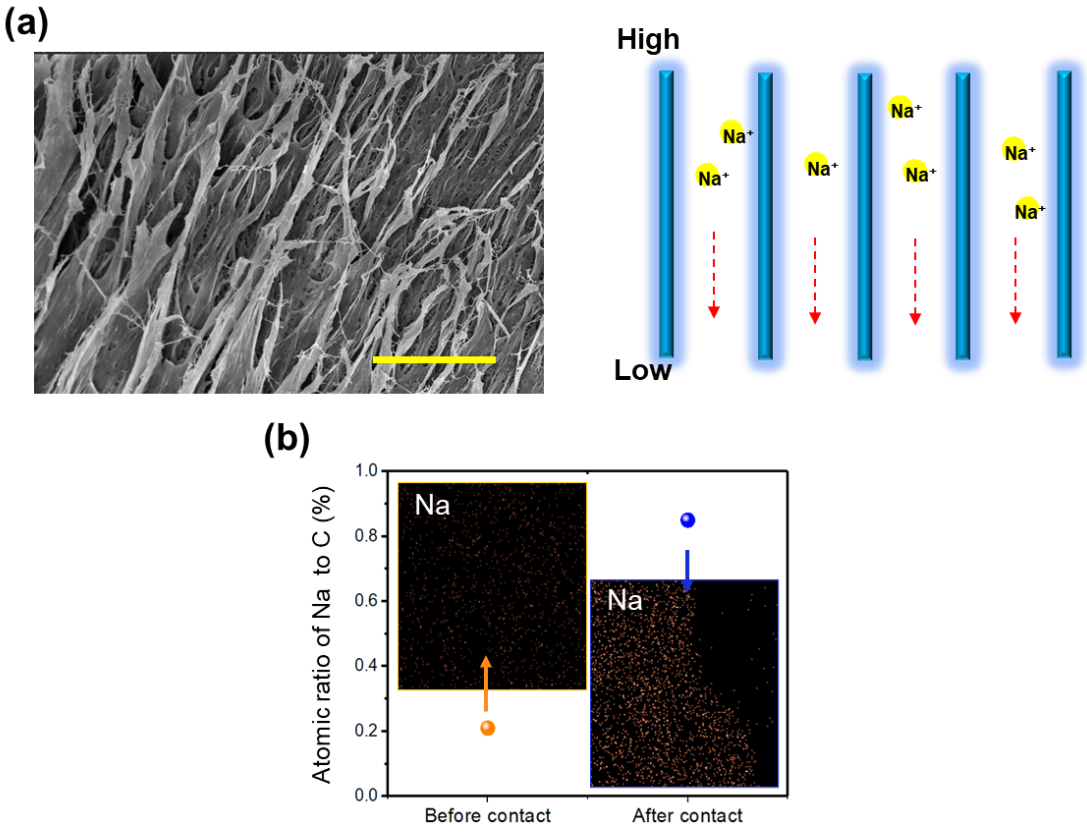

Figure 4.7 a) The 3D holes inside the PVA hydrogel can be applied as channels for Na^+

emigration. Scale bar:10 µm. b) Changes in the Na content of the original PVA hydrogel and the PVA hydrogel that has been placed under the PVA–LS hydrogel of PGHEG.

Although PVA and PVA-LS (100 wt.%) hydrogels also have 3D pores, the two individual hydrogels produce output voltages much lower than those of the bi-layer hydrogel assembly (the existence of the initial low voltage is caused by the non-uniform distribution of LS in the PVA–LS hydrogel) **(**Figure 4.8a). The above results support the idea that the polyelectrolyte/Na^+-gradient in the bi-layered hydrogel is the ultimate driving force for electric power generation.[207] The same absolute output voltages can be obtained by reversing the stacking direction of PVA–LS (100 wt.%) hydrogel and PVA hydrogel, yet with opposite signs (Figure 4.8b). This further demonstrates that the directional Na^+ diffusion is responsible for the polarity of the output voltage.[208] In addition, the output voltage of the device was also shown to be independent of size (Figure 4.8c).

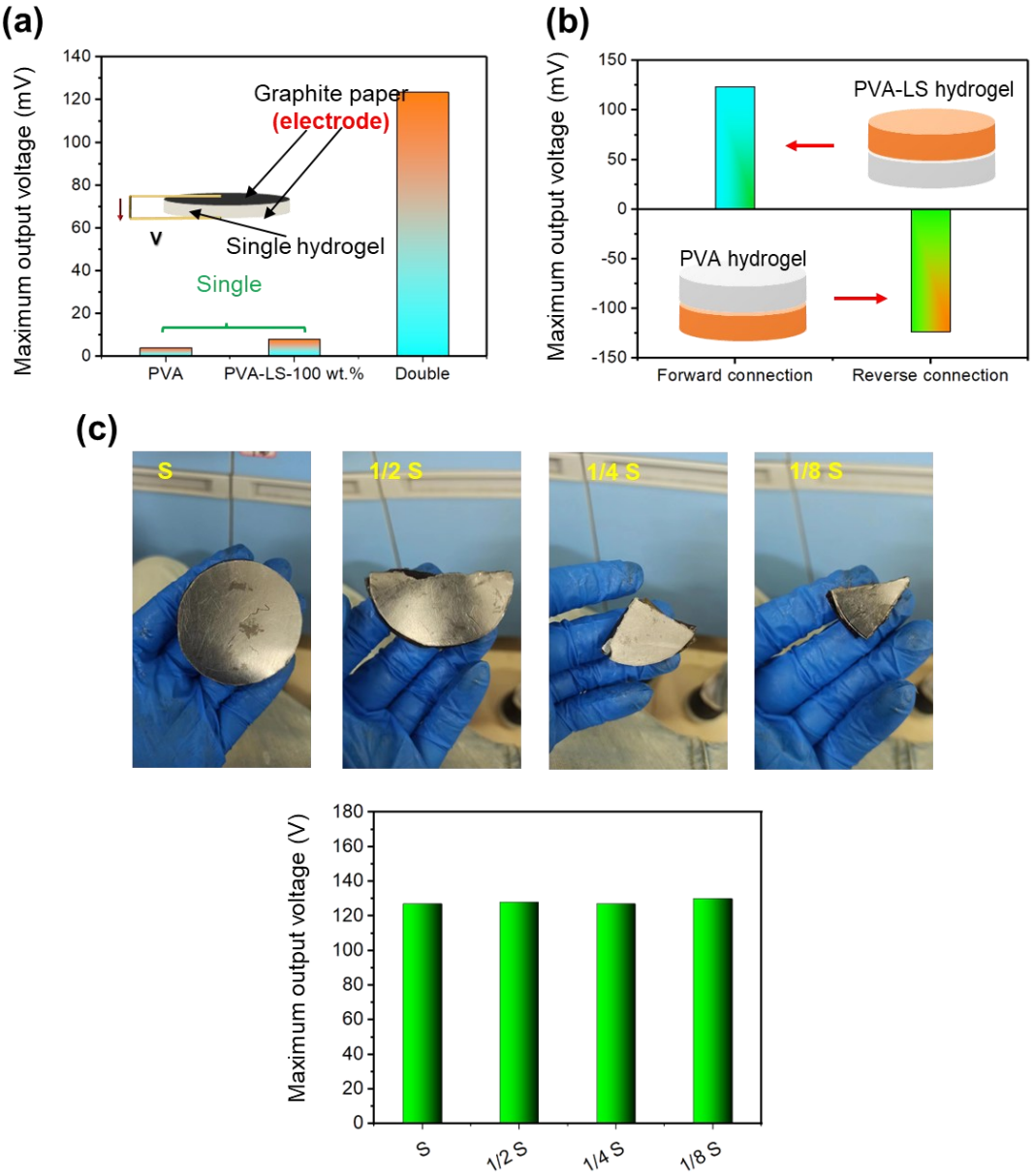

Figure 4.8 a) The device's output voltage is assembled by a single hydrogel or a bi-layer hydrogel. b) The output voltage of the bi-layer hydrogel device under different hydrogel stacking directions. c) Appearance and output voltage of different size devices (S=23.75 cm^2).

The optimized PVA–LS (100 wt.%) hydrogel-assembled PGHEG can generate output voltages up to ~130 mV and a stable current density of ~2.11 μA/cm^2 (Figure 4.9a and b). In addition, the device's output voltage can be maintained at >100 mV for nearly 10 hours, allowing it to supply power or charge a capacitor without being restricted by the external environment. This device has also been proven to have high output stability in a wide temperature range (Figure 4.9c). Further, the plastic wrap was used to seal the device to prevent dehydration of the hydrogel, thus the stability of the device was significantly improved (Figure 4.9d).

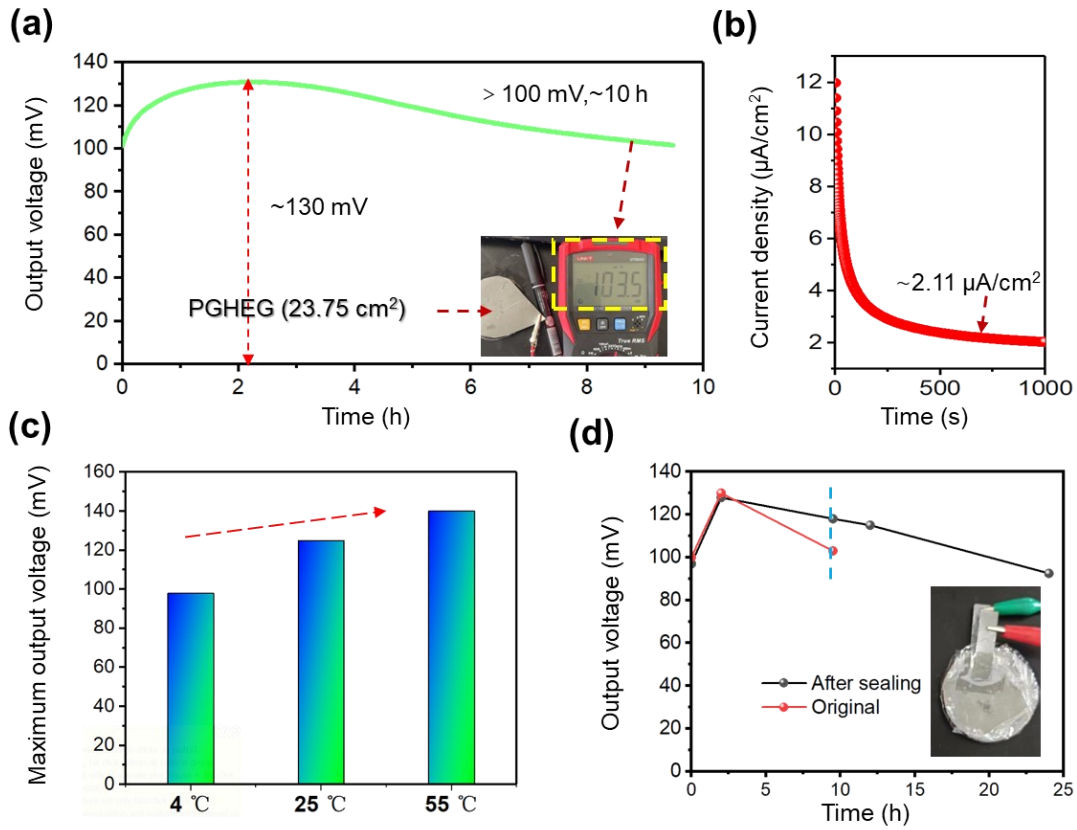

Figure 4.9 The real-time a) output voltage and b) current of the electric generator assembled by PVA–LS (100 wt.%) hydrogel at room temperature. c) The output voltage of PVA–LS (100 wt.%) hydrogel assembled PGHEG at various temperatures. d)This plastic-sealed device demonstrates better output stability.

Similarly, the hydrogel-based PGHEG exhibits good flexibility, presenting an additional advantage compared to traditional hard electronics. The device can maintain a stable output voltage even after being bent at different angles (Figure 4.10a and b). During the cyclic bending of the device, the hydrogel will be stretched and compressed, resulting in changes in the concentration of local ions. This will lead to small fluctuations in the voltage of the device. However, the output of the device is basically stable in the case of multiple cycles of bending, benefiting from the flexibility of the hydrogel.

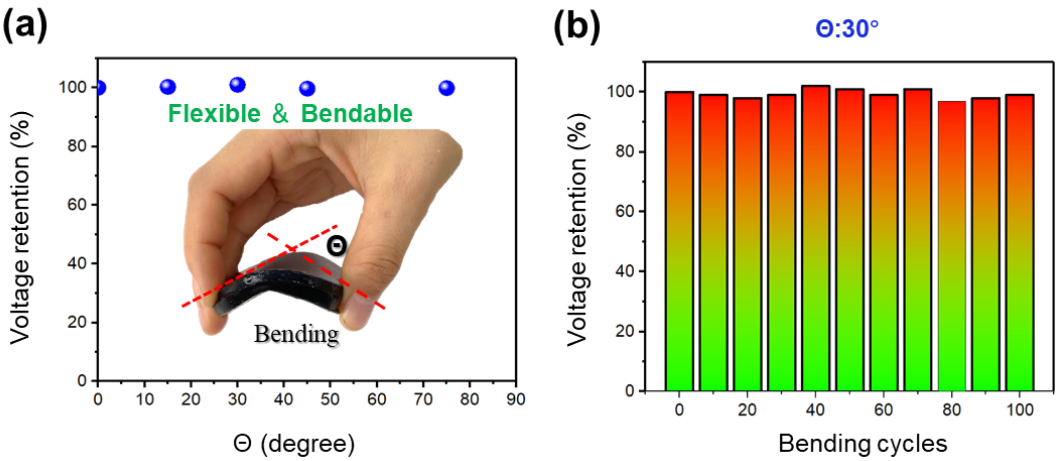

Figure 4.10 a) Voltage retention of PVA-LS (100 wt.%) hydrogel assembled PGHEG under different bending angles. b) Voltage retention of PVA–LS (100 wt.%) hydrogel assembled PGHEG after various bending cycles at an angle of 30°.

4.2.3 The performance of PGHEG constructed by cationic QC

In addition to the anionic LS, the PGHEG assembled by the QC (cationic polyelectrolyte)-doped PVA (PVA–QC) hydrogel has also been investigated. The QC can significantly improve the conductivity of solutions and hydrogels (Figure 4.11a-c), because it can ionize a large amount of Cl^-. The Cl^- content in the pristine PVA hydrogel that has been exposed to a PVA–QC hydrogel increased significantly, confirming the occurrence of directional migration of Cl^- (Figure 4.11d).

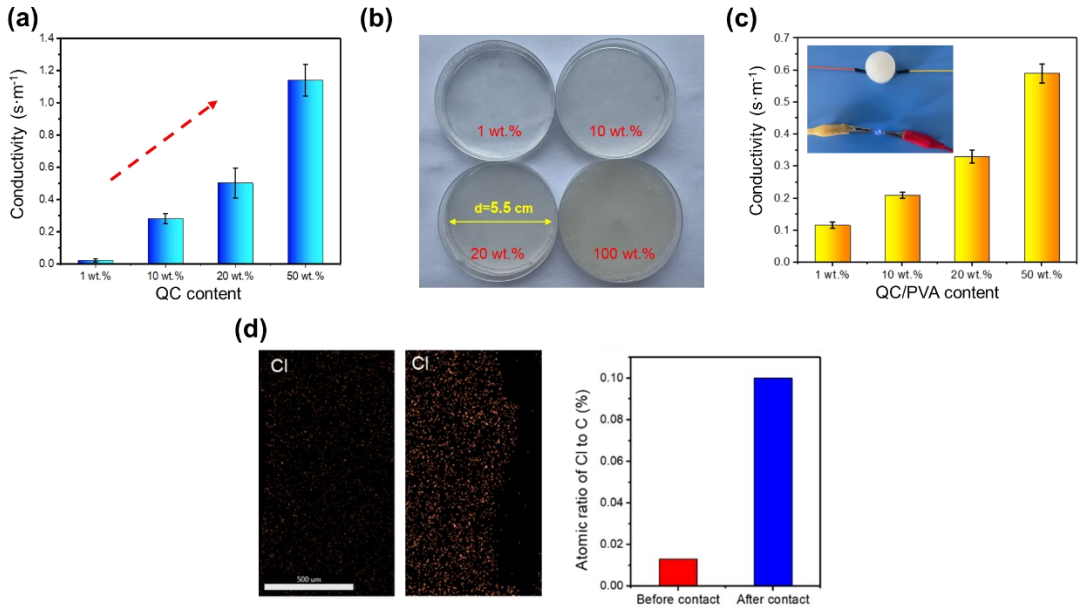

Figure 4.11 a) The conductivity of the QC solution. b) The actual appearance of PVA–QC hydrogel with various QC content (1 wt.% means the mass ratio of QC and PVA is 1%). c) The

ionic conductivity of PVA–QC hydrogel with varying QC content (detailed composition can be seen in Table 2.4). d) Changes in the Cl content of the original PVA hydrogel and the PVA hydrogel that has been in contact with the PVA–QC hydrogel of PGHEG.

The increase in the QC content of the PVA–QC hydrogel also significantly increases the output voltage of the PGHEG from ~8 to ~70 mV (Figure 4.12a). However, both QC and PVA are thickeners and, therefore cannot continue to dissolve more QC (>50 wt.%) in the PVA solution. In particular, a 50 wt.% PVA–QC hydrogel-stacked device obtains a max output voltage of ~71 mV and a current density of ~0.674 μA/cm^2 (Figure 4.12a -c). The difference in power generation performance of QC and LS-doped devices may be affected by the size of ions, the properties of the materials themselves, and the structure of the composite hydrogel.[149] To generate a positive voltage, it is necessary to place the PVA–QC hydrogel beneath the PVA hydrogel (Figure 4.4d). Otherwise, the device will cause a negative output voltage.[209] This device is similar to an inverted AA-size battery (positive at the bottom). These results support the conclusion that voltage can be generated for both polycation electrolytes and polyanion electrolytes, and the current direction of the device depends entirely on the charged type and diffusion direction of ions.[155]

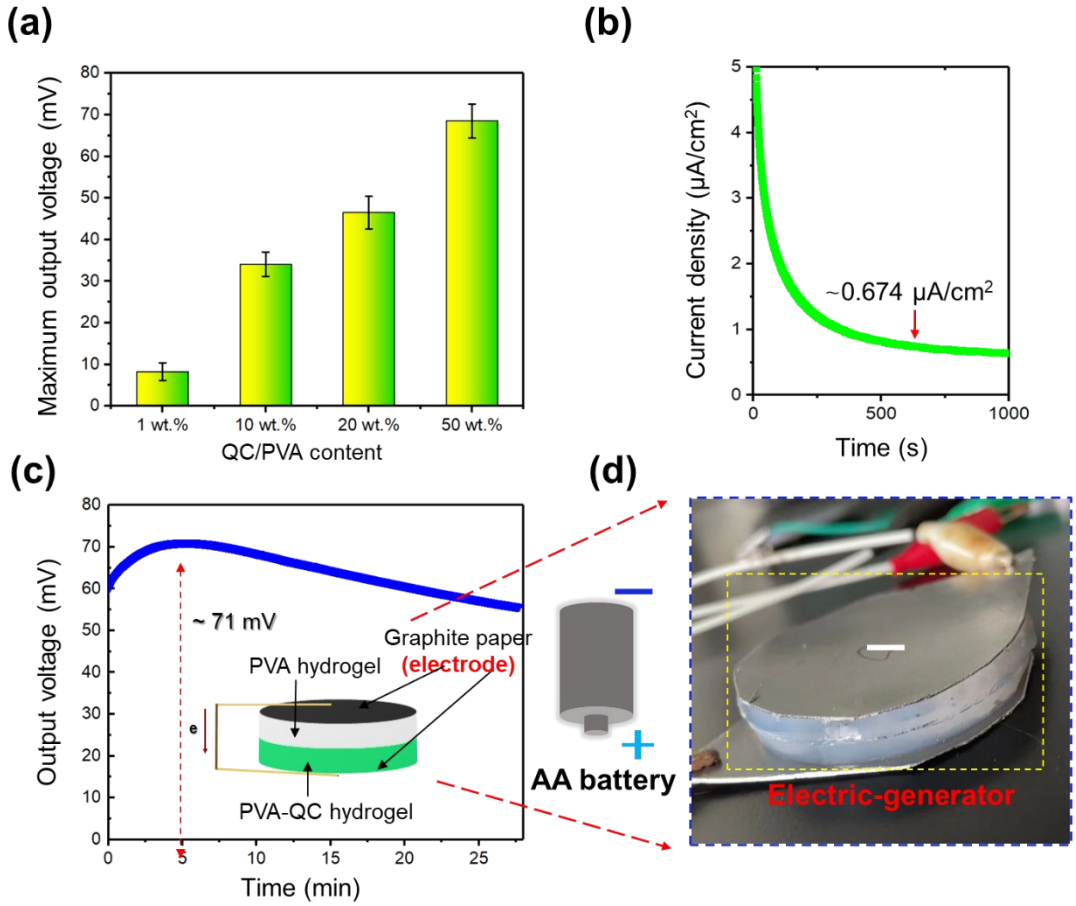

Figure 4.12 a) The output voltages of the device assembled by various PVA–QC hydrogels and pure PVA hydrogel (hydrogel diameter: 5.5 cm, hydrogel thickness: 5 mm). b) The real-time current of PGHEG assembled by PVA–QC (50 wt.%) hydrogel at room temperature. c) The real-time output voltage of a PGHEG assembled by PVA–QC (50 wt.%) hydrogel at room temperature. d) Comparison of pictures of PGHEG and AA batteries.

4.2.4 Application

Once the optimized concentration of LS and QC has been found, we can further assemble PGHEG devices in a series circuit to significantly increase the output voltage (Figure 4.13a). As shown in Figure 4.13b, various units of PGHEG (PVA–LS hydrogel (100%)/PVA hydrogel) were connected in series. The 10 PGHEG unit device can generate DC voltages up to ~1.29 V, autonomously supplying power to a small calculator (Figure 4.13c).

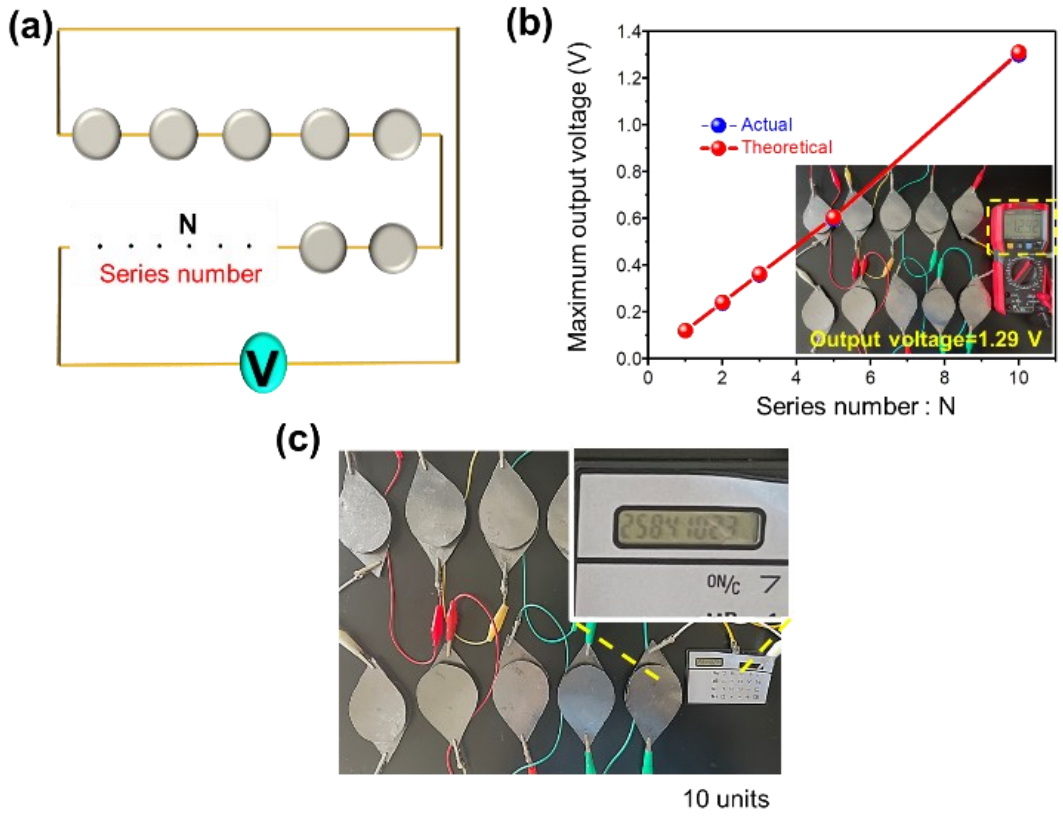

Figure 4.13 a) Schematic of PGHEG in series connection. b) The relationship between the actual and theoretical output voltage and the serial number of the PGHEG unit. This PGHEG unit is composed of 100 wt.% PVA–LS hydrogel (T: 5 mm, S=23.75 cm^2) and the same size pure PVA hydrogel. c) Demonstration of 10 PGHEGs connected in series as a power supply for a commercial calculator.

Additionally, a pressure sensor was assembled using the PVA–LS/PVA-based PGHEG device to evaluate its ability to sense pressure through direct current output (Figure 4.14a). As shown in Figure 4.14b and c, the device responds to varying pressure levels—such as finger pressing or different weights—by generating distinguishable changes in DC voltage, enabling effective pressure detection.

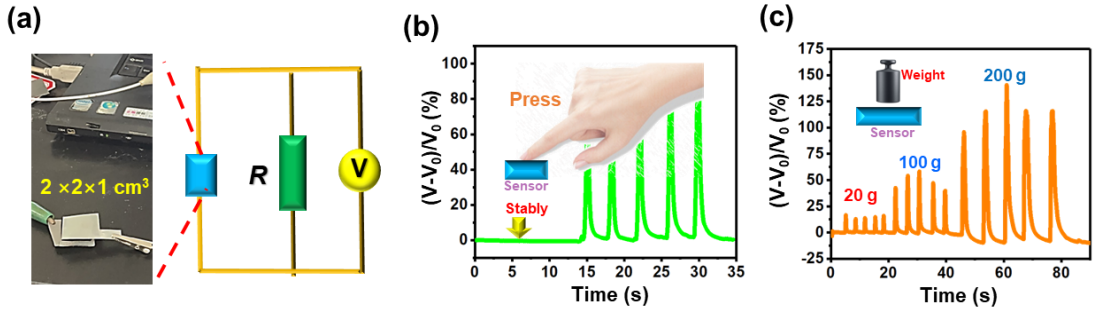

Figure 4.14 a) Schematic diagram of the self-powered sensor based on PGHEG; b–c) Illustrations of self-powered responses under different pressure levels.

Finally, unlike commercial AA-size batteries, the PGHEG unit is fully biocompatible because it is made of reusable Zn and graphite paper electrodes, biodegradable PVA, LS, and QC.[198, 210, 211] PVA–LS, PVA, and PVA–QC hydrogels can quickly dissolve using hot water (Figure 4.15).

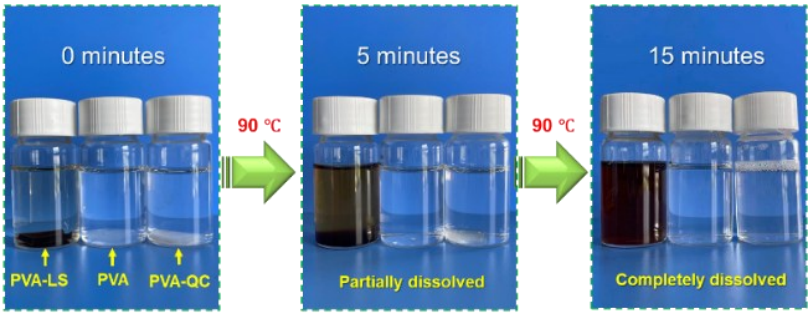

Figure 4.15 PVA-LS, PVA, and PVA-QC hydrogels (1×1×0.5 cm^3) can be quickly dissolved and recovered using hot water.

4.3 Conclusions

We described the design, fabrication, and testing of a PGHEG. The biomass-based anionic LS and cationic QC were used as two examples of polyelectrolytes to assemble the PGHEG. The LS-assembled PGHEG can obtain a maximum output voltage of ~130 mV. By assembling 10 PGHEG units in series, an output voltage as high as ~1.29 V can be obtained, which is sufficient to power a small electronic. The device has been demonstrated to enable self-powered pressure sensing with a DC output. Therefore, this low-cost, flexible, portable, and bio-degradable hydrogel generator is promising as a green energy source for wearable electronics.

5 PAPER–HYDROGEL GENERATOR AND SELF-POWERED PRESSURE SENSOR

In the previous chapter, we constructed an asymmetric polyelectrolyte-gradient hydrogel that produced over 100 mV of DC output from a single device, enabling self-powered pressure sensing and powering small electronics when stacked. However, the voltage of a single unit was still limited. In this chapter, we redesigned the structure by placing metal-coated paper on the hydrogel surface. Hydrogel moisture enters the paper, causing ionization of cellulose of paper and forming a concentration gradient that drives ions back into the hydrogel. Meanwhile, contact with the metal surface triggers a galvanic reaction, boosting the voltage. This boosts the output voltage to ~600 mV, allowing a single device to both sense pressure and power other electronics reliably.

5.1 Introduction

Electricity generation from moisture is a promising green self-powered technology that can be used for several applications, *e.g.*, small wearable electronic devices. [188, 214] The appeal of moist-electric generators stems from their innate ability to effortlessly draw in moisture from the surrounding environment, whether from the air, rivers, or lakes. This moisture triggers a gradient ionization process within the active materials of the generator. As a result of this ion concentration gradient, ions naturally diffuse from areas of high concentration to those of lower concentration, thereby producing a DC once the generator is linked to an external circuit. [183] Moisture-electricity generators offer many advantages, including small size, low cost, eco-friendliness green, and high efficiency. [215] Recently, a series of ionizable materials such as films, aerogel, wood, microorganisms, and graphene have been extensively studied for electricity generation from moisture. [216] Some of these devices have already demonstrated the capacity to generate voltages exceeding 0.8 V in high-humidity environments, where relative humidity levels (RH) surpass 80%.[217]

However, the performance of such devices is highly dependent on moisture content, which poses significant challenges for efficient operation in low-humidity environments, such as arid deserts with relative humidity levels below 50 % RH. [218] Moreover, maintaining a stable voltage output becomes challenging due to the continuous fluctuations in ambient humidity. [113, 219] Most moisture-electricity

generators encounter limitations in achieving self-powered pressure or strain sensing because external pressure obstructs the entry of moisture, leading to a disruption in voltage output. [156] Consequently, their application as self-powered pressure or strain sensors poses considerable challenges. [185]

Hydrogel, an elastomer with a solid-like elastomer comprising a 3D polymer network and water, possesses remarkable attributes of high-water content and good flexibility. [220, 221] The water within the hydrogel facilitates proton/ion transport, making them well-suited for moist-electric generation. However, hydrogels by themselves typically cannot generate electricity directly without external moisture stimulation. To address this limitation, we developed a PHEG, which was assembled by attaching commercial cellulose-based filter paper with viscous PAM hydrogel. The evaporation of moisture in the hydrogel can deprotonate the paper fibers and triggers a galvanic reaction at the asymmetric electrode, resulting in a voltage of ~0.6 V, a current density of ~12.5 $\mu A/cm^2$, and a power density output of 1.61 $\mu W/cm^2$.To increase voltage output, multiple 10-unit PHEGs were easily stacked into a battery-like power generation component, capable of providing a DC voltage output of ~6 V, which is sufficient to power electronic devices such as calculators. Furthermore, a PHEG device assembled with PAM gel containing 50% glycerol content can continuously generate a voltage output of 0.4 V for over 1000 h without external stimulation. Equally significant, PHEG has been showcased as an effective self-powered strain and pressure sensor. Considering its ease of assembly and cost-effectiveness, the combination of gel and commercial paper in PHEG holds excellent potential for integration into wearable electronic devices.

5.2 Results and Discussions

5.2.1 Preparation of integrated PHEG

Figure 5.1a presents a schematic diagram illustrating the preparation and application of PHEG. The device comprises a graphite paper electrode positioned at the bottom for energy transmission and collection, with a PAM hydrogel layer in the middle. Instead of physically affixing rigid metal electrodes, we employed a top layer of filter paper coated with Ag flakes, which exhibit better integrity and electrical collection capabilities (Table 2.2) while retaining the flexibility of the paper. The filter paper, which is a compact membrane formed by stacking layers of cellulose network, was used

for solid-liquid separation due to its advantages such as light weight, flexibility, hydrophilicity, and customizable nature (Figure 5.1b). [222] Moreover, the surface of the filter paper features roughness and abundant -OH groups, making it easy to load Ag flakes (Figure 5.1c and d). The Ag flakes on the filter paper do not come into contact with the hydrogel; rather, they serve for both energy transmission and collection purposes.

PAM hydrogels, elastomers formed by covalently crosslinking PAM polymers in water, demonstrate remarkable elasticity and stretchability (Figure 5.1e). The pores of the polymer 3D network are filled with water (Figure 5.1f). In addition, PAM hydrogel exhibits excellent adhesion properties, effectively adhering its upper to flexible graphite paper and its lower surfaces to filter paper (Figure 5.1g). Figure 5.1h demonstrates that the maximum adhesive strength of PAM hydrogel to filter paper exceeds 130 N/m. Even after the peel test, part of the paper fibers remains attached to the PAM hydrogel, highlighting the excellent integrity and flexibility of the layered PHEG. Unless otherwise stated, the PHEG devices here are made of 2×2 cm^2 Ag-coated filter paper, 2×2×0.5 cm^3 PAM hydrogel, and graphite papers. In addition, the ambient temperature during the tests was 25 ± 5 ℃.

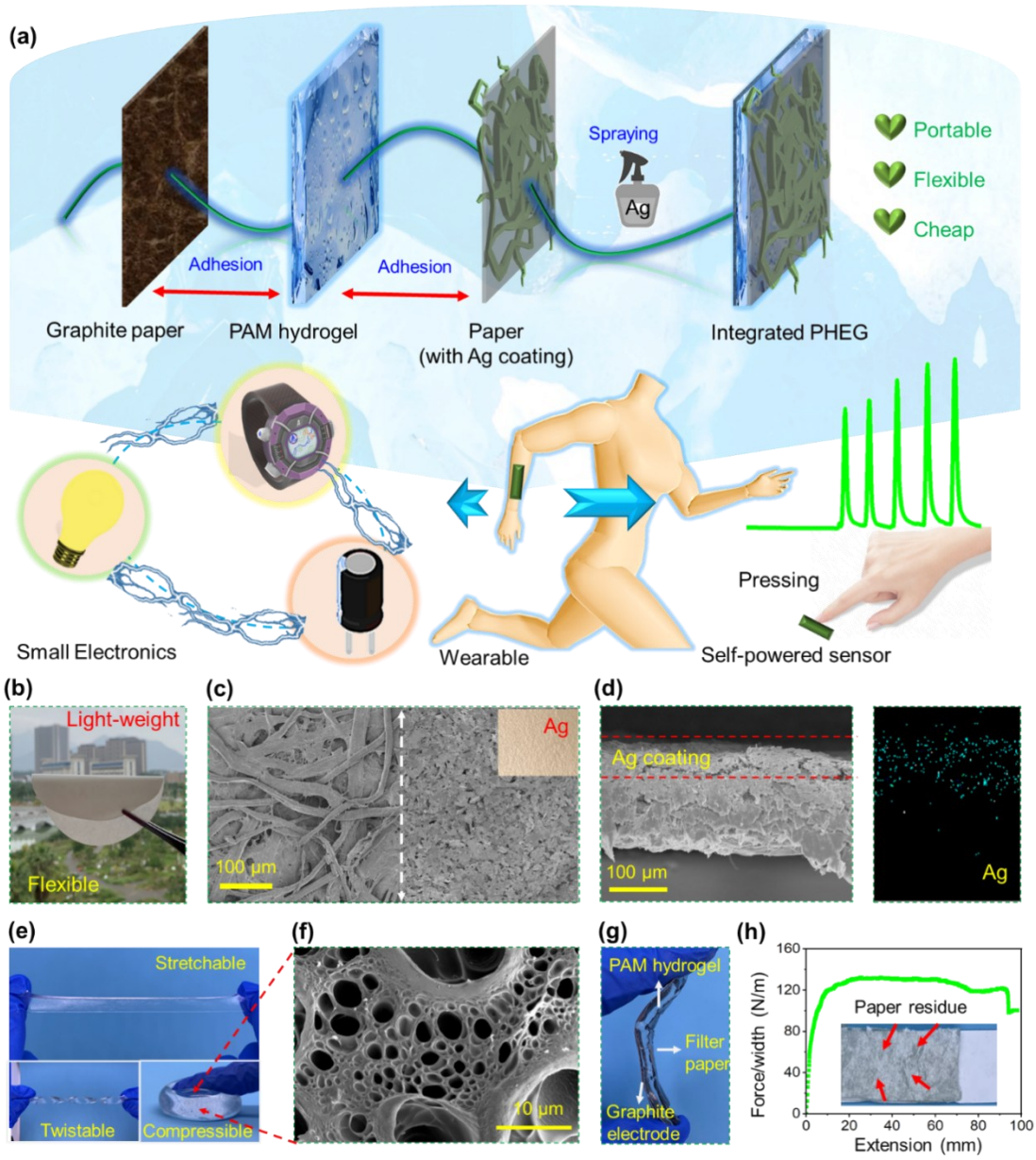

Figure 5.1 a) Schematic diagram of the preparation, composition, and application of PHEG. b) Actual photograph of filter paper. c) SEM image of original filter paper and Ag coating. d) Cross-sectional SEM and Ag distribution images of filter paper with Ag coating. e) Photographs of the mechanical behavior of PAM hydrogels. f) SEM image of PAM hydrogel. g) Actual photograph of integrated filter paper/hydrogel device. h) Adhesion force between filter paper and PAM hydrogel.

Furthermore, the device cost was calculated to be \$0.0277 per PHEG unit (2×2 cm^2) (the details can be found in Chapter 2.12). We also evaluated the stretchability of the device (Figure 5.2a), and its water retention capacity (Figure 5.2b). The mechanical strength of the sandwich-structured PHEG was measured using uniaxial stretching, revealing a fracture process comprising three distinct stages, each corresponding to the deformation of specific components. The tensile strength of the device was found to be

~17 kPa. The sandwich structure and partial tape fixation of PHEG can inhibit the loss of water in the PAM hydrogel to the air to a certain extent.

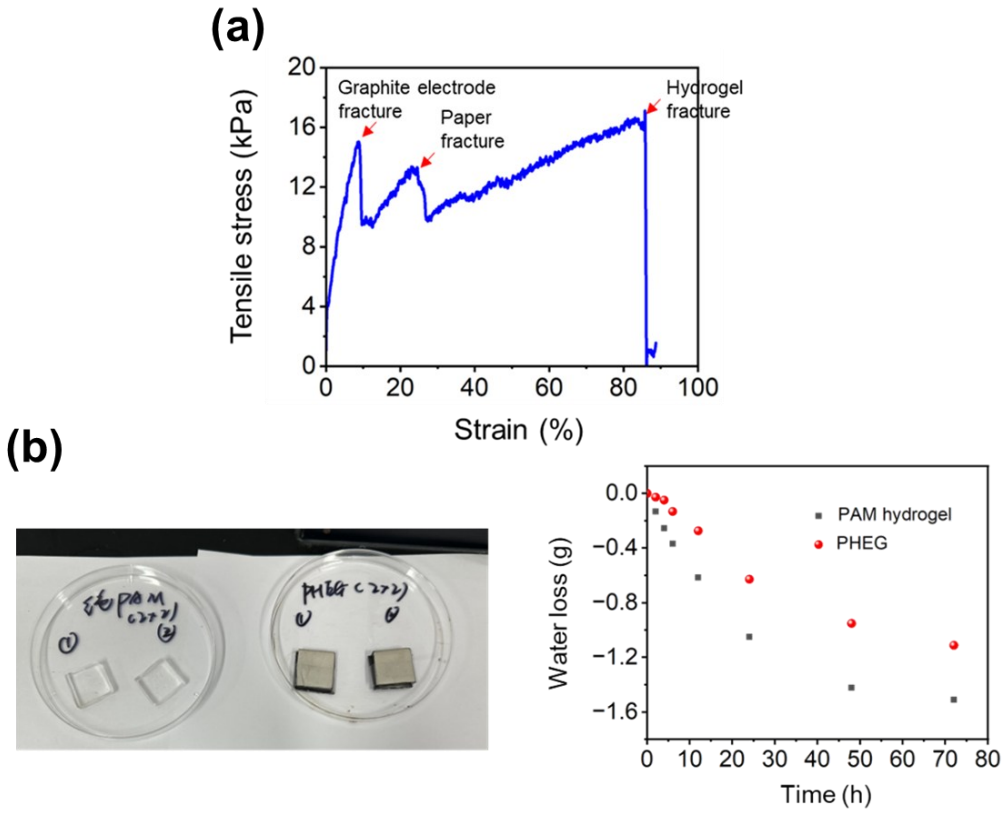

Figure 5.2 a) Stress-strain curves of the PHEG device. b) Water loss results of PHEG and PAM hydrogels at room temperature over time.

5.2.2 Working mechanism of PHEG

As shown in Figure 5.3a and b, the open circuit voltages of HEG and PEG, assembled from separate PAM hydrogel or filter paper, are close to 0 V. In contrast, the output voltage of integrated PHEG is close to 0.6 V, suggesting that the PHEG is responsible for the observed voltages. XPS reveals the presence of C–OH groups in the cellulose-based filter paper (Figure 5.3c). The hydroxyl group (–OH) can undergo mild ionization and release protons (H^+) in water. [223]

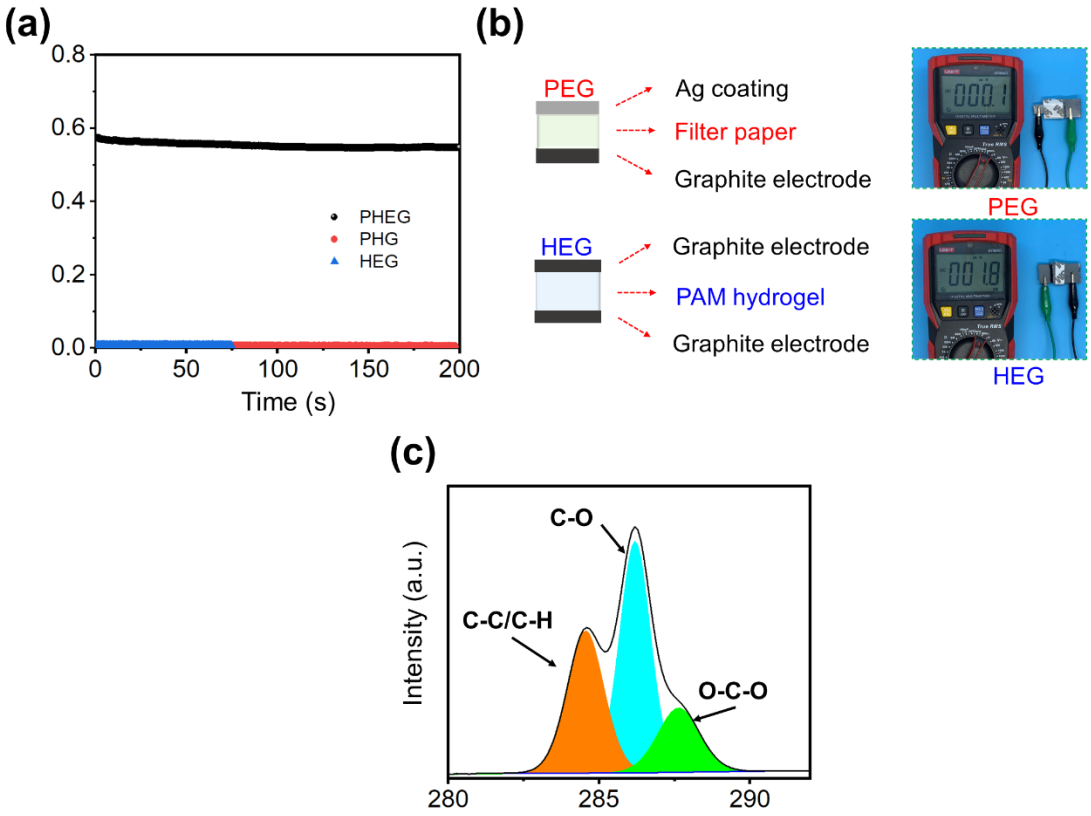

Figure 5.3 a-b) Output voltage of devices with paper/hydrogel, single paper, or single hydrogel compositions, respectively. c) C1s XPS spectrum of filter paper.

This is further supported by the observation of a negative zeta potential of filter paper and increased conductivity in PHEG (Figure 5.4-5.8), which were not present in non-ionizable materials such as glass, silicone, and PET films. We believe that the mobile ions within PHEG play a crucial role in initiating power generation. Generally, filter paper comprises many cellulose fibers and a very small number of fillers. Although cellulose and filter paper cannot be dissolved in water, contact with water can cause wetting and swelling, so their –OH groups can ionize a bit protons/H^+ so that the zeta potential shows a negative value.

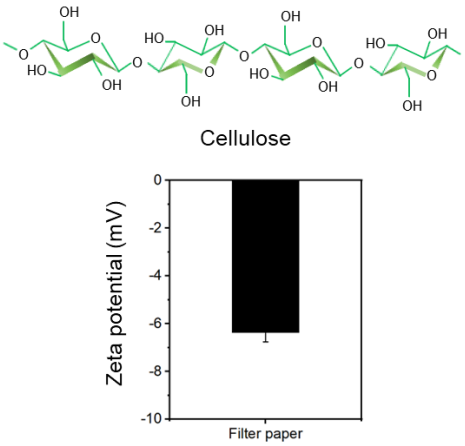

Figure 5.4 Schematic of cellulose's chemical structure and filter paper's zeta potential.

Deionized water itself is non-conductive, yet here it can promote the ionization of protons in the paper, thereby improving the conductivity of the paper and the water.

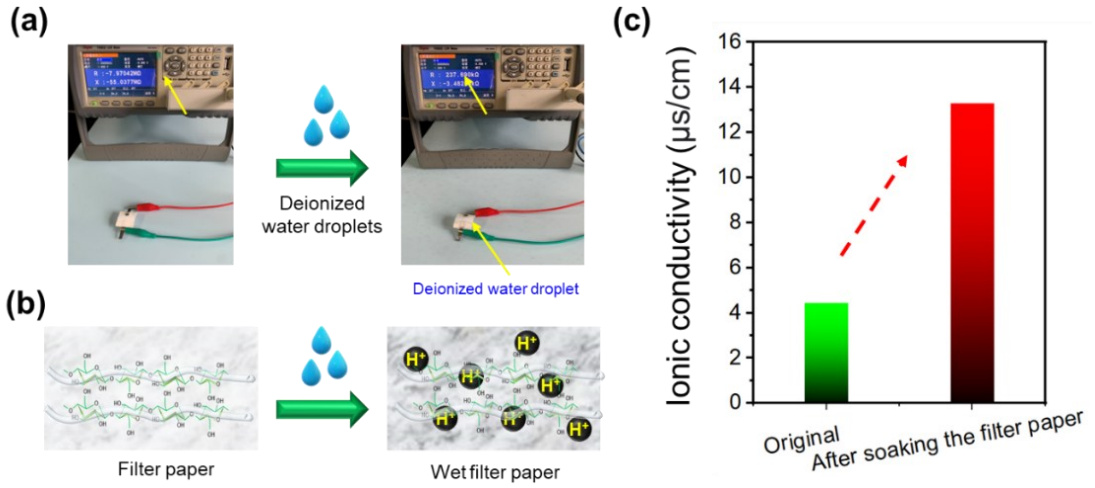

Figure 5.5 a) Photograph and b) Mechanism diagram of filter paper's electric resistance before and after wetting. The paper size is 2*2 cm^2. c) Conductivity of original deionized water and conductivity of four 4 cm2 filter papers soaked in 10 mL of deionized water for 30 minutes.

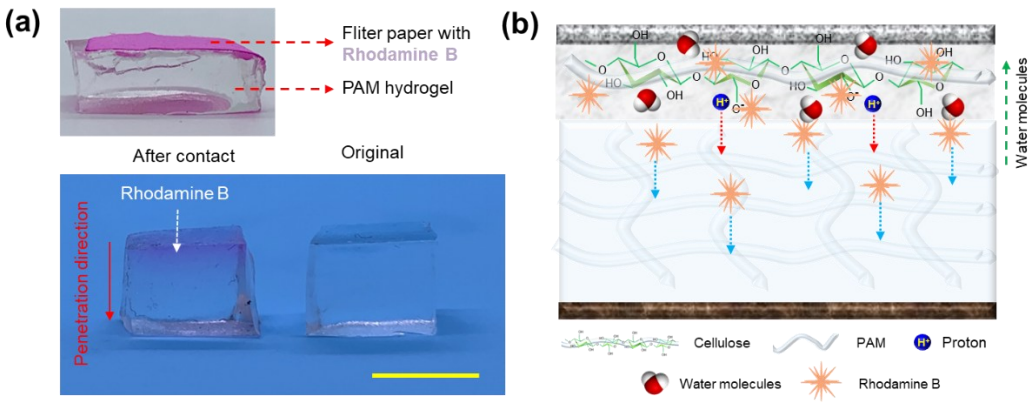

Figure 5.6 a) The filter paper soaked with rhodamine B dye will transfer the dye from the paper to the hydrogel after contact with the PAM hydrogel. b) Schematic diagram of the dye movement process. Scale bar: 2 cm.

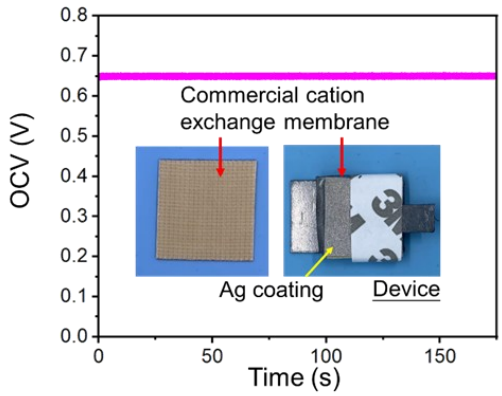

Figure 5.7 The output voltage of devices assembled with commercial cation exchange membranes instead of filter paper. The membrane size is 2*2 cm^2, and the thickness of the PAM hydrogel is 5 mm.

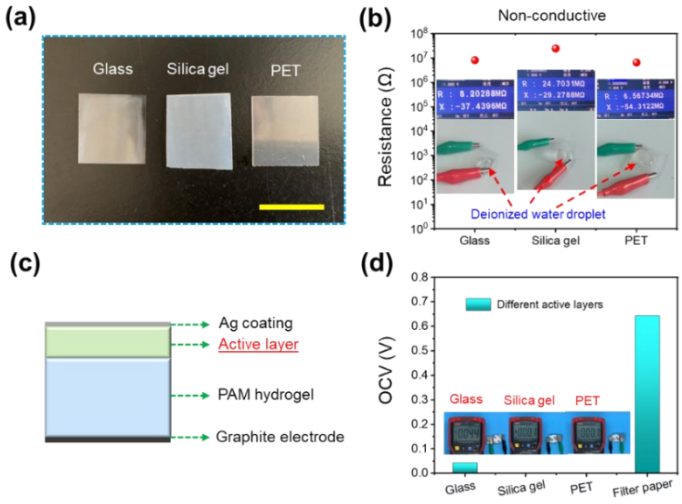

Figure 5.8 a) Photographs and b) electrical resistance of different materials. c) Schematic diagram of the electric-generation device assembled with the above materials as the active layer. d) Output voltage of devices using different active layer materials. The membrane size is 2×2 cm^2, and the thickness of the PAM hydrogel is 5 mm.

The water in the PAM hydrogel is another critical factor for the functionality of PHEG. When assembled with dry hydrogel and filter paper, the device's voltage remained at 0 V (Figure 5.9).

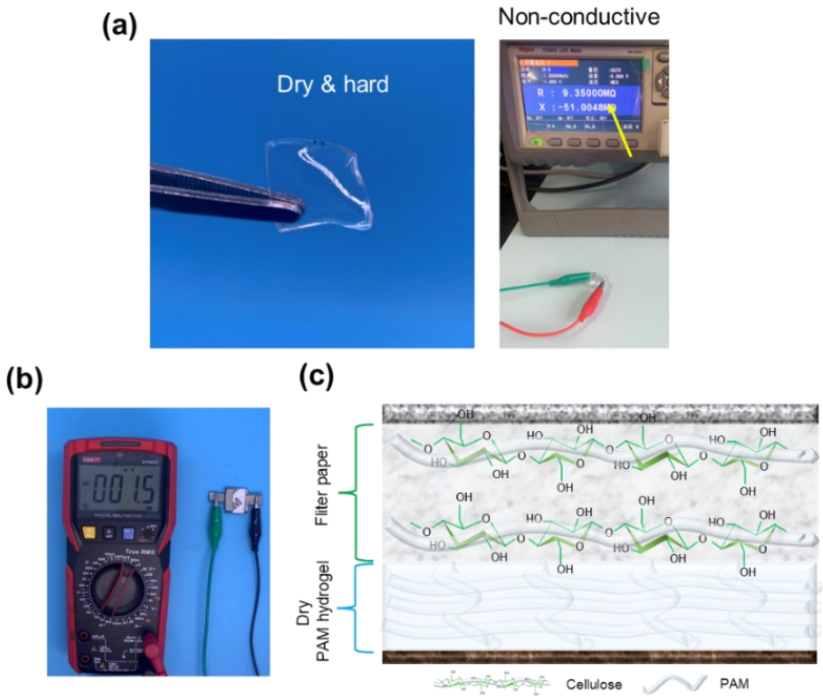

Figure 5.9 a) The photograph and electrical resistance of the dried PAM hydrogel. b) Output voltage of devices assembled with dry PAM hydrogel. c) Schematic diagram of device composition.

As depicted in Figure 5.10a and b, both the filter paper and PAM hydrogel exhibit small water CA, demonstrating great hydrophilicity. The paper with hydrophilic dyes was attached to the bottom surface of the hydrogel film, recording the process of water diffusion from the hydrogel to the paper (Figure 5.10c).

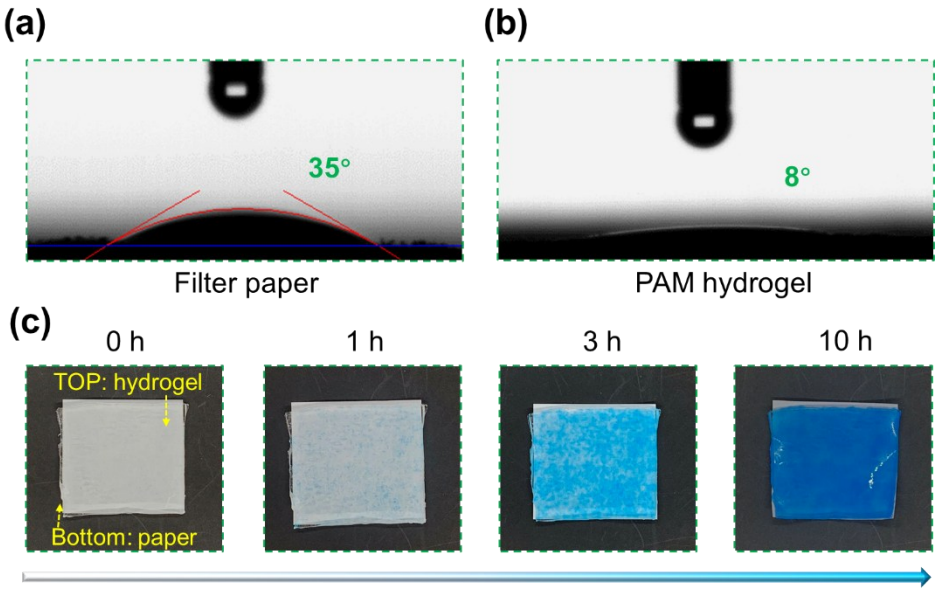

Figure 5.10 Water CA of the a) filter paper and b) PAM hydrogel. c) Photographs of the wetting process of PAM hydrogel on the paper with hydrophilic dyes.

The resistance (R) of PHEG also showed a cliff-like drop immediately after device fabrication (Figure 5.11). This indicates that the water in the hydrogel diffuses into the filter paper, facilitating the ionization and transport of H^+.

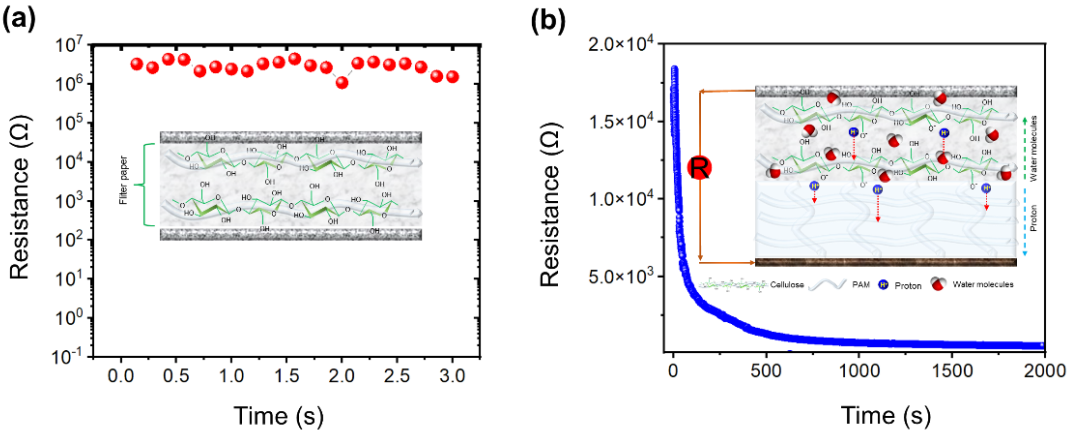

Figure 5.11 a) The electrical resistance of filter paper. b) The electrical resistance of the paper-hydrogel electric generator (PHEG) was recorded from when the filter paper and PAM hydrogel were bonded together. The filter paper size is 2×2 cm^2, and the thickness of the PAM hydrogel is 5 mm.

Further, KPFM was used to demonstrate the apparent difference in surface potential between the filter paper and the filter paper with bottom PAM hydrogel [156]. As shown in Figure 5.12a and b, the average potential of the latter is much higher than that of

filter paper alone. The uneven distribution of potential may be attributed to the fiber roughness of the paper surface (Figure 5.12c).

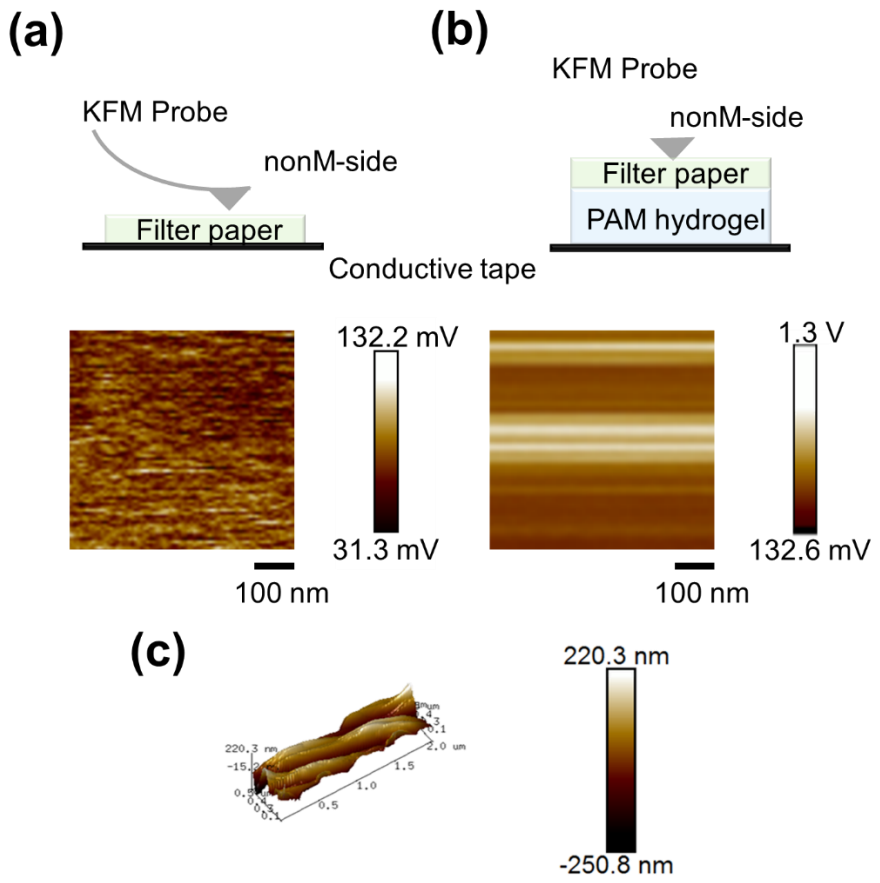

Figure 5.12 The potential results of a) filter paper and h) hydrogel-filter paper surfaces were acquired from a KPFM. c)The surface roughness of the filter paper.

When water contacts filter paper or a negatively charged membrane, it usually carries protons together for directional diffusion movement. [207] In such a case, the output voltage of PHEG should be negative (<0 V). However, the movement direction of protons here is opposite to the diffusion route of the water. This may be attributed to the negatively charged PAM hydrogel, which has an electrostatic attraction to the protons (positively charged) dissolved on the surface (Figure 5.13). [184]

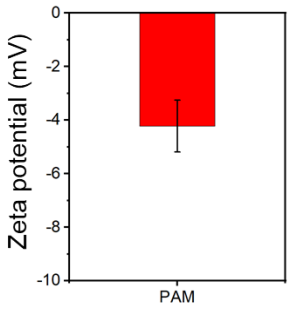

Figure 5.13 a) Zeta potential of the PAM hydrogel.

The proposed working mechanism of PHEG is summarized in Figure 5.14a. When the filter paper absorbs water within the PAM hydrogel, protons are rapidly generated and transported downwards through the aqueous medium within the hydrogel. At the same time, the metal coating of the asymmetric electrode ionizes upon contact with water, producing electrons that contribute to the device's voltage. As water continues to diffuse upwards through the paper, it replenishes protons that are transported downward due to the driving force, leading to a gradual increase in device voltage during the initial operation phase. [221, 224]

To validate this mechanism, the individual voltage of the paper (V_1) and the hydrogel (V_2) were recorded immediately after disassembling the running PHEG. Both V_1 and V_2 were positive (>0), and their sum equaled the original V_{oc} (Figure 5.14b), indicating the presence of proton downward motion in both the paper and the hydrogel. In particular, after 6 h of PHEG separation, the voltages of paper and gel dropped by 93% and 87%, respectively (Figure 5.14c). The device gradually loses its ability to generate electricity when there is no paper to provide protons or hydrogel to supply water. Overall, these findings strongly support the proposed mechanism.

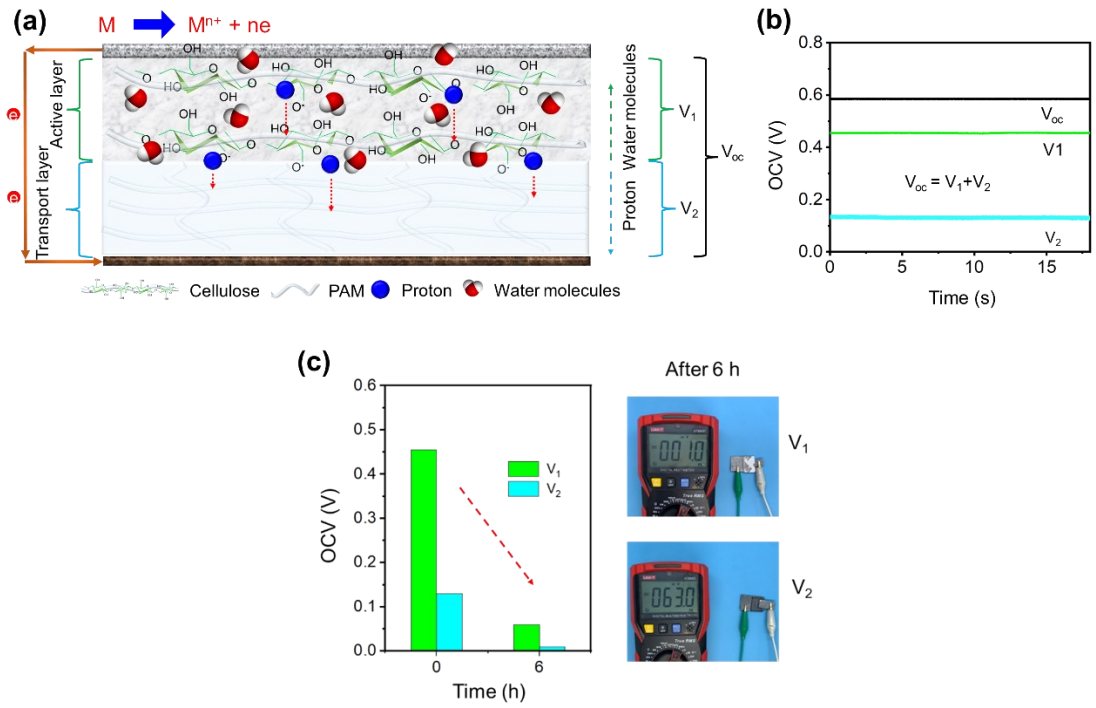

Figure 5.14 a) Schematic diagram of the power generation mechanism. b) Instantaneous output voltage after running PHEG is split into PEG and HEG. c)The running PHEG was instantaneously split independently into PEG (paper electric generator, V_1) and HEG (hydrogel electric generator, V_2). The output voltages of the different devices were recorded immediately after separation and 6 hours after separation.

The output voltage of devices assembled using other assembly methods was also tested (Figure 5.15a). For example, a reverse-PHEG (R–PHEG) connected inversely to the electrometer yielded a negative voltage. In the case of the device assembled by sandwiching the hydrogel between two filter papers, the output voltage was close to 0 V. This indicates that both layers of paper can provide almost the same number of mobile protons to the hydrogel, resulting in a net proton displacement of approximately zero (Figure 5.15b). At the same time, the voltage outputs from the asymmetric electrodes are also canceled out.

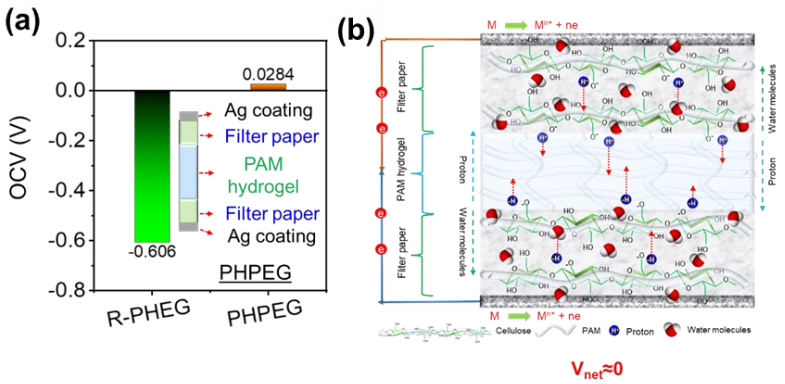

Figure 5.15 a) The output voltage of devices using different assembly methods. b) Schematic illustration of the power generation mechanism of the paper-hydrogel-paper structure.

To evaluate the stability and adaptability of PHEG, we recorded the voltage output of the device under varying temperatures and humidity was recorded (Figure 5.16). Temperature and humidity have a significant impact on the output performance of such devices. To study the effect of temperature on the device's output voltage, we first placed the device in a 4°C refrigerator for voltage measurement. Then, the device was removed and tested at room temperature, followed by testing in a 50°C oven. The results showed that the device's output voltage increased with temperature. This may be because higher temperatures speed up water molecule movement, leading to higher voltage output.

Testing in a controlled low-humidity (5 RH%) environment (with a desiccant) and high-humidity (95 RH%, using a humidifier) environment confirmed that the device's voltage output remains unaffected by external humidity variations. This highlights that its output is derived solely from the internal hydrogel moisture. Additionally, materials including tape, graphite paper, and paper also partially block external moisture, further differentiating PHEG from typical moist-electric generation devices.

Unlike traditional moisture-based power generation devices that rely on external moisture, PHEG derives its functionality from the moisture retained within its internal hydrogel. [225] As a result, its voltage output remains consistent across a wide range of humidity levels, including low humidity (5% RH), normal humidity (50% RH), and high humidity (95% RH).

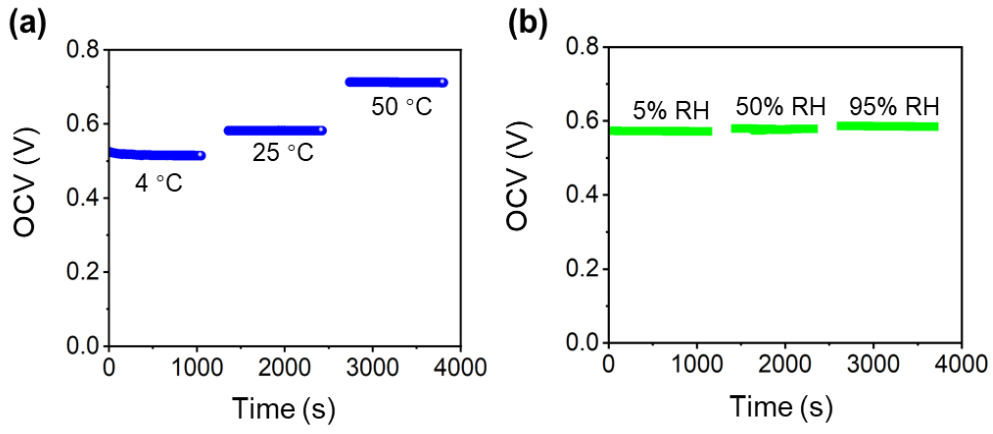

Figure 5.16 a) Output voltage curves of PHEG device at different temperatures. b) Output voltage curves of PHEG device at different humidity.

In addition, the device's voltage output increases with rising temperature, likely due to the accelerated movement of water molecules at higher temperatures, resulting in a higher voltage output. [221] The short-circuit current of the device over time (Figure 5.17) was also measured and found to resemble the discharge current profiles of similar devices. [225]Similar to moisture-powered devices, the current of the device rapidly drops after discharging. However, when not discharging, the open-circuit voltage remains relatively stable. Therefore, the duration of the voltage output is often used to estimate the device's lifespan.

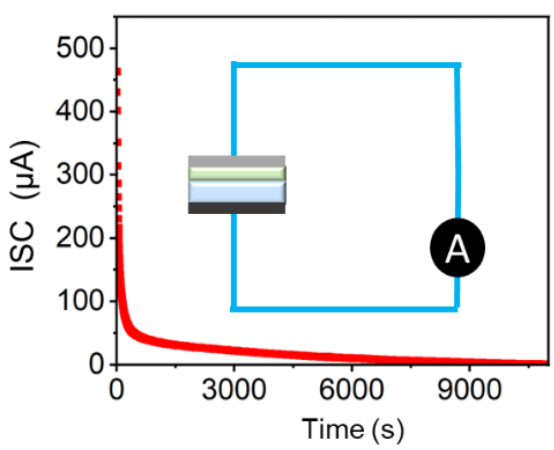

Figure 5.17 Short-circuit current curve of the PHEG device over time.

Furthermore, PHEG demonstrates self-charging capabilities without requiring external stimulation after discharge, similar to other moisture generators (Figure 5.18). [226] This process is similar to how a capacitor works. When protons diffuse into the hydrogel, the device becomes charged. After short-circuit discharge, electrons return through the external circuit, and the internal protons diffuse back to their original position. As a result, the current quickly drops to zero, and the voltage also returns to around 0 V. However, because there is still a concentration gradient of ions, protons start to diffuse again, allowing the device to recharge.

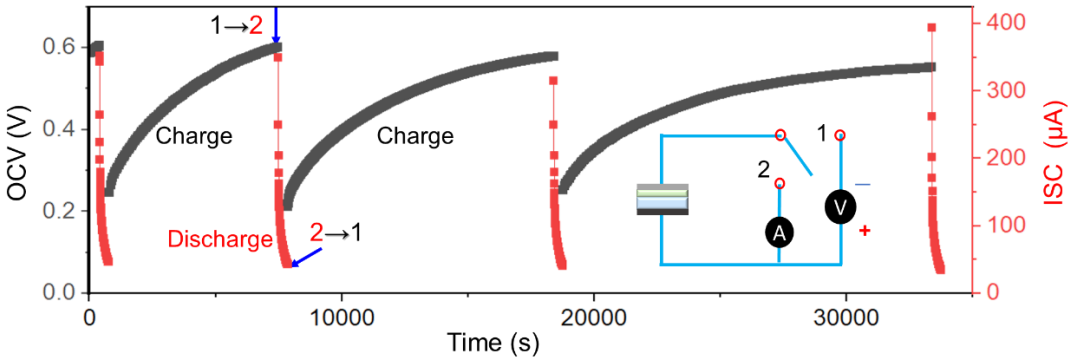

Figure 5.18 The circular charge and discharge process of PHEG.

5.2.3 The output performance of PHEG using different papers

Upon grasping the underlying operational mechanism, the output performance of PHEG assembled with other commercial papers was also assessed. Figure 5.19a displays the visual appearance of the original and Ag-coated papers. Parameters related to distinct papers are documented in Tables 2.1 and 2.2. Figure 5.19b exhibits the CA of water (<90°) on different paper surfaces, revealing their capacity to absorb water. However, while hydrophilicity is a necessary condition for power generation in the device, it alone does not guarantee functionality. For example, the glass (hydrophilicity)-assembled PHEG cannot generate electricity (as mentioned above). Furthermore, the zeta potentials of these papers were also negative (<0, Figure 5.19c). As a result, these papers can ionize and provide protons, which is similar to the filter paper.

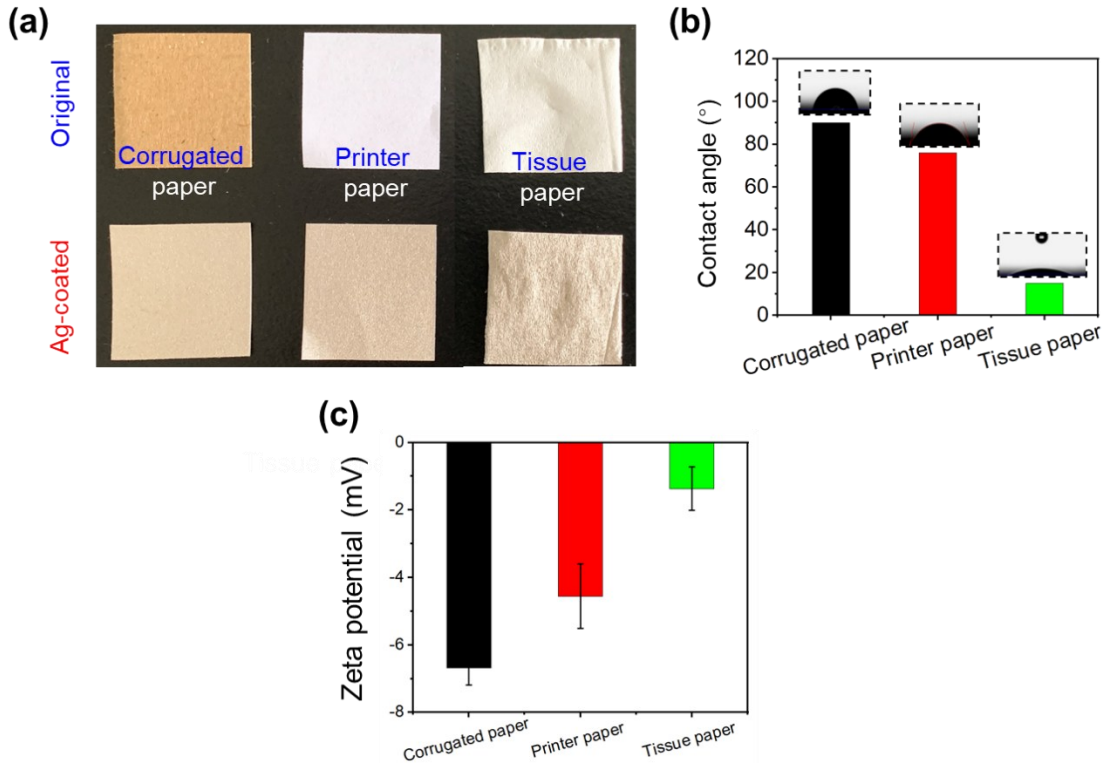

Figure 5.19 a) Photographs of various papers with or without Ag coating. b) Water CA of different papers. c) Zeta potential of different papers.

Figure 5.20a depicts the output voltages of PHEGs assembled with different papers over the first 10 hours, revealing a gradual increase in voltage that supports the previous hypothesis. Analysis of the average voltage during this period indicates that tissue paper and printing paper produce relatively lower voltages (Figure 5.20b), which may be attributed to their loose structure or a higher concentration of fillers (Figure 5.20c).

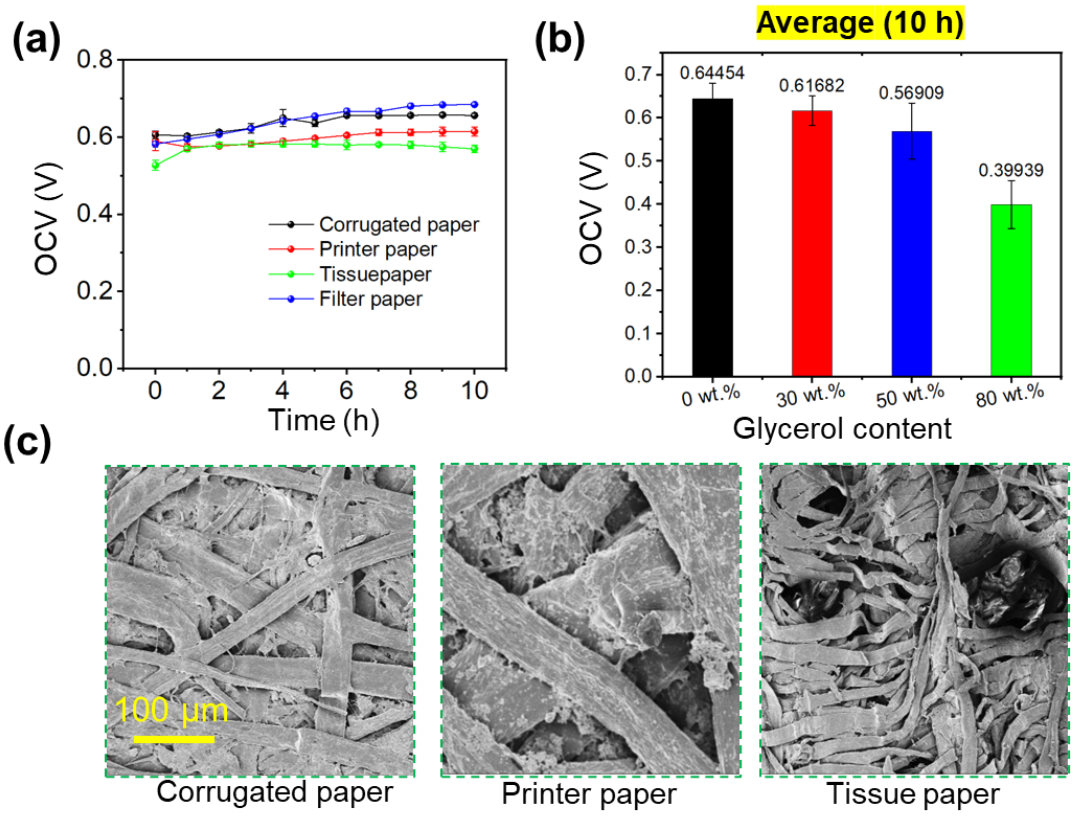

Figure 5.20 a) The output voltage (0-10 h) of PHEG assembled from different papers. b) Average voltage of the first 10 h for different PHEG. c) SEM images of different papers. The detailed parameters of the paper and hydrogels are provided in Tables 2.1, 2.2, and 2.5. respectively. The ambient temperature during the test was 25 ± 5 ℃.

5.2.4 Output performance of PHEG using various hydrogel films

In addition to the proton transport layer, the performance of PHEG is influenced by the PAM hydrogel layer. As demonstrated in Figure 5.21a, modifications to the crosslinker of the hydrogel film resulted in a consistent output voltage across the assembled PHEG device. In addition, alterations in the thickness of the hydrogel had minimal effect on the device's output voltage (Figure 5.21b).

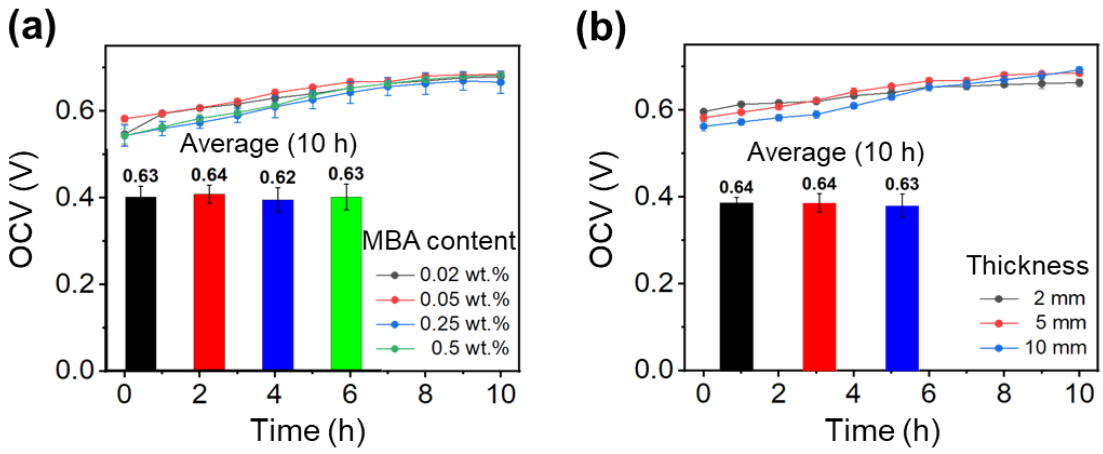

Figure 5.21 The output performance of PHEG using various hydrogel compositions and the same filter paper. The output voltage (0–10 h) of PHEG assembled from different a) cross-linking agents, and b) thickness of hydrogels.

However, devices utilizing thicker hydrogels exhibited prolonged output lifetime due to an extended water delivery capability (Figure 5.22). Paper deformation due to moisture absorption presents a challenge in maintaining structural stability. To address this issue, we propose to remove the moisture from the detached paper through hot pressing or by incorporating the paper into industrial recycling processes for waste paper. These approaches would significantly enhance paper utilization and reduce the manufacturing costs of the device. During operation, progressive deformation of the paper substrate may occur. To minimize this effect, a stabilization method involving the use of adhesive tape has been adopted to secure the device effectively.

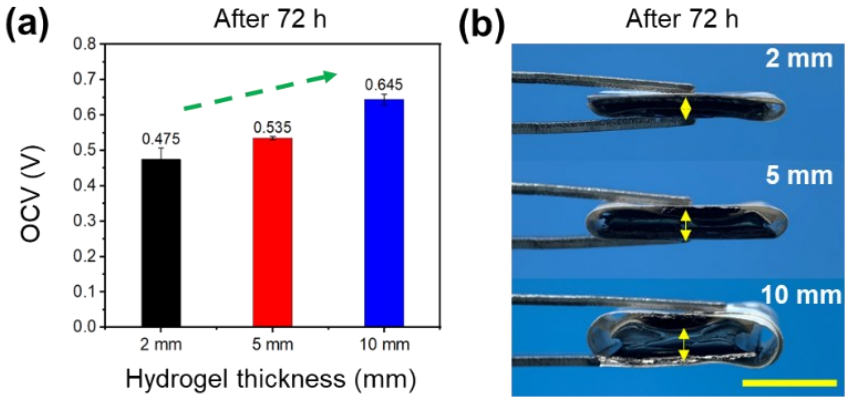

Figure 5.22 a) After 72 h of operation, the voltage of PMEGs with different thicknesses of PAM hydrogels. b) After 72 h of operation, the appearance of PMEG devices with different thicknesses of PAM hydrogels.

Furthermore, varying glycerol contents in the PAM hydrogels were achieved by

substituting a portion of water with glycerol. As shown in Figure 5.23a, it is evident that the output voltage of the device experiences a substantial decrease as the glycerol content in the hydrogel increases. This observation implies that the water content at the interface between the hydrogel and the paper holds a more substantial impact on the device's voltage. The conductivity of the hydrogel decreased gradually with increasing glycerol content (Figure 5.23b).

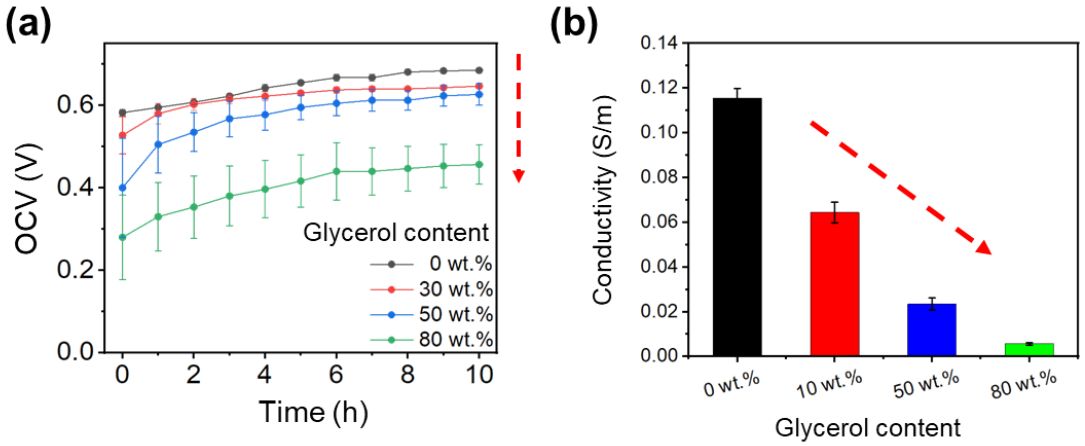

Figure S5.23 a) The output voltage (0-10 h) of PHEG assembled from different glycerol content of hydrogels. b) The conductivity of PAM hydrogels composed of different glycerol contents.

However, glycerol exerted a favorable impact on enhancing the moisture-retaining capability of the hydrogel [60, 72]. The higher the glycerol content, the greater the weight and shape retention of the hydrogel during storage (Figure 5.24a and b). The effect of glycerol content on device performance is demonstrated in Figure 5.24c. Devices assembled with PAM hydrogels containing 50 wt.% glycerol exhibited an operational lifespan exceeding 1000 h, significantly longer than that of pristine PHEG. This enhancement can be attributed to the role of graphite paper and filter paper in reducing water volatilization evaporation from the hydrogel, as compared to bare hydrogel films. Most importantly, the strong hydrogen bonding between glycerol and water effectively enhances water retention and regulates its diffusion. [72] The fact that the device's output drops after reaching its peak is primarily due to the limited availability of protons provided by the paper substrate [195].

Besides experiencing water loss, hydrogels are susceptible to freezing in colder conditions, leading to device malfunctions. As illustrated in Figure 5.24d, both the pristine and low glycerol (30 wt.%) hydrogels became entirely white and lost their

electrical conductivity after exposure to –24 °C for 24 h. In contrast, the hydrogel with high glycerol content (50 and 80 wt.%) retained its transparency and partial conductivity, thereby preserving the flexibility of the device. The compressive strength of the pure PAM hydrogel (Figure 5.24e) was observed to be much greater than that of the 50 wt.% glycerol hydrogels, suggesting that the original hydrogel resembled an ice cube and lost its elasticity completely (Figure 5.24f). In particular, the device's output voltage is 0 V because the water is frozen. Simultaneously, the device's voltage assembled with 50 wt.% glycerol hydrogels also decreased, likely due to the slower movement of water molecules and protons at low temperatures. Achieving a balance between the device's output performance, operational lifespan, and extreme environmental adaptation is imperative. [227]

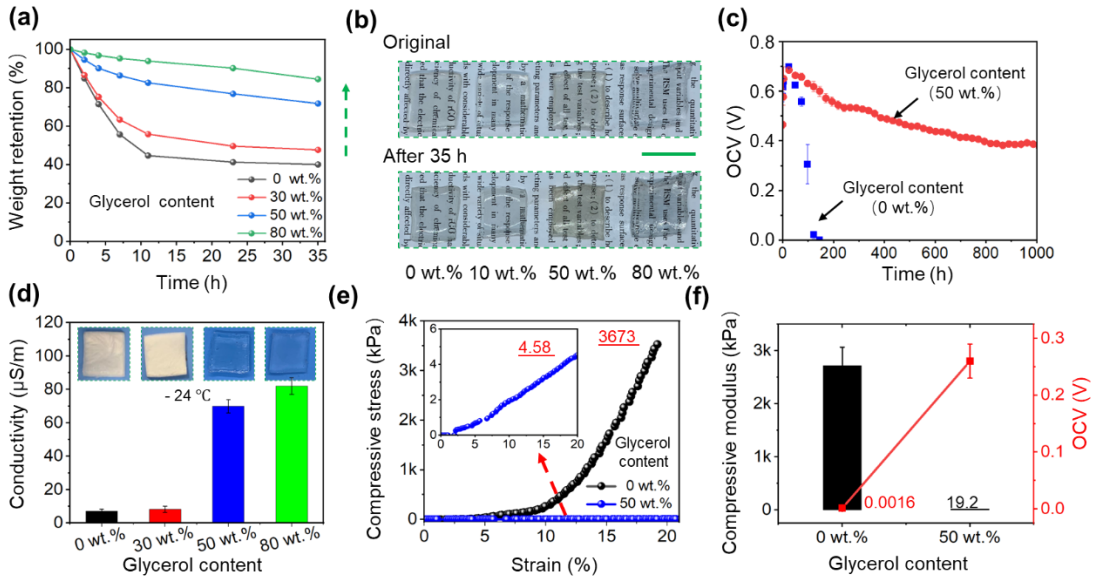

Figure 5.24 a) The weight retention rate of bare PAM hydrogel with various glycerol contents. b) Photographs of PAM hydrogels with different glycerol contents before and after 35 h storage (25 ± 5 °C). Scale bar: 2 cm. c) The output voltage of PHEG using PAM hydrogels with 0 wt.% and 50 wt.% glycerol contents at different storage times (25 ± 5 °C). d) The conductivity of PAM hydrogels with different glycerol content at –24 °C. The inserted images represent the actual appearance of PAM hydrogels with different glycerol contents after storage at –24 °C for 24 h. e) The typical compressive stress-strain curves, f) compressive modulus and output voltage of PAM hydrogels with 0 wt.% and 50 wt.% glycerol contents after storage at –-24 °C for 24 h.

Additionally, we evaluated the output voltage of devices assembled using PAA and PVA hydrogels (Figure 5.25). The adhesion of PVA devices is too poor, and it is difficult to adhere to paper and graphite electrodes, making it difficult to transfer moisture. On the contrary, PAA is too adhesive and is easily pulled and damaged during the assembly

process, resulting in a low yield rate of the device. PAM hydrogel has moderate adhesion and does not have this problem. So, PAM hydrogel was finally chosen.

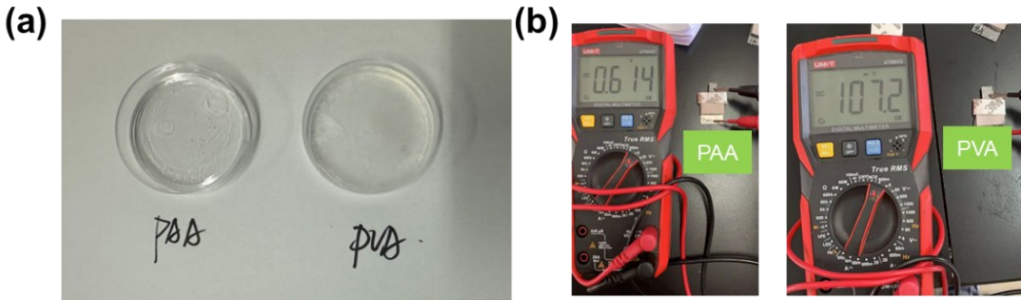

Figure 5.25 a) Appearance of PAA and PVA hydrogels. b) Output voltage of devices assembled with PAA and PVA hydrogels.

5.2.5 Comprehensive application of PHEG

The robust endurance and environmental adaptability of the glycerol-doped PAM hydrogel and its assembled PHEG were highlighted above. However, it is commonly observed that PHEG assembled from glycerol-free PAM gel tends to possess a higher initial voltage, rendering it more suitable for immediate use. The PHEG depicted below comprises glycerol-free PAM hydrogel and filter paper. As illustrated in Figure 5.26a, the device's output power was evaluated immediately after attaching the paper, hydrogel, and electrode, yielding a maximum output power of ~1.61 $\mu W/cm^2$. This significantly surpasses the performance of most wet electric generators under normal conditions (RH < 50%) (Table 5.1). Figure 5.26b also demonstrates that the freshly assembled PHEG can directly charge capacitors of different capacitances without the need for waiting.

Table 5.1 Performance comparison between PHEG and moist generator at regular RH%

Material	RH/ ΔRH (%)	Voltage (V)	Area (cm^2)	Maximum areal current density ($nAcm^{-2}$)	Maximum areal power density ($nW\ cm^{-2}$)	Reference
Protein nanowire	35	0.32	0.25	140	44.8	[152]
Graphene oxide bulk	25	0.2	0.04	90	18	[228]
Gradient graphene oxide and graphene oxide	20	0.52	0.16	94	48.9	[229]
Graphene oxide and sodium polyacrylate	40	0.45	0.1	-	-	[187]
Graphene oxide film	20	0.08	0.25	-	-	[230]
TiO_2 nanowire	40	0.07	1.44	430	30	[231]
Biological nanofiber	55	0.02	1	-	-	[189]
Gradient polypyrrole foam	40	0.012	-	2000	24	[232]
Paper	20	0.05	1.5	-	-	[207]
Bilayer of polyelectrolyte film	27	0.95	0.6	80	76	[195]
Filter paper/PAM hydrogel	**-**	**0.6**	**4**	**12500**	**1610**	**This work**

"**—**": not available in the references.

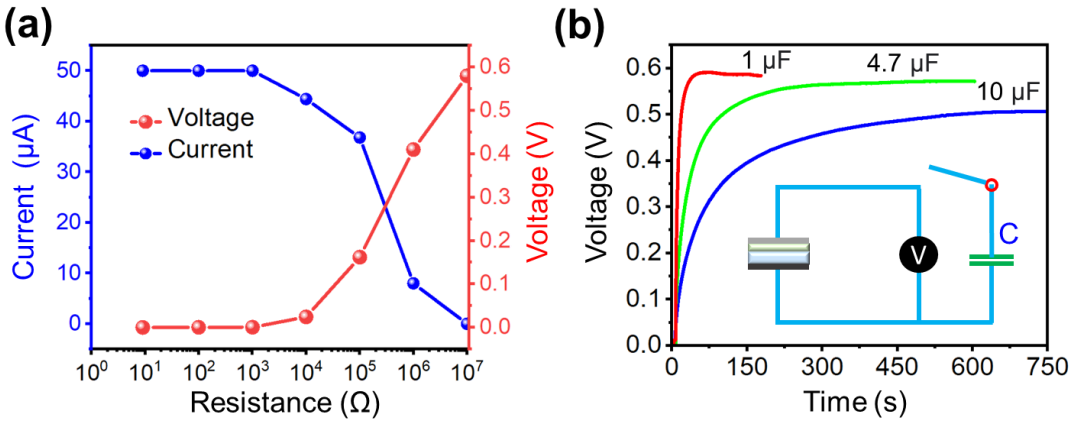

Figure 5.26 a) Dependence of PHEG's output current and voltage on the electrical resistance of the external circuit. b) Voltage-time curves of commercial capacitors charged by a PHEG. The inset is a charge storage circuit.

Furthermore, the output voltage of the device can be gradually increased by stacking PHEGs in series (Figure 5.27a). Similarly, stacking PHEGs in parallel results in a stepwise increase in the device's output current (Figure 5.27b). Figure 5.27c demonstrates the assembly of 10 PHEG units stacked together, occupying a volume of only ~26.62 cm^3. Its volume is smaller than that of four AA batteries (~30.78 cm^3), yet it yields a comparable output voltage of ~6V. Significantly, the 5-unit PHEG configuration effortlessly fulfills the power requirements of a large-sized calculator (Figure 5.27d).

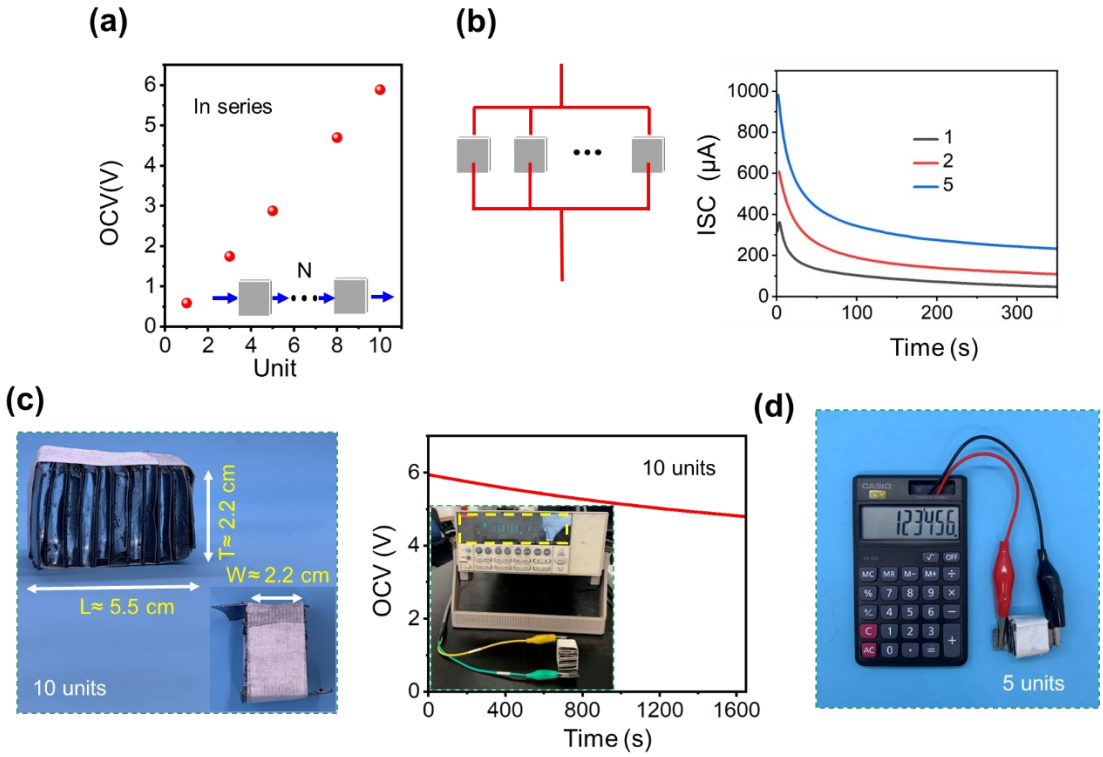

Figure 5.27 a) Linear relationship between the in-series units of PHEG and voltage. b) Schematic diagram of different PHEGs connected in parallel. The output current of different numbers of PHEGs is connected in parallel. c) The appearance and size of PHEG assembled by 10 units. Real-time output voltage curve of PHEG assembled by 10 units. d) Demonstration of a PHEG assembled from 10 units as a commercial calculator power supply.

PHEG displays a voltage variation upon application of pressure (Figure 5.28a). In contrast, both PEG and HEG fail to generate discernible voltage signals. As shown in Figure 5.28b, pressing the PHEG with a finger results in a voltage drop followed by a subsequent recovery, effectively functioning as a self-powered pressure sensor. This sensing mechanism is attributed to the compression of the elastic hydrogel by pressure, resulting in a change in the local proton concentration. [133, 155] Figure 5.28c depicts the dynamic pressure detection of the sensor up to 1230 cycles, showcasing its impressive stability.

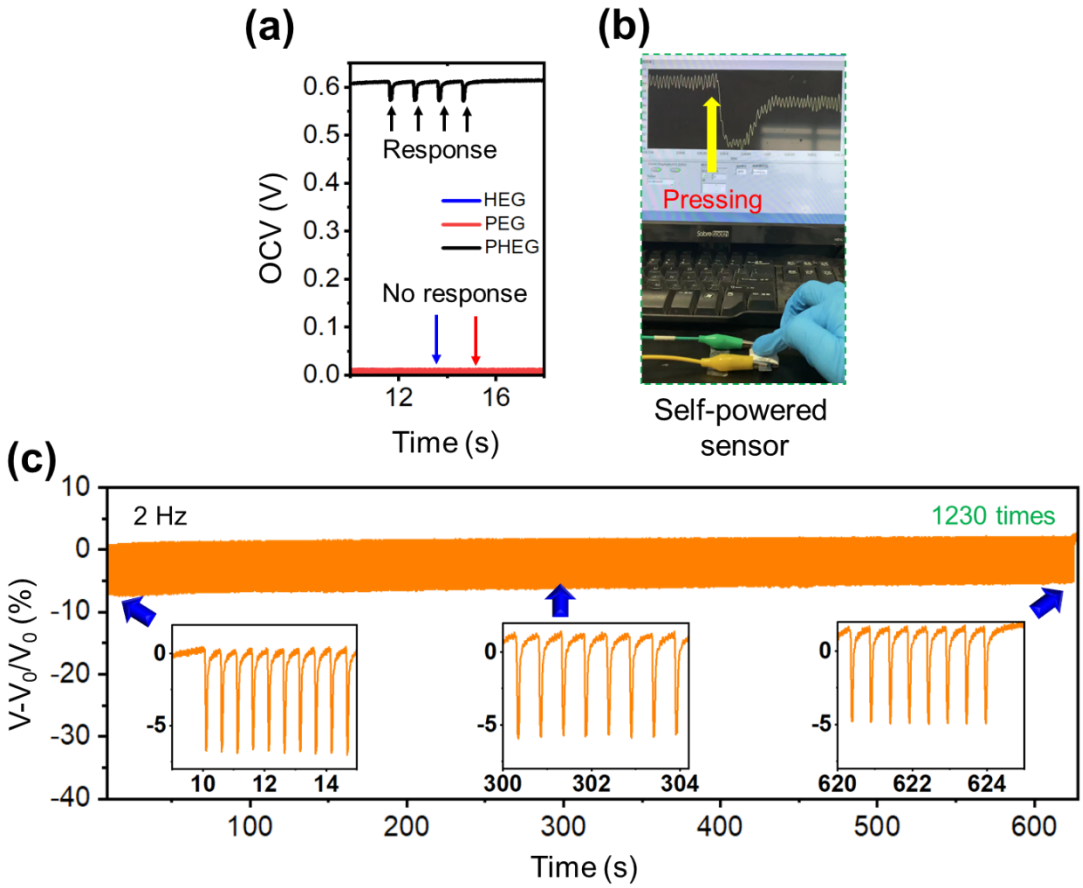

Figure 5.28 a) The voltage response of different devices (HEG, PEG, and PHEG) for dynamic pressing operation. b) Schematic diagram of the self-powered PHEG sensor responding to the pressing process. c) The pressing response stability of the self-powered PHEG sensor (2 Hz; 1230 times).

The device has been successfully utilized as a self-powered strain sensor for detecting finger bending (Figure 5.29a). In addition, the glycerol-doped PAM hydrogel-assembled PHEG has also demonstrated utility in strain detection at -24 °C (Figure 5.29b).

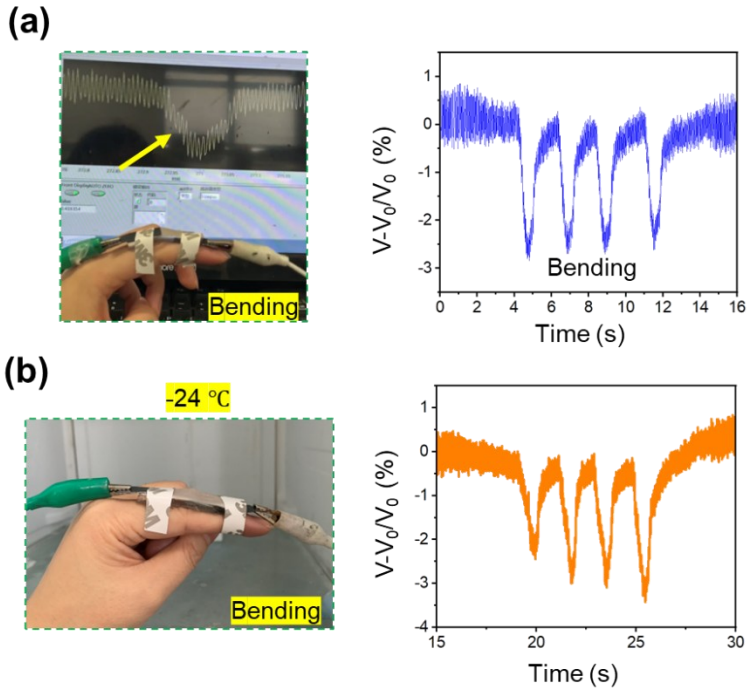

Figure 5.29 a) PHEG as strain sensor for finger bending sensing. b) PHEG assembled from 50% glycerol PAM hydrogel as a strain sensor for finger bending sensing.

5.3 Conclusions

In conclusion, we have designed and prepared an electricity-generating integrated PHEG. The device is simple to fabricate, using PAM hydrogel as a bonding layer to easily adhere the top filter paper coated with Ag and the bottom graphite paper electrode firmly together. Through the permeation of water from the hydrogel to the filter paper, cellulose in the filter paper is ionized, producing protons. The concentration gradient of protons drives their diffusion towards the hydrogel section, generating direct current in the external circuit. At the same time, the metal coating of the asymmetric electrode will also ionize when it comes into contact with water, generating electrons, which in turn supply part of the output voltage of the device. The PHEG efficiently produces a voltage of ~0.6 V, a current of ~12.5 μA/cm^2, and a max power of ~1.61 μW/cm^2. By stacking 10 units of PHEG, a battery-like power component is formed, providing a reliable 6 V DC voltage. Moreover, the PHEG featuring PAM gel enriched with 50% glycerol showcases enduring voltage generation for over 1000 hours without external stimulation. Other types of paper, such as printing paper, tissue paper, and corrugated paper, have been shown to possess similar power generation capabilities. Interestingly, the PHEG can serve as steady self-powered strain and pressure sensors (1230 times).

PHEG is thus promising as a low-cost, environmentally friendly device. Unlike other moisture-electricity generators, it is not subject to continuous disruptions from unstable external moisture supply. Therefore, its application in wearable electronic devices, such as small-scale generators and self-powered sensors, holds immense potential for the development of self-sufficient portable energy devices.

In addition, we present three key innovations in our moisture-powered device. First, traditional moisture-powered devices typically use either paper or hydrogel and rely on external moisture sources. We creatively combined paper with hydrogel, where the hydrogel can continuously supply water to stable device operation over long periods (1000 h). As a result, this device no longer depends on external moisture, greatly improving its portability and stability. Second, the excellent adhesive properties of PAM hydrogel facilitate a strong bond between the paper and the electrodes, ensuring high device integration and eliminating gaps that are typically present between the electrodes and active layer in moisture-powered devices. Lastly, the inclusion of an elastic hydrogel provides excellent compression deformability, enabling stable performance under pressure. This feature makes the device suitable for use as a flexible sensor. Unlike traditional hydrogel sensors that require an external power supply, our device is self-powered, thus expanding its potential applications in wearable devices and smart sensing systems.

6 CONCLUSIONS AND PERSPECTIVES

Conclusions

This study systematically explores the design and development of hydrogel-based devices capable of generating DC and functioning as self-powered pressure sensors. Starting from the fundamental mechanism of ion movement under mechanical deformation in a single hydrogel, the research progresses toward an output-enhanced, bioinspired bilayer polyelectrolyte hydrogel, and finally achieves a high-output, stable paper–hydrogel hybrid power generator. The main findings and innovations are summarized as follows:

Part I: We developed a highly elastic and conductive hydrogel based on polyelectrolyte PAA. By exploiting the mobility difference between cations and immobile anions under compression, this hydrogel converts mechanical pressure into a measurable DC output. Specifically, mechanical stress increases the local ion concentration inside the hydrogel; while the fixed anionic backbone remains stationary, protons migrate toward the region of lower concentration, thereby generating a continuous DC signal in the external circuit. The device responds reliably to varying pressure levels and can serve as a self-powered position or even sound sensor. Importantly, this mechanism is also applicable to other polyelectrolyte hydrogels, demonstrating broad potential for mechanical energy harvesting.

Part II: Inspired by the asymmetric ion distribution in red blood cell membranes, we constructed a bilayer polyelectrolyte gradient hydrogel to enhance output voltage. This structure combines an ion-containing PVA hydrogel layer (with LS as the anionic source or QC as the cationic source) with a neutral PVA layer. The interface forms a strong ionic concentration gradient. Devices based on PVA-LS and PVA show an initial DC output over 100 mV—an order of magnitude higher than the single-layer PAA hydrogel. Connecting 10 of these devices in series can generate up to 1.29 V, enough to power small electronics like calculators. This bilayer system also functions well as a self-powered pressure sensor.

Part III: To further improve device stability and practicality, we developed a paper–hydrogel hybrid generator (PHEG), integrating PAM hydrogel with a silver-coated cellulose paper electrode. Water from the hydrogel diffuses into the paper, triggering

ion release from cellulose and inducing a mild galvanic reaction with the Ag layer, thus producing stable electrical output. The device can deliver up to 0.6 V and shows excellent long-term performance. After adding glycerol to maintain hydration, the generator continues working for over 1000 hours. Its modular design allows multiple units to be connected in series for higher voltages—up to 6 V with 10 units—making it suitable for powering larger electronics or charging storage devices. In addition to power generation, the PHEG also functions as a flexible and reliable pressure sensor.

This research outlines a clear path from fundamental principles to practical applications in hydrogel-based energy devices. The proposed systems are low-cost, eco-friendly, and easy to fabricate—relying only on water-soluble polymers, biomass-derived polyelectrolytes, and paper materials, without the need for complex microfabrication. Their flexibility and biocompatibility make them especially suitable for integration into wearable electronics, such as self-powered electronic skin and flexible sensors, offering promising potential for future applications.

Perspectives

Although this study successfully developed a series of hydrogel-based DC generators and self-powered pressure sensors, and gradually improved their voltage output through structural optimization—showing potential for powering small electronics and pressure sensing applications—several key challenges remain before practical use can be achieved:

Water loss and stability of hydrogels: Hydrogels are soft and skin-friendly, making them ideal materials for skin-contact wearable electronic devices. However, unlike traditional elastomers, their high-water content makes them highly prone to evaporation, which leads to reduced flexibility and long-term performance degradation. In open environments or under high temperatures, hydrogel-based devices are more likely to dry out and become brittle, compromising their structural integrity and functional stability.

One commonly used approach to mitigate water loss is incorporating humectants such as glycerol, inorganic salts, ethylene glycol, (ILs, or DES into the hydrogel system. For example, in this study, glycerol was added to help slow down water evaporation. While these additives can improve water retention in the short term, they are still insufficient

to fully prevent dehydration, and challenges remain in maintaining structural and functional stability over time.

To improve anti-drying performance, more effective protection strategies are needed. For instance, Jian Xu's team proposed an innovative method by forming a flexible elastomer coating directly on the surface of PAM hydrogels via surface-confined copolymerization (Figure 6.1). This elastomer layer significantly reduces water evaporation and enhances environmental adaptability. However, it is important to note that although elastomer coatings can effectively reduce water loss, most elastomers differ greatly from hydrogels in mechanical properties, such as modulus and softness. This mismatch may cause delamination or mechanical failure at the interface during repeated bending or deformation. Therefore, the mechanical compatibility between the coating and hydrogel should be carefully considered when designing encapsulation strategies to ensure long-term stability in practical applications.

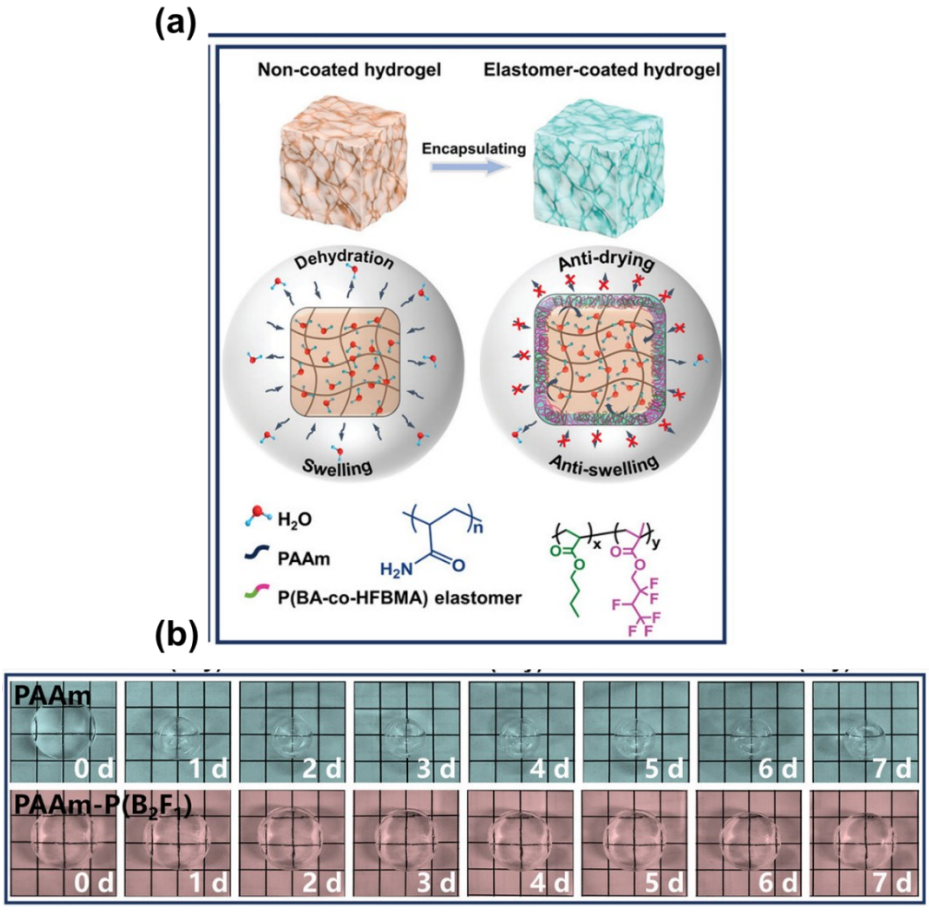

Figure 6.1 a) Schematic illustration of the anti-drying and anti-swelling for the elastomer-encapsulated hydrogels. b) Photographs documenting the changes in PAM (top) and elastomer-encapsulated PAM hydrogels (bottom) hydrogels overtime during the air-drying test. [233]

In another study, Zisheng Luo's group reported in *Science* Journal a new method to protect hydrogels by treating PAM-polysaccharide hydrogels with concentrated sulfuric acid. This reaction forms glycosidic polymer fragments and branching structures, which carbonize in place after drying for 48 hours, resulting in a dense carbon dot layer (Figure 6.2). This carbon layer acts as a moisture barrier, preventing water loss even at temperatures up to 143 °C, while maintaining the flexibility and stretchability of the hydrogel. Although this method shows excellent anti-drying performance, the use of concentrated sulfuric acid may affect the hydrogel's biocompatibility, which calls for the development of gentler yet effective alternatives.

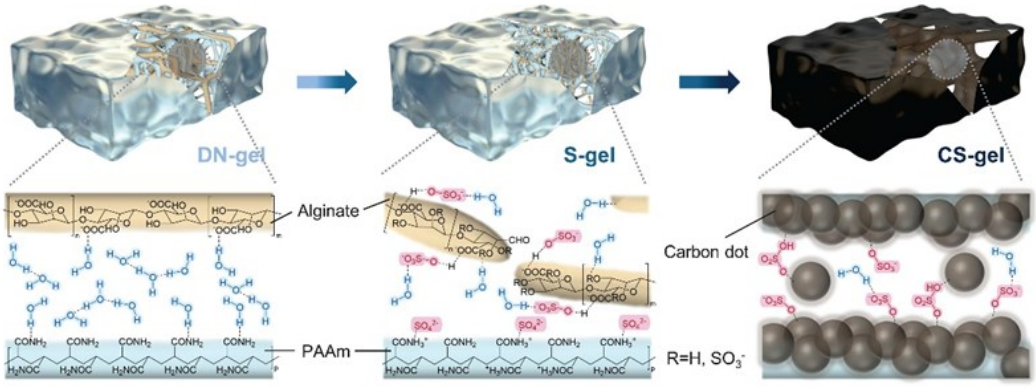

Figure 6.2 Schematic illustration of in situ formation of a carbon dot barrier on the surface of PAM hydrogel.[234]

Additionally, Hongbo Zeng's team highlighted that free water in hydrogels evaporates easily, while bound water is much more stable. Inspired by the structure of the stratum corneum, they developed a zwitterionic hydrogel that retains bound water after removing most free water (Figure 6.3). This design significantly improves water retention under various conditions while preserving the hydrogel's soft mechanical properties. The strong interaction between the bound water and the zwitterionic polymer network is considered a key factor in improving anti-drying performance.

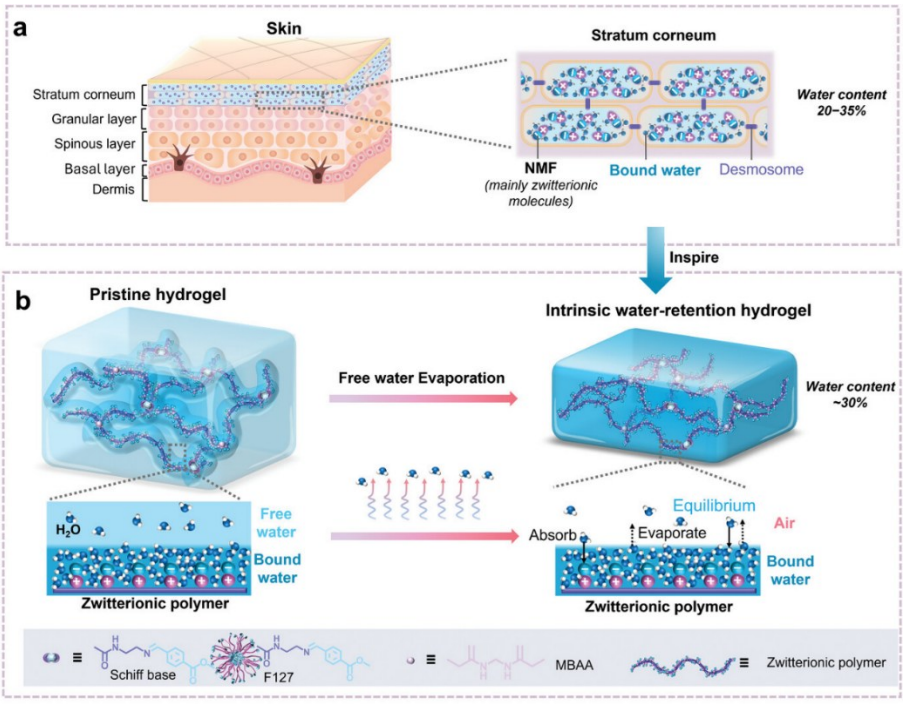

Figure 6.3 Design of intrinsically anti-dehydration hydrogels composed of zwitterionic polymers and bound water. a) Schematic illustration of the structures of skin and stratum corneum. b) Fabrication process and structure of stratum corneum-inspired hydrogels composed of zwitterionic polymers and bound water.[235]

In summary, these strategies offer promising solutions to enhance the structural stability and functional reliability of hydrogel-based devices, paving the way for their broader application in challenging environments.

Low voltage output and the need for hybrid strategies: Even though the performance of hydrogel-based DC generators has improved, their output voltage is still much lower than that of other technologies like TENGs. This is mainly because the electric potential generated by ion movement in hydrogels is relatively weak, usually in the range of hundreds of millivolts to ~1 volts—too low to meet the needs of many electronic devices.

To overcome this, two strategies are recommended: (1) strengthen the internal ion gradient or double-layer structure through material design, and (2) increase the total voltage by connecting multiple hydrogel units in series.

The first strategy focuses on enhancing the output of individual units, but the improvement is often limited. In contrast, connecting multiple units in series is a more

effective and straightforward way to boost overall device performance.

Inspired by the electric eel, Thomas B. H. Schroeder and colleagues reported in Nature a hydrogel-based power generation system that uses ion gradients between micro-compartments made of cation- and anion-selective hydrogel membranes (Figure 6.4). By arranging these compartments in a scalable stacked or folded structure—similar to series connections—they achieved synchronized activation through mechanical contact. This setup enabled self-powered energy generation, with the device reaching an open-circuit voltage of up to 110 V.

We could stack or fold multiple devices together using 3D printing to boost the output. However, this would need precise fabrication methods, so more research is still needed.

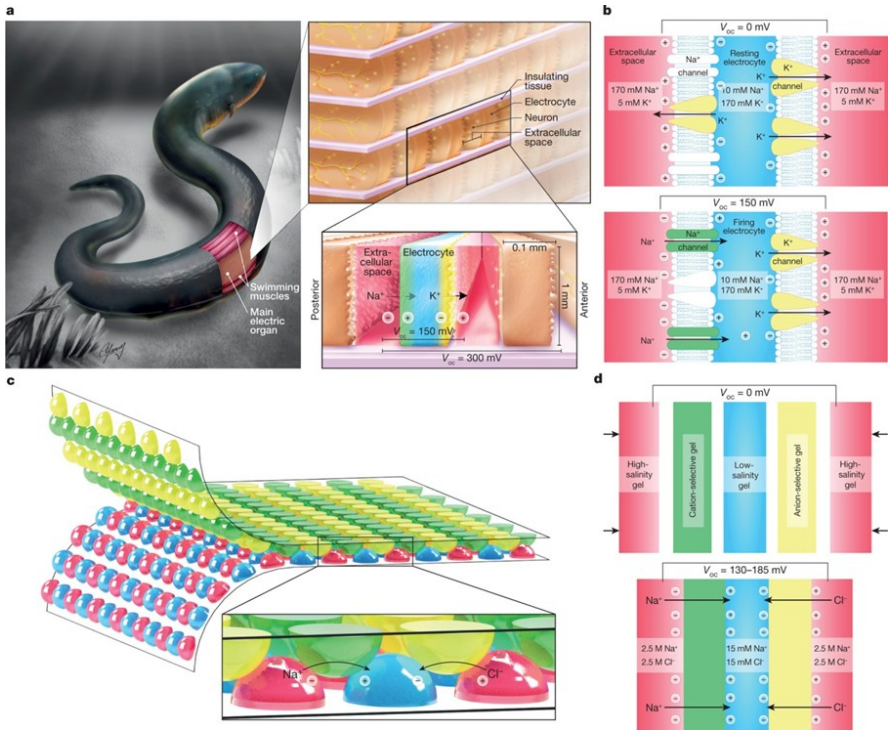

Figure 6.4 Morphology and mechanism of action of the eel's electric organ and the artificial electric organ.[143]

Slow response and signal instability

Hydrogel sensors based on ion movement work well for slow or static pressure changes, but they struggle with fast, high-frequency inputs. This is because ions move slowly in the hydrogel network, which leads to delayed or unstable voltage signals, signal drift, and noise—making it hard to get accurate, real-time data. In addition, the voltage output

of devices is unstable, which makes it more difficult to accurately read the pressure signals.

To address these issues, one approach is to enhance the material properties by tuning the crosslinking density, pore structure, or ion transport pathways to accelerate ion mobility. Additionally, advanced signal processing techniques—such as machine learning algorithms—can be employed to denoise and correct the raw electrical signals in real time. Together, these strategies can significantly improve both the stability and accuracy of sensor outputs, particularly under complex or dynamic conditions.

7 BIBLIOGRAPHIE

[1] D. Won, J. Bang, S.H. Choi, K.R. Pyun, S. Jeong, Y. Lee, S.H. Ko, Transparent Electronics for Wearable Electronics Application, Chemical Reviews 123(16) (2023) 9982-10078.
[2] N.A. Choudhry, L. Arnold, A. Rasheed, I.A. Khan, L. Wang, Textronics—A Review of Textile-Based Wearable Electronics, Advanced Engineering Materials 23(12) (2021) 2100469.
[3] S.M.A. Iqbal, I. Mahgoub, E. Du, M.A. Leavitt, W. Asghar, Advances in healthcare wearable devices, npj Flexible Electronics 5(1) (2021) 9.
[4] K. Meng, X. Xiao, W. Wei, G. Chen, A. Nashalian, S. Shen, X. Xiao, J. Chen, Wearable Pressure Sensors for Pulse Wave Monitoring, Advanced Materials 34(21) (2022) 2109357.
[5] Y. Li, Y.A. Samad, K. Liao, From cotton to wearable pressure sensor, Journal of Materials Chemistry A 3(5) (2015) 2181-2187.
[6] J. Kim, E.-F. Chou, J. Le, S. Wong, M. Chu, M. Khine, Soft Wearable Pressure Sensors for Beat-to-Beat Blood Pressure Monitoring, Advanced Healthcare Materials 8(13) (2019) 1900109.
[7] K. Liu, M. Wang, C. Huang, Y. Yuan, Y. Ning, L. Zhang, P. Wan, Flexible Bioinspired Healable Antibacterial Electronics for Intelligent Human-Machine Interaction Sensing, Advanced Science 11(10) (2024) 2305672.
[8] P. Di, Y. Yuan, M. Xiao, Z. Xu, Y. Liu, C. Huang, G. Xu, L. Zhang, P. Wan, A Flexible Skin Bionic Thermally Comfortable Wearable for Machine Learning-Facilitated Ultrasensitive Sensing, Advanced Science 11(32) (2024) 2401800.
[9] M.A. Butt, N.L. Kazanskiy, S.N. Khonina, Revolution in Flexible Wearable Electronics for Temperature and Pressure Monitoring—A Review, Electronics 11(5) (2022) 716.
[10] R.B. Mishra, N. El-Atab, A.M. Hussain, M.M. Hussain, Recent Progress on Flexible Capacitive Pressure Sensors: From Design and Materials to Applications, Advanced Materials Technologies 6(4) (2021) 2001023.
[11] H. Li, Z. Wang, M. Sun, H. Zhu, H. Liu, C.Y. Tang, L. Xu, Breathable and Skin-Conformal Electronics with Hybrid Integration of Microfabricated Multifunctional Sensors and Kirigami-Structured Nanofibrous Substrates, Advanced Functional Materials 32(32) (2022) 2202792.
[12] A. Chortos, J. Liu, Z. Bao, Pursuing prosthetic electronic skin, Nature Materials 15(9) (2016) 937-950.
[13] S. Sharma, A. Chhetry, M. Sharifuzzaman, H. Yoon, J.Y. Park, Wearable Capacitive Pressure Sensor Based on MXene Composite Nanofibrous Scaffolds for Reliable Human Physiological Signal Acquisition, ACS Applied Materials & Interfaces 12(19) (2020) 22212-22224.
[14] J.C. Yang, J. Mun, S.Y. Kwon, S. Park, Z. Bao, S. Park, Electronic Skin: Recent Progress and Future Prospects for Skin-Attachable Devices for Health Monitoring, Robotics, and Prosthetics, Advanced Materials 31(48) (2019) 1904765.
[15] C.-C. Kim, H.-H. Lee, K.H. Oh, J.-Y. Sun, Highly stretchable, transparent ionic touch panel, Science 353(6300) (2016) 682-687.
[16] X. Pan, J. Guan, S. Cao, X. Ma, Y. Ni, Q. Wang, An oxidative metal ions-free lignin-catalyzed multifunctional hydrogel bioelectronics for codable eye communication, Journal of Colloid and Interface Science 680 (2025) 753-761.
[17] F. Lin, Y. Qiu, X. Zheng, Z. Duanmu, Q. Lu, B. Huang, L. Tang, B. Lu, One-pot mechanochemical assembly of lignocellulose nanofiber/graphite nanocomposites for

wearable electronic devices, Chemical Engineering Journal 437 (2022) 135286.
[18] T. Huang, M. Lu, H. Yu, Q. Zhang, H. Wang, M. Zhu, Enhanced Power Output of a Triboelectric Nanogenerator Composed of Electrospun Nanofiber Mats Doped with Graphene Oxide, Scientific Reports 5(1) (2015) 13942.
[19] Z. Pengyu, L. Zihan, P. Jinbo, H. Peng, Z. Shuye, Latest developments and trends in electronic skin devices, Soft Science 4(2) (2024) 17.
[20] U. Yaqoob, A.S.M.I. Uddin, G.-S. Chung, A high-performance flexible NO2 sensor based on WO3 NPs decorated on MWCNTs and RGO hybrids on PI/PET substrates, Sensors and Actuators B: Chemical 224 (2016) 738-746.
[21] L. Wang, T. Xu, X. Zhang, Multifunctional conductive hydrogel-based flexible wearable sensors, TrAC Trends in Analytical Chemistry 134 (2021) 116130.
[22] H. Yuk, B. Lu, X. Zhao, Hydrogel bioelectronics, Chemical Society Reviews 48(6) (2019) 1642-1667.
[23] F. Ullah, M.B.H. Othman, F. Javed, Z. Ahmad, H.M. Akil, Classification, processing and application of hydrogels: A review, Materials Science and Engineering: C 57 (2015) 414-433.
[24] S. Ma, B. Yu, X. Pei, F. Zhou, Structural hydrogels, Polymer 98 (2016) 516-535.
[25] S. Bashir, M. Hina, J. Iqbal, A.H. Rajpar, M.A. Mujtaba, N.A. Alghamdi, S. Wageh, K. Ramesh, S. Ramesh, Fundamental Concepts of Hydrogels: Synthesis, Properties, and Their Applications, Polymers 12(11) (2020) 2702.
[26] L. Hu, P.L. Chee, S. Sugiarto, Y. Yu, C. Shi, R. Yan, Z. Yao, X. Shi, J. Zhi, D. Kai, H.-D. Yu, W. Huang, Hydrogel-Based Flexible Electronics, Advanced Materials 35(14) (2023) 2205326.
[27] B. Ying, X. Liu, Skin-like hydrogel devices for wearable sensing, soft robotics and beyond, iScience 24(11) (2021) 103174.
[28] A.H. Karoyo, L.D. Wilson, A Review on the Design and Hydration Properties of Natural Polymer-Based Hydrogels, Materials 14(5) (2021) 1095.
[29] L. Zhao, Y. Zhou, J. Zhang, H. Liang, X. Chen, H. Tan, Natural Polymer-Based Hydrogels: From Polymer to Biomedical Applications, Pharmaceutics 15(10) (2023) 2514.
[30] Z. Bao, C. Xian, Q. Yuan, G. Liu, J. Wu, Natural Polymer-Based Hydrogels with Enhanced Mechanical Performances: Preparation, Structure, and Property, Advanced Healthcare Materials 8(17) (2019) 1900670.
[31] F. Jiang, X.-W. Xu, F.-Q. Chen, H.-F. Weng, J. Chen, Y. Ru, Q. Xiao, A.-F. Xiao, Extraction, Modification and Biomedical Application of Agarose Hydrogels: A Review, Marine Drugs 21(5) (2023) 299.
[32] S. Thakur, B. Sharma, A. Verma, J. Chaudhary, S. Tamulevicius, V.K. Thakur, Recent progress in sodium alginate based sustainable hydrogels for environmental applications, Journal of Cleaner Production 198 (2018) 143-159.
[33] S.H. Zainal, N.H. Mohd, N. Suhaili, F.H. Anuar, A.M. Lazim, R. Othaman, Preparation of cellulose-based hydrogel: a review, Journal of Materials Research and Technology 10 (2021) 935-952.
[34] C. Chang, L. Zhang, Cellulose-based hydrogels: Present status and application prospects, Carbohydrate Polymers 84(1) (2011) 40-53.
[35] U.S.K. Madduma-Bandarage, S.V. Madihally, Synthetic hydrogels: Synthesis, novel trends, and applications, Journal of Applied Polymer Science 138(19) (2021) 50376.
[36] S. Awasthi, J.K. Gaur, M.S. Bobji, C. Srivastava, Nanoparticle-reinforced polyacrylamide

hydrogel composites for clinical applications: a review, Journal of Materials Science 57(17) (2022) 8041-8063.
[37] R.J. Senden, P. De Jean, K.B. McAuley, L.J. Schreiner, Polymer gel dosimeters with reduced toxicity: a preliminary investigation of the NMR and optical dose–response using different monomers, Physics in Medicine & Biology 51(14) (2006) 3301.
[38] J.-Y. Sun, X. Zhao, W.R.K. Illeperuma, O. Chaudhuri, K.H. Oh, D.J. Mooney, J.J. Vlassak, Z. Suo, Highly stretchable and tough hydrogels, Nature 489(7414) (2012) 133-136.
[39] Y. Gu, W. Wu, C. Zhang, X. Li, X. Guo, Y. Wang, Y. Yuan, B. Jiang, Y. Jin, Multi-Solvent-Induced Gradient Aggregation Rendered Superstrong, Tough, Stretchable, and Fatigue-Resistant Lignin-Based Supramolecular Hydrogels, Advanced Functional Materials 35(11) (2025) 2417206.
[40] H. Adelnia, R. Ensandoost, S. Shebbrin Moonshi, J.N. Gavgani, E.I. Vasafi, H.T. Ta, Freeze/thawed polyvinyl alcohol hydrogels: Present, past and future, European Polymer Journal 164 (2022) 110974.
[41] Y. Hui, Y. Yao, Q. Qian, J. Luo, H. Chen, Z. Qiao, Y. Yu, L. Tao, N. Zhou, Three-dimensional printing of soft hydrogel electronics, Nature Electronics 5(12) (2022) 893-903.
[42] Z. Sun, C. Dong, B. Chen, W. Li, H. Hu, J. Zhou, C. Li, Z. Huang, Strong, Tough, and Anti-Swelling Supramolecular Conductive Hydrogels for Amphibious Motion Sensors, Small 19(44) (2023) 2303612.
[43] J. Hua, P.F. Ng, B. Fei, High-strength hydrogels: Microstructure design, characterization and applications, Journal of Polymer Science Part B: Polymer Physics 56(19) (2018) 1325-1335.
[44] Q. Chen, H. Chen, L. Zhu, J. Zheng, Fundamentals of double network hydrogels, Journal of Materials Chemistry B 3(18) (2015) 3654-3676.
[45] J. Shojaeiarani, D. Bajwa, A. Shirzadifar, A review on cellulose nanocrystals as promising biocompounds for the synthesis of nanocomposite hydrogels, Carbohydrate Polymers 216 (2019) 247-259.
[46] H. Huang, Z. Dong, X. Ren, B. Jia, G. Li, S. Zhou, X. Zhao, W. Wang, High-strength hydrogels: Fabrication, reinforcement mechanisms, and applications, Nano Research 16(2) (2023) 3475-3515.
[47] X. Du, J. Zhou, J. Shi, B. Xu, Supramolecular Hydrogelators and Hydrogels: From Soft Matter to Molecular Biomaterials, Chemical Reviews 115(24) (2015) 13165-13307.
[48] Q. Wang, J. Lan, Z. Hua, X. Ma, L. Chen, X. Pan, Y. Li, S. Cao, Y. Ni, An oriented Fe3+-regulated lignin-based hydrogel with desired softness, conductivity, stretchability, and asymmetric adhesiveness towards anti-interference pressure sensors, International Journal of Biological Macromolecules 184 (2021) 282-288.
[49] L. Tang, S. Wu, J. Qu, L. Gong, J. Tang, A Review of Conductive Hydrogel Used in Flexible Strain Sensor, Materials 13(18) (2020) 3947.
[50] Q. Peng, J. Chen, T. Wang, X. Peng, J. Liu, X. Wang, J. Wang, H. Zeng, Recent advances in designing conductive hydrogels for flexible electronics, InfoMat 2(5) (2020) 843-865.
[51] T. Zhu, Y. Ni, G.M. Biesold, Y. Cheng, M. Ge, H. Li, J. Huang, Z. Lin, Y. Lai, Recent advances in conductive hydrogels: classifications, properties, and applications, Chemical Society Reviews 52(2) (2023) 473-509.
[52] L. Han, L. Yan, M. Wang, K. Wang, L. Fang, J. Zhou, J. Fang, F. Ren, X. Lu, Transparent, Adhesive, and Conductive Hydrogel for Soft Bioelectronics Based on Light-Transmitting

Polydopamine-Doped Polypyrrole Nanofibrils, Chemistry of Materials 30(16) (2018) 5561-5572.
[53] G. Li, C. Li, G. Li, D. Yu, Z. Song, H. Wang, X. Liu, H. Liu, W. Liu, Development of Conductive Hydrogels for Fabricating Flexible Strain Sensors, Small 18(5) (2022) 2101518.
[54] Z. Deng, R. Yu, B. Guo, Stimuli-responsive conductive hydrogels: design, properties, and applications, Materials Chemistry Frontiers 5(5) (2021) 2092-2123.
[55] W. Zhang, P. Feng, J. Chen, Z. Sun, B. Zhao, Electrically conductive hydrogels for flexible energy storage systems, Progress in Polymer Science 88 (2019) 220-240.
[56] A. Madhusudhan, T.A. Suhagia, C. Sharma, S.K. Jaganathan, S.D. Purohit, Carbon Based Polymeric Nanocomposite Hydrogel Bioink: A Review, Polymers 16(23) (2024) 3318.
[57] D. Mawad, A. Lauto, G.G. Wallace, Conductive Polymer Hydrogels, in: S. Kalia (Ed.), Polymeric Hydrogels as Smart Biomaterials, Springer International Publishing, Cham, 2016, pp. 19-44.
[58] S. Azadi, S. Peng, S.A. Moshizi, M. Asadnia, J. Xu, I. Park, C.H. Wang, S. Wu, Biocompatible and Highly Stretchable PVA/AgNWs Hydrogel Strain Sensors for Human Motion Detection, Advanced Materials Technologies 5(11) (2020) 2000426.
[59] H. Zhu, J. Zeng, S. Jiang, S. Huang, Z. Xie, Y. Huang, S. Lin, B. Wang, Poly(vinyl alcohol)/borax/modified silver nanowire composite hydrogel with self-healing, high conductivity, and electromagnetic interference shielding properties, Journal of Alloys and Compounds 1011 (2025) 178437.
[60] L. Han, K. Liu, M. Wang, K. Wang, L. Fang, H. Chen, J. Zhou, X. Lu, Mussel-Inspired Adhesive and Conductive Hydrogel with Long-Lasting Moisture and Extreme Temperature Tolerance, Advanced Functional Materials 28(3) (2018) 1704195.
[61] Q. Wang, X. Pan, C. Lin, D. Lin, Y. Ni, L. Chen, L. Huang, S. Cao, X. Ma, Biocompatible, self-wrinkled, antifreezing and stretchable hydrogel-based wearable sensor with PEDOT:sulfonated lignin as conductive materials, Chemical Engineering Journal 370 (2019) 1039-1047.
[62] C. Yang, Z. Suo, Hydrogel ionotronics, Nature Reviews Materials 3(6) (2018) 125-142.
[63] J.-Y. Sun, C. Keplinger, G.M. Whitesides, Z. Suo, Ionic skin, Advanced Materials 26(45) (2014) 7608-7614.
[64] X. Yao, S. Zhang, L. Qian, N. Wei, V. Nica, S. Coseri, F. Han, Super Stretchable, Self-Healing, Adhesive Ionic Conductive Hydrogels Based on Tailor-Made Ionic Liquid for High-Performance Strain Sensors, Advanced Functional Materials 32(33) (2022) 2204565.
[65] Y. Gao, Y. Gao, Z. Zhang, Y. Wang, X. Ren, F. Jia, G. Gao, Highly conductive hydrogel sensors driven by amylose with freezing and dehydration resistances, Journal of Materials Chemistry C 10(35) (2022) 12873-12882.
[66] Introduction: Ionic Liquids, Chemical Reviews 117(10) (2017) 6633-6635.
[67] B.B. Hansen, S. Spittle, B. Chen, D. Poe, Y. Zhang, J.M. Klein, A. Horton, L. Adhikari, T. Zelovich, B.W. Doherty, B. Gurkan, E.J. Maginn, A. Ragauskas, M. Dadmun, T.A. Zawodzinski, G.A. Baker, M.E. Tuckerman, R.F. Savinell, J.R. Sangoro, Deep Eutectic Solvents: A Review of Fundamentals and Applications, Chemical Reviews 121(3) (2021) 1232-1285.
[68] J. Bai, R. Wang, X. Wang, S. Liu, X. Wang, J. Ma, Z. Qin, T. Jiao, Biomineral calcium-ion-mediated conductive hydrogels with high stretchability and self-adhesiveness for sensitive iontronic sensors, Cell Reports Physical Science 2(11) (2021).

[69] H. Zhang, N. Tang, X. Yu, M.-H. Li, J. Hu, Strong and Tough Physical Eutectogels Regulated by the Spatiotemporal Expression of Non-Covalent Interactions, Advanced Functional Materials 32(41) (2022) 2206305.
[70] C.-J. Lee, H. Wu, Y. Hu, M. Young, H. Wang, D. Lynch, F. Xu, H. Cong, G. Cheng, Ionic Conductivity of Polyelectrolyte Hydrogels, ACS Applied Materials & Interfaces 10(6) (2018) 5845-5852.
[71] X. Fan, Z. Chen, H. Sun, S. Zeng, R. Liu, Y. Tian, Polyelectrolyte-based conductive hydrogels: from theory to applications, Soft Sci 2(10) (2022).
[72] X. Pan, Q. Wang, R. Guo, Y. Ni, K. Liu, X. Ouyang, L. Chen, L. Huang, S. Cao, M. Xie, An integrated transparent, UV-filtering organohydrogel sensor via molecular-level ion conductive channels, Journal of Materials Chemistry A 7(9) (2019) 4525-4535.
[73] Y. Yang, Y. Yang, Y. Cao, X. Wang, Y. Chen, H. Liu, Y. Gao, J. Wang, C. Liu, W. Wang, J.-K. Yu, D. Wu, Anti-freezing, resilient and tough hydrogels for sensitive and large-range strain and pressure sensors, Chemical Engineering Journal 403 (2021) 126431.
[74] Y. Jian, S. Handschuh-Wang, J. Zhang, W. Lu, X. Zhou, T. Chen, Biomimetic anti-freezing polymeric hydrogels: keeping soft-wet materials active in cold environments, Materials Horizons 8(2) (2021) 351-369.
[75] F. Chen, D. Zhou, J. Wang, T. Li, X. Zhou, T. Gan, S. Handschuh-Wang, X. Zhou, Rational Fabrication of Anti-Freezing, Non-Drying Tough Organohydrogels by One-Pot Solvent Displacement, Angewandte Chemie International Edition 57(22) (2018) 6568-6571.
[76] X.P. Morelle, W.R. Illeperuma, K. Tian, R. Bai, Z. Suo, J.J. Vlassak, Highly Stretchable and Tough Hydrogels below Water Freezing Temperature, Advanced Materials 30(35) (2018) 1801541.
[77] C. Huang, Y. Zhong, W. Cai, L. Cao, Q. Wang, W. Li, Z. Lin, P. Zhang, Highly sensitive, anti-freeze, and ion-conductive polyelectrolyte-based hydrogel for flexible sensor applications in sub-zero temperatures, Polymer 323 (2025) 128226.
[78] Y. Wang, Y. Xia, P. Xiang, Y. Dai, Y. Gao, H. Xu, J. Yu, G. Gao, K. Chen, Protein-assisted freeze-tolerant hydrogel with switchable performance toward customizable flexible sensor, Chemical Engineering Journal 428 (2022) 131171.
[79] Y. Ye, Z. Wan, P.D.S.H. Gunawardane, Q. Hua, S. Wang, J. Zhu, M. Chiao, S. Renneckar, O.J. Rojas, F. Jiang, Ultra-Stretchable and Environmentally Resilient Hydrogels Via Sugaring-Out Strategy for Soft Robotics Sensing, Advanced Functional Materials 34(26) (2024) 2315184.
[80] L.X. Hou, H. Ju, X.P. Hao, H. Zhang, L. Zhang, Z. He, J. Wang, Q. Zheng, Z.L. Wu, Intrinsic Anti-Freezing and Unique Phosphorescence of Glassy Hydrogels with Ultrahigh Stiffness and Toughness at Low Temperatures, Advanced Materials 35(21) (2023) 2300244.
[81] Y. Feng, S. Wang, Y. Li, W. Ma, G. Zhang, M. Yang, H. Li, Y. Yang, Y. Long, Entanglement in Smart Hydrogels: Fast Response Time, Anti-Freezing and Anti-Drying, Advanced Functional Materials 33(21) (2023) 2211027.
[82] J. Yu, Q. Wang, X. Pan, X. Ma, S. Cao, Y. Ni, Fruit Peel-Inspired Super-Stable Ionic Organohydrogel Electronics with Dense Hydrophobic Skin, ACS Applied Polymer Materials 4(7) (2022) 4673-4680.
[83] D.L. Taylor, M. in het Panhuis, Self-Healing Hydrogels, Advanced Materials 28(41) (2016) 9060-9093.
[84] T. Qin, W. Liao, L. Yu, J. Zhu, M. Wu, Q. Peng, L. Han, H. Zeng, Recent progress in

conductive self-healing hydrogels for flexible sensors, Journal of Polymer Science 60(18) (2022) 2607-2634.
[85] W.-P. Chen, D.-Z. Hao, W.-J. Hao, X.-L. Guo, L. Jiang, Hydrogel with Ultrafast Self-Healing Property Both in Air and Underwater, ACS Applied Materials & Interfaces 10(1) (2018) 1258-1265.
[86] X. Pan, J. Yu, X. Lu, Q. Wang, X. Ma, S. Cao, Y. Ni, A multifunctional MXene-assembled anhydrous gel electronics, Journal of Colloid and Interface Science 623 (2022) 1151-1159.
[87] S. Li, Y. Cong, J. Fu, Tissue adhesive hydrogel bioelectronics, Journal of Materials Chemistry B 9(22) (2021) 4423-4443.
[88] X. Qu, S. Wang, Y. Zhao, H. Huang, Q. Wang, J. Shao, W. Wang, X. Dong, Skin-inspired highly stretchable, tough and adhesive hydrogels for tissue-attached sensor, Chemical Engineering Journal 425 (2021) 131523.
[89] X. Liu, H. Yu, L. Wang, Z. Huang, F. Haq, L. Teng, M. Jin, B. Ding, Recent Advances on Designs and Applications of Hydrogel Adhesives, Advanced Materials Interfaces 9(2) (2022) 2101038.
[90] L. Han, X. Lu, K. Liu, K. Wang, L. Fang, L.-T. Weng, H. Zhang, Y. Tang, F. Ren, C. Zhao, G. Sun, R. Liang, Z. Li, Mussel-Inspired Adhesive and Tough Hydrogel Based on Nanoclay Confined Dopamine Polymerization, ACS Nano 11(3) (2017) 2561-2574.
[91] C. Shao, M. Wang, L. Meng, H. Chang, B. Wang, F. Xu, J. Yang, P. Wan, Mussel-Inspired Cellulose Nanocomposite Tough Hydrogels with Synergistic Self-Healing, Adhesive, and Strain-Sensitive Properties, Chemistry of Materials 30(9) (2018) 3110-3121.
[92] Y. Xia Zhang, Y. He, Y. Liang, J. Tang, Y. Yang, H. Ming Song, M. Zrínyi, Y. Mei Chen, Sensitive piezoresistive pressure sensor based on micropyramid patterned tough hydrogel, Applied Surface Science 615 (2023) 156328.
[93] Y.-Z. Zhang, K.H. Lee, D.H. Anjum, R. Sougrat, Q. Jiang, H. Kim, H.N. Alshareef, MXenes stretch hydrogel sensor performance to new limits, Science Advances 4(6) (2018) eaat0098.
[94] X. Pan, Q. Wang, R. Guo, S. Cao, H. Wu, X. Ouyang, F. Huang, H. Gao, L. Huang, F. Zhang, L. Chen, Y. Ni, K. Liu, An adaptive ionic skin with multiple stimulus responses and moist-electric generation ability, Journal of Materials Chemistry A 8(34) (2020) 17498-17506.
[95] Y. Luo, J. Li, Q. Ding, H. Wang, C. Liu, J. Wu, Functionalized Hydrogel-Based Wearable Gas and Humidity Sensors, Nano-Micro Letters 15(1) (2023) 136.
[96] Z. Lei, Q. Wang, S. Sun, W. Zhu, P. Wu, A Bioinspired Mineral Hydrogel as a Self-Healable, Mechanically Adaptable Ionic Skin for Highly Sensitive Pressure Sensing, Advanced Materials 29(22) (2017) 1700321.
[97] J. Bai, Y. Huang, H. Cheng, L. Qu, Moist-electric generation, Nanoscale 11(48) (2019) 23083-23091.
[98] W. Tang, Q. Sun, Z.L. Wang, Self-Powered Sensing in Wearable Electronics—A Paradigm Shift Technology, Chemical Reviews 123(21) (2023) 12105-12134.
[99] Z. Zhao, Y.-P. Hu, K.-Y. Liu, W. Yu, G.-X. Li, C.-Z. Meng, S.-J. Guo, Recent Development of Self-Powered Tactile Sensors Based on Ionic Hydrogels, Gels 9(3) (2023) 257.
[100] C. Wu, A.C. Wang, W. Ding, H. Guo, Z.L. Wang, Triboelectric Nanogenerator: A Foundation of the Energy for the New Era, Advanced Energy Materials 9(1) (2019) 1802906.
[101] Z.L. Wang, Triboelectric Nanogenerators as New Energy Technology for Self-Powered Systems and as Active Mechanical and Chemical Sensors, ACS Nano 7(11) (2013) 9533-9557.

[102] F.G. Torres, O.P. Troncoso, G.E. De-la-Torre, Hydrogel-based triboelectric nanogenerators: Properties, performance, and applications, International Journal of Energy Research 46(5) (2022) 5603-5624.
[103] X. Pu, M. Liu, X. Chen, J. Sun, C. Du, Y. Zhang, J. Zhai, W. Hu, Z.L. Wang, Ultrastretchable, transparent triboelectric nanogenerator as electronic skin for biomechanical energy harvesting and tactile sensing, Science Advances 3(5) (2017) e1700015.
[104] C. Zhang, S.H. Kwon, L. Dong, Piezoelectric Hydrogels: Hybrid Material Design, Properties, and Biomedical Applications, Small 20(28) (2024) 2310110.
[105] T. Vijayakanth, S. Shankar, G. Finkelstein-Zuta, S. Rencus-Lazar, S. Gilead, E. Gazit, Perspectives on recent advancements in energy harvesting, sensing and bio-medical applications of piezoelectric gels, Chemical Society Reviews 52(17) (2023) 6191-6220.
[106] R. Freer, A.V. Powell, Realising the potential of thermoelectric technology: a Roadmap, Journal of Materials Chemistry C 8(2) (2020) 441-463.
[107] C. Zhang, X.-L. Shi, Q. Liu, Z.-G. Chen, Hydrogel-Based Functional Materials for Thermoelectric Applications: Progress and Perspectives, Advanced Functional Materials 34(51) (2024) 2410127.
[108] L. Liu, D. Zhang, P. Bai, Y. Mao, Q. Li, J. Guo, Y. Fang, R. Ma, Strong Tough Thermogalvanic Hydrogel Thermocell With Extraordinarily High Thermoelectric Performance, Advanced Materials 35(32) (2023) 2300696.
[109] Y. Han, H. Wei, Y. Du, Z. Li, S.-P. Feng, B. Huang, D. Xu, Ultrasensitive Flexible Thermal Sensor Arrays based on High-Thermopower Ionic Thermoelectric Hydrogel, Advanced Science 10(25) (2023) 2302685.
[110] X. Yang, X. Ma, Y. Niu, Y. Yao, S.A. Khan, H. Zhang, X. Cui, Thermoelectric hydrogels for self-powered wearable biosensing, Nano Trends 7 (2024) 100050.
[111] J. Chen, L. Zhang, Y. Tu, Q. Zhang, F. Peng, W. Zeng, M. Zhang, X. Tao, Wearable self-powered human motion sensors based on highly stretchable quasi-solid state hydrogel, Nano Energy 88 (2021) 106272.
[112] Y. Cao, B. Xu, Z. Li, H. Fu, Advanced Design of High-Performance Moist-Electric Generators, Advanced Functional Materials 33(31) (2023) 2301420.
[113] S. Yang, X. Tao, W. Chen, J. Mao, H. Luo, S. Lin, L. Zhang, J. Hao, Ionic Hydrogel for Efficient and Scalable Moisture-Electric Generation, Advanced Materials 34(21) (2022) 2200693.
[114] Z. Lei, P. Wu, A highly transparent and ultra-stretchable conductor with stable conductivity during large deformation, Nature Communications 10(1) (2019) 3429.
[115] F. Zhao, H. Cheng, Z. Zhang, L. Jiang, L. Qu, Direct Power Generation from a Graphene Oxide Film under Moisture, Advanced Materials 27(29) (2015) 4351-4357.
[116] X. Zhu, P. Qi, W. Fan, H. Wang, K. Sui, Bioinspired multifunctional self-powered ionic receptors derived by gradient polyelectrolyte hydrogels, Chemical Engineering Journal 438 (2022) 135610.
[117] H. Liu, M. Li, C. Ouyang, T.J. Lu, F. Li, F. Xu, Biofriendly, Stretchable, and Reusable Hydrogel Electronics as Wearable Force Sensors, Small 14(36) (2018) 1801711.
[118] Q. Wen, A. Basu, P.A. Janmey, A.G. Yodh, Non-affine deformations in polymer hydrogels, Soft Matter 8(31) (2012) 8039-8049.
[119] Y. Chang, L. Wang, R. Li, Z. Zhang, Q. Wang, J. Yang, C.F. Guo, T. Pan, First Decade of

Interfacial Iontronic Sensing: From Droplet Sensors to Artificial Skins, Advanced Materials 33(7) (2021) 2003464.
[120] Y. Ren, Z. Liu, G. Jin, M. Yang, Y. Shao, W. Li, Y. Wu, L. Liu, F. Yan, Electric-Field-Induced Gradient Ionogels for Highly Sensitive, Broad-Range-Response, and Freeze/Heat-Resistant Ionic Fingers, Advanced Materials 33(12) (2021) 2008486.
[121] X. Liu, J. Liu, S. Lin, X. Zhao, Hydrogel machines, Materials Today 36 (2020) 102-124.
[122] D. Gan, W. Xing, L. Jiang, J. Fang, C. Zhao, F. Ren, L. Fang, K. Wang, X. Lu, Plant-inspired adhesive and tough hydrogel based on Ag-Lignin nanoparticles-triggered dynamic redox catechol chemistry, Nature Communications 10(1) (2019) 1487.
[123] G. Ge, Y. Lu, X. Qu, W. Zhao, Y. Ren, W. Wang, Q. Wang, W. Huang, X. Dong, Muscle-Inspired Self-Healing Hydrogels for Strain and Temperature Sensor, ACS Nano 14(1) (2020) 218-228.
[124] Y. Zhou, C. Wan, Y. Yang, H. Yang, S. Wang, Z. Dai, K. Ji, H. Jiang, X. Chen, Y. Long, Highly Stretchable, Elastic, and Ionic Conductive Hydrogel for Artificial Soft Electronics, Advanced Functional Materials 29(1) (2019) 1806220.
[125] C. Li, Y. Xue, M. Han, L.C. Palmer, J.A. Rogers, Y. Huang, S.I. Stupp, Synergistic photoactuation of bilayered spiropyran hydrogels for predictable origami-like shape change, Matter 4(4) (2021) 1377-1390.
[126] M. Liao, P. Wan, J. Wen, M. Gong, X. Wu, Y. Wang, R. Shi, L. Zhang, Wearable, Healable, and Adhesive Epidermal Sensors Assembled from Mussel-Inspired Conductive Hybrid Hydrogel Framework, Advanced Functional Materials 27(48) (2017) 1703852.
[127] B. Ying, R.Z. Chen, R. Zuo, J. Li, X. Liu, An Anti-Freezing, Ambient-Stable and Highly Stretchable Ionic Skin with Strong Surface Adhesion for Wearable Sensing and Soft Robotics, Advanced Functional Materials 31(42) (2021) 2104665.
[128] X. Liu, Q. Zhang, G. Gao, Solvent-Resistant and Nonswellable Hydrogel Conductor toward Mechanical Perception in Diverse Liquid Media, ACS Nano 14(10) (2020) 13709-13717.
[129] X. Pei, H. Zhang, Y. Zhou, L. Zhou, J. Fu, Stretchable, self-healing and tissue-adhesive zwitterionic hydrogels as strain sensors for wireless monitoring of organ motions, Materials Horizons 7(7) (2020) 1872-1882.
[130] S. Li, H. Pan, Y. Wang, J. Sun, Polyelectrolyte complex-based self-healing, fatigue-resistant and anti-freezing hydrogels as highly sensitive ionic skins, Journal of Materials Chemistry A 8(7) (2020) 3667-3675.
[131] Q. Wang, X. Pan, C. Lin, X. Ma, S. Cao, Y. Ni, Ultrafast gelling using sulfonated lignin-Fe3+ chelates to produce dynamic crosslinked hydrogel/coating with charming stretchable, conductive, self-healing, and ultraviolet-blocking properties, Chemical Engineering Journal 396 (2020) 125341.
[132] Q. Wang, X. Pan, J. Guo, L. Huang, L. Chen, X. Ma, S. Cao, Y. Ni, Lignin and cellulose derivatives-induced hydrogel with asymmetrical adhesion, strength, and electriferous properties for wearable bioelectrodes and self-powered sensors, Chemical Engineering Journal 414 (2021) 128903.
[133] B. Ying, Q. Wu, J. Li, X. Liu, An ambient-stable and stretchable ionic skin with multimodal sensation, Materials Horizons 7(2) (2020) 477-488.
[134] X. Wu, M. Ahmed, Y. Khan, M.E. Payne, J. Zhu, C. Lu, J.W. Evans, A.C. Arias, A potentiometric mechanotransduction mechanism for novel electronic skins, Science Advances

6(30) (2020) eaba1062.
[135] Z. Ma, J. Ai, Y. Shi, K. Wang, B. Su, A Superhydrophobic Droplet-Based Magnetoelectric Hybrid System to Generate Electricity and Collect Water Simultaneously, Advanced Materials 32(50) (2020) 2006839.
[136] X. Zhang, J. Ai, Z. Ma, Y. Yin, R. Zou, B. Su, Liquid Metal Based Stretchable Magnetoelectric Films and Their Capacity for Mechanoelectrical Conversion, Advanced Functional Materials 30(45) (2020) 2003680.
[137] B. Jiang, Y. Long, X. Pu, W. Hu, Z.L. Wang, A stretchable, harsh condition-resistant and ambient-stable hydrogel and its applications in triboelectric nanogenerator, Nano Energy 86 (2021) 106086.
[138] W. Xu, L.-B. Huang, M.-C. Wong, L. Chen, G. Bai, J. Hao, Environmentally Friendly Hydrogel-Based Triboelectric Nanogenerators for Versatile Energy Harvesting and Self-Powered Sensors, Advanced Energy Materials 7(1) (2017) 1601529.
[139] X. Wu, J. Zhu, J.W. Evans, C. Lu, A.C. Arias, A Potentiometric Electronic Skin for Thermosensation and Mechanosensation, Advanced Functional Materials 31(17) (2021) 2010824.
[140] Y. Jia, Y. Pan, C. Wang, C. Liu, C. Shen, C. Pan, Z. Guo, X. Liu, Flexible Ag Microparticle/MXene-Based Film for Energy Harvesting, Nano-Micro Letters 13(1) (2021) 201.
[141] Q.-Y. Wu, C. Wang, R. Wang, C. Chen, J. Gao, J. Dai, D. Liu, Z. Lin, L. Hu, Salinity-Gradient Power Generation with Ionized Wood Membranes, Advanced Energy Materials 10(1) (2020) 1902590.
[142] L. Ding, D. Xiao, Z. Lu, J. Deng, Y. Wei, J. Caro, H. Wang, Oppositely charged Ti3C2Tx MXene membranes with 2D nanofluidic channels for osmotic energy harvesting, Angewandte Chemie 132(22) (2020) 8798-8804.
[143] T.B.H. Schroeder, A. Guha, A. Lamoureux, G. VanRenterghem, D. Sept, M. Shtein, J. Yang, M. Mayer, An electric-eel-inspired soft power source from stacked hydrogels, Nature 552(7684) (2017) 214-218.
[144] H.J. Kim, B. Chen, Z. Suo, R.C. Hayward, Ionoelastomer junctions between polymer networks of fixed anions and cations, Science 367(6479) (2020) 773.
[145] A. Guha, T.J. Kalkus, T.B.H. Schroeder, O.G. Willis, C. Rader, A. Ianiro, M. Mayer, Powering Electronic Devices from Salt Gradients in AA-Battery-Sized Stacks of Hydrogel-Infused Paper, Advanced Materials 33(31) (2021) 2101757.
[146] Y. Zhang, C.K. Jeong, J. Wang, X. Chen, K.H. Choi, L.-Q. Chen, W. Chen, Q.M. Zhang, Q. Wang, Hydrogel Ionic Diodes toward Harvesting Ultralow-Frequency Mechanical Energy, Advanced Materials 33(36) (2021) 2103056.
[147] X. Zhao, D. Shen, W.W. Duley, C. Tan, Y.N. Zhou, Water-Enabled Electricity Generation: A Perspective, Advanced Energy and Sustainability Research 3(4) (2022) 2100196.
[148] A. Sohn, Y. Zhang, A. Chakraborty, C. Yu, Sustainable Power Generation via Hydro-Electrochemical Effects, Nanoscale 14(11) (2022) 4188-4194.
[149] Y. Dobashi, D. Yao, Y. Petel, T.N. Nguyen, M.S. Sarwar, Y. Thabet, C.L.W. Ng, E. Scabeni Glitz, G.T.M. Nguyen, C. Plesse, F. Vidal, C.A. Michal, J.D.W. Madden, Piezoionic mechanoreceptors: Force-induced current generation in hydrogels, Science 376(6592) (2022) 502-507.
[150] W. Fan, X. Zhang, H. Cui, C. Liu, Y. Li, Y. Xia, K. Sui, Direct Current-Powered High-

Performance Ionic Hydrogel Strain Sensor Based on Electrochemical Redox Reaction, ACS Applied Materials & Interfaces 11(27) (2019) 24289-24297.
[151] H. Wang, Y. Sun, T. He, Y. Huang, H. Cheng, C. Li, D. Xie, P. Yang, Y. Zhang, L. Qu, Bilayer of polyelectrolyte films for spontaneous power generation in air up to an integrated 1,000 V output, Nature Nanotechnology 16(7) (2021) 811-819.
[152] X. Liu, H. Gao, J.E. Ward, X. Liu, B. Yin, T. Fu, J. Chen, D.R. Lovley, J. Yao, Power generation from ambient humidity using protein nanowires, Nature 578(7796) (2020) 550-554.
[153] Z.-H. Lin, W.-S. Hsu, A. Preet, L.-H. Yeh, Y.-H. Chen, Y.-P. Pao, S.-F. Lin, S. Lee, J.-C. Fan, L. Wang, Y.-P. Chiu, B.-S. Yip, T.-E. Lin, Ingestible polysaccharide battery coupled with a self-charging nanogenerator for controllable disinfection system, Nano Energy 79 (2021) 105440.
[154] G. Bian, N. Pan, Z. Luan, X. Sui, W. Fan, Y. Xia, K. Sui, L. Jiang, Anti-Swelling Gradient Polyelectrolyte Hydrogel Membranes as High-Performance Osmotic Energy Generators, Angewandte Chemie International Edition 60(37) (2021) 20294-20300.
[155] M. Xia, N. Pan, C. Zhang, C. Zhang, W. Fan, Y. Xia, Z. Wang, K. Sui, Self-Powered Multifunction Ionic Skins Based on Gradient Polyelectrolyte Hydrogels, ACS Nano 16(3) (2022) 4714-4725.
[156] T. Xu, X. Ding, Y. Huang, C. Shao, L. Song, X. Gao, Z. Zhang, L. Qu, An efficient polymer moist-electric generator, Energy & Environmental Science 12(3) (2019) 972-978.
[157] H. Zhou, J. Lai, X. Jin, H. Liu, X. Li, W. Chen, A. Ma, X. Zhou, Intrinsically adhesive, highly sensitive and temperature tolerant flexible sensors based on double network organohydrogels, Chemical Engineering Journal 413 (2021) 127544.
[158] C. Tan, Z. Dong, Y. Li, H. Zhao, X. Huang, Z. Zhou, J.-W. Jiang, Y.-Z. Long, P. Jiang, T.-Y. Zhang, B. Sun, A high performance wearable strain sensor with advanced thermal management for motion monitoring, Nature Communications 11(1) (2020) 3530.
[159] Z. Yang, Y. Pang, X.-l. Han, Y. Yang, J. Ling, M. Jian, Y. Zhang, Y. Yang, T.-L. Ren, Graphene Textile Strain Sensor with Negative Resistance Variation for Human Motion Detection, ACS Nano 12(9) (2018) 9134-9141.
[160] Z. Lei, W. Gao, P. Wu, Double-network thermocells with extraordinary toughness and boosted power density for continuous heat harvesting, Joule 5(8) (2021) 2211-2222.
[161] X. Luo, L. Zhu, Y.-C. Wang, J. Li, J. Nie, Z.L. Wang, A Flexible Multifunctional Triboelectric Nanogenerator Based on MXene/PVA Hydrogel, Advanced Functional Materials 31(38) (2021) 2104928.
[162] R. Fu, L. Tu, Y. Zhou, L. Fan, F. Zhang, Z. Wang, J. Xing, D. Chen, C. Deng, G. Tan, P. Yu, L. Zhou, C. Ning, A Tough and Self-Powered Hydrogel for Artificial Skin, Chemistry of Materials 31(23) (2019) 9850-9860.
[163] P. Saxena, P. Shukla, A comprehensive review on fundamental properties and applications of poly(vinylidene fluoride) (PVDF), Advanced Composites and Hybrid Materials 4(1) (2021) 8-26.
[164] Z. Liu, G. Li, Q. Qin, L. Mi, G. Li, G. Zheng, C. Liu, Q. Li, X. Liu, Electrospun PVDF/PAN membrane for pressure sensor and sodium-ion battery separator, Advanced Composites and Hybrid Materials 4(4) (2021) 1215-1225.
[165] M. Zhang, H. Du, K. Liu, S. Nie, T. Xu, X. Zhang, C. Si, Fabrication and applications of cellulose-based nanogenerators, Advanced Composites and Hybrid Materials 4(4) (2021) 865-884.

[166] B. Chen, Q. Chen, S. Xiao, J. Feng, X. Zhang, T. Wang, Giant negative thermopower of ionic hydrogel by synergistic coordination and hydration interactions, Science Advances 7(48) (2021) eabi7233.
[167] C.-G. Han, X. Qian, Q. Li, B. Deng, Y. Zhu, Z. Han, W. Zhang, W. Wang, S.-P. Feng, G. Chen, W. Liu, Giant thermopower of ionic gelatin near room temperature, Science 368(6495) (2020) 1091-1098.
[168] X. Pan, Q. Wang, P. He, K. Liu, Y. Ni, L. Chen, X. Ouyang, L. Huang, H. Wang, S. Xu, A bionic tactile plastic hydrogel-based electronic skin constructed by a nerve-like nanonetwork combining stretchable, compliant, and self-healing properties, Chemical Engineering Journal 379 (2020) 122271.
[169] F. Chen, D. Zhou, J. Wang, T. Li, X. Zhou, T. Gan, S. Handschuh-Wang, X. Zhou, Rational fabrication of anti-freezing, non-drying tough organohydrogels by one-pot solvent displacement, Angewandte Chemie 130(22) (2018) 6678-6681.
[170] Q. Ding, Z. Wu, K. Tao, Y. Wei, W. Wang, B.-R. Yang, X. Xie, J. Wu, Environment tolerant, adaptable and stretchable organohydrogels: preparation, optimization, and applications, Materials Horizons 9(5) (2022) 1356-1386.
[171] F. He, X. You, H. Gong, Y. Yang, T. Bai, W. Wang, W. Guo, X. Liu, M. Ye, Stretchable, Biocompatible, and Multifunctional Silk Fibroin-Based Hydrogels toward Wearable Strain/Pressure Sensors and Triboelectric Nanogenerators, ACS Applied Materials & Interfaces 12(5) (2020) 6442-6450.
[172] K. Hu, Z. Zhao, Y. Wang, L. Yu, K. Liu, H. Wu, L. Huang, L. Chen, Y. Ni, A tough organohydrogel-based multiresponsive sensor for triboelectric nanogenerator and supercapacitor toward wearable intelligent devices, Journal of Materials Chemistry A 10(22) (2022) 12092-12103.
[173] Y. Feng, J. Yu, D. Sun, C. Dang, W. Ren, C. Shao, R. Sun, Extreme environment-adaptable and fast self-healable eutectogel triboelectric nanogenerator for energy harvesting and self-powered sensing, Nano Energy 98 (2022) 107284.
[174] D. Sun, Y. Feng, S. Sun, J. Yu, S. Jia, C. Dang, X. Hao, J. Yang, W. Ren, R. Sun, C. Shao, F. Peng, Transparent, Self-Adhesive, Conductive Organohydrogels with Fast Gelation from Lignin-Based Self-Catalytic System for Extreme Environment-Resistant Triboelectric Nanogenerators, Advanced Functional Materials 32(28) (2022) 2201335.
[175] W. Zhao, Z. Shi, S. Hu, G. Yang, H. Tian, Understanding piezoelectric characteristics of PHEMA-based hydrogel nanocomposites as soft self-powered electronics, Advanced Composites and Hybrid Materials 1(2) (2018) 320-331.
[176] Z. Wang, Z. Liu, G. Zhao, Z. Zhang, X. Zhao, X. Wan, Y. Zhang, Z.L. Wang, L. Li, Stretchable Unsymmetrical Piezoelectric BaTiO3 Composite Hydrogel for Triboelectric Nanogenerators and Multimodal Sensors, ACS Nano 16(1) (2022) 1661-1670.
[177] J. Kim Hyeong, B. Chen, Z. Suo, C. Hayward Ryan, Ionoelastomer junctions between polymer networks of fixed anions and cations, Science 367(6479) (2020) 773-776.
[178] S. Chen, J. Jiang, F. Xu, S. Gong, Crepe cellulose paper and nitrocellulose membrane-based triboelectric nanogenerators for energy harvesting and self-powered human-machine interaction, Nano Energy 61 (2019) 69-77.
[179] C. Lin, J. Yu, Z. Hua, J. Lan, H. Huang, D. Lu, S. Cao, X. Ma, Development progress, performance enhancement routes, and applications of paper-based triboelectric

nanogenerators, Chemical Engineering Journal 430 (2022) 132559.
[180] X. Peng, K. Dong, Y. Zhang, L. Wang, C. Wei, T. Lv, Z.L. Wang, Z. Wu, Sweat-Permeable, Biodegradable, Transparent and Self-powered Chitosan-Based Electronic Skin with Ultrathin Elastic Gold Nanofibers, Advanced Functional Materials 32(20) (2022) 2112241.
[181] Y. Dobashi, D. Yao, Y. Petel, T.N. Nguyen, M.S. Sarwar, Y. Thabet, C.L.W. Ng, E.S. Glitz, G.T.M. Nguyen, C. Plesse, F. Vidal, C.A. Michal, J.D.W. Madden, Piezoionic mechanoreceptors: Force-induced current generation in hydrogels, Science 376(6592) (2022) 502-507.
[182] S. Du, N. Zhou, Y. Gao, G. Xie, H. Du, H. Jiang, L. Zhang, J. Tao, J. Zhu, Bioinspired hybrid patches with self-adhesive hydrogel and piezoelectric nanogenerator for promoting skin wound healing, Nano Research 13(9) (2020) 2525-2533.
[183] Y. Huang, H. Cheng, L. Qu, Emerging Materials for Water-Enabled Electricity Generation, ACS Materials Letters 3(2) (2021) 193-209.
[184] C. Liu, S. Wang, X. Wang, J. Mao, Y. Chen, N.X. Fang, S.-P. Feng, Hydrovoltaic energy harvesting from moisture flow using an ionic polymer–hydrogel–carbon composite, Energy & Environmental Science 15(6) (2022) 2489-2498.
[185] Z. Sun, X. Wen, L. Wang, J. Yu, X. Qin, Capacitor-inspired high-performance and durable moist-electric generator, Energy & Environmental Science 15(11) (2022) 4584-4591.
[186] H.J. Kim, B. Chen, Z. Suo, R.C. Hayward, Ionoelastomer junctions between polymer networks of fixed anions and cations, Science 367(6479) (2020) 773-776.
[187] Y. Huang, H. Cheng, C. Yang, H. Yao, C. Li, L. Qu, All-region-applicable, continuous power supply of graphene oxide composite, Energy & Environmental Science 12(6) (2019) 1848-1856.
[188] W. Yang, X. Li, X. Han, W. Zhang, Z. Wang, X. Ma, M. Li, C. Li, Asymmetric ionic aerogel of biologic nanofibrils for harvesting electricity from moisture, Nano Energy 71 (2020) 104610.
[189] M. Li, L. Zong, W. Yang, X. Li, J. You, X. Wu, Z. Li, C. Li, Biological Nanofibrous Generator for Electricity Harvest from Moist Air Flow, Advanced Functional Materials 29(32) (2019) 1901798.
[190] A. Guha, T.J. Kalkus, T.B.H. Schroeder, O.G. Willis, C. Rader, A. Ianiro, M. Mayer, Powering Electronic Devices from Salt Gradients in AA-Battery-Sized Stacks of Hydrogel-Infused Paper, Advanced Materials 33(31) (2021) 2101757.
[191] Z. Wu, P. Ji, B. Wang, N. Sheng, M. Zhang, S. Chen, H. Wang, Oppositely charged aligned bacterial cellulose biofilm with nanofluidic channels for osmotic energy harvesting, Nano Energy 80 (2021) 105554.
[192] R. Latorre, J.E. Hall, Dipole potential measurements in asymmetric membranes, Nature 264(5584) (1976) 361-363.
[193] A.A. Gurtovenko, I. Vattulainen, Lipid Transmembrane Asymmetry and Intrinsic Membrane Potential: Two Sides of the Same Coin, Journal of the American Chemical Society 129(17) (2007) 5358-5359.
[194] Y. Ma, K. Poole, J. Goyette, K. Gaus, Introducing Membrane Charge and Membrane Potential to T Cell Signaling, Frontiers in Immunology 8 (2017) 1513.
[195] H. Wang, Y. Sun, T. He, Y. Huang, H. Cheng, C. Li, D. Xie, P. Yang, Y. Zhang, L. Qu, Bilayer of polyelectrolyte films for spontaneous power generation in air up to an integrated 1,000 V output, Nature Nanotechnology 16(7) (2021) 811-819.
[196] Y. Qian, Y. Zhou, M. Lu, X. Guo, D. Yang, H. Lou, X. Qiu, C.F. Guo, Direct Construction of

Catechol Lignin for Engineering Long-Acting Conductive, Adhesive, and UV-Blocking Hydrogel Bioelectronics, Small Methods 5(5) (2021) 2001311.
[197] E. Lizundia, M.H. Sipponen, L.G. Greca, M. Balakshin, B.L. Tardy, O.J. Rojas, D. Puglia, Multifunctional lignin-based nanocomposites and nanohybrids, Green Chemistry 23(18) (2021) 6698-6760.
[198] X. Zhang, W. Liu, D. Yang, X. Qiu, Biomimetic Supertough and Strong Biodegradable Polymeric Materials with Improved Thermal Properties and Excellent UV-Blocking Performance, Advanced Functional Materials 29(4) (2019) 1806912.
[199] T. Wang, X. Ren, Y. Bai, L. Liu, G. Wu, Adhesive and tough hydrogels promoted by quaternary chitosan for strain sensor, Carbohydrate Polymers 254 (2021) 117298.
[200] L. Min, M. Liu, L. Liu, Z. Rao, C. Zhu, L. Fan, Enzymatic synthesis of quaternary ammonium chitosan-silk fibroin peptide copolymer and its characterization, International Journal of Biological Macromolecules 109 (2018) 1125-1131.
[201] W. Sajomsang, P. Gonil, S. Tantayanon, Antibacterial activity of quaternary ammonium chitosan containing mono or disaccharide moieties: Preparation and characterization, International Journal of Biological Macromolecules 44(5) (2009) 419-427.
[202] H. Wang, T. He, X. Hao, Y. Huang, H. Yao, F. Liu, H. Cheng, L. Qu, Moisture adsorption-desorption full cycle power generation, Nature Communications 13(1) (2022) 2524.
[203] W. He, H. Wang, Y. Huang, T. He, F. Chi, H. Cheng, D. Liu, L. Dai, L. Qu, Textile-based moisture power generator with dual asymmetric structure and high flexibility for wearable applications, Nano Energy 95 (2022) 107017.
[204] T. Cai, L. Lan, B. Peng, C. Zhang, S. Dai, C. Zhang, J. Ping, Y. Ying, Bilayer Wood Membrane with Aligned Ion Nanochannels for Spontaneous Moist-Electric Generation, Nano Letters 22(16) (2022) 6476-6483.
[205] Q. Xia, C. Chen, Y. Yao, S. He, X. Wang, J. Li, J. Gao, W. Gan, B. Jiang, M. Cui, L. Hu, In Situ Lignin Modification toward Photonic Wood, Advanced Materials 33(8) (2021) 2001588.
[206] X. Pan, Q. Wang, D. Benetti, Y. Ni, F. Rosei, Polyelectrolyte hydrogel: A versatile platform for mechanical-electric conversion and self-powered sensing, Nano Energy 103 (2022) 107718.
[207] X. Gao, T. Xu, C. Shao, Y. Han, B. Lu, Z. Zhang, L. Qu, Electric power generation using paper materials, Journal of Materials Chemistry A 7(36) (2019) 20574-20578.
[208] X. Zhou, W. Zhang, C. Zhang, Y. Tan, J. Guo, Z. Sun, X. Deng, Harvesting Electricity from Water Evaporation through Microchannels of Natural Wood, ACS Applied Materials & Interfaces 12(9) (2020) 11232-11239.
[209] Y. Liang, F. Zhao, Z. Cheng, Y. Deng, Y. Xiao, H. Cheng, P. Zhang, Y. Huang, H. Shao, L. Qu, Electric power generation via asymmetric moisturizing of graphene oxide for flexible, printable and portable electronics, Energy & Environmental Science 11(7) (2018) 1730-1735.
[210] P.S. Chauhan, Lignin nanoparticles: Eco-friendly and versatile tool for new era, Bioresource Technology Reports 9 (2020) 100374.
[211] C. Chen, Q. Wu, Z. Wan, Q. Yang, Z. Xu, D. Li, Y. Jin, O.J. Rojas, Mildly processed chitin used in one-component drinking straws and single use materials: Strength, biodegradability and recyclability, Chemical Engineering Journal 442 (2022) 136173.
[212] J.A. Buswell, E. Odier, T.K. Kirk, Lignin Biodegradation, Critical Reviews in Biotechnology 6(1) (1987) 1-60.

[213] K.-E.L. Eriksson, R.A. Blanchette, P. Ander, Biodegradation of Cellulose, in: K.-E.L. Eriksson, R.A. Blanchette, P. Ander (Eds.), Microbial and Enzymatic Degradation of Wood and Wood Components, Springer Berlin Heidelberg, Berlin, Heidelberg, 1990, pp. 89-180.
[214] T. Xu, X. Ding, H. Cheng, G. Han, L. Qu, Moisture-Enabled Electricity from Hygroscopic Materials: A New Type of Clean Energy, Advanced Materials 36(12) (2023) 2209661.
[215] T. He, H. Wang, B. Lu, T. Guang, C. Yang, Y. Huang, H. Cheng, L. Qu, Fully printed planar moisture-enabled electric generator arrays for scalable function integration, Joule 7(5) (2023) 935-951.
[216] J. Tan, X. Wang, W. Chu, S. Fang, C. Zheng, M. Xue, X. Wang, T. Hu, W. Guo, Harvesting Energy from Atmospheric Water: Grand Challenges in Continuous Electricity Generation, Advanced Materials 36(12) (2023) 2211165.
[217] H. Zhang, N. He, B. Wang, B. Ding, B. Jiang, D. Tang, L. Li, High-Performance, Highly Stretchable, Flexible Moist-Electric Generators via Molecular Engineering of Hydrogels, Advanced Materials 35(20) (2023) 2300398.
[218] Y. Cao, B. Xu, Z. Li, H. Fu, Advanced Design of High-Performance Moist-Electric Generators, Advanced Functional Materials 33(31) (2023) 2301420.
[219] X. Wen, Z. Sun, X. Xie, Q. Zhou, H. Liu, L. Wang, X. Qin, S.C. Tan, High-Performance Fully Stretchable Moist-Electric Generator, Advanced Functional Materials 34(11) (2024) 2311128.
[220] S. Lin, H. Yuk, T. Zhang, G.A. Parada, H. Koo, C. Yu, X. Zhao, Stretchable Hydrogel Electronics and Devices, Advanced Materials 28(22) (2016) 4497-4505.
[221] K. Zhao, J.W. Lee, Z.G. Yu, W. Jiang, J.W. Oh, G. Kim, H. Han, Y. Kim, K. Lee, S. Lee, H. Kim, T. Kim, C.E. Lee, H. Lee, J. Jang, J.W. Park, Y.-W. Zhang, C. Park, Humidity-Tolerant Moisture-Driven Energy Generator with MXene Aerogel–Organohydrogel Bilayer, ACS Nano 17(6) (2023) 5472-5485.
[222] H. Wu, L. Wu, S. Lu, X. Lin, H. Xiao, X. Ouyang, S. Cao, L. Chen, L. Huang, Robust superhydrophobic and superoleophilic filter paper via atom transfer radical polymerization for oil/water separation, Carbohydrate Polymers 181 (2018) 419-425.
[223] L. Chen, X. Wei, H. Wang, M. Yao, L. Zhang, G. Gellerstedt, M.E. Lindström, M. Ek, S. Wang, D. Min, A modified ionization difference UV–vis method for fast quantitation of guaiacyl-type phenolic hydroxyl groups in lignin, International Journal of Biological Macromolecules 201 (2022) 330-337.
[224] Z. Sun, L. Feng, X. Wen, L. Wang, X. Qin, J. Yu, Nanofiber fabric based ion-gradient-enhanced moist-electric generator with a sustained voltage output of 1.1 volts, Materials Horizons 8(8) (2021) 2303-2309.
[225] G. Kim, J.W. Lee, K. Zhao, T. Kim, W. Kim, J.W. Oh, K. Lee, J. Jang, G. Zan, J.W. Park, S. Lee, Y. Kim, W. Jiang, S. Li, C. Park, A deformable complementary moisture and tribo energy harvester, Energy & Environmental Science 17(1) (2024) 134-148.
[226] X. Liu, H. Gao, L. Sun, J. Yao, Generic Air-Gen Effect in Nanoporous Materials for Sustainable Energy Harvesting from Air Humidity, Advanced Materials 36(12) (2023) 2300748.
[227] Q. Wang, X. Pan, H. Zhang, S. Cao, X. Ma, L. Huang, L. Chen, Y. Ni, Fruit-battery-inspired self-powered stretchable hydrogel-based ionic skin that works effectively in extreme environments, Journal of Materials Chemistry A 9(7) (2021) 3968-3975.
[228] H. Cheng, Y. Huang, F. Zhao, C. Yang, P. Zhang, L. Jiang, G. Shi, L. Qu, Spontaneous power source in ambient air of a well-directionally reduced graphene oxide bulk, Energy &

Environmental Science 11(10) (2018) 2839-2845.
[229] Y. Huang, H. Cheng, C. Yang, P. Zhang, Q. Liao, H. Yao, G. Shi, L. Qu, Interface-mediated hygroelectric generator with an output voltage approaching 1.5 volts, Nature Communications 9(1) (2018) 4166.
[230] T. Xu, X. Ding, C. Shao, L. Song, T. Lin, X. Gao, J. Xue, Z. Zhang, L. Qu, Electric Power Generation through the Direct Interaction of Pristine Graphene-Oxide with Water Molecules, Small 14(14) (2018) 1704473.
[231] D. Shen, M. Xiao, G. Zou, L. Liu, W.W. Duley, Y.N. Zhou, Self-Powered Wearable Electronics Based on Moisture Enabled Electricity Generation, Advanced Materials 30(18) (2018) 1705925.
[232] J. Xue, F. Zhao, C. Hu, Y. Zhao, H. Luo, L. Dai, L. Qu, Vapor-Activated Power Generation on Conductive Polymer, Advanced Functional Materials 26(47) (2016) 8784-8792.
[233] H. Yuan, T. Zhu, Y. Huang, Z. Wang, P. Han, L. Tan, J. Wu, X. Chen, P. Yao, C. Zhu, J. Xu, Hydrophobic and Adhesive Elastomer Encapsulation for Anti-Drying, Non-Swelling, and Adhesive Hydrogels, Advanced Functional Materials 34(51) (2024) 2409703.
[234] X. Zhang, D. Li, X. Yang, L. Wang, G. Li, T.-W. Wong, T. Li, W. Yang, Z. Luo, Hydro-locking in hydrogel for extreme temperature tolerance, Science 387(6737) (2025) 967-973.
[235] M. Wu, C. Qiao, P.-F. Sui, J.-L. Luo, Z. Li, Y. Cao, R. Pei, X. Peng, H. Zeng, Stratum Corneum-Inspired Zwitterionic Hydrogels with Intrinsic Water Retention and Anti-Freezing Properties for Intelligent Flexible Sensors, Advanced Functional Materials (2025) 2422755.

8 SOMMAIRE RÉCAPITULATIF

Générateurs électriques portables à base d'hydrogel, actionnés par des ions, et capteurs de pression autonomes

8.1 Introduction

Pour améliorer l'interaction entre l'homme et la machine, les dispositifs électroniques portables attirent de plus en plus d'attention. Leur souplesse, leur légèreté et leur réactivité en temps réel leur permettent de jouer un rôle important dans la surveillance de la santé, le contrôle intelligent et la rééducation. Les capteurs de pression portables, en particulier, peuvent transformer de légères pressions mécaniques en signaux électriques, permettant ainsi de suivre avec précision des signes vitaux comme le rythme cardiaque, la respiration ou la démarche. Comparés aux matériaux rigides classiques, les hydrogels, grâce à leur teneur élevée en eau, leur douceur et leur bonne compatibilité avec la peau, sont mieux adaptés au contact cutané. Ils sont aujourd'hui considérés comme des matériaux prometteurs pour la fabrication de capteurs de pression flexibles de nouvelle génération.

Les hydrogels sont des réseaux polymères hydrophiles en trois dimensions, dotés d'une grande souplesse de conception. Leurs propriétés mécaniques, conductrices, antigel, anti-dessèchement, auto-réparatrices et adhésives peuvent être modulées par des stratégies moléculaires adaptées. Dans le développement des capteurs de pression portables, les hydrogels sont généralement classés en trois catégories selon leur origine : naturels (comme la gélatine ou la chitine), synthétiques (comme le poly(acrylamide) (PAM) ou le poly(alcool vinylique) (PVA)), et composites (par exemple la lignine combinée au PVA). L'adoption de structures à double réseau, de renforts nanométriques ou de liaisons dynamiques permet d'en améliorer la solidité et la stabilité à long terme. Sur le plan de la conductivité, trois approches sont couramment utilisées : l'introduction de matériaux carbonés, de nanoparticules métalliques ou de polymères conducteurs pour favoriser la conduction électronique ; l'ajout de sels métalliques, de liquides ioniques ou de solvants eutectiques profonds pour assurer une conduction ionique ; et l'emploi de polymères électrolytes contenant des groupes ionisables, tels que –COOH ou $–SO_3Na$, capables de libérer des ions mobiles et de former des voies conductrices internes. Ces derniers présentent l'avantage de combiner souplesse, efficacité électrique et absence de charges conductrices externes, ce qui en fait des candidats

particulièrement adaptés aux dispositifs électroniques souples de nouvelle génération.
L'adaptabilité des hydrogels à l'environnement ne doit pas être négligée. Pour répondre aux conditions extrêmes telles que le gel à basse température et le dessèchement à haute température, des approches consistant à incorporer des sels, des solvants organiques, des liquides ioniques ou de petites molécules biologiques ont été mises en œuvre afin d'abaisser le point de congélation et d'améliorer la rétention d'eau. Par ailleurs, les réseaux de liaisons dynamiques et réversibles confèrent aux hydrogels une capacité d'auto-réparation, permettant de restaurer leurs propriétés mécaniques et électriques après endommagement, prolongeant ainsi leur durée d'utilisation. Enfin, l'introduction de molécules riches en groupes fonctionnels, telles que l'acide tannique ou la gélatine, améliore significativement leur adhérence, garantissant une fixation stable à la surface de la peau, même dans des environnements complexes impliquant des mouvements ou la transpiration.
À l'heure actuelle, la plupart des capteurs de pression à base d'hydrogel dépendent encore d'une source d'alimentation externe, ce qui limite considérablement leur liberté d'utilisation dans les dispositifs portables. Pour atteindre une autonomie réelle, les technologies triboélectriques (TENGs) et piézoélectriques (PENGs) ont été largement explorées afin de générer un courant alternatif (AC) à partir de stimuli mécaniques. Toutefois, ces approches nécessitent généralement un circuit de redressement supplémentaire pour convertir l'AC en courant continu (DC), ce qui augmente la complexité et l'encombrement du système. Ainsi, le développement de mécanismes de génération directe de courant continu à partir d'hydrogels est devenu un axe de recherche prioritaire.
Des travaux récents ont montré que certains effets thermoélectriques, tels que l'effet Soret ou les batteries thermiques, ainsi que les gradients d'humidité, peuvent induire un transport ionique orienté dans l'hydrogel, générant ainsi une sortie DC stable dans un circuit externe. Cependant, ces mécanismes sont fortement dépendants des conditions environnementales, ce qui entraîne souvent une instabilité de la sortie et limite leur utilisation pratique. Dans cette optique, la conception d'hydrogels intégrant des canaux sélectifs au transport ionique apparaît prometteuse. Sous une stimulation mécanique, ces structures peuvent induire un flux ionique directionnel, permettant une génération directe de courant continu ou une modulation de celui-ci en réponse à la force appliquée. Cette stratégie ouvre la voie à des capteurs autonomes sans alimentation externe,

contribuant au développement de systèmes électroniques flexibles plus intelligents et entièrement autonomes.

8.2 Objectifs

Cette étude vise à concevoir et développer un dispositif hydrogel flexible capable de générer un courant DC tout en assurant une fonction de détection de pression auto-alimentée. L'objectif principal est d'améliorer les performances de sortie DC en contrôlant la migration ionique directionnelle au sein du réseau hydrogel. Pour atteindre ce but, la composition chimique du matériau a été étudiée en profondeur, la structure du dispositif a été optimisée, et une conception multicouche fonctionnelle a été introduite afin de renforcer les performances globales.

L'ensemble des travaux permet de démontrer la faisabilité de ce type de système en tant que capteur de pression auto-alimenté. Le manuscrit se divise en trois parties :

Première partie: Nous présentons un capteur de pression auto-alimenté à base d'hydrogel, capable de générer un courant continu en exploitant la différence de mobilité entre cations et anions en solution, selon un principe similaire à celui de la conversion d'énergie par gradient salin. Un hydrogel de poly (acide acrylique) (PAA), à la fois élastique et conducteur, a été synthétisé. Ce polyelectrolyte contient des protons mobiles (H^+) et des groupements carboxylates ($–COO^–$) fixés sur le réseau polymère. Sous compression mécanique, la concentration ionique locale augmente : les anions restent immobiles tandis que les protons migrent dans une direction donnée, générant ainsi un signal électrique DC dans un circuit externe. Ce mécanisme de conversion mécano-électrique a été validé par modélisation théorique et expériences. Le dispositif montre également un potentiel pour des applications telles que la détection de position ou la reconnaissance de sons. Le concept a été généralisé à d'autres hydrogels polyelectrolytiques.

Deuxième partie: Bien que la migration ionique induite mécaniquement dans les hydrogels polyelectrolytes permette de générer un signal DC, la tension reste limitée (<10 mV), restreignant son applicabilité. Pour surmonter cette limite, un système hydrogel avec gradient de concentration ionique intégré a été développé, permettant d'obtenir une tension supérieure à 100 mV. Il repose sur l'assemblage vertical d'un hydrogel de PVA dopé en polyelectrolyte et d'un hydrogel de PVA neutre, créant ainsi un gradient naturel qui favorise la migration ionique. L'influence du type de polyelectrolyte, de son taux d'incorporation et de la structure interfaciale a été analysée.

Les résultats démontrent l'efficacité du dispositif en tant que micro-générateur et capteur de pression auto-alimenté.

Troisième partie : Afin d'améliorer encore les performances, une architecture papier–hydrogel a été introduite, dans laquelle la surface du papier est recouverte d'une couche d'argent. Cette structure permet de dépasser 500 mV en sortie. Le papier favorise la libération d'ions, tandis que l'argent réagit avec l'humidité du gel selon un effet électrochimique de type pile, amplifiant ainsi la tension générée. Ce système est simple, peu coûteux et facilement intégrable. L'effet de divers paramètres (type de papier, taux de réticulation, épaisseur du gel, teneur en glycérol) a été évalué, ainsi que les performances en courant de court-circuit, puissance de sortie et comportement de charge.

Enfin, nous démontrons la capacité du dispositif à produire un signal DC modulable sous contrainte mécanique, confirmant son potentiel pour des applications concrètes de détection de pression. En résumé, ce travail explore les mécanismes fondamentaux, conçoit des structures optimisées et aboutit à un générateur hydrogel performant intégré à un capteur de pression auto-alimenté. Il offre ainsi une base solide pour le développement de dispositifs électroniques souples, autonomes et intelligents.

8.3 Résultats et Discussions

8.3.1 Hydrogel poly électrolyte pour la conversion mécanique–électrique

Dans les hydrogels polyélectrolytiques, bien que les ions dissociés soient mobiles, les chaînes polymères qui forment le squelette du réseau restent immobiles. Lorsqu'une compression mécanique est appliquée, la concentration locale en polymère augmente dans la zone supérieure du gel, ce qui induit une diffusion ionique directionnelle (Figure 8.1a). Cette migration, non compensée par un déplacement des chaînes fixes, génère un flux d'électrons mesurable dans le circuit externe. Le système est ainsi capable de convertir une contrainte mécanique en signal électrique. Lorsque la pression est relâchée, la structure du gel se rétablit progressivement, entraînant une décroissance puis une extinction du signal de sortie (Figure 8.1b).

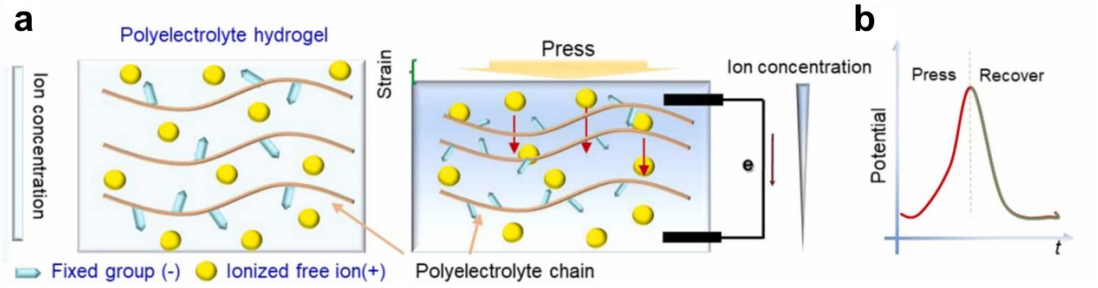

Figure 8.1 a) Sous compression, l'hydrogel polyélectrolyte anionique présente une répartition ionique déséquilibrée, ce qui entraîne une diffusion directionnelle des ions et la conversion de l'énergie mécanique en signal électrique. b) Après relâchement, le réseau élastique retrouve sa forme initiale et les ions se redistribuent de manière homogène, permettant une détection de contrainte auto-alimentée.

La Figure 8.2a illustre un modèle de convertisseur mécano-électrique composé d'un hydrogel cylindrique de PAA, un polyélectrolyte anionique, d'un diamètre de 2,5 cm, associé à une électrode en papier graphite flexible. Les résultats expérimentaux (Figure 8.2b) montrent qu'une compression appliquée par le haut entraîne une augmentation rapide de la tension de sortie, suivie d'un signal stable tant que la pression est maintenue, ce qui témoigne d'une bonne réactivité et stabilité. Ce comportement confirme notre hypothèse : la compression induit un gradient de concentration de H^+ du haut vers le bas, générant une diffusion directionnelle des protons responsable de la tension observée. Étant donné que les charges des H^+ et celles des chaînes PAA s'équilibrent globalement, le signal électrique ne provient pas directement de la pression appliquée, mais bien du transport ionique induit. Lors de la compression inverse de l'hydrogel, la tension de sortie diminue progressivement (Figure 8.2c), ce qui démontre clairement la migration inverse des protons (Figure 8.2d). Ces deux processus sont pratiquement symétriques.

Des analyses complémentaires révèlent qu'après compression, la densité du réseau polymère de l'hydrogel augmente (Figure 8.2e). Les résultats de la simulation par éléments finis (Figure 8.2f) indiquent une différence de déformation entre les surfaces supérieure et inférieure. Cette différence s'accentue avec l'augmentation de la contrainte appliquée, renforçant ainsi le gradient de concentration en H^+ entre les deux faces.

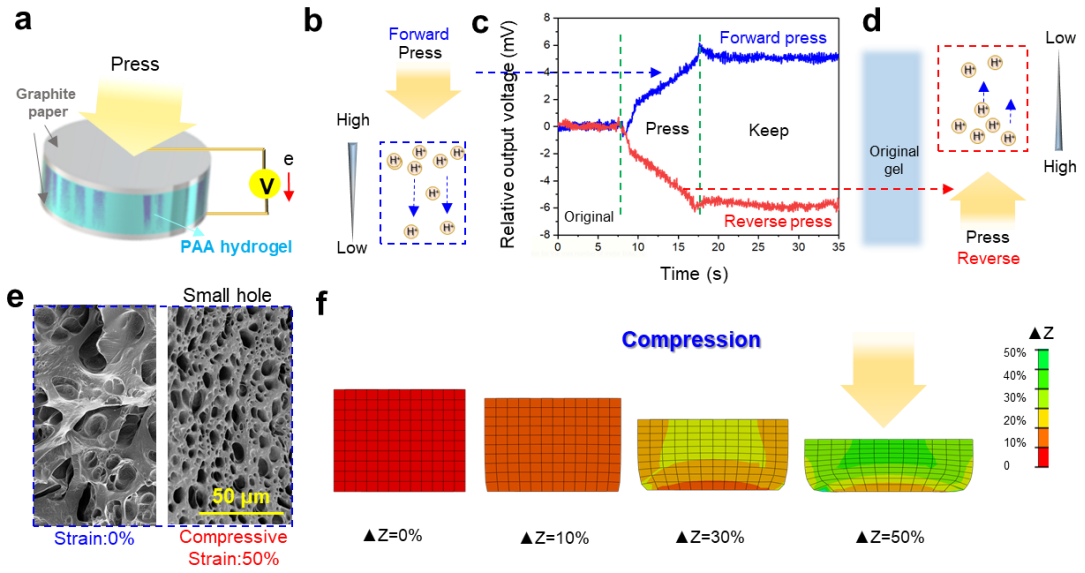

Figure 8.2 a) Schéma du modèle de conversion mécano-électrique basé sur un hydrogel de PAA. b) Principe de fonctionnement de l'hydrogel de PAA convertissant l'énergie mécanique en énergie électrique lors d'une compression vers l'avant. c) Variation de la tension de sortie relative (impulsion) de l'hydrogel de PAA en réponse à une compression dynamique externe. d) Principe de fonctionnement de l'hydrogel de PAA convertissant l'énergie mécanique en électricité lors d'une compression vers l'arrière. e) Images MEB de la structure interne des hydrogels de PAA soumis à différentes déformations en compression. f) Simulation par éléments finis de la répartition locale du déplacement et de l'état du réseau de PAA dans les hydrogels sous différentes déformations en compression (ΔZ représente le déplacement).

Nous avons mis en évidence la capacité directionnelle de détection auto-alimentée de l'hydrogel à base de PAA et développé, sur cette base, un capteur capable de reconnaître l'orientation d'une stimulation mécanique. Comme illustré dans la Figure 8.3a, le dispositif se compose d'un hydrogel de PAA encadré par deux électrodes en papier graphite, l'ensemble étant divisé en trois zones : A (gauche), O (centre) et B (droite), chacune générant une réponse électrique distincte. Une pression sur la zone A entraîne une augmentation locale des protons (H^+), qui diffusent vers la droite, induisant une élévation rapide de la tension de sortie. Inversement, une pression sur la zone B provoque une migration des H^+ vers la gauche, accompagnée d'une chute de tension. Lorsque la pression est appliquée sur la zone centrale O, les diffusions gauche/droite s'équilibrent, entraînant un déplacement net quasi nul et donc un signal électrique négligeable (Figure 8.3b). Ce capteur permet ainsi une reconnaissance simultanée de la position et de la direction, à la manière d'un commutateur logique. Il peut également être adapté pour des applications de reconnaissance vocale auto-alimentée. Les Figure 8.3c et d en illustrent le potentiel dans le domaine des systèmes de perception intelligente.

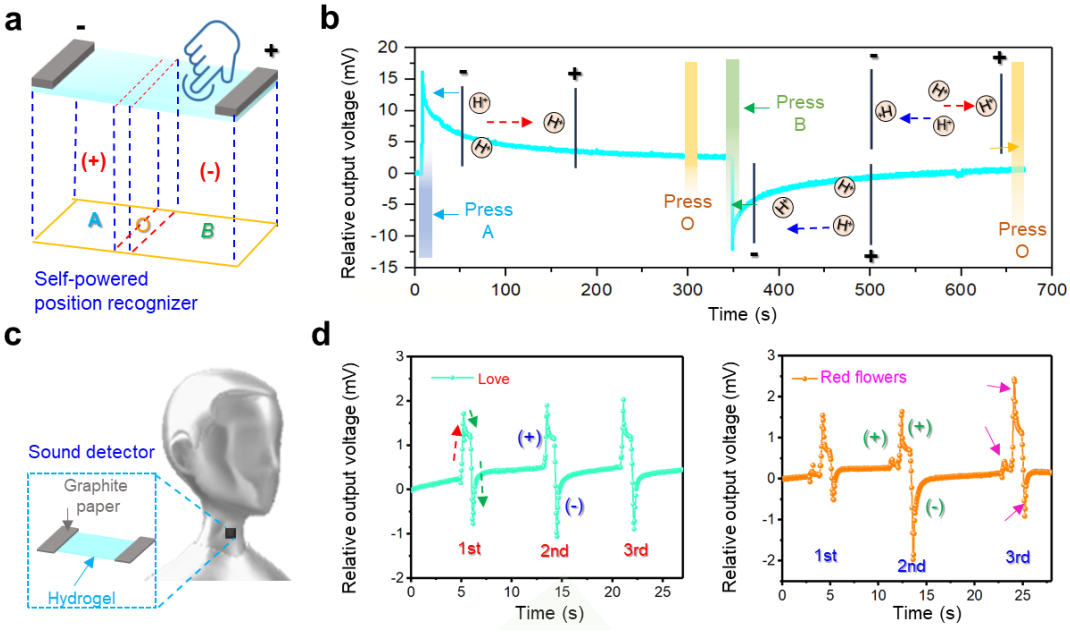

Figure 8.3 a) Schéma d'application d'un dispositif de reconnaissance de position auto-alimenté. b) Variation de la tension de sortie en fonction de la zone pressée sur le détecteur. c) Schéma de principe d'un détecteur acoustique à base d'hydrogel de PAA. d) Réponse en tension du détecteur à différents sons prononcés : « love » et « red flowers ».

Il convient de souligner que l'hydrogel de PAA présente une excellente aptitude au façonnage ainsi qu'un fort potentiel de production à grande échelle. Par exemple, comme le montre la Figure 8.4a, des hydrogels transparents de grande surface (jusqu'à 300 cm²) peuvent être fabriqués. L'hydrogel de PAA offre également une bonne capacité de personnalisation : la Figure 8.4b illustre une semelle réalisée à partir d'un hydrogel de PAA découpé et intégré, pouvant être insérée dans n'importe quel type de chaussure pour capter l'énergie mécanique issue des mouvements du corps.

Cette semelle permet de convertir efficacement l'énergie générée par la marche ou les mouvements des jambes en énergie électrique (Figure 8.4c). En raison d'une légère hétérogénéité interne du gel, un faible signal électrique initial peut exister ; toutefois, seules les impulsions électriques induites par les mouvements mécaniques sont prises en compte dans les mesures. De plus, comme montré dans la Figure 8.4d, la version organohydrogel obtenue par remplacement partiel du solvant par du glycérol permet un fonctionnement à basse température (–24 °C), tout en conservant sa capacité de conversion d'énergie.

Bien que la puissance de sortie reste limitée, la simplicité structurelle et le faible coût de fabrication confèrent à cette semelle un fort potentiel pour la récupération continue de l'énergie mécanique au cours de la marche. Ce concept peut également être

généralisé à d'autres hydrogels polyélectrolytiques. Comme illustré dans les Figure 8.4e à g, des matériaux tels que les hydrogels de PVA, de gomme de guar ou d'alginate de sodium présentent également la capacité de convertir une contrainte mécanique en signal électrique.

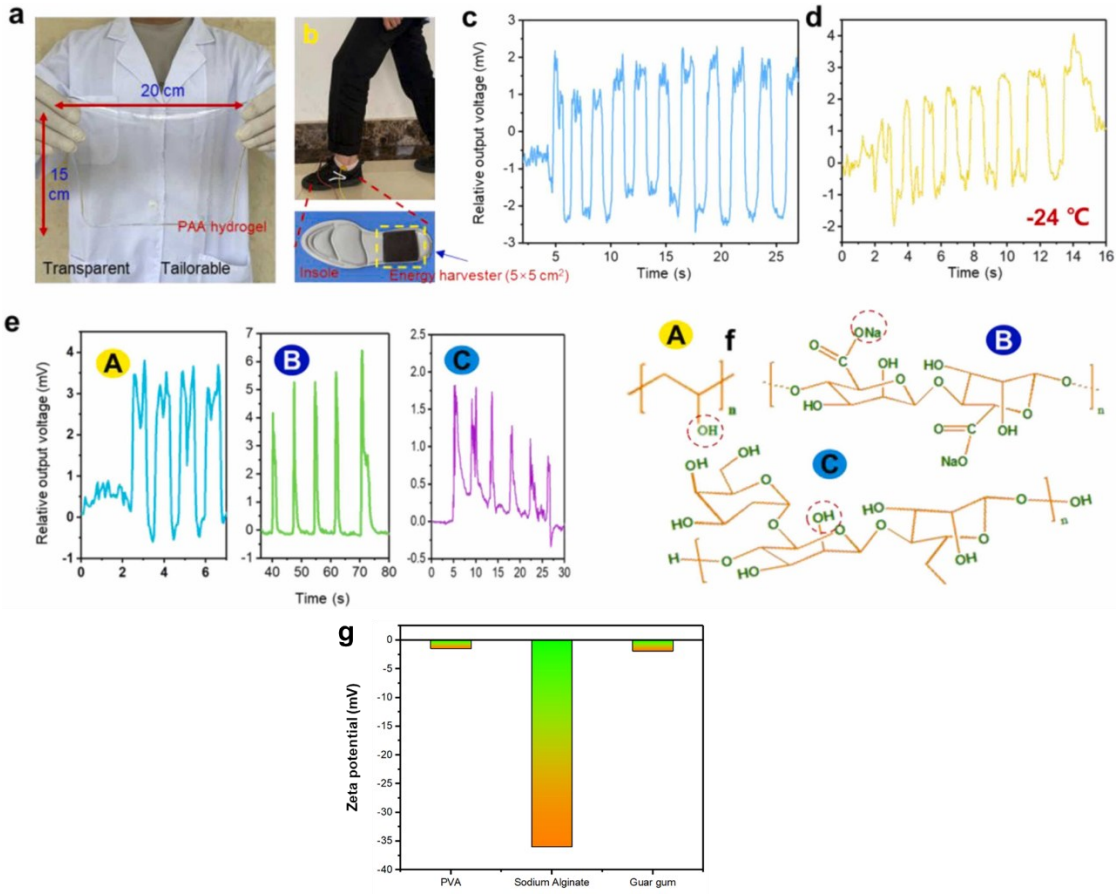

Figure 8.4 a) Les hydrogels de PAA présentent une grande transparence et une capacité de personnalisation. b) La semelle récolteuse d'énergie, assemblée avec l'hydrogel de PAA et des électrodes en papier de graphite, permet de capter l'énergie mécanique. c) Variation de la tension de sortie de la semelle contenant l'hydrogel de PAA en réponse à la marche humaine.d) Variation de la tension de sortie de la semelle contenant l'organohydrogel de PAA en réponse à la marche humaine. e) Performances de récolte d'énergie mécanique de différents hydrogels polyélectrolytes.
f) Structure chimique de différents polyélectrolytes: A. polyalcool vinylique (PVA), B. alginate de sodium, C. gomme de guar. g) Potentiels zêta du PVA (–), de l'alginate de sodium (–) et de la gomme de guar (–).

8.3.2 Générateur à gradient de polyelectrolyte et capteur de pression auto-alimenté

Afin de créer un gradient de concentration ionique plus marqué dans l'hydrogel et ainsi améliorer les performances de sortie du dispositif, nous avons utilisé un hydrogel de PVA non réticulé et exempt d'impuretés comme couche neutre, et introduit deux

polyélectrolytes d'origine biosourcée : un polyanion, le lignosulfonate de sodium (LS), et un polycation, le chitosane quaternaire (QC), afin de former les couches chargées. En solution aqueuse, LS se dissocie en libérant des ions Na^+ mobiles, tandis que les groupes sulfonate ($–SO_3^-$) restent fixés sur la chaîne polymère ; son incorporation dans le PVA permet donc d'obtenir un hydrogel PVA–LS à charge négative (Figure 8.5a). De même, QC libère des ions Cl^- en solution, tandis que les groupes ammonium quaternaires ($–N^+$) restent ancrés dans la matrice, formant un hydrogel PVA–QC à charge positive (Figure 8.5b).

L'empilement successif des couches PVA–QC et PVA–LS sur la couche de PVA neutre permet de constituer l'architecture finale du dispositif. Cette configuration, qui s'inspire de la distribution ionique asymétrique des cellules sanguines, favorise une migration ionique directionnelle génératrice d'électricité. Par exemple, l'hydrogel dopé au LS libère davantage de Na^+ que le PVA pur. Au contact des deux couches, les ions Na^+ diffusent naturellement du côté à forte concentration vers le côté à faible concentration. Les groupes fonctionnels fixés sur la chaîne polymère étant non mobiles, le mécanisme de génération électrique repose donc sur le gradient ionique interne préétabli comme force motrice.

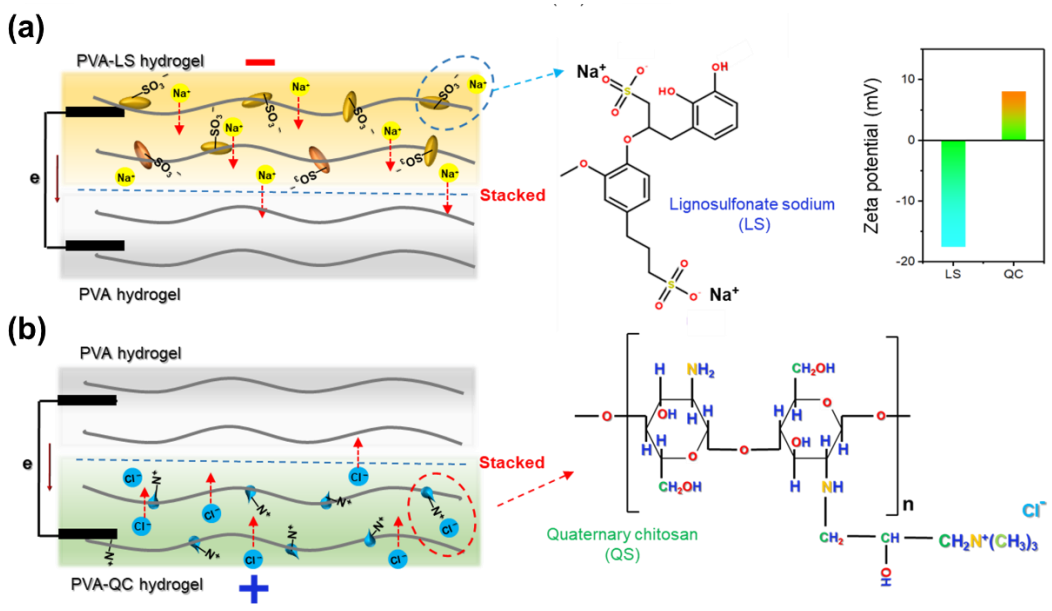

Figure 8.5 a) Principe de fonctionnement du générateur électrique basé sur un hydrogel à gradient de polyélectrolyte biomasse LS (–). b) Principe de fonctionnement du générateur électrique basé sur un hydrogel à gradient de polyélectrolyte biomasse QC (+).

Pour étudier l'effet de la teneur en LS sur les propriétés électriques des hydrogels

composites, des hydrogels PVA–LS ont été préparés avec différentes concentrations de LS. Comme montré sur la Figure 8.6a, l'aspect du gel passe progressivement d'un état transparent à une teinte brun foncé et opaque à mesure que la teneur en LS augmente. Cette augmentation entraîne une libération plus importante de Na^+, ce qui améliore la conductivité de l'hydrogel (Figure 8.6b).

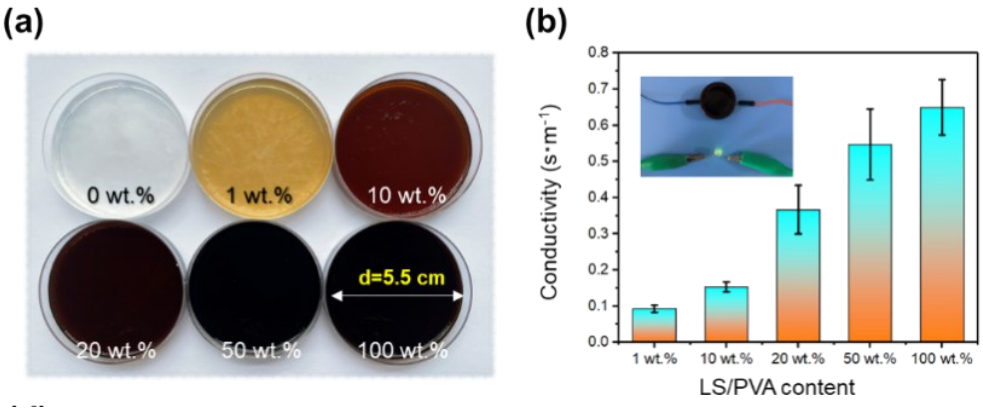

Figure 8.6 a) Aspect visuel des hydrogels PVA–LS avec différentes teneurs en LS (1 % en poids correspond à un rapport massique LS/PVA de 1 %). b) Conductivité ionique de la solution de LS.

Des échantillons d'hydrogel PVA–LS en forme de disque (diamètre : 5,5 cm ; épaisseur : 5 mm) ont été préparés avec différentes teneurs en LS, puis placés sur une couche de PVA pur de mêmes dimensions pour former une structure bilayer. Cet ensemble a ensuite été inséré entre deux électrodes en papier graphite (épaisseur : 0,5 mm) afin d'assembler le dispositif final, désigné sous le nom de générateur d'électricité à gradient de polyelectrolyte à base d'hydrogel (PGHEG). La Figure 8.7 présente l'influence de la concentration en LS sur la tension de sortie du dispositif. Les résultats montrent qu'à température ambiante, l'augmentation de la teneur en LS entraîne une élévation progressive de la tension, passant d'environ 20 mV à un maximum d'environ 125 mV. Cette amélioration s'explique par l'introduction de quantités croissantes de Na^+ mobiles, qui renforcent le gradient de concentration ionique entre les couches PVA–LS et PVA pur, assurant ainsi une force motrice plus importante. Les particules de LS, contenant des groupes $–SO_3^-$, restent fixées dans le réseau du gel. Toutefois, au-delà d'un certain seuil, l'augmentation de la tension tend à se stabiliser. En prenant en compte à la fois l'efficacité et le coût, le gel PVA–LS à 100 % en poids a été retenu comme formulation de référence pour les expériences ultérieures.

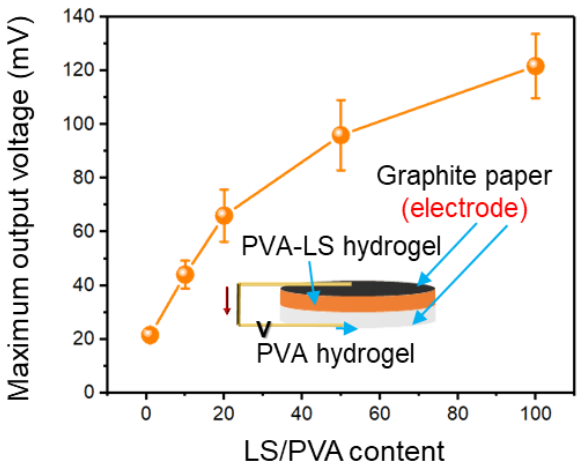

Figure 8.7 Tensions de sortie des dispositifs PGHEG assemblés à partir de différents hydrogels PVA–LS et d'un hydrogel de PVA pur.

La structure tridimensionnelle poreuse de l'hydrogel de PVA offre des canaux de diffusion directionnelle pour les ions Na^+, ce qui est essentiel à la génération d'électricité (Figure 8.8a). La Figure 8.8b confirme par ailleurs l'accumulation significative de Na^+ dans l'hydrogel de PVA neutre après contact avec le gel PVA–LS, indiquant une migration ionique effective entre les deux couches.

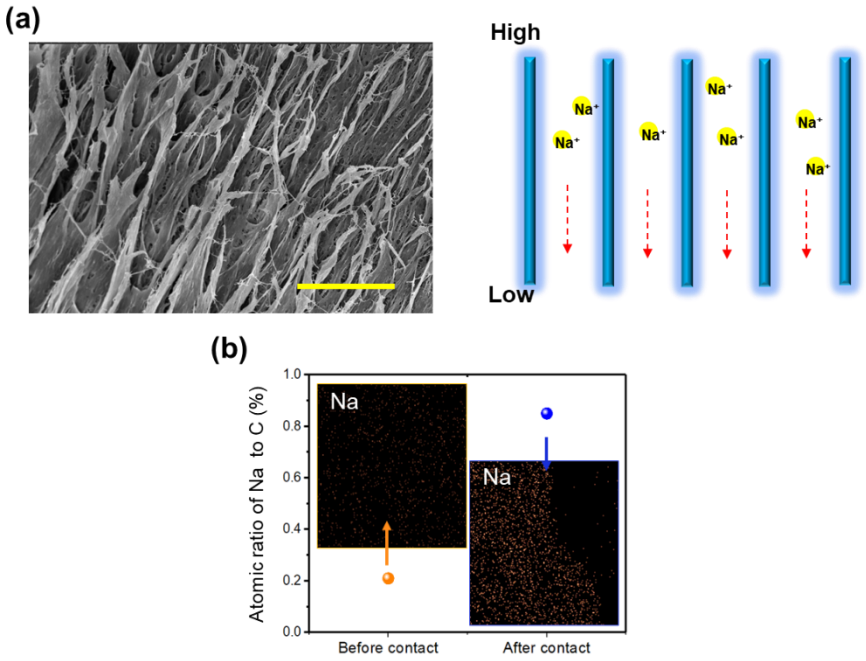

Figure 8.8 a) Les pores tridimensionnels à l'intérieur de l'hydrogel de PVA servent de canaux pour la migration des ions Na^+. Barre d'échelle : 10 µm. b) Évolution de la teneur en sodium dans l'hydrogel de PVA initial et dans l'hydrogel de PVA placé sous l'hydrogel PVA–LS dans le dispositif PGHEG.

Le dispositif PGHEG, basé sur l'hydrogel PVA–LS optimisé (100 % en poids), atteint une tension de sortie maximale d'environ 130 mV ainsi qu'une densité de courant stable de l'ordre de 2,11 µA/cm² (Figure 8.9a et b). Par ailleurs, la tension de sortie peut se maintenir au-dessus de 100 mV pendant près de 10 heures, démontrant une excellente stabilité dans le temps.

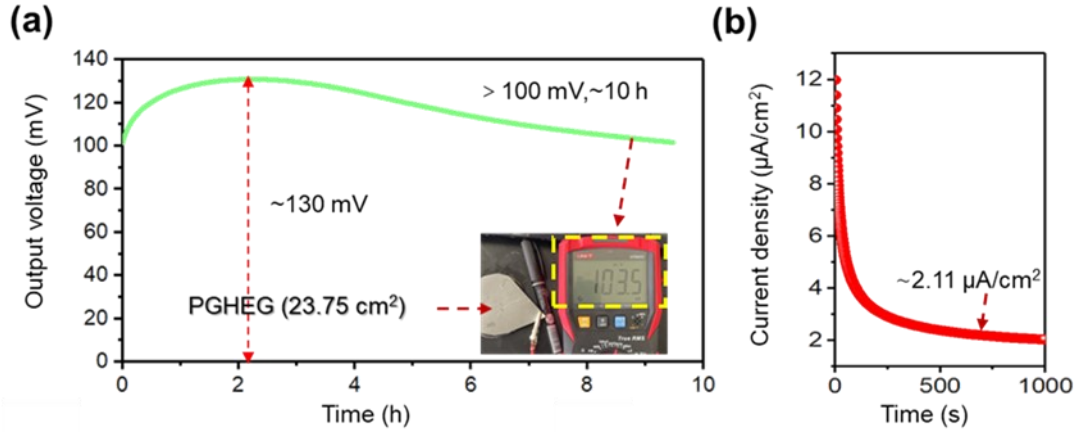

Figure 8.9 Tension (a) et courant (b) de sortie en temps réel du générateur électrique assemblé avec l'hydrogel PVA–LS (100 % en poids) à température ambiante.

Outre l'utilisation du polyanion LS, nous avons également étudié des dispositifs PGHEG fabriqués à partir d'hydrogels de PVA dopés avec le polyélectrolyte cationique QC (PVA–QC). Grâce à la libération importante d'ions Cl^- par le QC, la conductivité du système (solution + hydrogel) s'en trouve considérablement améliorée (Figure 8.10a à c). Par ailleurs, une augmentation notable de la concentration en Cl^- a été observée dans l'hydrogel de PVA pur après contact avec le gel PVA–QC, ce qui confirme la migration directionnelle des ions Cl^- (Figure 8.10d).

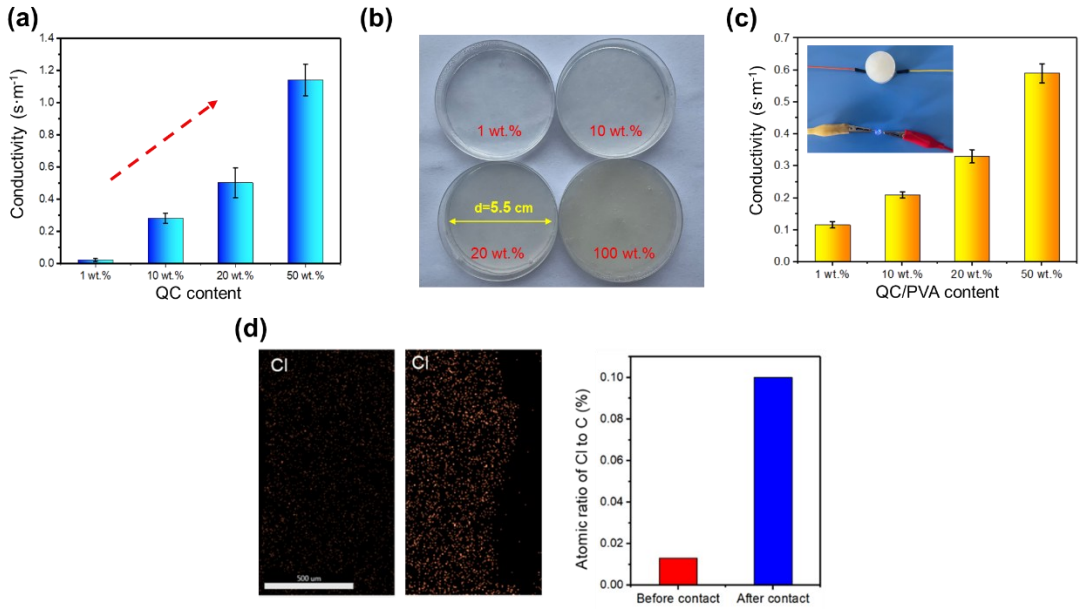

Figure 8.10 a) Conductivité de la solution de QC. b) Aspect visuel des hydrogels PVA–QC avec différentes teneurs en QC (1 % en poids correspond à un rapport massique QC/PVA de 1 %).c) Conductivité ionique des hydrogels PVA–QC en fonction de la teneur en QC (la composition détaillée est présentée dans le Tableau 2.4). d) Variation de la teneur en ions Cl^- dans l'hydrogel de PVA initial et dans l'hydrogel de PVA ayant été en contact avec l'hydrogel PVA–QC du dispositif PGHEG.

L'augmentation de la teneur en QC dans l'hydrogel PVA–QC améliore significativement la tension de sortie du dispositif PGHEG, passant d'environ 8 mV à près de 70 mV (Figure 8.11a). Toutefois, comme le QC et le PVA sont tous deux des agents épaississants, une solubilisation complète du QC au-delà de 50 % en poids dans la solution de PVA s'avère difficile. À cette concentration maximale, le dispositif empilé à base de PVA–QC atteint une tension de sortie de 71 mV et une densité de courant de 0,674 µA/cm² (Figure 8.11b et c). Les différences de performance entre les dispositifs dopés au QC et ceux dopés au LS peuvent être liées à la taille des ions, à la nature des matériaux utilisés, ainsi qu'à la structure du réseau hydrogel formé. Afin d'obtenir une tension positive, il est nécessaire de positionner la couche de PVA–QC en dessous de celle en PVA pur (Figure 8.11d); sinon, une tension de sortie négative est observée. Cette configuration rappelle une pile AA inversée, avec l'électrode positive placée en bas. Ces résultats montrent que des polyélectrolytes cationiques comme anioniques peuvent induire une génération de tension, la direction du courant dépendant uniquement du signe des charges ioniques et du sens de leur diffusion.

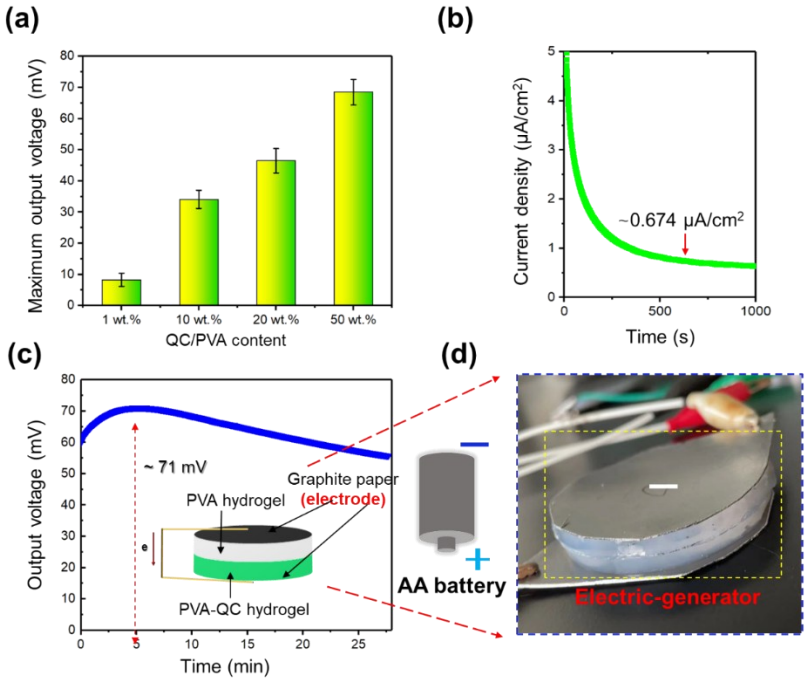

Figure 8.11 a) Tensions de sortie des dispositifs assemblés à partir de différents hydrogels PVA–QC et d'un hydrogel de PVA pur (diamètre de l'hydrogel : 5,5 cm ; épaisseur : 5 mm). b) Courant en temps réel d'un dispositif PGHEG assemblé avec un hydrogel PVA–QC à 50 % en poids, à température ambiante. c) Tension de sortie en temps réel du même dispositif PGHEG assemblé avec un hydrogel PVA–QC à 50 %, à température ambiante. d) Comparaison visuelle entre le dispositif PGHEG et des piles AA.

Après avoir déterminé les concentrations optimales de LS et de QC, nous avons procédé à l'assemblage en série de plusieurs dispositifs PGHEG afin d'augmenter significativement la tension de sortie (Figure 8.12a). Comme illustré dans la Figure 8.12b, plusieurs unités PGHEG (composées d'une couche de PVA–LS à 100 % et d'une couche de PVA neutre) ont été connectées en série. Un module comprenant 10 unités permet de générer une tension continue atteignant environ 1,29 V, suffisante pour alimenter de manière autonome une petite calculatrice (Figure 8.12c).

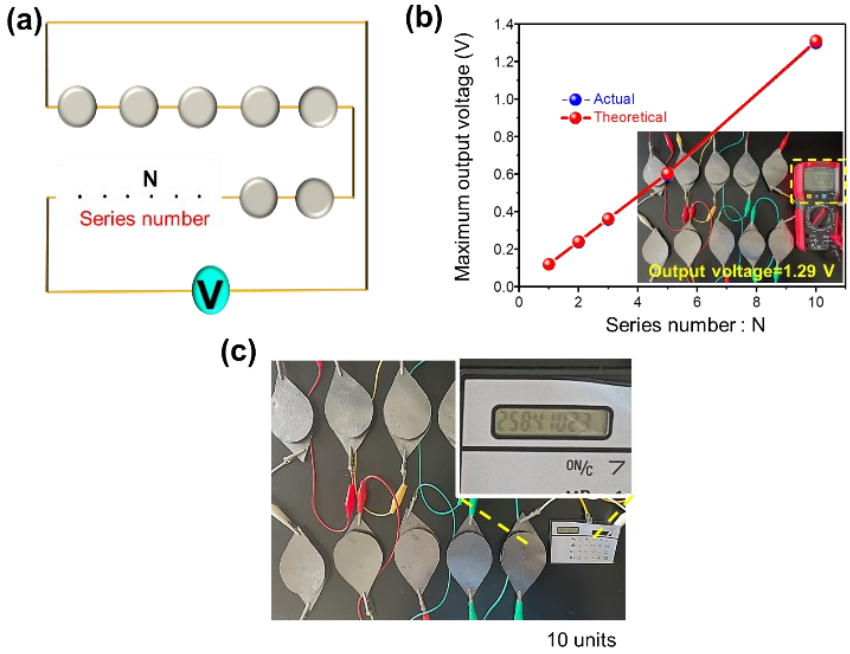

Figure 8.12 a) Schéma de connexion en série des dispositifs PGHEG. b) Relation entre la tension de sortie réelle et théorique en fonction du nombre d'unités PGHEG connectées en série. Chaque unité est composée d'un hydrogel PVA–LS à 100 % en poids (épaisseur : 5 mm, surface : 23,75 cm²) et d'un hydrogel PVA pur de même taille. c) Démonstration de 10 unités PGHEG connectées en série alimentant une calculatrice commerciale.

Par ailleurs, un capteur de pression PGHEG a été conçu sur la base de la structure PVA–LS/PVA afin d'évaluer sa capacité à détecter la pression via une sortie en courant continu (Figure 8.13a). Comme montré dans les Figure 8.13b et c, le dispositif génère des variations de tension clairement distinctes en réponse à différents niveaux de pression, tels qu'une pression du doigt ou des poids variés, démontrant ainsi son efficacité pour la détection de pression.

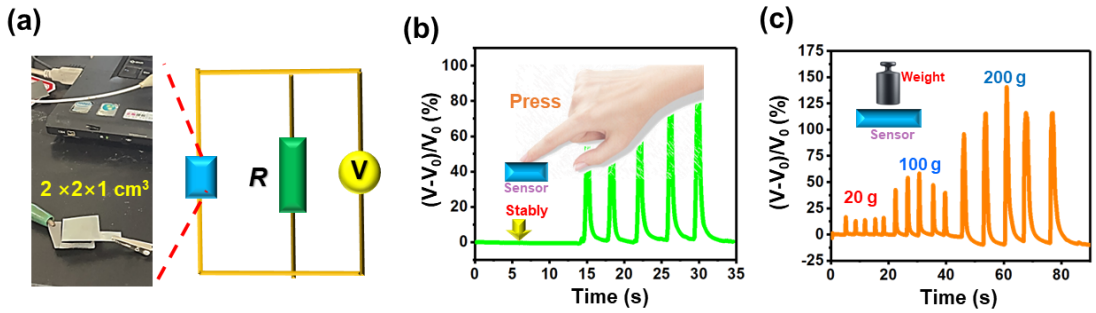

Figure 8.13 a) Schéma du capteur auto-alimenté basé sur le dispositif PGHEG; b–c) Illustrations des réponses auto-alimentées sous différents niveaux de pression.

8.3.3 Générateur papier–hydrogel et capteur de pression auto-alimenté

La Figure 8.14a montre le schéma de fabrication et d'application du générateur d'électricité papier-hydrogel (PHEG). Ce dispositif est composé d'une électrode inférieure en papier graphite, d'une couche intermédiaire d'hydrogel de PAM, et d'une électrode supérieure constituée d'un papier filtre recouvert de paillettes d'argent (Ag). Contrairement aux électrodes métalliques rigides conventionnelles, l'électrode supérieure utilise un papier filtre conducteur, léger, souple, hydrophile et facilement personnalisable (Figure 8.14b).

La surface du papier, rugueuse et riche en groupes –OH, facilite le dépôt de paillettes d'argent (Figure 8.14c et d). Ces paillettes ne sont pas en contact direct avec l'hydrogel, mais servent à la conduction et à la collecte de l'énergie. L'hydrogel de PAM est un matériau élastique formé par réticulation covalente de polymères de PAM dans l'eau, présentant une excellente extensibilité et élasticité (Figure 8.14e). Son réseau tridimensionnel est rempli d'eau, comme le montre la Figure 8.14f. Le PAM possède également de bonnes propriétés adhésives, assurant une liaison stable avec le papier graphite flexible (en haut) et le papier filtre (en bas) (Figure 8.14g). La Figure 8.14h montre que la force maximale de pelage du PAM sur le papier filtre dépasse 130 N/m. Après le test de pelage, des fibres de papier restent partiellement collées à la surface du gel, ce qui confirme la bonne cohésion et flexibilité de la structure stratifiée.

Sauf indication contraire, les dispositifs PHEG utilisés dans cette étude sont constitués de papier filtre recouvert d'Ag (2 × 2 cm^2), d'un hydrogel de PAM (2 × 2 × 0,5 cm^3), et de papier graphite, testés à température ambiante (25 ± 5 °C).

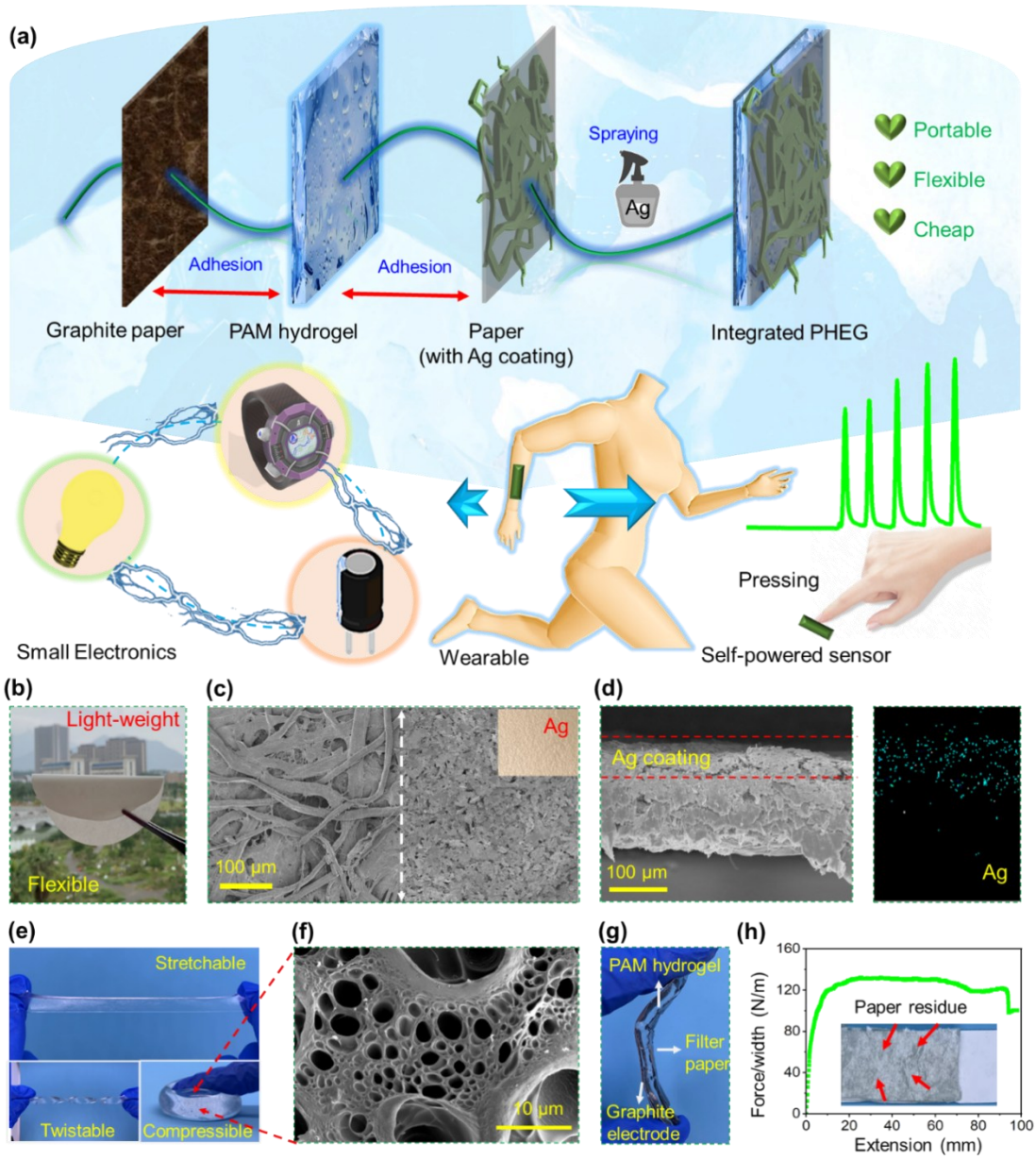

Figure 8.14 a) Schéma représentant la préparation, la composition et l'application du dispositif PHEG. b) Photo réelle du papier filtre. c) Image MEB du papier filtre avant et après dépôt d'argent.
d) Image en coupe transversale du papier filtre avec revêtement d'argent et répartition de l'argent.
e) Photographies montrant le comportement mécanique des hydrogels de PAM. f) Image MEB de l'hydrogel de PAM. g) Photo réelle du dispositif intégré papier filtre/hydrogel. h) Force d'adhésion entre le papier filtre et l'hydrogel de PAM.

Comme illustré dans les Figure 8.15a et b, les dispositifs HEG et PEG, constitués respectivement d'un hydrogel de PAM ou d'un papier filtre seul, présentent une tension en circuit ouvert proche de 0 V. En revanche, le dispositif PHEG intégré génère une tension avoisinante 0,6 V, ce qui indique que la production de tension provient

principalement des effets interfaciaux entre les différentes couches du système. Une analyse par spectroscopie photoélectronique à rayons X (XPS) révèle en outre la présence de groupes C–OH dans le papier filtre à base de cellulose (Figure 8.15c).

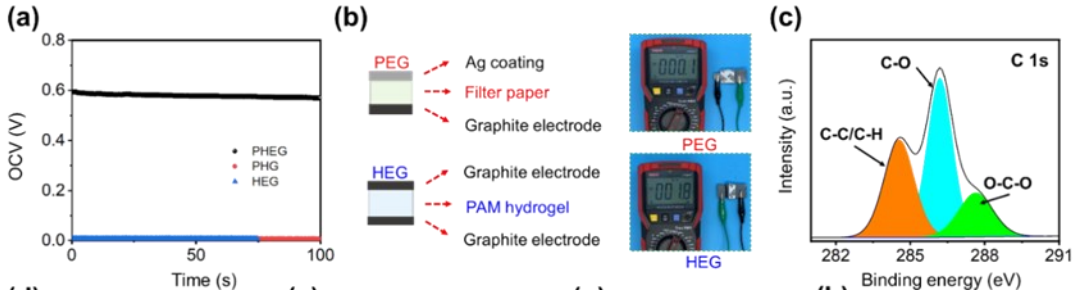

Figure 8.15 a–b) Tension de sortie des dispositifs composés de papier/hydrogel, de papier seul ou d'hydrogel seul, respectivement. c) Spectre XPS C1s du papier filtre.

Ces groupes hydroxyle (–OH) peuvent subir une légère ionisation dans l'eau, libérant des protons (H^+). Une chute brutale de la résistance (R) du PHEG est observée immédiatement après l'assemblage du dispositif (Figure 8.16), ce qui indique une diffusion rapide de l'eau contenue dans l'hydrogel vers le papier filtre, facilitant ainsi l'ionisation et le transport des protons.

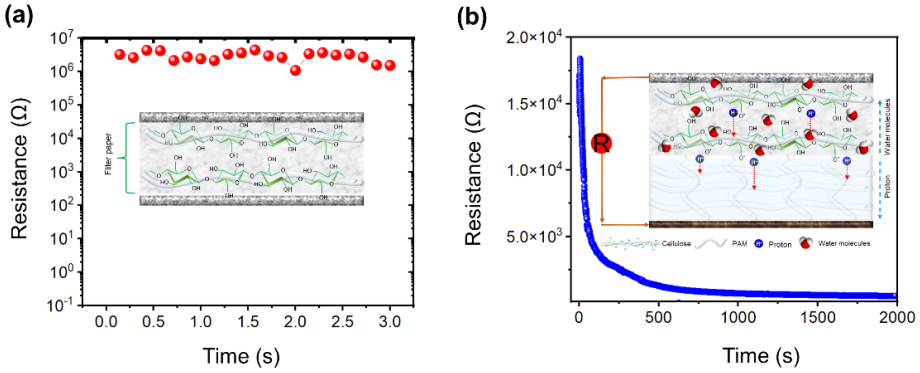

Figure 8.16 a) Résistance électrique du papier filtre. b) La résistance électrique du générateur papier-hydrogel (PHEG) a été enregistrée à partir du moment où le papier filtre et l'hydrogel PAM ont été assemblés. Le papier filtre mesure 2 × 2 cm² et l'épaisseur de l'hydrogel PAM est de 5 mm.

La Figure 8.17 résume le mécanisme de fonctionnement du PHEG : lorsque le papier filtre absorbe l'eau provenant de l'hydrogel de PAM, les protons migrent rapidement vers le bas à travers le gel. Parallèlement, le revêtement métallique asymétrique des électrodes entre en contact avec l'eau et initie une réaction de type pile galvanique, libérant des électrons et générant une tension. À mesure que l'eau continue de se

propager vers le haut, elle alimente en protons le flux descendant à travers le papier filtre, ce qui entraîne une montée progressive de la tension en phase initiale.

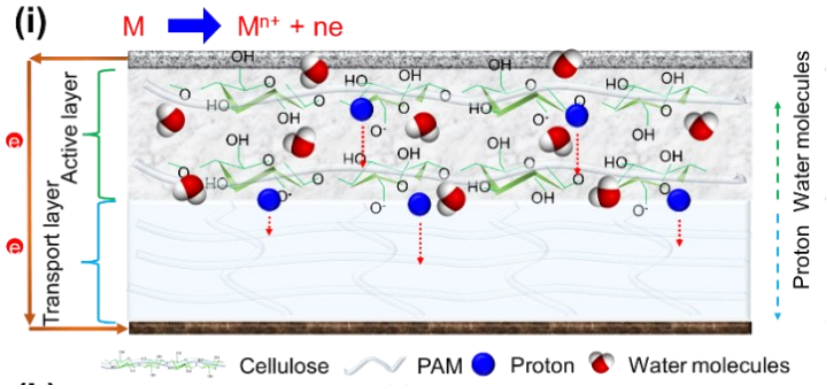

Figure 8.17 Schéma du mécanisme de génération d'électricité.

Après avoir élucidé le mécanisme de fonctionnement de base du PHEG, l'étude a également évalué les performances de sortie des dispositifs assemblés avec d'autres papiers commerciaux. La Figure 8.18a présente l'aspect des papiers d'origine avant et après dépôt de la couche d'argent. La Figure 8.18b montre les angles de contact avec l'eau mesurés sur les différentes surfaces : tous inférieurs à 90°, ce qui indique leur capacité à absorber l'humidité.

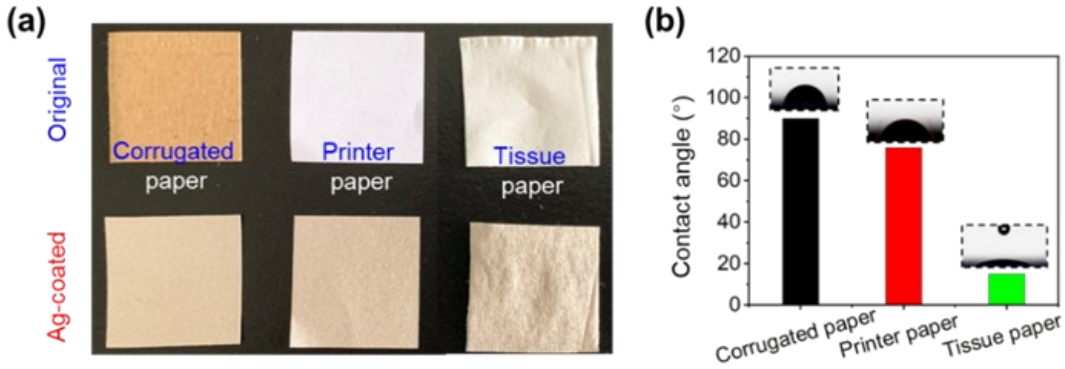

Figure 8.18 a) Photographies de différents papiers avec ou sans revêtement d'argent. b) Angle de contact de l'eau sur différents papiers.

La Figure 8.19a illustre l'évolution de la tension de sortie des dispositifs PHEG assemblés avec différents types de papier durant les 10 premières heures. Les résultats montrent une augmentation progressive de la tension, confirmant l'hypothèse formulée précédemment. L'analyse de la tension moyenne sur cette période (Figure 8.19b) révèle que les papiers mouchoirs et les papiers pour imprimante génèrent des tensions

relativement faibles, ce qui pourrait être attribué à une structure plus lâche ou à une teneur plus élevée en charges minérales (Figure 8.19c).

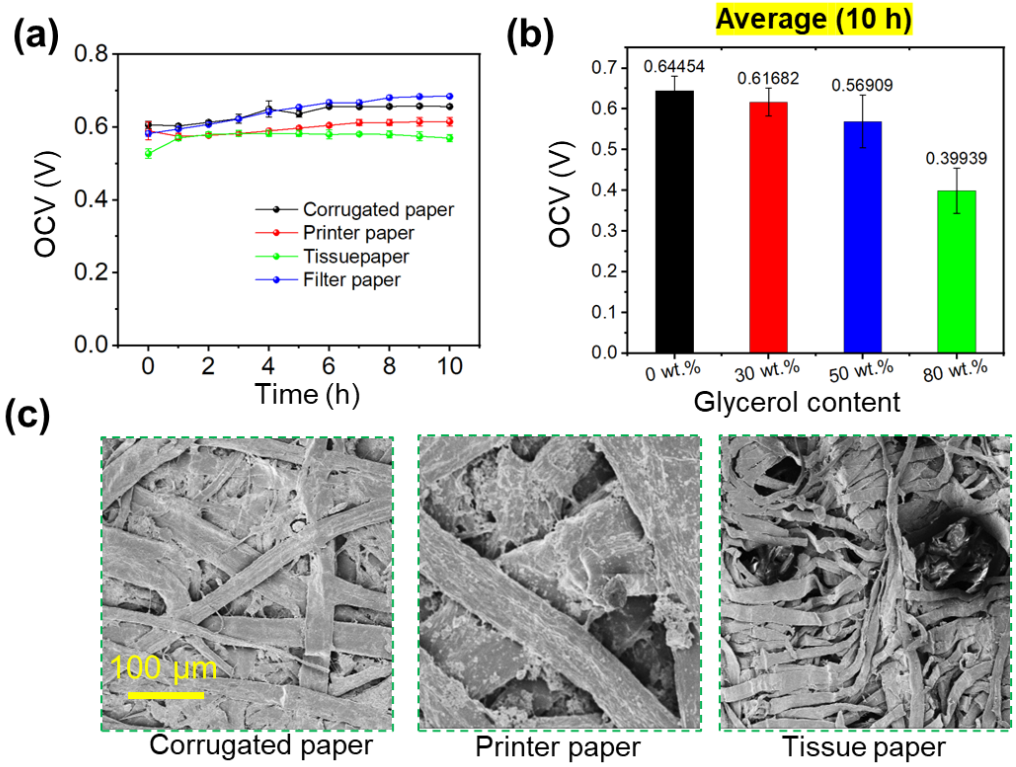

Figure 8.19 a) Tension de sortie (0–10 h) du générateur PHEG assemblé à partir de différents papiers. b) Tension moyenne pendant les 10 premières heures pour les différents PHEG. c) Images MEB des différents papiers.

Les performances du dispositif PHEG dépendent non seulement de la couche de transport de protons, mais également des propriétés de l'hydrogel de PAM. Les résultats indiquent que ni le type d'agent de réticulation ni l'épaisseur du gel n'ont d'effet significatif sur la tension de sortie (Figure 8.20a et b). En revanche, l'utilisation de glycérol pour remplacer partiellement l'eau dans la préparation du gel a un impact notable. À mesure que la teneur en glycérol augmente, la tension produite diminue, ce qui suggère que la quantité d'eau disponible à l'interface entre le gel et le papier est déterminante pour la génération de tension (Figure 8.20c).

Malgré cette diminution de performance électrique, le glycérol améliore fortement la rétention d'eau de l'hydrogel, ce qui favorise la stabilité de sa structure et de ses propriétés au cours du stockage (Figures 8.20d et e). Notamment, un dispositif à base de gel contenant 50 % de glycérol en poids présente une durée de fonctionnement supérieure à 1000 heures, bien au-delà de celle d'un échantillon non modifié. Ce comportement s'explique par la formation de fortes liaisons hydrogène entre l'eau et le

glycérol, qui limitent efficacement l'évaporation de l'eau (Figure 8.20f).

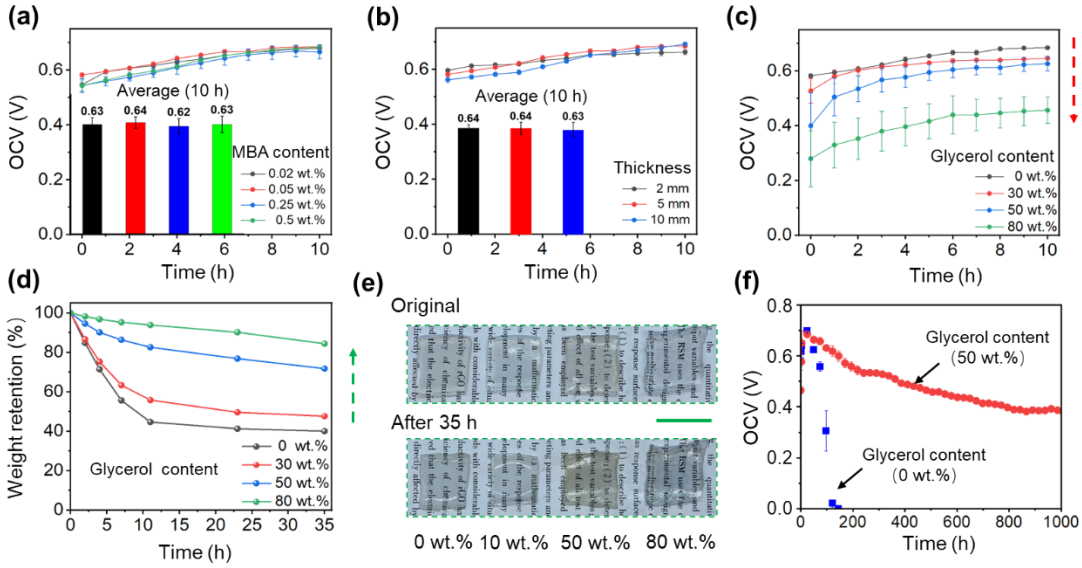

Figure 8.20 Performances de sortie du PHEG utilisant différentes compositions d'hydrogel avec le même papier filtre : a) Tension de sortie (0–10 h) du PHEG assemblé à partir de divers agents de réticulation. b) Tension de sortie (0–10 h) du PHEG assemblé à partir d'hydrogels de différentes épaisseurs. c) Tension de sortie (0–10 h) du PHEG assemblé à partir d'hydrogels contenant différentes teneurs en glycérol. d) Taux de rétention en masse des hydrogels PAM sans protection avec différentes teneurs en glycérol. e) Photographies des hydrogels PAM avec différentes teneurs en glycérol avant et après 35 heures de stockage (25 ± 5 °C). Échelle : 2 cm. f) Tension de sortie du PHEG utilisant des hydrogels PAM contenant 0 % et 50 % de glycérol à différents temps de stockage (25 ± 5 °C).

Le paragraphe précédent a mis en évidence l'excellente durabilité et l'adaptabilité environnementale du PAM-hydrogel dopé au glycérol et des dispositifs PHEG qui en sont issus. Cependant, il est généralement observé que les PHEG fabriqués à partir d'hydrogel PAM sans glycérol présentent une tension initiale plus élevée, ce qui les rend plus adaptés à une utilisation immédiate. Le dispositif PHEG illustré ci-dessous est composé d'un hydrogel PAM sans glycérol et de papier filtre. Comme le montre la figure 8.21a, le test de puissance de sortie a été réalisé immédiatement après l'assemblage du papier, de l'hydrogel et des électrodes, avec une puissance maximale atteignant environ 1,61 μW/cm². La figure 8.21b montre en outre que ce dispositif peut directement charger des condensateurs de différentes capacités.

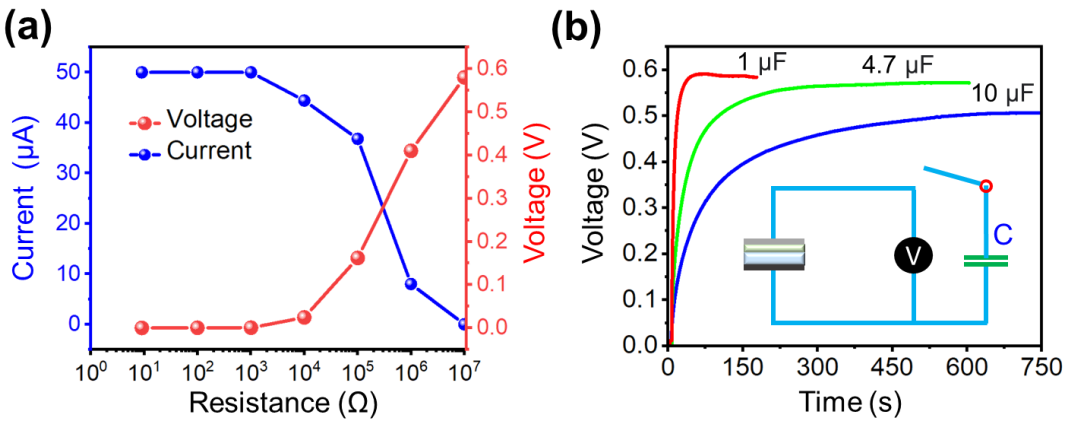

Figure 8.21 a) Dépendance du courant et de la tension de sortie du PHEG par rapport à la résistance électrique du circuit externe. b) Courbes tension–temps de condensateurs commerciaux chargés par un PHEG. L'encadré montre un circuit de stockage de charge.

Par ailleurs, la connexion en série de plusieurs dispositifs PHEG permet d'augmenter progressivement la tension de sortie (Figure 8.22a), tandis qu'un montage en parallèle entraîne une élévation graduelle du courant généré (Figure 8.22b). La Figure 8.22c illustre une configuration composée de 10 unités PHEG empilées, dont le volume total est d'environ 26,62 cm^3, inférieur à celui de quatre piles AA (≈ 30,78 cm^3), tout en atteignant une tension de sortie d'environ 6 V, comparable à celle de ces dernières.

Fait notable, comme le montre la Figure 8.22d, une configuration ne comportant que cinq unités suffit à alimenter facilement une calculatrice de grande taille, démontrant ainsi le potentiel pratique du système pour des applications électroniques à faible consommation.

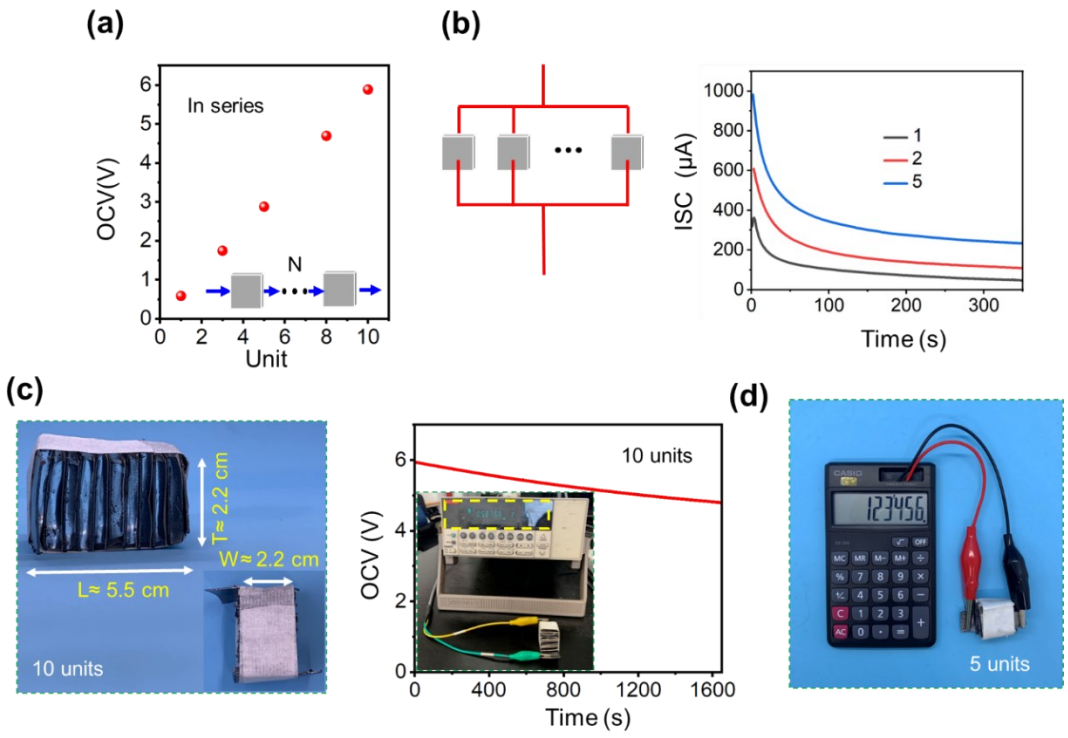

Figure 8.22 a) Relation linéaire entre le nombre d'unités PHEG en série et la tension de sortie. b) Schéma de différents PHEG connectés en parallèle. Courant de sortie en fonction du nombre d'unités connectées en parallèle. c) Apparence et dimensions d'un PHEG assemblé à partir de 10 unités. Courbe de la tension de sortie en temps réel du PHEG à 10 unités. d) Démonstration de l'alimentation d'une calculatrice commerciale par un PHEG composé de 10 unités.

Le PHEG présente une variation nette de tension lorsqu'il est soumis à une compression (Figure 8.23a), alors que ni le PEG ni le HEG ne génèrent de signal de tension identifiable. Comme illustré dans la Figure 8.23b, l'appui d'un doigt sur le PHEG provoque une diminution de la tension, suivie d'une récupération, démontrant son aptitude à servir de capteur de pression auto-alimenté. Ce mécanisme de détection s'explique par la compression du gel élastique, qui induit une variation locale de la concentration en protons. Par ailleurs, la Figure 8.23c montre que le capteur conserve une réponse dynamique stable même après 1230 cycles de chargement.

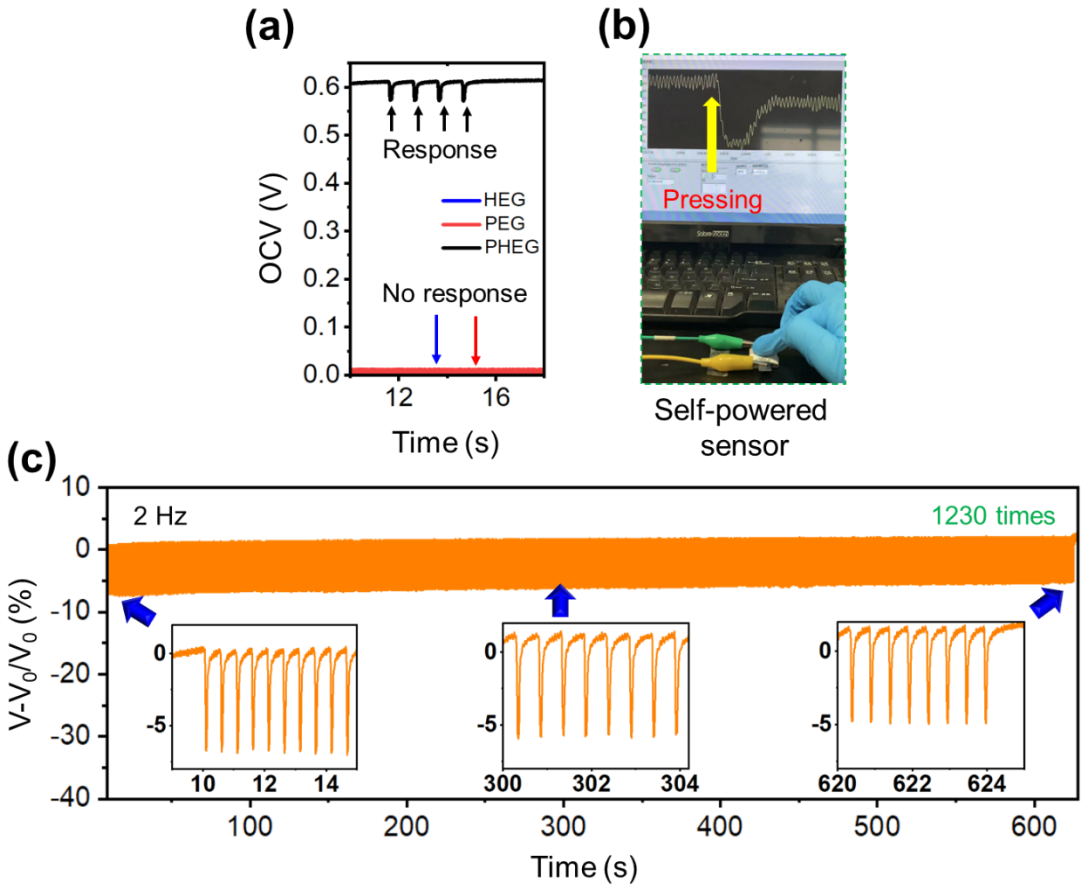

Figure 8.23 a) Réponse en tension de différents dispositifs (HEG, PEG et PHEG) lors d'un appui dynamique. b) Schéma illustrant la réponse du capteur PHEG auto-alimenté au processus d'appui. c) Stabilité de la réponse à l'appui du capteur PHEG auto-alimenté (2 Hz ; 1230 cycles).

8.4 Conclusions et perspectives

Conclusions

Cette étude propose une exploration systématique de la conception et du développement de dispositifs à base d'hydrogel capables de générer un courant continu et de fonctionner comme capteurs de pression auto-alimentés. Partant des mécanismes fondamentaux de migration ionique dans les hydrogels polyélectrolytiques sous contrainte mécanique, le travail a conduit à des architectures biomimétiques multicouches, pour aboutir à un générateur papier–hydrogel à haute performance et stabilité. Les principales avancées et contributions se déclinent comme suit :

Première partie

Un hydrogel conducteur, élastique et souple, à base de PAA, a été développé. Ce gel exploite la différence de mobilité entre les cations mobiles (H^+) et les groupements anioniques fixes ($–COO^–$) lors d'une compression pour convertir l'énergie mécanique en courant continu mesurable. Sous contrainte, la concentration ionique locale augmente ; les anions restent fixes tandis que les protons migrent vers la région de plus faible concentration, générant un signal électrique continu dans un circuit externe. Ce dispositif peut fonctionner comme capteur auto-alimenté de position ou même de vibration acoustique. Le principe a été validé pour d'autres hydrogels polyélectrolytiques, démontrant son applicabilité étendue dans la récupération d'énergie mécanique.

Deuxième partie: Inspirés de la répartition ionique asymétrique observée dans les membranes cellulaires, nous avons conçu une structure hydrogel en double couche à gradient ionique. Celle-ci associe une couche de PVA dopée avec un polyélectrolyte (LS pour fournir des cations, ou QC pour fournir des anions) à une couche de PVA neutre. Un fort gradient de concentration ionique est ainsi généré à l'interface. Les dispositifs basés sur PVA–LS/PVA atteignent une tension initiale supérieure à 100 mV, soit un ordre de grandeur supérieur à celui des gels PAA monocouches. En connectant 10 unités en série, une tension de 1,29 V est obtenue, suffisante pour alimenter un petit appareil électronique comme une calculatrice. Ces structures peuvent également servir de capteurs de pression auto-alimentés.

Troisième partie: Pour améliorer encore la stabilité et la praticité, nous avons développé

un générateur composite papier–hydrogel basé sur un hydrogel de PAM associé à un papier cellulosique recouvert d'argent. L'eau diffusant depuis le gel vers le papier induit une réaction électrochimique de type pile avec les couches d'argent, produisant une tension stable pouvant atteindre 0,6 V. L'introduction de glycérol renforce la rétention d'eau, prolongeant la durée de fonctionnement à plus de 1000 heures. Grâce à une conception modulaire, plusieurs unités peuvent être assemblées ; dix modules permettent d'atteindre 6 V, suffisants pour alimenter des dispositifs plus complexes ou charger des condensateurs. Par ailleurs, le PHEG agit aussi comme capteur de pression souple et fiable.

Conclusion générale: Ce travail trace une voie cohérente allant des principes de base aux applications concrètes dans le domaine des dispositifs d'énergie souples. Les systèmes proposés sont peu coûteux, écologiques, faciles à fabriquer, reposant sur des polymères hydrosolubles, des polyélectrolytes biosourcés et des matériaux à base de papier, sans nécessiter de microfabrication complexe. Leur flexibilité et leur biocompatibilité les rendent particulièrement adaptés à l'électronique portable, notamment pour des applications en peau électronique auto-alimentée ou en capteurs flexibles, ouvrant la voie à de nombreuses perspectives pratiques.

Perspectives

Bien que cette étude ait permis de développer avec succès une série de générateurs à courant continu et de capteurs de pression auto-alimentés à base d'hydrogel, tout en améliorant progressivement leur tension de sortie grâce à l'optimisation structurelle — démontrant ainsi leur potentiel pour alimenter de petits dispositifs électroniques et pour des applications de détection de pression — plusieurs défis clés restent à surmonter avant une mise en œuvre pratique à grande échelle.

1. Perte d'eau et stabilité des hydrogels

Les hydrogels, de par leur douceur et leur compatibilité avec la peau, sont des matériaux prometteurs pour les dispositifs portables en contact direct avec le corps humain. Toutefois, leur forte teneur en eau les rend très sensibles à l'évaporation, ce qui réduit leur flexibilité et entraîne une dégradation progressive de leurs performances. En environnement ouvert ou sous haute température, les hydrogels ont tendance à se dessécher et devenir cassants, compromettant leur intégrité structurelle et leur stabilité

fonctionnelle.

Une approche courante pour limiter la perte d'eau consiste à incorporer des agents humectants tels que le glycérol, des sels inorganiques, l'éthylène glycol, des liquides ioniques ou des solvants eutectiques profonds dans le réseau hydrogel. Dans cette étude, le glycérol a été utilisé pour ralentir l'évaporation. Ces additifs améliorent la rétention d'eau à court terme, mais ne suffisent pas à assurer une stabilité à long terme, ce qui soulève la nécessité de stratégies de protection plus efficaces.

Par exemple, l'équipe de Jian Xu a proposé une méthode innovante basée sur la formation d'un revêtement élastomère souple à la surface de l'hydrogel de PAM par copolymérisation confinée. Cette couche limite fortement l'évaporation de l'eau et améliore la stabilité environnementale du gel. Cependant, l'incompatibilité mécanique entre l'élastomère et l'hydrogel (notamment en termes de module de Young) peut provoquer un délaminage ou une rupture sous déformation répétée. Il est donc essentiel d'assurer une bonne compatibilité mécanique pour garantir la durabilité de l'encapsulation.

Dans une autre étude publiée dans Science, l'équipe de Zisheng Luo a mis en œuvre un traitement à l'acide sulfurique concentré sur des hydrogels PAM-polysaccharide. Ce procédé génère in situ une couche dense de carbone après 48 h de séchage, agissant comme barrière contre l'évaporation, même à des températures allant jusqu'à 143 °C. Malgré son efficacité, cette méthode soulève des préoccupations quant à la biocompatibilité en raison de l'utilisation d'acide fort.

Par ailleurs, l'équipe de Hongbo Zeng a démontré que l'eau libre dans l'hydrogel s'évapore facilement, tandis que l'eau liée est bien plus stable. En s'inspirant de la structure de la couche cornée, ils ont conçu un hydrogel zwitterionique capable de retenir efficacement l'eau liée tout en maintenant des propriétés mécaniques souples. Cette interaction forte entre les polymères zwitterioniques et l'eau constitue une voie prometteuse pour améliorer la résistance au dessèchement.

En résumé, ces stratégies ouvrent de nouvelles perspectives pour améliorer la stabilité structurelle et fonctionnelle des dispositifs à base d'hydrogel dans des environnements contraignants.

2. Faible tension de sortie et nécessité de stratégies hybrides

Malgré les progrès réalisés, la tension de sortie des générateurs DC à base d'hydrogel reste bien inférieure à celle d'autres technologies, comme les TENG. Cette faiblesse est liée à la faible intensité du potentiel généré par la migration ionique, généralement limitée à quelques centaines de millivolts à environ 1 volt — insuffisant pour de nombreuses applications électroniques.

Deux approches sont envisageables :

Renforcer les gradients ioniques internes ou les structures à double couche via la conception des matériaux ; Connecter plusieurs unités hydrogel en série pour accroître la tension globale.Si la première approche vise à améliorer le rendement unitaire, l'effet reste souvent limité. En revanche, la connexion en série de plusieurs unités constitue une méthode plus efficace et directe pour augmenter les performances globales.

Inspiré de l'anguille électrique, Thomas B. H. Schroeder et ses collaborateurs ont publié dans Nature un système de génération d'énergie basé sur des compartiments microstructurés de gels ioniques sélectifs (pour cations et anions). En empilant ces compartiments de manière contrôlée, ils ont obtenu une activation synchronisée et une tension de sortie pouvant atteindre 110 V. Une telle approche pourrait être transposée par impression 3D, mais nécessite encore des procédés de fabrication de haute précision.

3. Réponse lente et instabilité des signaux

Les capteurs à base d'hydrogel fonctionnent bien pour les pressions lentes ou statiques, mais rencontrent des difficultés face à des entrées rapides ou à haute fréquence. En effet, la mobilité ionique limitée dans le réseau du gel induit des délais de réponse, du bruit de fond et une dérive du signal, compromettant la précision des mesures en temps réel.

Pour pallier ces limitations, deux axes sont envisageables :

Optimiser les propriétés du matériau (densité de réticulation, porosité, voies de conduction ionique) pour accélérer la mobilité ionique ; Intégrer des techniques avancées de traitement de signal, notamment des algorithmes d'apprentissage automatique, afin de filtrer, corriger et stabiliser les signaux électriques bruts en temps réel. L'association de ces stratégies permettrait d'améliorer significativement la précision et la stabilité des capteurs dans des conditions dynamiques ou complexes.